Reliability – based Performance Assessment of Damaged Ships

By

Y.W. Lee, Y. Pu, H.S Chan, A. Incecik and R.S. Dow
School of Marine Science and Technology, Newcastle University, Newcastle Upon Tyne NE1 7RU United Kingdom

I. Khan and P.K. Das
Department of Naval Architecture and Marine Engineering, Universities of Glasgow and Strathclyde, Henry Dyer Building, 100 Montrose Street, Glasgow G4 OLZ United Kingdom

P.E. Hess,
Formerly, Code 654, Naval Surface Warfare Center Carderock Division
9500 MacArthur Blvd, West Bethesda, MD 20817, USA

October 2006

REPORT DOCUMENTATION PAGE

Form Approved
OMB No. 0704-0188

1. REPORT DATE *(DD-MM-YYYY)*	2. REPORT TYPE	3. DATES COVERED *(From - To)*
10-10-2006	Technical, Research	15-JUL-2004 to 14-JUL-2006

4. TITLE AND SUBTITLE
Reliability - Based Performance Assessment of Damaged Ships

5a. CONTRACT NUMBER
N00014-04-1-0757

5b. GRANT NUMBER
N00014-04-1-0757

5c. PROGRAM ELEMENT NUMBER
05PR08631-00

6. AUTHOR(S)
Lee, Y.; Pu, Y.; Chan, H.; Incecik, A.; Dow, R.S.;
Khan, I.; Das, P.K.
Hess, P.E.

5d. PROJECT NUMBER

5e. TASK NUMBER

5f. WORK UNIT NUMBER

7. PERFORMING ORGANIZATION NAME(S) AND ADDRESS(ES)
a) Newcastle University, Newcastle Upon Tyne NE1 7RU United Kingdom
b) Universities of Glasgow and Strathclyde, Henry Dyer Building, 100 Montrose Street, Glasgow G4 OLZ United Kingdom

8. PERFORMING ORGANIZATION REPORT NUMBER

9. SPONSORING/MONITORING AGENCY NAME(S) AND ADDRESS(ES)
Office of Naval Research, Ballston Centre Tower One, 800 North Quincy Street, Arlington VA 22217 - 5660

10. SPONSOR/MONITOR'S ACRONYM(S)
ONR

11. SPONSOR/MONITOR'S REPORT NUMBER(S)

12. DISTRIBUTION/AVAILABILITY STATEMENT
Approved for Public Release; distribution is Unlimited.

13. SUPPLEMENTARY NOTES
This report is prepared in cooperation with Naval Surface Warfare Center Carderrock Division, USA.

14. ABSTRACT

The objective of this research is to develop a reliability-based procedure for the ship operators to make the immediate repair actions by evaluating the effects of the damage on the safety of the ship using residual strength assessment procedure. In this study, a procedure has been developed to assess structural integrity of damaged ships. The procedure consists of four steps: (1) Identify the location and size of the openings; (2) Calculate the still water bending moment and wave-induced loadings including vertical bending moment, horizontal bending moment and torsion; (3) Calculate the ultimate strength of the damaged cross-section considering the interaction of vertical bending moment, horizontal bending moment and torsion; (4) Assess the structural integrity by deterministic and probabilistic approaches. The state of the art of the methods for predicting environmental loads and assessing the structural safety has been reviewed. The developed procedure is applied to a sample vessel, HULL5415, to demonstrate the applicability of the proposed procedure. Overall the developed procedure and the methods are working well.

15. SUBJECT TERMS
Residual strength of damaged ships; Wave-induced loads on damaged ships; Hull girder strength; Reliability analysis of damaged ships; Model tests of hydrodynamic loads; Interaction of vertical and horizontal bending moment.

16. SECURITY CLASSIFICATION OF:			17. LIMITATION OF ABSTRACT	18. NUMBER OF PAGES	19a. NAME OF RESPONSIBLE PERSON
a. REPORT	b. ABSTRACT	c. THIS PAGE			Dr Yongchang Pu
UU	UU	UU	UU	220	19b. TELEPHONE NUMBER *(Include area code)* +44-191-222 6243

CONTENTS

1. EXECUTIVE SUMMARY

When a ship is damaged, the operators need to decide the immediate repair actions by evaluating the effects of the damage on the safety of the ship using residual strength assessment procedure. In this study, a procedure has been developed to assess structural integrity of damaged ships. The procedure consists of four steps: (1) Identify the location and size of the openings; (2) Calculate the still water bending moment and wave-induced loadings including vertical bending moment, horizontal bending moment and torsion; (3) Calculate the ultimate strength of the damaged cross-section considering the interaction of vertical bending moment, horizontal bending moment and torsion; (4) Assess the structural integrity by deterministic and probabilistic approaches. The state of the art of the methods for predicting environmental loads and assessing the structural safety has been reviewed. The developed procedure is applied to a sample vessel, HULL5415, to demonstrate the applicability of the proposed procedure.

The hydrodynamic loads in regular waves have been calculated by a 2D linear method. Experimental tests on a ship model with a scale of 1/100 have also been carried out to predict the hydrodynamic loads in regular waves. The results of the theoretical method and experimental tests are compared to validate the theoretical method and to calculate the model uncertainties of the theoretical method for probabilistic strength assessment. The comparison of theoretical results with experimental results has revealed that the prediction of vertical bending moment of the 2D linear method agrees reasonably well with the experimental results, while the prediction of horizontal bending moment is acceptable although it is not as well as that of vertical bending moment. However the accuracy of torsion moment is generally poor. Further research is required to improve the accuracy in this area.

The extreme wave-induced loads have been calculated by short term and long term prediction. For the loads in intact condition, long term prediction with duration of 20 years is used, while for loads in damaged conditions short term prediction is used. The maximum values of the most probable extreme amplitudes of dynamic wave induced loads in damaged conditions are much less than those in intact condition, because the most probable extreme load in intact condition is based on long term prediction, while the most probable extreme load for damaged conditions is based on short term prediction (sea state 3 for 96 hours).

An opening could change the distribution of not only stillwater bending moment but also wave-induced bending moment. It is observed that although some cross sections are not structurally damaged, the total loads (including stillwater bending moment and wave-induced bending moment) acting on these cross sections after damage (in other locations) may be increased dramatically compared to the original design load in intact condition. In this case the strength of these cross sections also needs to be assessed.

The ultimate strength of the hull 5415 has been predicted using the progressive analysis, the results of which compare well with those of another program developed by Bureau Veritas (BV). Although the strength assessment of all the critical cross sections should be carried out in practice, not all the cross sections have structural details for this hypothetical vessel. Therefore only those critical cross sections with structural details are assessed to demonstrate the applicability of the developed methods.

The residual strength for the different damage scenarios has been compared. In damage scenarios 1 and 2, since the location of the damages have been around the elastic neutral axis, the residual strength has been about 96.6% and 93 % of the ultimate strength during hogging

condition. Similarly the residual strength damage scenarios 3 and 4 shows significant decrease compared to the ultimate strength.

Deterministic strength assessment of the damaged ships is carried out by considering the interaction of vertical and horizontal bending moments for intact condition and damage scenario 2. It is found that the damaged ship is quite safe with a fairly high safety margin. This is due to the relatively small wave-induced loads, which is based on a short term prediction, and at the same time the extent of damage is fairly moderate, which does not reduce the ultimate strength too much.

The residual strength has also been assessed by a probabilistic approach. The limit state function used for reliability analysis is derived from the interaction equation including vertical and horizontal bending moments, which was developed in the deterministic strength assessment. The reliability index for HULL 5415 in intact condition has been calculated.

Overall the developed procedure and the methods are working well, although further research is required in some areas. The information, which is produced by this procedure, should be very useful for the operators to make a well-informed decision.

2. INTRODUCTION

2.1 Background

A large number of ship accidents continue to occur despite the advance with the navigation system. These accidents would cause the loss of cargos, pollution of environment, even loss of human beings. Based on statistical data of Lloyd's Register of Shipping (Lloyd's Register, 2000), a total of 1336 ships were lost with 6.6 million gross tonnage cargo loss between 1995 and 2000. 2727 people were reported killed or missing as a result of total losses in this period. So it is very important to ensure an acceptable safety level for damaged ships. Unfortunately adequate structural strength in intact condition does not necessarily guarantee an acceptable safety margin in damaged conditions. Conventionally only the structural strength in intact condition was assessed in the design.

Recognising the importance of the residual strength of ships, International Maritime Organisation (IMO) has proposed an amendment, which states: 'All oil tankers of 5000 tonnes deadweight or more shall have prompt access to computerised, shore-based damage stability and residual structural strength calculation programmes.'

When a ship is damaged, the operators need to decide the immediate repair actions by evaluating the effects of the damage on the safety of the ship using residual strength assessment procedure.

Various publications have concerned at, as summarised in the following, the local and overall structural behaviour of a damaged ship. Smith and Dow (1981) carried out pioneer work in assessing residual strength of damaged ships and offshore structures. Strength reduction of dented stiffened panels was investigated. The effect of this reduction on the ultimate strength of hull girder was further assessed.

Qi, et al (1999) have derived a simplified method for assessing residual strength of hull girders of damaged ships. Reliability of the ship was also estimated by a first order and second moment method.

Wang, et al (2002) have tried to use the section modulus to indicate the residual strength of damaged ships. Both section modulus and ultimate strength of damaged ships were calculated. A regression analysis was carried out to derive an empirical formula for predicting safety level of damaged ships.

A few more papers (Ghoneim and Tadros, 1992, Paik, 1992, Paik, et al, 1995, Zhang, et al,1996, Paik, et al, 1998, Ghose, et al, 1995) have discussed the residual strength of damaged ships from different view points.

All the above work only studied the ultimate vertical bending moment capacity without considering the effect of horizontal bending moment and torsion and critical load case was not evaluated. This means that the worst load case was assumed to be the vertical bending moment, and the horizontal bending moment and torsion are negligible. This methodology was, strictly speaking, only valid for ships in intact condition.

In the design of ships, structural strength is conventionally assessed only in intact condition. Under this condition, the critical load case for mono-hull ship is the vertical bending moment, which reaches maximum in head seas. Both horizontal bending moment and torsion are

insignificant. The torsion will be considered only when there are large openings on ships. This methodology has been successfully applied to ship design for many years. Because of this, the prediction of environmental loads and assessment of structural strength were normally carried out separately by two groups of people. When the ultimate strength of hull girder is assessed, only vertical bending moment is considered. Although some researchers have tried to evaluate the effect of horizontal bending moment and shear on the ultimate strength, it is concluded that these effects are insignificant. But this conclusion is only valid for intact condition.

When a ship is in damaged condition its floating condition could be changed dramatically. Its draught is increased and it may heel. It could also have large holes in the structure. If the methodology used for intact condition is blindly applied to damaged condition, the results could be misleading. Ideally the environmental loads should be calculated together with the assessment of the residual strength of the ship. In another words, a systematic approach should be used for a more accurate assessment of residual strength of a damaged ship. Chan, et al, (2001) have shown that the most critical condition for a damaged Ro-Ro ship is in quartering seas. Although the vertical bending moment in quartering seas is smaller than that in head seas, the horizontal bending moment is quite large. The ratio of horizontal bending moment to vertical bending moment could be as large as 1.73. So the combined effect of vertical bending moment and horizontal bending moment is more serious. In addition, torsion, which is not considered in the above study, normally reaches maximum in quartering seas. So the effect of horizontal bending moment and torsion on the ultimate hull girder strength should be considered in the assessment of residual strength of damaged ships.

2.2 Objectives and Scope of Work

The objective of the proposed research is to develop a reliability-based procedure to assess the residual strength of damaged ships. A systematic approach will be adopted in this research. The wave excitation loads will be predicted by a linear and non-linear method. Experimental study will also be carried out to compare the results obtained from the prediction with those obtained from measurements. The ultimate hull girder strength of damaged ships will then be evaluated in which the effect of horizontal bending moment and shear will be considered. The reliability of damaged ships will be estimated. This procedure could be applied to develop a reliability-based performance assessment format for damaged ships.

Damage on ships could have various forms, such as dents, cracks, corrosion and openings. The work presented in this report will concentrate on large openings, which could lead to water ingress. The effects of dents, cracks and corrosion will not be considered in this project. However it should be noted that the combined effects of dents, cracks and corrosion with openings should, strictly speaking, be considered because a ship is quite likely being sustained certain level of defects in the form of dents, cracks and corrosion. This could be the work of further research.

This project is a joint effort of Naval Surface Warfare Centre Carderock Division (NSWCCD), USA, Newcastle University, and University of Strathclyde & Glasgow. Because NSWCCD is funded by a different funding mechanism, the details of the work of NSWCCD will not be presented in this report unless it is essential to explain the developed process.

2.3 The developed procedure for assessing performance of damaged ships

The procedure could be used by ship operators to assess the residual strength of damaged ships. The procedure is described as follows:

(1) Identify the location and size of the openings
(2) Calculate the still water bending moment and wave-induced loadings including vertical bending moment, horizontal bending moment and torsion
(3) Calculate the ultimate strength of the damaged cross-section considering the interaction of vertical bending moment, horizontal bending moment and torsion
(4) Assess the structural integrity by deterministic and probabilistic approaches

The key methods used in this procedure will be fully explained in chapters 3 and 4. The procedure will be applied to a sample vessel in chapter 7.

3. THE STATE OF THE ART

3.1 The State of the Art in Wave-Induced Loading Prediction

The prediction of ship motions and dynamic wave induced loads acting on a ship has been a main theme in the field of ship hydrodynamics. The development of a two-dimensional harmonic flow solution was accomplished by Ursell (1949). Korvin-Kroukovsky (1955) introduced the heuristically-derived strip theory to ship motions as the first strip theory. This theory was modified by his sequel paper (Korvin-Kroukovsky and Jacobs, 1957) and Jacobs (1958), and the theory restricted on heaving and pitching only. Jacobs (1960) carried out correlation works with the analytical calculation of ship bending moments and the results of model tests in regular waves. The validity of the strip theory on a high-speed destroyer hull was shown in (Gerritsma and Beukelman, 1967). Salvesen et al. (1970) expanded the original theory for more general modes of motions and wave headings. Further a number of improved strip theories have been developed. Among them there are rational strip theory (Ogilvie and Tuck, 1969) and unified strip theory (Newman, 1978). Good agreement between strip theory predictions and experimental data has been found for many classes of mono-hull forms (Kim et al., 1980) and twin-hull ships (Lee and Curphey, 1977). Fully three-dimensional numerical solutions of the slender ship motion problem at forward speed have been attempted by Chang (1977), Inglis (1980) and Chan (1992, 1993 and 1995). In spite of practical success of these linear two-dimensional and three-dimensional theories, their applications are limited to small amplitude motions.

However, large amplitude motions and resulting structural responses, which cannot be accurately predicted by linear theory, are key issues for assessments of ultimate hull girder strength of intact ship and residual strength of damaged ship in extreme wave conditions. There is a need to use techniques being capable to take into account these non-linear effects. Although non-linear boundary element technique is applicable to solving full non-linear ship motion problem, its computational cost is prohibitively expensive in practical applications. On the other hand, alternative practical approaches to solving non-linear problem have been attempted. For the past decades, practical tools have been developed based on the calculations of the hydrodynamic and hydrostatic forces at the instantaneous positions of the ship body sections for intact vessels motions with or without forward speed. In these practical, so called quasi-non-linear, time domain methods the hydrodynamic forces are obtained from the solution of linear frequency domain. These time dependent hydrodynamic coefficients, wave exciting forces and hydrostatic forces are employed in the coupled equations of motion. Various applications of the quasi-non-linear time domain method to the prediction of mono and multi-hull ship motions and loads can be found in Yamamato et al. (1978), Borresen & Tellsgard (1980), Chiu & Fujino (1989), Fang & Her (1995), Fang et al. (1997) and Tao & Incecik (1996). No oblique waves were considered in these studies. On the other hand, Fujino & Yoo (1985) investigated wave loads acting on a ship in large amplitude oblique waves. The predicted peak values of the wave loads and their non-linear behaviour are in good agreement with experimental measurements. Although large amplitude motions have been investigated in the above studies, the equations of motion were solved in a linear sense where Euler angles are implicitly assumed to be small.

The above works only studied ship motions and dynamic wave loads acting on a ship in intact condition. In the last decade the study on wave induced loads in damage conditions have been accomplished, but fairly limited. De Kat (1990) and Alegeest (1995) solved the non-linear Euler equations of motion respectively for studying ship capsize events in following seas and

non-linear hull girder loads in head waves. The former has considered both linear hydrodynamic forces and empirical viscous forces while the latter has employed a three-dimensional panel method to calculate linear hydrodynamic forces in time domain. The behaviour of the damaged ship in waves is different from that in intact condition, so it could be analysed in time domain rather than in frequency domain (Santos et al., 2002). A nonlinear time-domain simulation method for the prediction of large amplitude motions of a Ro-Ro ship in intact and damaged conditions was introduced by Chan et al. (2002). In this study numerical computations and model tests have been carried out to investigate the dynamic motion responses of Ro-Ro ship Dextra to various wave amplitudes at different wave headings. Chan et al. (2003) also described global wave load predictions on a Ro-Ro ship in intact and damaged condition. In order to evaluate the method used, results of the vertical bending moment, horizontal bending moment and dynamic torsion as well as dynamic shear force were correlated with model test results. Recently six degrees of freedom motion response tests of a Ro-Ro model (completed for EU project DEXTREMEL) have been reported in regular waves for intact and damaged conditions by Korkut et al. (2004). Korkut et al. (2005) mentioned measurements of global loads acting on a Ro-Ro ship. The stationary model was tested in different wave heights and wave frequencies for the head, beam and stern quartering seas in order to explore the effect of damage and wave heights on the global loads acting on the model. Recently Lee at al. (2005) has introduced the framework for damage survivability assessment system that can evaluate and improve the ship safety. The importance of predicting accurate wave induced loads and residual strength in a damaged ship was mentioned.

3.2 The state of the art in ultimate strength prediction of hull girders

The longitudinal strength of a vessel, as is otherwise known the ability of a ship to withstand longitudinal bending under operational and extreme loads without suffering failure, is one of the most fundamental aspects of the strength of a ship and of primary importance for Naval Architects. Assessment of the ability of the ship hull girder to carry such loads involves the evaluation of the capacity of the hull girder under longitudinal bending and also the estimation of the maximum bending moment which may act on it. From the initial work of pioneers in the area of ship structural design such as the likes of Thomas Young and Sir Isambard K. Brunel and Stephen P. Timoshenko, the fundamental idea to assess longitudinal strength of a ship's hull was first presented by John in 1874. By calculating the bending moment assuming the wave whose length is equal to the ship length, he proposed an approximate formula to evaluate the bending moment at amid-ship section. He also calculated the deck maximum stress and by comparing that to the material breaking strength he managed to determine the panel optimum thickness. Although John's theory remains in use until today, subsequent methods of stress analysis and wave loading have improved substantially with criteria that help to determine optimal thickness changing from breaking strength to yield strength

From the beginning of the 20th century, it has become common to consider the buckling as a design criterion, and in 21st century it shall be supplemented by the ultimate strength. Caldwell (1965) was originally the first one to attempt theoretically to evaluate the ultimate hull-girder strength of a vessel. He introduced "Plastic Design", as it is known today, by considering the influence of buckling and yielding of structural members composing a ship's hull. By introducing a stress reduction factor at the compression side of bending he managed to calculate the bending moment produced by the reduced stress which he considered as the ultimate hull-girder strength. By not taking into account the reduction in the capacity of structural members beyond their ultimate strength his method overestimates the hull-girder's ultimate strength in general and since exact values of reduction factors for structural members were not known, the "real" value could not be calculated, only an approximation. Since then it

has been improved by work carried out by Maestro and Marino (1989) and Nishihara (1983) who extended the formulation to include bi-axial bending so that it is able to estimate the influence of damage due to grounding and to improve the accuracy of the strength reduction factor. By proposing their own formulae Edo et al. (1988) and Mansour et al. (1990) performed simple calculations that lead to further development of the methods, which were proposed by Paik and Mansour (1995). By applying these methods Paik et al. (1993), (1997) performed reliability analysis considering corrosion damage, and similar work that includes corrosion effects has also been published by Wei-Biao (1992). Although these methods do not explicitly take into account of the strength reduction in the members, the evaluated ultimate strength showed good correlation with measured/calculated results from other cases. Paik and Mansour (1995) compared the predicted results with those by experiments and Idealized Structural Unit Method (ISUM) analysis and the differences between the two were found to be between -1.9% and +9.1%.

By taking into account of the strength reduction (load shedding) of structural members when the collapse behaviour of a ship's hull is simulated, a number of methods were developed which can be grouped under the overall term "Progressive Collapse Analysis" whose fundamental part could be the application of the Finite Element Method (FEM) considering both geometrical and material nonlinearities. Unfortunately the large amount of computer resources required to perform such type of analysis and lack of validation of the subsequent results have led to the development of simplified methods such as the one proposed by Smith (1977). Progressive Collapse Analysis takes into account the strength reduction of structural members after their ultimate strength as well as the time lag in collapse of individual members and Smith was also the first to demonstrate that the cross-section cannot sustain fully plastic bending moment. The accuracy of the derived results depends largely on the accuracy of the average stress-strain relationships of the elements. Problems in the use of the method occur from modelling of initial imperfections (deflection and welding residual stresses) and the boundary conditions (multi-span model, interaction between adjacent elements). To improve this recent research is focusing on the development of more reliable stress-strain curves and it can be seen in the work of Gordo & Guedes Soares (1993) and Paik (1999). Smith also performed a series of elasto-plastic large deflection analysis by FEM to derive the average stress-strain relationships of elements and analytical methods have been proposed such as the one by Ostapenko (1981) which includes in-plane bending, shear, thrust and lateral pressure. Rutherford and Caldwell (1990) proposed an analytical method combining the ultimate strength formulae and solution of the rigid-plastic mechanism analysis. In both methods, the strength reduction after the ultimate strength is considered. Yao (1993) also proposed an analytical method to derive average stress-strain relationship for the element composed of a stiffener and attached plating by combining the elastic large deflection analysis and the rigid-plastic mechanism analysis in analytical forms from work performed by Yao and Nikolov (1991) & (1992). Then by taking into account the equilibrium condition of forces and bending moments acting on the element the relationships are derived. When the stiffener is in elastic region, a sinusoidal deflection mode is assumed, whereas after the yielding has started, a plastic deflection component is introduced which gives constant curvature at the yielded mid-span region.

Rutherford & Caldwell (1990) presented a comparison between the ultimate bending moment experienced by very large crude carrier, the *Energy Concentration* and results of retrospective strength calculations in which a simplified approach to stiffened plates collapse was used, but without considering the post-buckling behaviour. Also the importance of lateral pressure, initial imperfections and corrosion rates were investigated. The validity of the model and the method was confirmed by a non-linear finite element analysis. Later Gordo et.al. (1993)

calculated the ultimate strength of *Energy Concentration* using simplified formula considering of the effects of corrosion and initial imperfections on flexural buckling. Recently Khan et al (2006) studied the ultimate strength of *Energy Concentration* considering the tripping, flexural buckling and post buckling behaviour of local elements, taking into account of corrosion, welding induced residual stresses and imperfection.

The applications of FEM to prediction of ultimate strength of hull girders are very few due to the large amount of computational time. A ship's hull-girder is, perhaps, too large for such a kind of analysis to get rational results easily, a number of significant works have, nevertheless, been published. Chen et al. (1983) and Kutt et al.(1985) performed static and dynamic FEM analyses modelling a part of a ship hull with plate and beam-column elements and orthotropic plate elements representing stiffened plates and discussed the sensitivities of the ultimate hull-girder strength with respect to yield stress, plate thickness and initial imperfections. Valsgaard et al.(1991) analysed the progressive collapse behaviour of the girder models tested by Mansour et al.(1995), but unfortunately the results of FEM analysis to evaluate ultimate hull-girder strength are not so many at the moment because the number of elements and nodal points become very huge if rational results are required.

Apart from Smith's method, the Idealized Structural Unit Method (ISUM) is another simple procedure that treats a large structural unit as one element so that the computational time is reduced. The essential point of this method is to develop effective and simple elements (dynamic model) considering the influences of both buckling and yielding. Ueda et al. (1984) developed plate and stiffened plate elements that accurately simulate buckling/plastic collapse behaviour under combined bi-axial compression/tension and shear loads. Paik improved this work and performed different progressive collapse analyses as published in Paik et al. (1990), (1992) and (1992b). Ueda and Rashed (1991) improved their results with Paik (1995) following with an attempt to introduce the influence of tensile behaviour of elements in ISUM. Finally Bai et al. (1993) developed a beam element, a plate element and a shear element based on the Plastic Node Method, as originally published by Ueda and Yao (1982) and managed to achieve progressive collapse analysis. While in Smith's method accurate results are obtained when only the bending moment is considered, the ISUM can be applicable for the case with any combination of compression/tension, bending, shear and torsion loadings but sophisticated elements are required to get accurate results and further improvement of these ISUM elements are still under development.

3.3 The state of the art in structural reliability analysis

Reliability theory of engineering structural systems has three significant parts: the identification of all possible dominant failure modes, the calculation of the failure probability of each failure modes and sensitivity with respect to the obtained dominant limit states and the determination of the upper and lower bounds of the overall structural system according to the correlation between the dominant failure modes and their failure probability. The identification of the dominant failure mode is performed by either traditional mechanics or a mathematical programming approach. Although all proposed methods in this field show a significant amount of effectiveness, the computational effort is still quite demanding for complex structural systems. No close form of the limit states can be obtained since numerical methods are required to calculate the structural responses. Work has also focused on the analysis of structural components or the local behaviour of a structural system.

The determination of the failure probability is the most researched part in the theory of reliability. A variety of second-moment based studies were carried out before the sixties, a

milestone was laid by the paper of Freudenthal (1956) who used complete probability models. However, it is the work of Cornell (1967) that heralds popular acceptance of second moment concept. Later, among many other researchers, Shinozuka (1983) presented a brand new interpretation to the theory. To date, second-moment approaches have become so popular that it always takes an important place in the text books concerning structural safety. Typical of them are those by Ang and Tang, Madsen, Krenk and Lind, Ditlevsen and Madsen , Zhao(1996), and Melcher (1999). The first order and second order moment theories (FOSM and SOSM) which are well established and have found an ever-increasing use in a significant amount of engineering fields. In this type of theories the integration of the joint probability density function (JPDF) of the design variables is circumvented by transformation of the actual problem into a least distance problem in a standard normalised space. Orthogonal transform is used to uncouple the correlated design variables which essentially show that the problem is in its core an optimization procedure.

A number of insurmountable problems in numerical integration of highly dimensional JPDFs in normal space lead research into the conclusion that the failure probability of the structural system has to be given in a "weak form". Instead of calculating the failure probability itself, an interval is given to bind the exact value. Two methods have been proposed to help achieve this, the Wide Bound Method as proposed by Cornell (1967) and the Narrow Bound Method as proposed by Ditlevsen (1979). They are first order and second order approximations respectively. However with the increase of failure modes and their correlation, the bounds will become too loose. In this case, formulation of higher order approximations can be developed or different point evaluation techniques can be used such as the ones proposed by Ang et al. (1981) and Song (1992). A modified bound method can also be found in Cornell's (1967) original work.

Monte Carlo Simulation (MSC) also plays a very important role in different levels of reliability analysis. The high accuracy that the method produces is only dependent on the sampling number and is not affected by the distribution type and the number of basic variables. The method can be used in even those cases where the limit state function is not known explicitly and it is the only approach to highly non-linear problems. A number of variation reduction techniques have been proposed such as the Importance Sampling Method but as always the computation cost in large complex structural systems is still significantly high.

The Response Surface Method (RSM) is one of the latest developments in the field of structural reliability analysis. It is very suitable in cases where the limit state function is known only point-wisely by such numerical methods as the FEM rather than in closed form. In essence, RSM is a system identification procedure, in which a transfer function relates the input parameters (loading and system conditions) to the output (response in terms of displacements or stresses). The observations required for the identification of the most suitable way to relate those two are usually taken from systematic numerical experiments with the full mechanical model and the transfer function obtained approximately defined as the response surface (RS). The basis of the RSM can be tracked back to the 50s in experiment field, but only recently, it has been introduced into the field of reliability analysis. It combines deterministic structural analysis software and the basic reliability ideas aforementioned. In addition to this, even for those problems that other approximate methods seem to be susceptible to, the RSM is shown to be superior in both accuracy and efficiency with its only drawbacks being the experiment design and the identification of unknown parameters in the RS which influence the whole algorithm. Work by Bucher (1990) and Rajashekhar (1993) have led the ways of future research. Advanced algorithms based on that work can be found in work published by Kim et al. (1997), Zheng & Das (2000, 2001) and Yu, Das & Zheng (2001) .

Reliability analysis on hull-girders against collapse is typically undertaken using simplified, closed form equations or progressive failure models. Downes and Pu (2005) evaluated the reliability of a notional high speed craft against hull-girder collapse using both the First Order Reliability Method (FORM) and Monte Carlo simulation with an embedded hull-girder ultimate strength code based on Smith's method. Load-shortening curves were from LR.PASS. A sensitivity analysis was also performed, and it was clarified that the location of a structural member influences which basic random variable is dominant. Another approach for predicting the hull-girder collapse reliability is proposed by Lua and Hess (2003) where the probability distribution of the hull-girder collapse strength modelled by ULTSTR is developed using Monte Carlo simulation. The probability distribution is then approximated by an automated piecewise curve-fit in PULSTR before use in a FORM analysis of the limit state equation for hull-girder collapse in a seaway. The number of simulation cycles is greatly reduced from what would be required for Monte Carlo simulation of the limit state function, without a significant reduction in accuracy.

Fang and Das (2005) use Monte Carlo simulation to predict hull-girder collapse reliability for intact and damaged ships. The strength predictions are based on the Smith's method which is presented in Fang and Das (2004). The mean hull-girder strength is determined using nominal values for the basic strength variables in the strength prediction. The coefficient of variation of the strength prediction is assumed to be 10 percent. A time-dependant reliability model is presented and exercised by Paik, et al.(2003) for a bulk carrier, a double hull-tanker and a FPSO. The reliability model accounts for the effects of fatigue-induced cracking and corrosion. Timelines are presented for each vessel relating the probability of hull-girder failure to ship age. Each timeline is heavily dependant upon the modelling assumptions such as severity and location of corrosion or cracking. The effects of various repair schemes on the reliability over time are shown. Qin and Cui (2003) present a discussion on current corrosion models and propose a new model that uses three piece-wise continuous stages to represent the corrosion process.

Das et al.(2003) present modelling uncertainty evaluations of strength predictions of ring stiffened shells and ring and stringer stiffened shells for various modes of buckling and various radius to thickness ratio values (range used in offshore structures). Model uncertainty factors in terms of bias and coefficient of variation (COV) are developed by comparing predictions to experimental results found in the literature. Comparisons are made for API BUL 2U and DNV buckling strength of shells models.

4. METHODOLOGIES

4.1 Methodologies for Wave-Induced Loading

4.1.1 Linear two-dimensional strip theory

A linear two-dimensional strip theory has been developed to predict the wave-induced motions and loads for both intact and damaged conditions. The details are briefly described below.

4.1.1.1 Equation of motions

Under the assumptions that the responses are linear and harmonic, the equation of motions of a vessel in regular waves can be written in the following general equation.

$$\sum_{k=1}^{6}[(M_{jk}+A_{jk})\cdot\ddot{\eta}_k+B_{jk}\cdot\dot{\eta}_k+C_{jk}\cdot\eta_k]=E_j\cdot e^{-i\omega t} \qquad (4.1\text{-}1)$$

where:

M_{jk} is the components of the generalised mass matrix

A_{jk} and B_{jk} are matrixes of the added mass and damping coefficients

C_{jk} is the matrix of hydrostatics and mooring restoring coefficients

E_j is the complex amplitudes of exciting forces and moments

j and k indicate the direction of fluid force and the modes of motion

(i and j =1 - surge, 2 - sway, 3 - heave, 4 - roll, 5 - pitch, 6 - yaw)

The derivations of the equation of motions and their components can be discovered in (Jacobs, 1958 and 1960; Salvesen et al., 1970; Raff, 1972). Within the framework of linearised potential flow theory, hydrodynamic coefficients and forces were calculated (Chan, 1992).

In this study, rigid body motions are considered. The elasticity of the hull girder is assumed to have the insignificant effect on wave induced loads (Adegeest, 1995). To describe wave and ship motions, two sets coordinate systems are considered (see Figure 4.1-1). One frame is a right handed coordinate system, which translates with the ship with its origin at the longitudinal centre of gravity (G-xyz). Another coordinate system is the space fixed frame (O-XYZ) as shown in Figure 4.1-1, OXY is in the plane of the undisturbed free surface. The vessel is considered to undergo six degree of freedom oscillations about its mean position. These oscillations are better known as surge, sway and heave for translatory oscillations (η_1, η_2, and η_3), and roll, pitch and yaw for angular oscillations (η_4, η_5, and η_6). Figure 4.1-2 shows the definition of wave heading angle (β).

4.1.1.2 Two-dimensional source distribution

Frank (1967) introduced a method in which the required velocity potential is represented by the distribution of the sources over the submersed cross section. The unknown function of the density of the sources along the cylinder contour is determined from the integral equations obtained by satisfying the kinematic boundary condition over the submersed cross section. The hydrodynamic pressures are obtained from velocity potential by using the linearised Bernoulli

Equation. Integration of these pressures over the immersed portion of the cylinder yields the hydrodynamic forces and moments (Frank, 1967; Chan, 2003).

In a pulsating source theory, we can describe it like the follows using source distribution σ and Green function G.

$$\phi(y,z) = -\int_C \sigma(y',z') \cdot G(y,z;y',z') \cdot ds(y',z') \tag{4.1-2}$$

The σ integral equation is

$$\frac{\partial \phi(y,z)}{\partial N} = \frac{\sigma(y,z)}{2} - \int_C \sigma(y',z') \cdot \frac{\partial G(y,z;y',z')}{\partial N} \cdot ds(y',z') \cdot ds(y',z') \tag{4.1-3}$$

After calculating equation (4.1-3), we can obtain the velocity potential from equation (4.1-2).

where, Green function $G(y,z;y',z')$ is

$$G(y,z;y',z') = \frac{1}{2\pi} \log \frac{\sqrt{(y-y')^2 + (z+z')^2}}{\sqrt{(y-y')^2 + (z-z')^2}}$$

$$+ \frac{1}{\pi} \lim_{\mu \to 0} \int_0^\infty \frac{e^{-k(z+z')+ik(y-y')}}{k - K + i\mu} dk \tag{4.1.4}$$

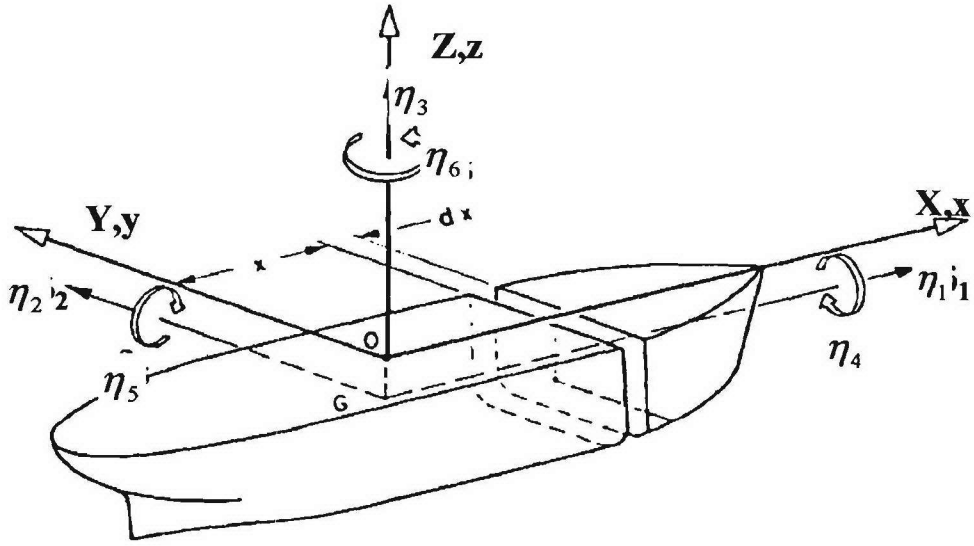

Figure 4.1-1: Co-ordinate systems and modes of motions (Aryawan, 2000)

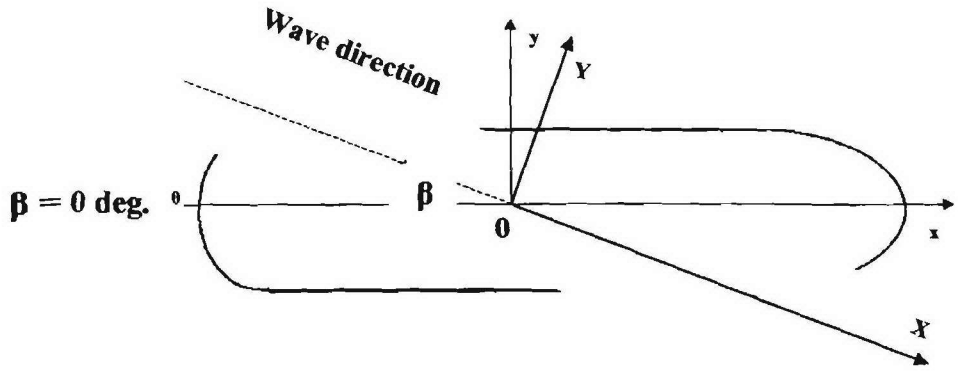

Figure 4.1-2: Definition of wave heading (Aryawan, 2000)

4.1.1.3 Global structural responses

For the calculation of static and dynamic structural loads due to waves, two-dimensional linear strip theory can be used to predict the dynamic loads in the linear frequency domain. The following load components are considered in the calculations (Aryawan, 2000; Incecik et al., 2001; Chan et al., 2003).

- Difference between the static weight and still water buoyancy distribution.
- Dynamic effects due to weight distribution.
- Wave excitation forces.
- Motion induced forces due to added-mass and damping.
- The loads due to the acceleration of structural members.

By neglecting loads due to slamming and springing, in vertical plane the dynamic loads at each section can be written as the following equation. The derivation of the equation can be found in (Aryawan, 2000; Incecik et al., 2001).

$$\frac{dF_3}{dx} = \left(M(x) + A_{33}(x)\right)\cdot\left(\ddot{\eta}_3 + x\cdot\ddot{\eta}_5\right) + B_{33}(x)\cdot\left(\dot{\eta}_3 + x\cdot\dot{\eta}_5\right) + C_{33}\cdot\left(\eta_3 + x\cdot\eta_5\right) - \frac{dE}{dx} \tag{4.1-5}$$

where:

F_3 is the vertical dynamic load at location x

$M(x)$ is the mass component at location x

A_{33} and B_{33} are the added mass and damping coefficient at location x

C_{33} is the restoring force coefficient at location x

η_3 and η_5 are the heave and pitch displacement respectively

E is the vertical exciting force at location x

In horizontal plane, the dynamic loads consist of horizontal dynamic loads and torsion moments. These equations can be found in (Aryawan, 2000).

$$\frac{dF_2}{dx} = \left[m\left(\ddot{\eta}_2 + \xi \ddot{\eta}_6 - \bar{z} \ddot{\eta}_4 \right) \right] d\xi + \left[\begin{array}{l} a_{22}\left(\ddot{\eta}_2 + \xi \ddot{\eta}_6 \right) + b_{22}\left(\dot{\eta}_2 + \xi \dot{\eta}_6 \right) + \\ a_{24} \ddot{\eta}_4 + b_{24} \dot{\eta}_4 \end{array} \right] d\xi - \frac{dE_2}{dx}$$

..... (4.1.6)

$$\frac{dF_4}{dx} = \left[i_{xx} \ddot{\eta}_4 - m\bar{z}\left(\ddot{\eta}_2 + \xi \ddot{\eta}_6 \right) \right] d\xi - \left[g \eta_4 \left(\rho S\overline{om} - m\bar{z} \right) \right] d\xi$$

$$+ \left[a_{44} \ddot{\eta}_4 + b_{44} \dot{\eta}_4 + a_{24}\left(\ddot{\eta}_2 + \xi \ddot{\eta}_6 \right) + b_{24}\left(\dot{\eta}_2 + \xi \dot{\eta}_6 \right) \right] d\xi - \frac{dE_4}{dx} \qquad (4.1\text{-}7)$$

Similar treatment with the vertical plane, the distribution of horizontal shear-forces over the length of ship is determined by integration of $\frac{dF_2}{dx}$, while the distribution of horizontal bending moment is obtained by integrating the shear-forces over the length.

4.1.1.4 Linear frequency domain solutions

Since the equations of motions are linear and harmonic, in which the exciting forces and moments can be written in complex terms, these equations are solved using complex response method. This means that the exciting forces and the responses can be represented as real and imaginary parts. The solutions are then in the forms of amplitudes and their phase-lags (Jacobs et al., 1960; Brebbia, 1979). Coordinate systems and modes of motions are shown in Figure 4.1-1. In addition Figure 4.1-2 describes the definition of wave heading (Aryawan, 2000).

4.1.2 Non-linear two-dimensional strip theory

The problem of a marine vehicle at sea is that of the dynamic equilibrium of forces and moments on an elastic body under wave excitations. In order to predict the resulting motions of a body in waves, the body is considered to be rigid. As long as no vibration problems are to be dealt with, the rigid body assumption can be made without hesitation. The body floating in waves experiences unsteady external fluid forces. The unsteady forces are contributed mainly from the hydrodynamic pressures due to incident, diffraction and radiation waves. The theoretical formulation of the problem is based on the framework of potential flow theory. A body freely floating in oblique regular wave of frequency ω_0 at an angle of incidence β undergoes oscillatory and drift motions. In order to simplify the analysis we assume that the body oscillates harmonically with waves (Chan, 1998; Chan et al, 2003).

To describe flow fields and motions of a rigid body floating in waves, it is convenient to refer the rigid body motion to a space-fixed co-ordinate system O-XYZ as well as a body-fixed co-ordinate system o-xyz as shown in Figure 4.1-3. The position and orientation of the body should be described with respect to the space-fixed system O-XYZ while the linear and angular velocities and accelerations of the body should be expressed in the body-fixed system o-xyz. The space-fixed system O-XYZ is the inertia system with the origin O lying on undisturbed free surface and the Z-axis pointing vertically upward. The body-fixed system o-xyz is moving rectangular co-ordinate system with the origin o being coincident with the centre of gravity of

the intact body. The x, y and z axes are directed respectively toward the bow, the port side and the sky (Chan, 1998; Chan et al, 2003).

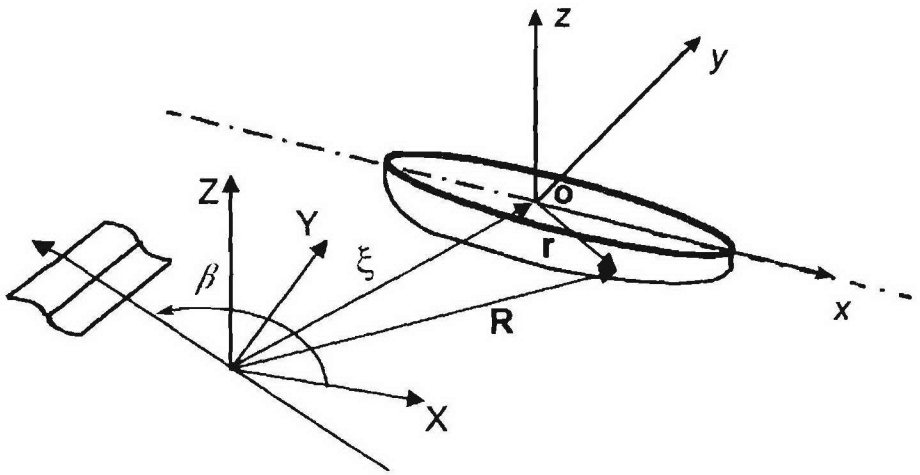

Figure 4.1-3: Co-ordinate systems (Chan at al, 2003)

The position and orientation vectors of the body-fixed axes with respect to the space-fixed frame are defined respectively in the form

$$\boldsymbol{X} = (\xi_1, \xi_2, \xi_3) \tag{4.1-8}$$

$$\boldsymbol{\Omega} = (\xi_4, \xi_5, \xi_6) \tag{4.1-9}$$

where ξ_j with j = 1, 2, 3 represent the surge, sway and heave displacements respectively while j = 4, 5, 6 refer to roll, pitch and yaw angles respectively.

The relationship between a body-fixed position vector $\boldsymbol{r}$ and a space-fixed position vector $\boldsymbol{R}$ can be written as

$$\boldsymbol{R} = \boldsymbol{X} + \boldsymbol{T}\boldsymbol{r} \tag{4.1-10}$$

where $\boldsymbol{T}$ is an orthogonal transformation matrix.

4.1.2.1 Euler equations of motion

The well known Euler equations of motion of a rigid body in six degrees of freedom with respect to the body-fixed co-ordinate system are defined by

$$\dot{m}\left(\mathbf{v} + \boldsymbol{\omega} \times r_G\right) + m\left(\dot{\mathbf{v}} + \boldsymbol{\omega} \times \mathbf{v} + \dot{\boldsymbol{\omega}} \times \boldsymbol{r}_G + \boldsymbol{\omega} \times \left(\boldsymbol{\omega} \times r_G\right)\right) = \boldsymbol{F} \tag{4.1-11}$$

$$\boldsymbol{I}\boldsymbol{\omega} + \dot{m}\boldsymbol{r}_G \times \mathbf{v} + \boldsymbol{I}\dot{\boldsymbol{\omega}} + \boldsymbol{\omega} \times \boldsymbol{I}\boldsymbol{\omega} + m\boldsymbol{r}_G \times \left(\dot{\mathbf{v}} + \boldsymbol{\omega} \times \mathbf{v}\right) = \boldsymbol{M} \tag{4.1-12}$$

in which m is the body mass; $\boldsymbol{I}$ is the matrix of second moment of inertia; $\mathbf{v}$ and $\boldsymbol{\omega}$ are linear and angular velocity vectors respectively; the dot stands for time derivative with respect to the body-fixed frame; $\boldsymbol{r}_G$ is a position vector of the centre of gravity of the body; $\boldsymbol{F}$ and $\boldsymbol{M}$ are the external force and moment vectors respectively. The body-fixed angular velocity vector $\boldsymbol{\omega}$ and the Euler angular velocity vector $d\boldsymbol{\Omega}/dt$ can be related through a transformation matrix $\boldsymbol{E}$.

$$\boldsymbol{\omega} = \boldsymbol{E}\, d\boldsymbol{\Omega}/dt \tag{4.1-13}$$

Equations (4.1-11) and (4.1-12) represent a set of six second-order ordinary differential equations and can be solved by numerically integration over time using 4th order Runge-Kutta method.

Within the framework of linear potential flow theory the components of the external force $\boldsymbol{F}$ and moment $\boldsymbol{M}$ can be generalised in the form

$$F_i = f_i - \sum_{j=1}^{6} \left(A_{ij}\dot{\mathrm{v}}_j + B_{ij}\mathrm{v}_j \right) + C_i - W_i \quad i = 1,2\ldots6 \tag{4.1-14}$$

where i and j indicate the direction of external force and velocity (acceleration) respectively in the body-fixed co-ordinate system; f_i is the wave exciting force; A_{ij} is the added mass; B_{ij} is the damping coefficient; C_i is the buoyancy force; W_i is the force due to gravitation. These hydrodynamic forces due to radiation and wave excitation at each time step can be calculated by integration of sectional values at the incident wave profile. The sectional values of hydrodynamic coefficients and wave exciting forces at various ship sections can be obtained by means of two-dimensional source distribution technique (Kim et al, 1980). The buoyancy force and moment of submerged body are calculated by integration of sectional area and moment of submerged section. For a damaged hull loss of buoyancy can be accounted for the calculations of buoyancy force and moment by means of loss buoyancy method or added weight method. The external force $\boldsymbol{F}$ and moment $\boldsymbol{M}$ are time dependent and become non-linear. The hydrodynamic coefficients are coupled with each other when the ship sections are no longer symmetrical.

The position vector $\boldsymbol{r}_G$ of an intact ship is equal to zero as the origin of the body-fixed system is defined at the centre of gravity of intact ship and the ship mass m and inertia matrix $\boldsymbol{I}$ is constant. The dynamic effects of flooding water in damaged compartment on ship motion are taken into account by adding time dependent mass of flooding water into the ship mass m. Consequently the mass m, inertia matrix $\boldsymbol{I}$ and the position vector $\boldsymbol{r}_G$ of a damaged ship varies with time. As it is difficult to simulate the free surface of flooding water, the sloshing effects are not considered in the present study. For simplicity the level of flooding water is assumed to be the same height as that of the incident wave profile.

Since the ship body is free to drift, she will inevitably drift away from the nominal heading angle β. In order to maintain the wave heading angle within a reasonable range, an artificial restoring yaw moment c_6 is introduced in the equations of motion and may be expressed by

$$c_6 = -a\zeta\omega_o^2 I_{zz} \tag{4.1-15}$$

where a is a constant; ζ is wave amplitude and I_{zz} is yaw moment of inertia. In the present study the constant a of 0.1 is used outside roll resonant region. In addition to potential roll

damping B_{44}, viscous roll damping b_{44} obtained from roll decay test is used in the prediction of roll motion in roll resonant region.

Although the equations of motion are fully non-linear, the hydrodynamic forces due to incident waves, radiation waves and diffraction waves are still linear and calculated up to the incident wave profile. No radiation and diffraction waves are considered on the free surface. As a consequence, drift motions predicted by the present numerical model may be unrealistic.

4.1.2.2 Dynamic global structural responses

The global structure responses of a vessel to waves, such as shear forces and bending moments, arise from various distributions of wave-induced forces and mass inertia forces. The wave-induced forces are those due to wave excitation as well as motion responses while the mass inertia forces are due to the acceleration of the vessel.

The wave-induced loads at any particular cut of the hull are the resultant forces and moments of the inertia forces, hydrodynamic and hydrostatic forces on one side of the cut. These wave loads consists of compression force P_1, lateral shear P_2, vertical shear P_3, torsion moment P_4, vertical bending moment P_5 and horizontal bending moment P_6.

After solving the non-linear Euler equations of motion at each time step, the dynamic global wave loads can be easily calculated. They are expressed as

$$\begin{aligned}(P_1, P_2, P_3) = \overline{\boldsymbol{F}} - \overline{\boldsymbol{F}_S} - \overline{m}\left(\mathbf{v} + \boldsymbol{\omega} \times \boldsymbol{r}_G\right) \\ - \overline{m}\left(\dot{\mathbf{v}} + \boldsymbol{\omega} \times \mathbf{v} + \boldsymbol{\omega} \times \boldsymbol{r}_G + \boldsymbol{\omega} \times \left(\boldsymbol{\omega} \times \boldsymbol{r}_G\right)\right)\end{aligned} \tag{4.1-16}$$

$$\begin{aligned}(P_4, P_5, P_6) = \overline{\boldsymbol{M}} - \overline{\boldsymbol{M}}_S - \boldsymbol{r}_c \times \boldsymbol{P} - \overline{\boldsymbol{I}}\boldsymbol{\omega} + \overline{\dot{m}}\,\boldsymbol{r}_G \times \mathbf{v} \\ - \overline{\boldsymbol{I}}\dot{\boldsymbol{\omega}} - \boldsymbol{\omega} \times \overline{\boldsymbol{I}}\boldsymbol{\omega} - m\boldsymbol{r}_G \times \left(\dot{\mathbf{v}} + \boldsymbol{\omega} \times \mathbf{v}\right)\end{aligned} \tag{4.1-17}$$

where the over-bar implies that the integration is carried out from one end to the particular cut. $\boldsymbol{F}_S$ and $\boldsymbol{M}_S$ are shear force and bending moment vectors due to still water loads. $\boldsymbol{r}_c$ is the position vector of the point of interest at which the dynamic shear force vector $\boldsymbol{P}$ acts.

4.1.3 Responses under irregular waves

The elevation of the ocean waves is irregular and has a random nature in seaway. In practice linear theory is used to simulate irregular sea and to obtain statistical estimates. The wave spectrum can be estimated from wave measurements during limited time period in the range from ½ hour to around 10 hours. In the literature this is often referred to as a short-term description of the sea. Pierson-Moskowitz and JONSWAP spectrum can be used to calculate significant values and other characteristics of wave exciting forces and responses in short term prediction method (ISSC Committee, 1979; Hasselmann at al, 1973; DNV, 2000).

The variance (m_0) is the area below the spectral density function.

$$m_0 = \int_0^\infty S(\omega)d\omega \tag{4.1-18}$$

From equation (4.1-18), the following characteristic parameters can be defined as follows (Ochi, 1973 and 1981; DNV, 2000).

Significant wave height is

$$H_s = 4\sqrt{m_0} \tag{4.1-19}$$

Average wave height is

$$H_{av} = \sqrt{2m_0} \tag{4.1-20}$$

Highest one tenth of all waves is

$$H_{1/10} = 5.1\sqrt{m_0} \tag{4.1-21}$$

Extreme design wave height is

$$H_{\max} = \sqrt{8m_0 \ln \frac{N}{0.01}} \tag{4.1-22}$$

where N is the number of waves.

Related to the wave spectrum $S(\omega)$ of the seaway, the response spectrum $RS(\omega)$ represents the energy distribution of the output signal.

$$\sigma_R^2 = \int_0^\infty S(\omega)|H(\omega)|^2 d\omega \tag{4.1-23}$$

If the wave height values are assumed to be Rayleigh distributed so are the response values. The probability density function of a response amplitude value R_0 can be written as (Faltinsen, 1990)

$$p(R_0) = \frac{R_0}{\sigma_R^2} e^{-R_0^2/2\sigma_R^2} \tag{4.1-24}$$

The probability of exceeding the value of R_0 is

$$Q(R > R_0) = e^{-R_0^2/2\sigma_R^2} \tag{4.1-25}$$

The most probable extreme response amplitude value in N waves can be written as

$$R_{\max} = \sqrt{2\sigma_R^2 \ln(N)} \tag{4.1-26}$$

The probability of exceeding the response value given in equation (4.1-26) for large N values is 0.632 (Ochi, 1973). The design extreme response amplitude value that will not be exceeded in N encounters with a probability of 0.99 is given by

$$R_{design} = \sqrt{2\sigma_R{}^2 \ln(N/0.01)} \qquad (4.1\text{-}27)$$

Since the probability function for the maxima of the wave elevation for given significant wave height follows a Rayleigh distribution, the long-term probability can be obtained from the following equation (Faltinsen, 1990; DNV, 2000).

$$P(H) = 1 - \sum_{j=1}^{M} e^{-2H^2/(H_s^{(j)})^2} p_j \qquad (4.1\text{-}28)$$

where $P(H)$ is the long term probability that the wave height does not exceed H. The Scatter diagram of the North Atlantic in DNV Classification Notes No. 30.5 was used for simulating the long term sea state.

The probability level can be also written as

$$Q = 1 - P(H) \qquad (4.1\text{-}29)$$

If the short term calculations summarised above are carried out for different sea states which may be represented by significant wave height and the associated average period, the long term statistics of the response values can be calculated as follows (Faltinsen, 1990; DNV, 2000).

The probability of not exceeding the value of R_0 is

$$P(R_0) = 1 - \sum_{j=1}^{M}\sum_{k=1}^{K} e^{-\frac{1}{2}R_0^2/(\sigma_R^{jk})^2} p_{jk} \qquad (4.1\text{-}30)$$

The probability level can be written as

$$Q(R > R_0) = \sum_{j=1}^{M}\sum_{k=1}^{K} e^{-\frac{1}{2}R_0^2/(\sigma_R^{jk})^2} p_{jk} \qquad (4.1\text{-}31)$$

where $\sigma_R{}^{jk}$ is the standard deviation of the response for a mean H_s and modal period in significant wave height interval j and modal wave period interval k. In addition p_{jk} is the joint probability for a significant wave height and a modal wave period to be in interval-numbers j and k respectively.

4.1.4 Experimental investigation

4.1.4.1 Introduction

The experiments have been carried out at the Newcastle University Towing Tank using a model with a scale of 1/100 of a Notional US Navy Destroyer Hull 5415. The tests measured 6 degree of freedom motion responses of the stationary model, as well as global loads in intact and damaged conditions for different headings in regular waves.

4.1.4.2 Description of the facility and equipment used

4.1.4.2.1 Towing tank

The towing tank is 37 metres long, 4 metres wide and has a water depth of 1.2 metres. Shown in Figure 4.1-4 are main dimensions of the Towing Tank. Figure 4.1-5 shows the general view of the towing tank. For the present experimental programme, waves were generated by a group of wave makers at one end of the tank, and were essentially absorbed by a parabolic beach, which is comprised of energy absorbing sheets, located at the other end of the tank.

4.1.4.2.2 Wave maker

Waves were generated by twelve rolling seal hinged paddle type wave makers normally operating in unison and driven by a sinusoidal source at the desired period and amplitude. The wave makers employ velocity feedback within the electronic control system to stabilise operation and to obtain the desired transfer function, additionally the wave makers incorporate absorption facilities to remove the effects of reflected waves.

4.1.4.2.3 Wave probes

The wave height and period were monitored and recorded using three Churchill resistance probes and an associated monitor. The probe consists of two parallel wires rigidly separated at both ends with the probe being partially immersed, high frequency current is passed through the wires, the magnitude of which is proportional to the depth of immersion. Thus the changing current is analogous to the wave height.

4.1.4.2.4 Optical co-ordinate measurement system (QUALISIS motion capture system)

6 degree of freedom motions of the model were measured using QUALISIS motion capture system. It is comprised of four infra emitters strategically placed on the vessel (see Figure 4.1-6). All stalks are 60 mm except ??* which is 80 mm height. Figure 4.1-7 shows QUALISIS motion capture system used in tests. The co-ordinates in the vertical and horizontal plane are registered by detectors located in two cameras suitably positioned above the vessel.

4.1.4.2.5 Force gauge

The forces and moments were obtained from a five component force gauge, type 206/5C manufactured by Danish Hydraulic Institute (DHI) with the following specifications: $F_y=F_z=125N$, $M_y=M_z=110Nm$ and $M_x=4.0Nm$. This is comprised of two vertical end pieces joined by four beams, one at each corner, machined from solid aluminium. The beams are strain gauged to obtain F_y, F_z, M_x, M_y and M_z. The force gauge was bolted to two substantial bulkheads mounted in the fore and aft parts of the model and the two sections made waterproof by the provision of a thin membrane across the cut. The gauge was located at 545.43 mm from AP longitudinally and at the centre of the depth to public spaces deck which is 62.83 mm from the base line. Table 4.1-1 represents amplifier connections and calibration details. A close photograph of the force gauge is given in Figure 4.1-8. The convention for the measured loads is described in Figure 4.1-9 (Atlar et al, 1999).

Table 4.1-1: Amplifier connections and calibration details

Fylde amplifier connection	Maximum value	Calibration with gauge clamped to desk	Maximum value
CH1 = Fy	*125 N*	*2.5 kg = 10 volt*	*24.53 N*
CH2 = Fz	*125 N*	*4.0 kg = 10 volt*	*39.24 N*
CH3 = My	*110 Nm*	*5.0 kg = 9.81 Nm = 5 volt*	*19.62 Nm, 200 mm lever*
CH4 = Mz	*110 Nm*	*5.0 kg = 9.81 Nm = 10 volt*	*9.81 Nm, 200 mm lever*
CH5 = Mx	*4 Nm*	*2.0 kg = 1.96 Nm = 10 volt*	*1.96 Nm, 100 mm lever*

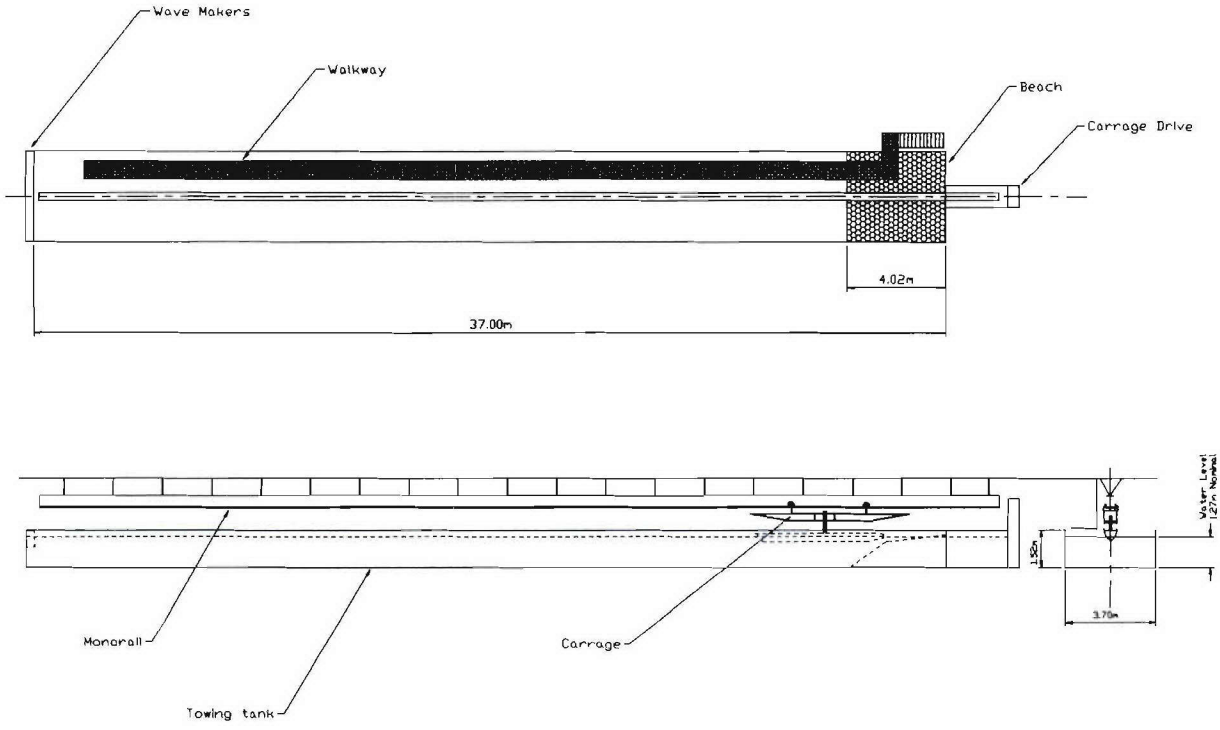

Figure 4.1-4: Main dimensions of Department of Marine Technology Towing Tank

Figure 4.1-5: General view of the towing tank

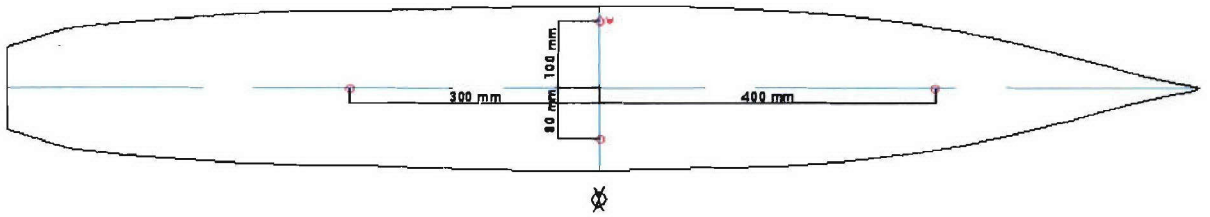

Figure 4.1-6: Four infra emitters placed on the vessel

Figure 4.1-7: QUALISIS motion capture system and three wave probes used in tests

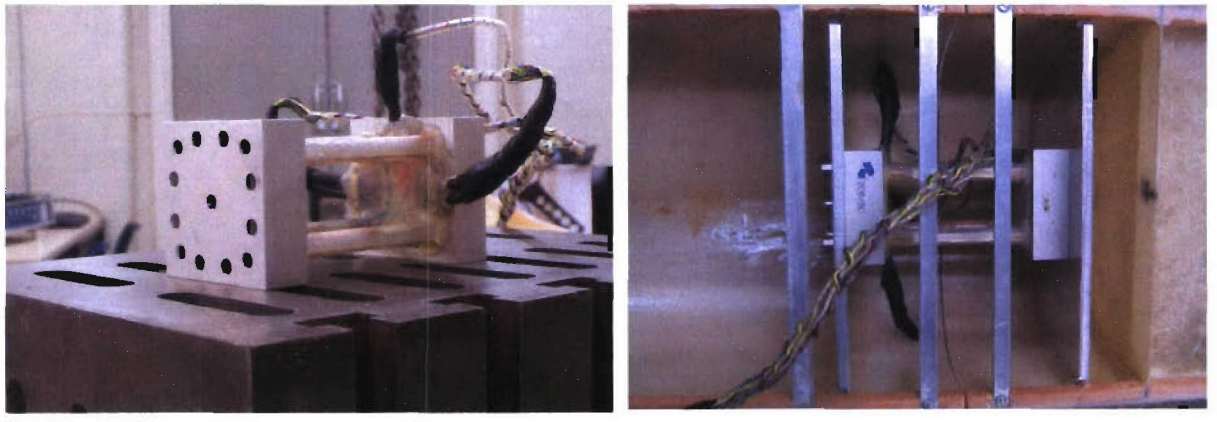

Figure 4.1-8: Force gauge installed at AP 545 mm

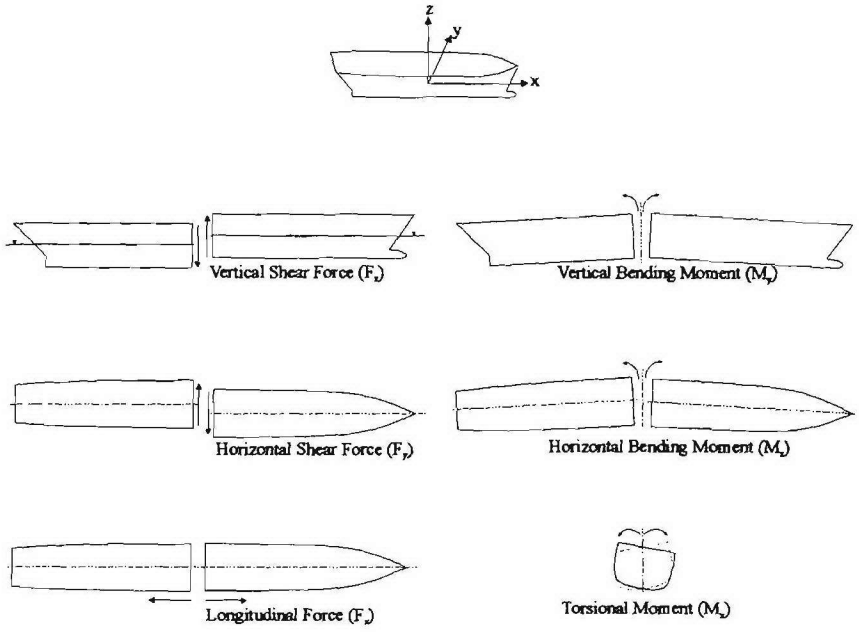

Figure 4.1-9: Convention for measured loads

4.1.4.3 Construction of model

4.1.4.3.1 Model vessel for motion tests

Intact model

The model was made from fibreglass based on the offsets of a sample vessel of Notional US Navy Destroyer Hull 5415 (See Appendix B). The ship to model ratio was 100 which is suitable for the size of the towing tank facility. The main particulars of the model are given in Table 4.1-2, while a view of the intact model is shown in Figure 4.1-10.

Table 4.1-2: Main particulars of Notional US Navy Destroyer Hull 5415

Particulars	Ship	Model (1/100)
L_{oa} (Length overall) in m	151.1800	1.5118
L_{pp} (Length between perpendiculars) in m	142.0400	1.4204
B (Breadth moulded) in m	20.0300	0.2003
D (Depth to public spaces deck) in m	12.7400	0.1274
T (Design draft) in m	6.3100	0.0631
∇ (Volume) in m^3	8811.9415	0.0088
Ax (Maximum section area) in m^2	96.7923	0.0097
C_B (Block coefficient)	0.4909	0.4909
C_P (Prismatic coefficient)	0.6409	0.6409
C_M (Midship section coefficient)	0.7658	0.7658
KM (Height of metacentre above keel) in m	9.4700	0.0947
KG (Height of centre of gravity above keel) in m	6.2830	0.0628
GM (Metacentric height) in m	3.1870	0.0316
LCG (Longitudinal position CoG from A.P.) in m	71.0200	0.7105
k_{xx} (Roll radius of gyration) in m	-	0.0601
k_{yy} (Pitch radius of gyration) in m	35.5100	0.3363
k_{zz} (Yaw radius of gyration) in m	35.5100	0.3363

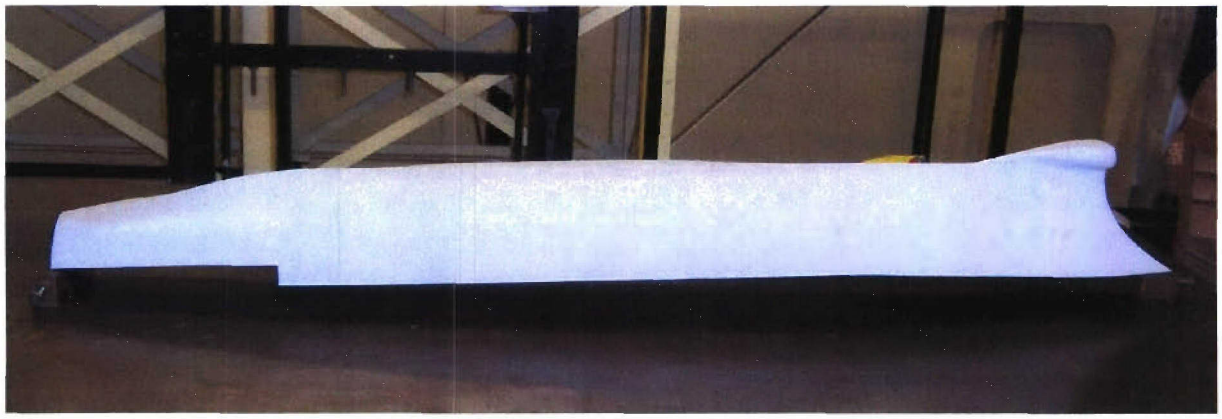

Figure 4.1-10: Intact model

Damaged model

As the model was to be tested in damaged conditions as well as in intact condition, an appropriate damage size had to be decided. A two-compartment damage scenario was assumed and the model was damaged at the starboard side in midship area. And a sonar zone damage case at the starboard side in fore body was considered. The details of damaged opening size and location are shown in Figure 4.1-12 while a general view of the damaged model are shown in Figure 4.1-11.

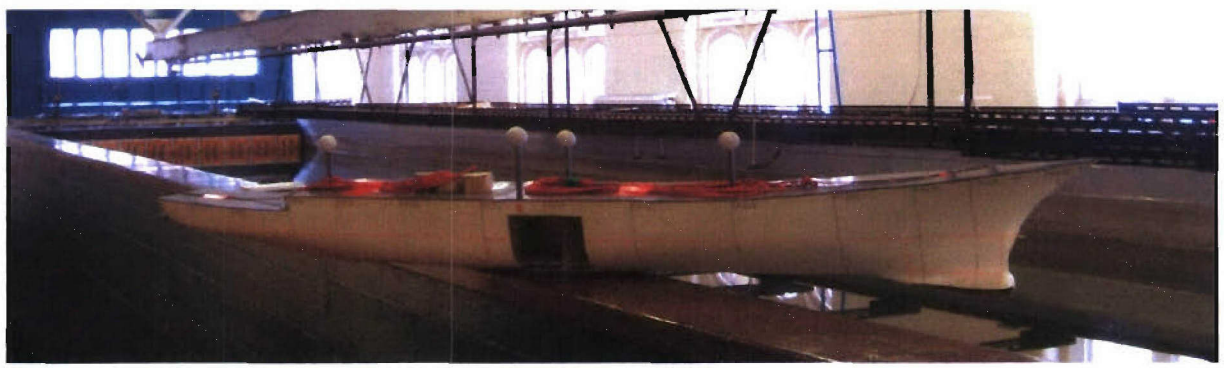

Figure 4.1-11: General view of the damaged model

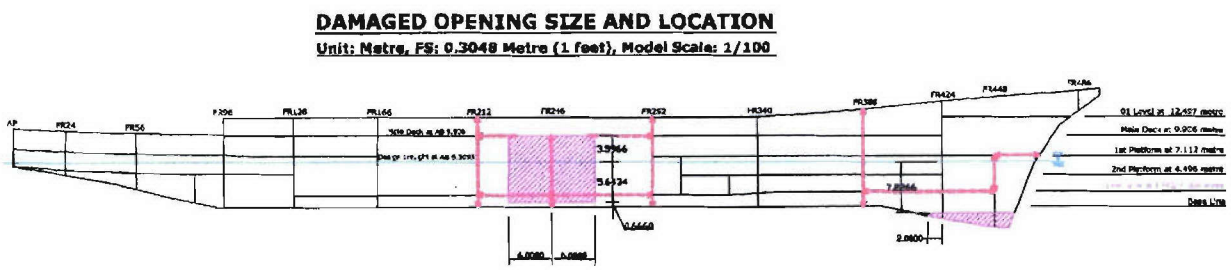

Figure 4.1-12: Damaged opening size and location

4.1.4.3.2 Model vessel for loading tests

Intact model

For the hull girder loading measurements the model used for motion tests was converted. A general view of the model for loading tests is shown in Figure 4.1-13. In order to accomplish damaged model tests additional parts were built. *T1 ~ T6* and *D1 ~ D4* stand for transverse bulkheads and decks respectively. *L1* and *L2* stand for longitudinal girders (see Figures 4.1-14).

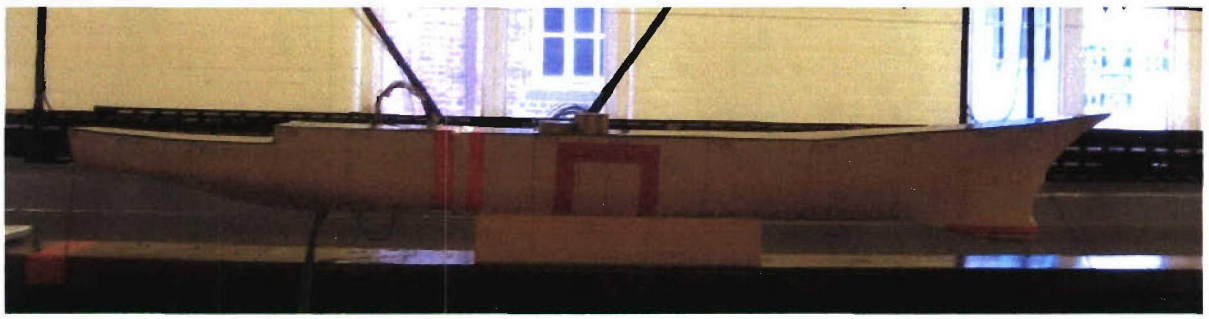

Figure 4.1-13: General view of the model for intact loading tests

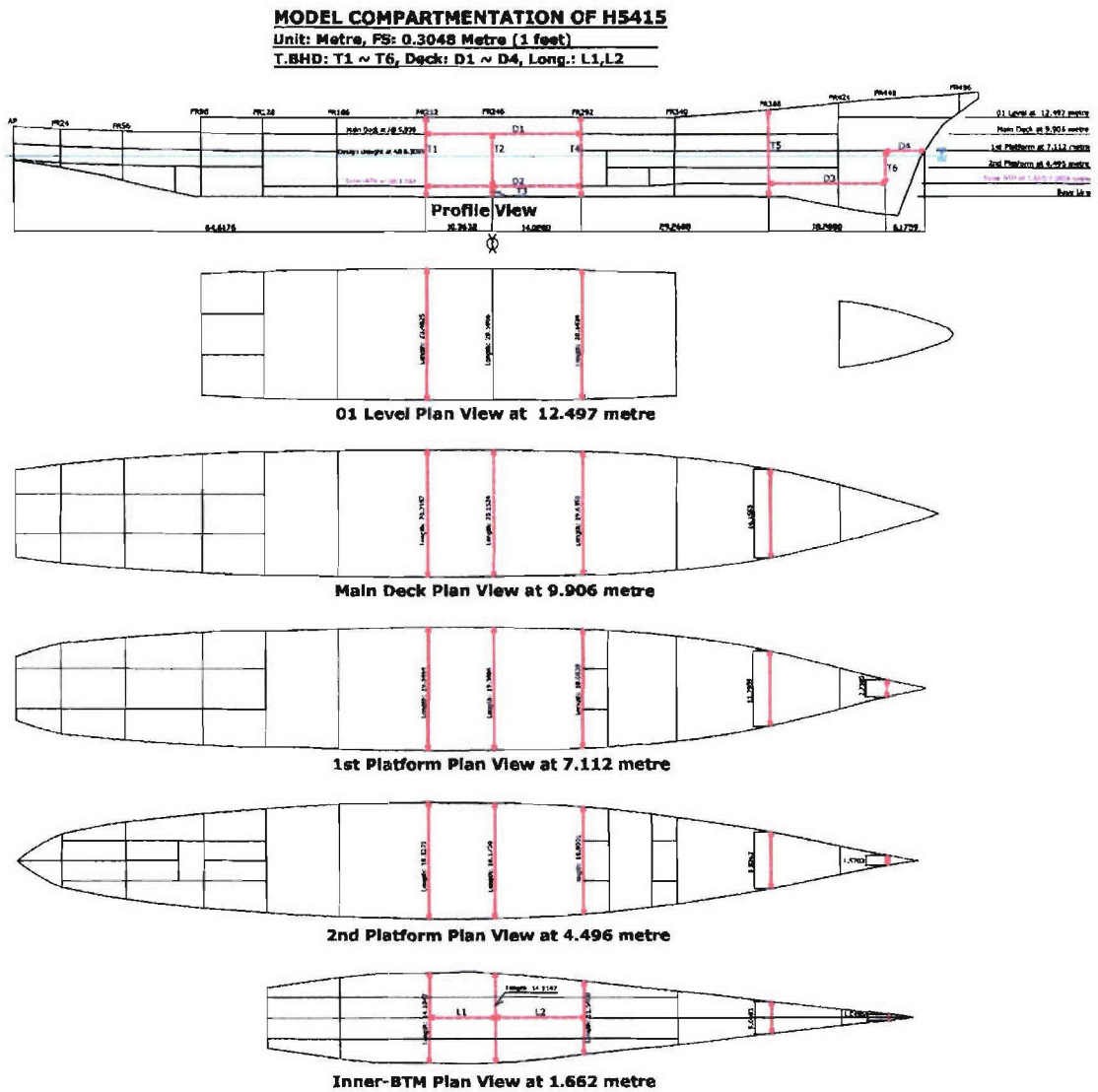

Figure 4.1-14: Model compartmentation

Damaged model

The details of damaged opening size and location were presented in Figure 4.1-12. A general view of the damaged model used in loading tests is shown in Figure 4.1-15.

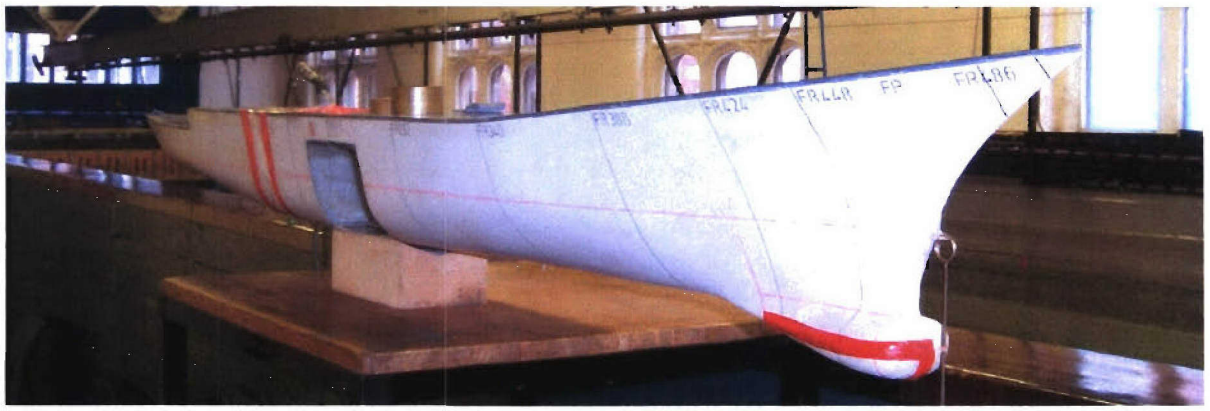

Figure 4.1-15: General view of the model for loading tests in damaged conditions

4.1.4.4 Preparation of model

4.1.4.4.1 Adjustment of centre of gravity

Longitudinal Centre of Gravity (LCG) of the Model

In order to obtain the longitudinal centre of gravity of the model vessel, the method described by Bhattacharyya (1978) was used. The longitudinal centre of gravity (*LCG*) of the model was obtained as 710.5 mm from A.P.

Vertical Centre of Gravity (KG) of the Model

An inclining test was carried out to determine the vertical centre of gravity (*KG*) of the model. This indicated a transverse *GM* value of 31.6 mm. Based on this value *KG* was calculated as 62.8 mm above the keel.

4.1.4.4.2 Adjustment of radii of gyration

In order to adjust the radii of gyration of the model in pitch, yaw and roll, first the radii of gyration of the model without the ballast was determined by using appropriate tests. The measured values of pitch radius of gyration (k_{yy}), yaw radius of gyration (k_{zz}) and roll radius of gyration (k_{xx}) are given in Table 4.1-2. In order to comply with the required radii of gyration and loading condition some weights were added to the model.

Pitch and Yaw Radii of Gyration

Bifilar suspension method was used to obtain the yaw radius of gyration given in Bhattacharyya (1978). By using this method the pitch and yaw radii of gyration of the bare model were obtained as:
$k_{yy} = k_{zz} = 336.3$ mm.

Roll Radius of Gyration

The roll radius of gyration of the model was found to be k_{xx} = 60.1 mm following the method given in Bhattacharyya (1978).

In order to satisfy the required draught, weight, *LCG*, *KG* and the radii of gyration some weights were added at strategic points. A typical mooring system used at the aft end of the model is shown in Figure 4.1-16.

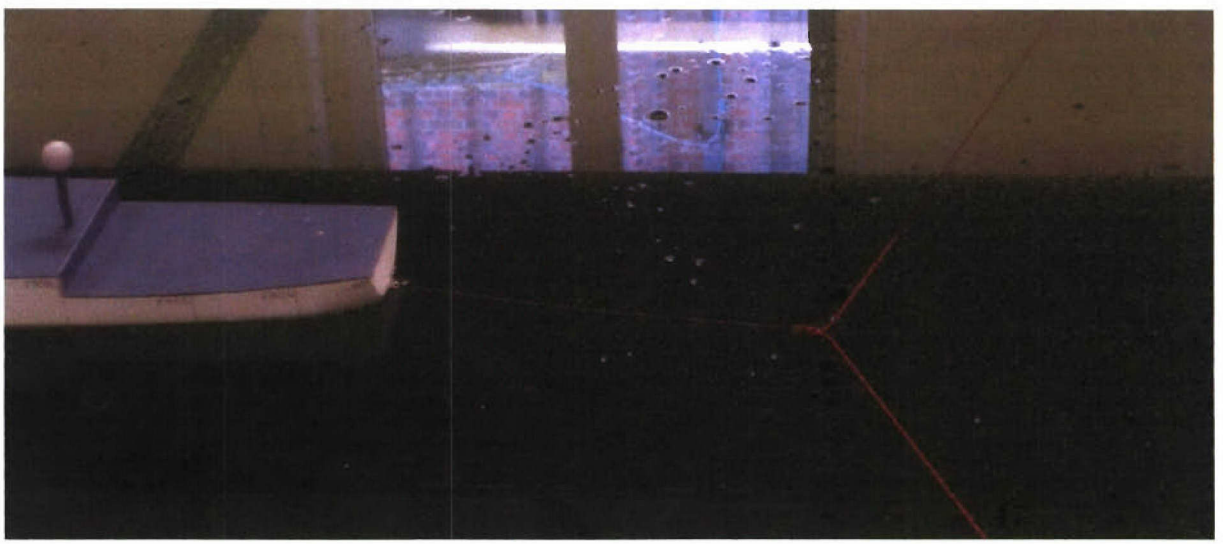

Figure 4.1-16: Typical mooring system used in the experiments

4.1.4.5 Description of test conditions and test trials

The stationary model tests were carried out in both intact and damage conditions. In motion tests the total number of recorded runs was 81, which consisted of 3 design conditions, 3 heading angles and 9 wave frequencies. The heading angles were 180°, 45° and 90°, which corresponded to the head, stern quartering and beam seas respectively. In beam and stern quartering conditions, the damage opening was situated in the seaward side.

Table 4.1-3: Motion test trials and identifications

condition	test ID	Hw	heading	wave freq.	total
intact	MT-ITS-1 ~ 27	small	3	9	27
DS2	MT-DS2S-1 ~ 27	small	3	9	27
DS3	MT-DS3S-1 ~ 27	small	3	9	27
total					81

Table 4.1-4: Loading test trials and identifications

condition	test ID	Hw	heading	wave freq.	total
intact	LT-ITS-1 ~ 27	small	3	9	27
	LT-ITL-1 ~ 27	large	3	9	27
DS2	LT-DS2S-1 ~ 45	small	5	9	45
	LT-DS2L-1 ~ 45	large	5	9	45
DS3	LT-DS3S-1 ~ 27	small	3	9	27
	LT-DS3L-1 ~ 27	large	3	9	27
total					198

For loading tests the total number of recorded runs was 198. Test trials and identifications are provided in Table 4.1-3 and Figure 4.1-4. Table 4.1-5 shows a summary of the experimental wave conditions and the corresponding full-scale conditions used in motion and loading tests. In motion tests small waves only were generated for measuring motion responses.

Table 4.1-5: Experimental wave conditions used in model tests

λ/L	λ (m)		ω (r/s)		T(s)		H1		H2	
	Model	Ship	Model	Ship	Model	Ship	Model	Ship	Model	Ship
3.347	5.061	506.055	3.490	0.349	1.800	18.003	small	small	large	large
2.645	3.999	399.897	3.926	0.393	1.600	16.004	small	small	large	large
2.171	3.281	328.149	4.334	0.433	1.450	14.497	small	small	large	large
1.882	2.845	284.452	4.655	0.466	1.350	13.498	small	small	large	large
1.032	1.560	156.041	6.285	0.629	1.000	9.997	small	small	large	large
0.837	1.265	126.514	6.980	0.698	0.900	9.002	small	small	large	large
0.506	0.764	76.436	8.980	0.898	0.700	6.997	small	small	large	large
0.437	0.661	66.053	9.660	0.966	0.650	6.504	small	small	large	large
0.313	0.473	47.262	11.420	1.142	0.550	5.502	small	small	large	large

where, "small": *(H1)M 4.28 ~ 26.35 mm, (H1)S 0.428 ~ 2.635 m*
"large": *(H2)M 8.39 ~ 45.51 mm, (H2)S 0.839 ~ 4.551 m*

where λ is the wave length
L is the length between perpendiculars
ω is the wave frequency
T is the wave period
H is the expected wave height
M and S denote model and ship, respectively.

The amplitude of the waves for each run was increased gradually to its maximum to minimise the impact effect of the waves. Once the model has reached the steady state condition then the load and pressure records were taken. As soon as the waves reached the beach at the far end of the towing tank, the recordings were stopped to avoid reflected waves reaching the model.

The above wave conditions were selected in order to maximise the possible test runs over a wide frequency range where the model was free from green water effects and the mooring lines did not apply excessive force to restrain the motions.

4.1.5 Model uncertainties of numerical methods

Model uncertainty is a very important source of uncertainties in structural design process. A coefficient of variation (COV) of a typical strength prediction could be about 10 – 15%, while a COV of wave-induced load prediction could be well above 30%. This means that model uncertainties of wave-induced load prediction is a major uncertainty in structural strength assessment.

Model uncertainty of wave-induced loads is defined as the ratio of real load to the predicted load, which could be expressed as:

$$X_{m0} = \frac{M_{exp}}{M_{pred}} \qquad (4.1-32)$$

where X_{m0} is model uncertainty of the formula or numerical method for predicting wave-induced loads. In this project model uncertainty of the 2D linear method for predicting wave-induced loads will be calculated. M_{exp} and M_{pred} are real and predicted extreme design wave-induced loads respectively. In practice the real extreme design wave-induced loads are very difficult to be obtained, so the experimental results would be used as the real values if the experiment is properly executed.

When the model uncertainty is calculated, the number of sample data should be fairly large so that reliable statistical mean and standard deviation could be obtained. However if the definition in Eq. (4.1-32) is directly used in model uncertainty calculation, there would be only one set of data for each wave headings, so the total number of sample data would be too few to calculate the model uncertainty of wave-induced load prediction. In addition, wave-induced loads for a given period can not be measured in the test. Therefore another definition is introduced, which is expressed as:

$$X_{m1} = \frac{RAO_{exp}}{RAO_{pred}} \tag{4.1-33}$$

where RAO stands for Response Amplitude Operator. Obviously X_{m1} is a function of wave frequency. However it is a good indicator of model uncertainty associated with wave-induced loads. When X_{m1} is a constant, it is equal to X_{m0} if the extreme design wave-induced load is calculated by a short term analysis. This can be proved as follows:

Substitute Eq. (4.1-26) into Eq. (4.1-32), so

$$X_{m0} = \frac{M_{exp}}{M_{pred}} = \frac{(\sigma_R)_{exp}\sqrt{2\ln(N)}}{(\sigma_R)_{pred}\sqrt{2\ln(N)}} = \frac{(\sigma_R)_{exp}}{(\sigma_R)_{pred}} \tag{4.1-34}$$

Because

$$(\sigma_R^2)_{exp} = \int_0^\infty S(\omega)\left|RAO_{exp}\right|^2 d\omega = \int_0^\infty S(\omega)\left|X_{m1} \times RAO_{pred}\right|^2 d\omega = X_{m1}^2 \int_0^\infty S(\omega)\left|RAO_{pred}\right|^2 d\omega = X_{m1}^2 \times (\sigma_R^2)_{pred} \tag{4.1-35}$$

Combine Eqs. (4.1-34) and (4.1-35)

$$X_{m0} = X_{m1} \tag{4.1-36}$$

Hence in this project X_{m1} is used as model uncertainty of wave-induced loads.

4.2 Methodologies for combining different load cases

There are various types of loads acting on ships, such as Stillwater bending moment, wave-induced loads, slamming forces. In this project, only Stillwater bending moment and wave-induced loads will be considered. It is very important to properly combine all these loads in the strength assessment. In the ship design rules the maximum loads for each type of load are simply added together. This could introduce unnecessary conservatism in the design. In the context of load combination of ship structures, there are two issues. The first issue is how to

combine different components of wave-induced loads. The second issue is how to combine Stillwater bending moment and wave-induced loads.

4.2.1 Combination of different load components of wave-induced loads

Wave-induced loads have generally six components, among which 5 components will be predicted by 2D methods in this project. Of these load components, vertical and horizontal bending moments, torsion and vertical shear force are potentially important in the strength assessment of damaged ships. Because all these load components have different phase angles, they reach maximum at different time. If the maximum amplitudes of each components are simply added together to assess the structural strength, the results could be too conservative. In this project a method is derived to combine different load components of wave-induced loads.

Fig. 4.2-1 shows two load components with different phase angles. Without losing generality, it is assumed that these two load components can be expressed as:

$$y_1 = y_{1m}\sin(\omega t + \delta_1) \tag{4.2-1}$$

$$y_2 = y_{2m}\sin(\omega t + \delta_2) \tag{4.2-2}$$

Where y_1 and y_2 are two load components, y_{1m} and y_{2m} are the maximum amplitudes of y_1 and y_2 respectively. δ_1 and δ_2 are initial phase angles of y_1 and y_2 respectively. ω is angular frequency, and t is time.

To combine these two components, two load cases should be considered.

Load case 1: $y_{1m} + \cos(\delta_1 - \delta_2) \times y_{2m} = y_{1m} + \cos(\Delta\delta) \times y_{2m}$ (4.2-3)

Load case 2: $\cos(\delta_1 - \delta_2) \times y_{1m} + y_{2m} = \cos(\Delta\delta) \times y_{1m} + y_{2m}$ (4.2-4)

In which $\Delta\delta$ is phase angle difference of the two components. These two load cases are also indicated by two vertical lines in Fig. 4.2-1. Obviously when load components are combined in this way, the combined load is the exact instantaneous load acting on the structure.

This principle can be applied to the cases with more than two components.
The phase angle difference could be obtained from time domain load calculation or experimental tests.

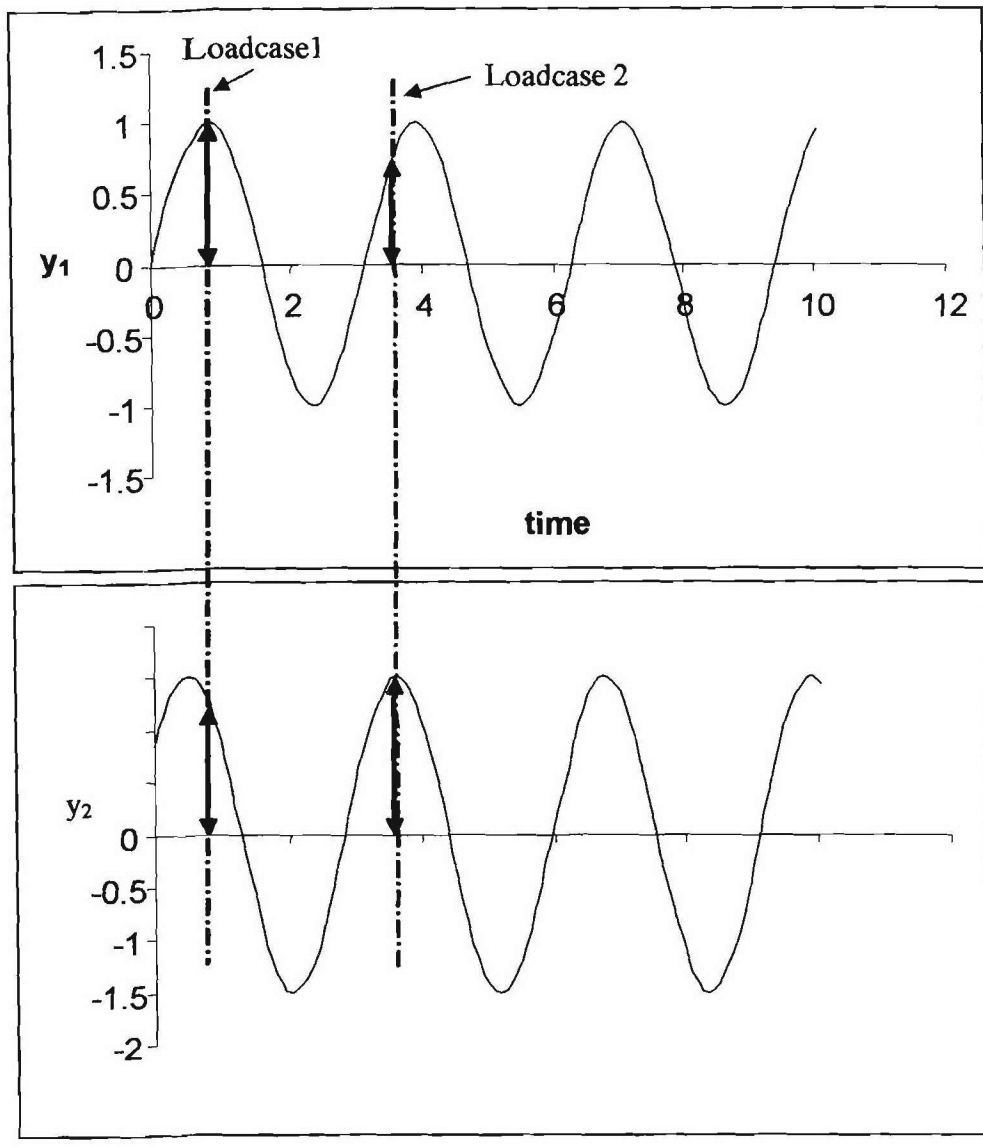

Fig. 4.2-1 Combination of two load components

4.2.2 Combination of Stillwater bending moment and wave-induced loads

Stillwater bending moment has quite different frequency from wave-induced loads. It is more difficult to combine these two loads than the previous case. In ship design rules, maximum Stillwater bending moment is added to maximum wave-induced loads to assess the strength in order to achieve a safe design. Wang (1996) have applied several methods, such as point-crossing method, load coincidence method, Ferry Borges method, peak coincidence method and Turkstra method, to combine Stillwater bending moment with wave-induced bending moments for an offshore production storage ship.

However when a ship is damaged, it would be used only for a short period until a repair is carried out. So the wave-induced loads to be used for the strength assessment of damaged ships should be predicted by short term analysis. The Navy ships rule developed by Lloyd's Register

of Shipping (LR) has recommended that a damaged ship should be able to survive under a seastate of 3 for 96 hours. This environmental condition is used to calculate the wave-induced loads in this study. Within this short period the Stillwater bending moment is obviously known. So the Stillwater bending moment will be directly combined with wave-induced loads, which are predicted by a short term analysis.

4.3 Methodologies for Ultimate Strength of Hull Girders

4.3.1. Smith's method

Failure of a ship hull girder is normally catastrophic and ends up being severe loss of human lives and wealth. So it is of great importance to calculate the ultimate hull-girder strength accurately so as to operate within the safety margin to avoid failure of the ship. Many researchers have applied the commercially available as well as independently developed Finite Element Software to calculate the ultimate strength of the ship panels. But using FEM to calculate the Moment-Curvature relationship to predict the Ultimate Strength of Ship has been a hugely challenging task due to various computational reasons.

However empirical formulae have been very popular in calculating the Moment-Curvature (M-Φ) relationship. It has been observed that the most significant factor in the complete analysis of the ultimate strength analysis of ship is the stress-strain relationship in the ultimate compressive strength analysis of individual elements of the ship section. Historically, the earliest attempts to incorporate the plate buckling and its effects on ship strength were made by Caldwell using simplified formula where the ultimate moment of a mid-ship cross-section in the sagging condition was calculated introducing the concept of a structural instability strength reduction factor for the compressed panels. This factor would account for the reduced strength of the cross-section due to early failure and uploading of some plate elements.

Smith developed a method to incorporate the load-shortening curves of the plate elements in the calculation of the hull girder collapse. The behaviour of each plate was calculated by finite-elements and their contribution to the overall behaviour of the girder was accounted as a function of the plate location in the cross-section. Other methods based on the same general approach were afterwards developed, including the simplified approaches by Billingsley, Adamchak and Dow *et al.* Rutherford and Caldwell presented a real life case study of a failed VLCC and compared ultimate bending moment of it during the failure and that calculated using a simplified approach to stiffened plate strength, without considering their post buckling behaviour and taking into account of lateral pressure, initial deformations and corrosion rates. The validity of the method was confirmed by comparing with the results of a nonlinear finite element program.

Many of the beam-column approaches used in the ISSC Technical Committee III.1 (Jansen et al, 1994) investigation, were developed from Smith's method, the main differences are in the derivation of the Stress-Strain relationship of the individual components. For this reason Jensen et al. investigated the theoretical stress-strain relationship of ten stiffened plates using different methods. Significant variances were noticed between the predictions of a series of stiffened plates. This was found to be a result of the use of different effective width formulations and the integration of initial large deflection of the plate.

In this project Smith's approach is used to calculate ultimate strength of the ship hull girder. During the calculation of stress-strain curve of each elements, the beam-column buckling, plate

failure and tripping have been taken in account. The details are presented in the following section.

4.3.1.1 Progressive collapse analysis

The present method follows the progressive collapse analysis approach presented initially by Smith and later by others for the contribution of each element to the hull strength. The stress-strain relationship of each element in the simplified method is determined on the basis of a rational theoretical background. The procedure for calculating the plate strength and the beam-column behaviour will be described in the remaining part of this report.

4.3.1.1.1 The Method and assumptions

The assessment of a moment-curvature relationship is obtained from the imposition of a sequence of increasing curvatures to the hull-girder. For each curvature, the state of average strain of beam-column element is determined. Entering these values in the model that represents the load- shortening behaviour of each element, the load that it sustains is calculated and consequently the bending moment resisted by the cross section is obtained from the summation of the contributions from the individual elements. The derived set of values defines the desired moment-curvature relation.

However, some problems arise in this implementation, because the sequence and the discretisation of the sequence of the imposed curvatures strongly influence the convergence of the method due to the shift of the neutral axis. In this method, the modelling of the ship's section and the determination of the position of the neutral axis are important issues. The basic assumptions in the progressive collapse analysis are:

- The transverse cross-section of the hull girder is regarded as an assembly of elements such as stiffened panels (longitudinal stiffener with associated plate panel) and hard corners.
- The interaction between adjacent elements is not considered. The interaction between the stiffener and attached plate is taken into account, as well as the influence of distortion of stiffeners on elastic-plastic collapse behaviour of stiffener, torsional-bending, buckling and local plate buckling.
- The relationship between average stress and average strain for an element is pre-evaluated considering the factors mentioned above.
- Assuming that each cross-section of the hull girder remains flat, a curvature increment is applied. The revised level of neutral axis of the cross-section for the subsequent step is calculated, based on the axial rigidities of individual elements at that time.
- At the same time, the bending rigidity of the cross-section around the revised neutral axis is calculated.
- The bending moment increment, corresponding to the curvature increment, is calculated and the axial strain and stress are also calculated for individual elements.
- The increment of the curvature, bending moment, axial strains and stresses of individual elements are added to those at the previous step in order to proceed to the next step.
- Finally, the entire relationship between the curvature and bending moment of a hull girder can be derived through this progressive analysis, in which the effects of the yielding and buckling of individual structural elements are considered.

As a first step it is necessary to estimate the position of the neutral axis through an elastic analysis, because when the curvature is small the section acts in the elastic domain. The elastic neutral axis passes through a point with coordinates given by:

$$\begin{cases} x_n = 0 \\ y_n = \dfrac{\sum y_i . A_i}{\sum A_i} \end{cases} \qquad (4.3\text{-}1)$$

The basic assumptions of this method are:

- The elements into which the cross-section is subdivided are considered to act and behave independently.
- When estimating the strain level of the elements, plane sections are assumed to remain plane when curvature is increasing,
- Overall grillage collapse is avoided by sufficiently strong transverse frames.

The vertical bending moment is indeed the most important load effect when considering the hull girder collapse. However, in many types of ships, the combined effect of the vertical and the horizontal bending moments is important, especially after the ship is damaged.

On the assumption that plane sections remain plane in bending, the strain corresponding to an applied curvature C can be calculated for each element of the cross-section using the simple theory of bending.

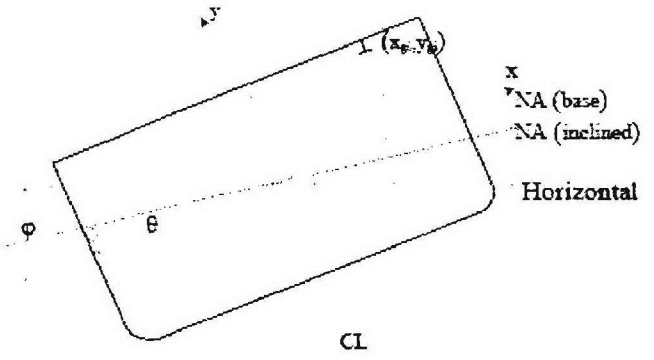

Figure 4.3-1: Combined Bending of Hull

The bending stress at a point (x_{gi},y_{gi}) is defined as:

$$\sigma = \sigma_V + \sigma_H = \frac{M\cos\varphi . y_{gi}}{I_{NA}} - \frac{M\sin\varphi . x_{gi}}{I_{CL}} \qquad (4.3\text{-}2)$$

Where φ is the angle that the bending moment vector makes with the base line and (x_{gi},y_{gi}) is the coordinate of a point with respect to a reference located in any point on the neutral axis. $M.\cos\varphi$ and $M.\sin\varphi$ are the vertical and horizontal bending moments respectively, M being the resultant bending moment. It may be expressed as a function of the total moment by

$$\frac{\sigma}{M} = \frac{y.\cos\varphi}{I_{NA}} - \frac{x.\sin\varphi}{I_{CL}} \tag{4.3-3}$$

Maximum values of stress occur at corners (decks or bilge strake), where both x_{gi} and y_{gi} are maximum.

$$\sigma_{max} = \frac{M\cos\varphi.y_{gi-max}}{I_{NA}} - \frac{M\sin\varphi.x_{gi-max}}{I_{CL}} \tag{4.3-4}$$

Equation (3) can be re-written as

$$\sigma_{max} = \frac{M\cos\varphi}{Z_{NA-deckedge}} - \frac{M\sin\varphi}{Z_{CL-deckedge}} \tag{4.3-5}$$

Maximum stress will occur at an angle of inclination φ, then

$$\frac{d\sigma_{max}}{d\varphi} = 0 \quad \Rightarrow \quad \tan\varphi = \frac{Z_{NA-deckedge}}{Z_{CL-deckedge}}$$
$$\varphi(\sigma_{max}) = \tan^{-1}\left(\frac{Z_{NA-deckedge}}{Z_{CL-deckedge}}\right) \tag{4.3-6}$$

For typical ships $\varphi(\sigma_{max}) \sim 30^{\circ}$. The bending stress is zero at the neutral axis of the mid-ship section, so equation (4.3-4) can be re-written as

$$\frac{y_{gi}.\cos\varphi}{I_{NA}} - \frac{x_{gi}.\sin\varphi}{I_{CL}} = 0 \quad \Rightarrow y_{gi} = \left[\frac{I_{NA}}{I_{CL}}\tan\varphi\right]x_{gi} \tag{4.3-7}$$

This is an equation for a straight line in Cartesian coordinate having a slope of $(I_{NA}/I_{CL})\tan\varphi$. The slope is given by

$$\tan\theta = \frac{y_{gi}}{x_{gi}} = \left[\frac{I_{NA}}{I_{CL}}\tan\varphi\right]$$
$$\theta = \tan^{-1}\left[\frac{I_{NA}}{I_{CL}}\tan\varphi\right] \tag{4.3-8}$$

Where θ is the angle the neutral axis makes with base (x-axis). The strain at the centroid of an element *i* (x_{gi}, y_{gi}), when curvature C_x and C_y are imposed in the vertical and horizontal planes respectively is given by:

$$\varepsilon_{ei} = C\left(x_{gi}.\sin\theta - y_{gi}.\cos\theta\right) \tag{4.3-9}$$

Where ε_{ei} =the longitudinal edge strain in the element.

$$C = \sqrt{\left(C_x^2 + C_y^2\right)} \tag{4.3-10}$$

Where

$$C_x = C.\cos\theta$$
$$C_y = C.\sin\theta \tag{4.3-11}$$

Once the strain state of each element is achieved, the corresponding average stress may be calculated and consequently the components of bending moment at a curvature C can be given as:

$$M_X = \Sigma y_{gi}.\sigma_i.A_i$$
$$M_Y = \Sigma x_{gi}.\sigma_i.A_i \qquad (4.3\text{-}12)$$

The modulus of the combined bending moment is

$$M = \sqrt{M_X^2 + M_Y^2} \qquad (4.3\text{-}13)$$

This is the bending moment on the cross-section if the instantaneous CG is placed at correct location. Along the step by step increment of the curvature the neutral axis shifts towards deck during the hogging and towards the bottom during sagging. The new neutral axis shifts to a position where the net load ($NL=\Sigma(A_i.\sigma_i)$) is zero, considering compressive and tensile stress with different signs. It is necessary to calculate the shift between the two imposed curvatures. For this reason a trial and error process need to be implemented, having a terminating criterion. For this study the following criterion proposed by Gordo and Guedes Soares (1996) has been used.

$$NL = \sum(A_i.\sigma_i) \leq 10^{-6}.\sigma_{yi}.\sum A_i \qquad (4.3\text{-}14)$$

Where A_i =area of the i^{th} element
σ_i= the stress developed in the i^{th} element when a curvature is applied.
σ_{yi}= the yield stress of the i^{th} element.

4.3.1.2 Collapse strength of stiffened plates

In the stiffened panels, the longitudinal stiffeners have the main function of providing the necessary support to the plates ensuring that they retain the required strength. To fulfil this function, stiffeners must have adequate rigidity and the spacing between them must be chosen according to the main characteristics of the plate namely, its thickness and yield stress. The slenderness of the plate has to be designed in such a way that the ultimate average stress is kept closer to the yield stress as much as possible.

The analysis of stiffened plates has been performed by several researchers and many solutions to the problem were presented over the years. The prediction of the panel behaviour has led to the development of several techniques such as non-linear finite element methods or more simplified formulations applying the beam-column concept. Common to all is the need for the application of an incremental end shortening if a realistic description of the post buckling behaviour is required. Also common to later formulation is the use of load end shortening curves for simply supported plates carried out on separate studies, which are able to describe the loss of plate stiffness after buckling.

Design methods to determine the ultimate load of the panels were presented among others by Faulkner et al based on John-Ostenfeld approach, by Carlson, and Dwight and Little based on Perry-Robertson formulation.

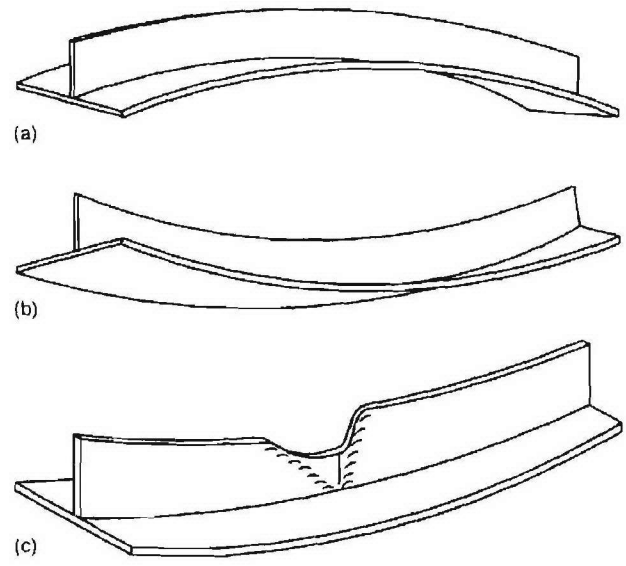

Figure 4.3-2: Possible collapse modes of stiffened panels under compressive loads. (a) Plate induced collapse, (b) Stiffener induced collapse, (c) Tripping failure.

Failure of panels is usually classified as:

1. plate induced failure
2. column like failure
3. tripping of stiffeners
4. overall grillage failure

Failure of a stiffened panel is usually classified, as shown in figure 4.3-2, as: plate induced failure, column like failure, tripping of stiffeners and over all grillage failure. The last one is normally avoided by ensuring that transverse frames are of adequate size therefore it is not considered generally. The first one occurs when the stiffener is sufficiently stocky and the plate has a critical elastic stress lower than yield stress. The second failure mode is mainly due to the excessive slenderness of the column (stiffener and associated effective plate acting together) and failure may be towards the plate or towards the stiffener, depending on the column's initial shape and the type of loading considered, i.e., eccentrically applied or not, following the shift of the neutral axis or not. In a continuous panel it is usual that the failure is towards the plate in one span and towards the stiffener in the adjacent span. The third mode of failure is the consequence of a lack of torsional rigidity of the stiffener. Interaction with the plate-buckling mode may also occur including premature tripping.

Sometimes the first and the second modes are incorporated in the same group because the buckled shape of the panel is similar and is normally towards the stiffener.

To obtain the average load-end shortening curve of the column it is assumed that the stiffener has an elastic-perfectly plastic behaviour given by

$$\Phi(\varepsilon) \equiv \Phi_{,} = \begin{cases} -1 & \text{when } \varepsilon < -1 \\ \varepsilon & \text{when } -1 < \varepsilon < 1 \\ 1 & \text{when } \varepsilon > 1 \end{cases} \qquad (4.3\text{-}15)$$

Where ε is the normalized strain ratio, i.e. $\varepsilon_e/\varepsilon_y$ = edge strain/yield strain. The slenderness ratio of the plate is given by

$$\beta_0 = \frac{b}{t}\sqrt{\frac{\sigma_y}{E}} \qquad (4.3\text{-}16)$$

Where β_0 is the slenderness ratio when the stress in the element is σ_y (yield stress).b,t and E are the breadth, thickness and Young's modulus respectively. It has become common to deal with the reduced strength of plates by equating it to the strength of another plate that has an effective width, ϕ and collapse at nominal yield stress. Therefore speaking of effective width or of ultimate strength becomes equivalent. Among different proposals in the existing literature, the formula proposed by Faulkner has been proven to be well accepted. According to it, imperfect plates with simply supported edges forced to remain straight under longitudinal loadings; here the effective width is given by:

$$\phi_b = \begin{cases} \dfrac{2}{\beta_0} - \dfrac{1}{\beta_0^2} & for \quad \beta_0 \geq 1 \\ 1 & for \quad \beta_0 \leq 1 \end{cases} \qquad (4.3\text{-}17)$$

The plate slenderness (β_0) depends on plate breadth (b), thickness (t), Young's modulus (E) and the yield stress (σ_y) of the plate. The load-shortening curve of the plate can be expressed as a function of normalised strain, and the slenderness at every level of normalized strain can be defined as

$$\beta = \frac{b}{t}\sqrt{\frac{\sigma_e}{E}} \qquad (4.3\text{-}18)$$

where σ_e is the edge stress of the plate when the given strain is ε_e. Dividing the equations (4.3-18) by equation (4.3-16) and replacing $\sigma_e/\sigma_y = \varepsilon_e/\varepsilon_y = \varepsilon$, the equation (4.3-18) can be re-written as

$$\beta = \beta_0\sqrt{\varepsilon} \qquad (4.3\text{-}19)$$

Therefore the effective width (ϕ_b)at a given strain can be given by, substituting β_0 by β in equation (14.3-17)

$$\phi_b = \begin{cases} \dfrac{2}{\beta} - \dfrac{1}{\beta^2} & for \quad \beta \geq 1 \\ 1 & for \quad \beta \leq 1 \end{cases} \qquad (4.3\text{-}20)$$

During the fabrication process, imperfections are induced in the structure in the form of initial deflections and residual stress. Both are a function of the welding process and have an influence on the local strength. When stiffening members are welded to the plate, the welding temperatures take on such extreme values that considerable residual stresses resulting from the process can seriously degrade the plate strength. As Fig.4.3-3 illustrates, the tension block is offset from the stiffener-plate centroid and thus bending occurs. To preserve equilibrium along the direction of the stiffener, the tension must be balanced by residual compression which exists largely in the plate. This equilibrium requirement provides a relationship between the magnitude of the compressive residual stress (σ_r) in the plating and the width ηt of the tension zones each side of the weld:

$$\frac{\sigma_r}{\sigma_y} = \frac{2\eta}{(b/t) - 2\eta} \qquad (4.3\text{-}21)$$

Values of η=4.5 to 6 are typical for as-welded ships, but values of 3 to 4.5 are more appropriate for ship design after allowing for the shakedown .

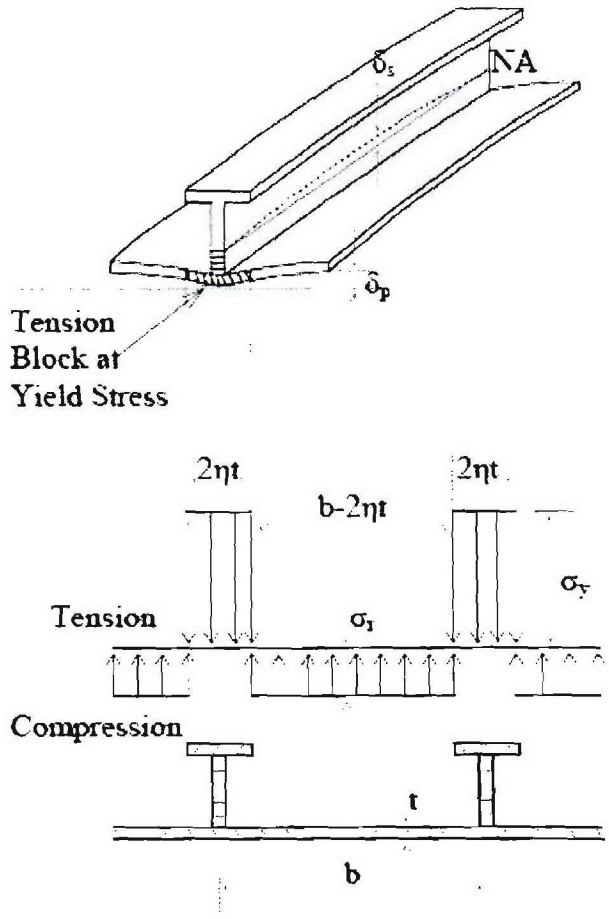

Fig.4.3-3: Idealized welding induced residual stress in plate

High tensile stresses which develop in the vicinity of a weld due to shrinkage are balanced by non-uniform compressive stresses across the plate. These compressive stresses affect the yielding process and hence reduce the pre-collapse stiffness of the structure. Depending on the slenderness of the plate panel involved, the collapse strength may be affected. The weld induced residual stresses have been shown to induce a reduction both in stiffness and strength of plate. The pattern of residual stresses due to welding stiffeners in a plate shows a zone of tension stresses near the welds and a zone of compressive stresses in the central region of the plate.

The interaction co-efficient for the residual stress (R_η) is given by Guedes Soares ( )

$$R_\eta = \left(1 - \frac{\Delta\phi_b}{1.08 \times \phi_b}\right)(1 + 0.0078\eta) \qquad (4.3\text{-}22)$$

Where $\Delta\phi_b$ is the compression strength reduction factor due to residual stresses in plate and given by:

$$\Delta\phi_b = \frac{\sigma_r}{\sigma_y}\frac{E_t}{E}$$

Where E_t is the structural tangent modulus for the stiffened plate in compression (Faulkner ,1975) given by:

$$\frac{E_t}{E} = \begin{cases} \dfrac{3.62\beta^2}{13.1 + 0.25\beta^2} & for \quad 0 \le \beta \le 2.7 \\ 1 & for \quad \beta > 2.7 \end{cases} \qquad (4.3\text{-}23)$$

Table 4.3-1: Deflection Levels

Level	Initial deflection w_{max}/t	Residual stresses σ_r / σ_y
Slight	$0.025\beta^2$	0.05
Average	$0.1\beta^2$	0.15
Severe	$0.3\beta^2$	0.3

According to the available sources, although the geometric configuration of initial deflection is quite complex, a simple approach can be adopted to design the initial deflections on the stiffened plate. Based on the experimental measurements, Smith classified the initial deflection as slight, average and severe, which is shown in the Table 4.3-1.

The interaction co-efficient for the initial deflection (R_δ) is given by Guedes Soares (1988):

$$R_\delta = 1 - (0.626 - 0.121\beta)\frac{\delta_0}{t} \qquad (4.3\text{-}24)$$

If the residual stress coexists with the initial deflection, the combining interaction coefficient ($R_{\eta\delta}$) is given by(Guedes Soares, 1988) :

$$R_{\eta\delta} = 0.665 + 0.006\eta + 0.36\frac{\delta_0}{t} + 0.14\beta \qquad (4.3\text{-}25)$$

The radius of gyration (r_{ce}) of the stiffened plate is given by

$$r_{ce}^2 = \frac{I_e'}{A_s + b_e \times t} \; ; \qquad (4.3\text{-}26)$$

$$I_e' = \frac{b_{te}.t^3}{12} + b_{te}.t.\left(z_p - \frac{t}{2}\right)^2 + \frac{t_w.h_w^3}{12} + h_w.t_w.\left(z_p - \frac{t}{2} - \frac{h_w}{2}\right)^2 + \frac{b_f.t_f^3}{12} + b_f.t_f.\left(z_p - \frac{t}{2} - h_w - \frac{t_f}{2}\right)^2$$

$$z_p = \frac{0.5b_{te}.t^2 + h_w.t_w.(t + 0.5h_w) + b_f.t_f.(t + h_w + 0.5t_f)}{(b_{te}.t + h_w.t_w + b_f.t_f)} \qquad (4.3\text{-}27)$$

I_e', z_p and b_{te} are the reduced moment of inertia, centre of mass and tangential effective width of the stiffened plate. EI_e' is the buckling flexural rigidity of the stiffener. The tangent effective width of the plate (b_{te}) is given by:

$$\frac{b_{te}}{b} = \begin{cases} \dfrac{1}{\beta_e} \times R_\eta \times R_\delta \times R_{\eta\delta} & \beta_e \ge 1 \\ R_\eta \times R_\delta \times R_{\eta\delta} & 0 \le \beta_e \le 1 \end{cases} \qquad (4.3\text{-}28)$$

The effective width of the plate is related to the slenderness as follows:

$$\frac{b_e}{b} = \begin{cases} 1.08 \times \phi_b \times R_\eta \times R_\delta \times R_{\eta\delta} & \beta_e \geq 1 \\ 1.08 \times R_\eta \times R_\delta \times R_{\eta\delta} & 0 \leq \beta_e \leq 1 \end{cases} \quad (4.3\text{-}29)$$

Based on the Johnson-Ostenfeld formulation, which accounts for inelastic effects of column's buckling, Faulkner proposed a model for the strength of thin stiffened plates where it is considered that the stiffener and an effective strip of the associated plate are subjected to an edge stress σ_e. The maximum edge stress that this column can sustain is related to the yield stress by the Johnson-Ostenfeld approach, but the model used to calculate the flexural buckling rigidity of the column must consider a tangent modulus in a bending situation. Considering post buckling behaviour, the ultimate strength of a stiffened plate, modelled as stiffener with an associated width of plate can be given by:

$$\phi = \frac{\sigma u}{\sigma y} = \Phi(\varepsilon)\frac{\sigma_e}{\sigma_y}\left[\frac{A_s + b_e \times t}{As + b \times t}\right] \quad (4.3\text{-}30)$$

Where

$$\frac{\sigma_e}{\sigma_y} = \begin{cases} 1 - \frac{1}{4}\frac{\varepsilon\sigma_y}{\sigma_E} & for \quad \sigma_E \geq 0.5\varepsilon\sigma_y \\ \frac{\sigma_E}{\varepsilon\sigma_y} & for \quad \sigma_E \leq 0.5\varepsilon\sigma_y \end{cases} \quad (4.3\text{-}31)$$

Where ε is the nomalised strain for a given edge stress of σ_e, A_s is the area of the stiffener and σ_E is the Euler stress and is given by

$$\sigma_E = \frac{\pi^2 \times E \times r_{ce}^2}{a^2} \quad (4.3\text{-}32)$$

Where E, r_{ce} and a are Young's modulus, radius of gyration and the length of the stiffened plate.

4.3.1.2.1 TRIPPING OF STIFFENERS

Tripping failure is one of the most dangerous failures, since it is always associated with very quick shed of load carrying capacity of the column. Torsional instability may occur alone by twisting of the stiffener about its line of attachment to the plating; developing a partial or full hinge at the intersection, or induced by flexural buckling especially if the deflected shape of the column is towards the plate. In that case, the stiffener will be subjected to a higher stress than the average column stress and the critical tripping stress could be easily reached, followed by a deep load shedding. Several authors have proposed analytical formulae for torsional buckling (tripping), but here those used by classsification societies have been implemented.

The tripping stress (σ_T) at a given normalised strain is given by

$$\sigma_T = \sigma_y \Phi(\varepsilon)\left[\frac{A_s\sigma_C + bt.\phi_b.\sigma_y}{A_s + bt}\right] \quad (4.3\text{-}33)$$

Where $\Phi(\varepsilon)$ and ϕ_b are obtained from equations (4.3-15) and (4.3-20) respectively. As is the area of the stiffener and

$$\sigma_C = \begin{cases} \dfrac{\sigma_{ET}}{\varepsilon} & if \quad \sigma_{ET} \le 0.5\varepsilon\sigma_y \\ \sigma_y\left(1 - \dfrac{\Phi(\varepsilon)\sigma_y.\varepsilon}{4\sigma_{ET}}\right) & if \quad \sigma_{ET} > 0.5\varepsilon\sigma_y \end{cases} \qquad (4.3\text{-}35)$$

According to classification societies' rules the Euler torsional buckling stress (σ_{ET}) can be given as follows:

$$\sigma_{ET} = \frac{\pi^2.E.I_w}{I_p.a^2}\left(m^2 + \frac{K_C}{m^2}\right) + 0.385.E.\frac{I_t}{I_p} \qquad (4.3\text{-}36)$$

The torsional co-efficient, K_C, can be given as :

$$K_C = \frac{C_O.a^4}{\pi^4 E.I_w} \qquad (4.3\text{-}37)$$

Where a is the length of the stiffened plate, C_o is the spring stiffness of the attached plating and I_w is the net sectorial moment of inertia.The number of half-waves (m) should be taken equal to be an integer number, such that

$$m^2(m-1)^2 \le KC < m^2(m+1)^2 \qquad (4.3\text{-}38a)$$

and the relationship between the half-waves (m) and the torsional coefficient (K_C) is as follows

$$m = \begin{cases} 1 & if \quad 0 \le K_C \le 4 \\ 2 & if \quad 4 \le K_C \le 36 \\ 3 & if \quad 36 \le K_C \le 144 \end{cases} \qquad (4.3\text{-}38b)$$

The spring stiffness (C_O) of the attached plating is given by

$$C_O = \frac{E.t^3}{2.73b} \qquad (4.3\text{-}39)$$

Where E,t and b are the Young's modulus, thickness and breadth of the stiffened plate respectively.The net sectorial moment of inertia (I_w) of the stiffener about its connection to the attached plating for T-sections can be given by

$$I_w = \frac{t_f.b_f^3 h_w^2}{12} \qquad (4.3\text{-}40)$$

Where t_f, b_f and h_w are the flange thickness, flange breadth and web height respectively.The net polar moment of Inertia (I_p) of the stiffener about its connection to the attached plating for stiffener with face plate is given by

$$I_p = h_w^2 b_f t_f + \frac{t_w.h_w^3}{3} \qquad (4.3\text{-}41)$$

The St. Venant's net moment of inertia (I_t) of the stiffener without attached plating for stiffeners with face plate is given by

$$I_t = \frac{1}{3}\left[h_w t_w^3 + b_f t_f^3\left(1 - 0.63\frac{t_f}{b_f}\right)\right] \quad (4.3\text{-}42)$$

Where t_w is the thickness of the web of the stiffened plate.

4.4 Methodologies for Reliability Analysis of Hull Girders

In an environment of increasingly complex engineering systems, the concern for the operational safety of these systems continues to play a major role in both their design and operation. A systematic, quantitative approach for assessing the failure probabilities and consequences of engineering systems is needed. Such an approach allows the engineer to evaluate complex engineering systems, for safety and risk under different operational conditions, with relative ease. The ability to evaluate these systems quantitatively helps to reduce the cost of unnecessary repairs or replacement of the system and lessens the risk posed on the system. The results of risk analysis can also be used in decision analysis based on cost–benefit tradeoffs. There are many events (hazards) that affect the safety of marine systems. Numerous sources of hazard include equipment failure, external events, human errors, and organizational errors. Equipment failure is the most recognized hazard on ships and can be divided into several sub-categories including independent failures and common cause failure. Hazards due to external events include collision, grounding, severe sea states, ice, or bad weather, etc. Risk studies can be classified into risk assessment, risk management, and risk communication. The concept of risk is used to assess and evaluate uncertainties associated with an event. Risk can be defined as the potential of losses as a result of a system failure, and can be measured as a pair of probability of occurrence of the event, and the outcomes or consequences associated with the event's occurrence. Risk is commonly evaluated as the product of likelihood of occurrence and the impact of an accident:

Risk=Likelihood* Impact

In the above equation, the likelihood can also be expressed as a probability. The reliability of a ship can be defined as its ability to fulfil its design functions for a specified time period. This ability is commonly measured using probabilities. Reliability is, therefore, the occurrence probability of complementary event to failure:

Reliability=1-Failure Probability

Based on this definition, reliability is one of the components of risk. Safety can be defined as the judgment of risk acceptability for the system. So, in the risk assessment of ship systems, the structural reliability is a key component. In this study the ship structural reliability, especially for the damaged ship, is reviewed and discussed emphatically.

Structural reliability methods are powerful tools for dealing with uncertainties in many engineering disciplines. The importance of using probability concepts in the design and evaluation of engineering systems is widely recognised, and many valuable contributions to improvement of design and evaluation of structural and mechanical system have been made from the research community. Structural reliability methods have reached a mature stage and are widely used in the development of codes and for the design and maintenance of engineering systems and structures.

In general, the objective in the structural design is to ensure that the strength of structure or the system is higher than the loads to which the system can be exposed. The problem is to account for the uncertainty associated with quantification of the load or the strength of the structure. The uncertainty stems from physical uncertainties (natural loads and materials), statistical uncertainty (sparse data) and model uncertainty. The overall objective of structural reliability method is to quantify these uncertainties to provide a better basis for decision-making regarding the dimensions of the structure or with respect to maintenance issues.

In general, about calculating structural reliability, the following procedure is suggested.

- Establish target reliability, i.e. reliability safety index, or a decision model.
- Identify all possible and significant failure modes of the structure or operation under consideration.
- Formulate failure criteria and establish a relevant failure limit state function for each of mode of failure.
- Choose and identify stochastic variables and parameters for each failure mode of the structure or operation under consideration.
- Calculate the reliability or failure probability of the structure of each failure mode of the structure or operation under consideration.
- Assess the structure reliability against the given reliability target whether the calculated reliability is sufficient or not and modify the concept if necessary.
- Evaluate the results of the reliability analysis with respect to parametric sensitivity considerations.
- Document to the structure design.

The above steps will be illustrated respectively in detail in the following sections of this report.

4.4.1 Criteria for the selection of methodology

A reliability method that gives acceptable estimates of the reliability for the structure or structural components shall be used. The choice of the reliability methods must be justified. The justification may be based on verification by other relevant methods. When the limit state is a linear function, the FORM and SORM can be used to verify the results of the simulation and direct integral methods. Analytical FORM and SORM reliability estimate can generally be verified by simulation. When the number of basic random variables is under 5, the integral methods can be used to verify the results of analytical methods and simulation methods. In general, the simulation methods can be used to verify the results of the other methods. A local reliability estimate by FORM at a single design point can be verified by a SORM estimate. Simulation can then be used to verify if this local estimate is sufficient as an estimate of the global reliability when there is more than one design point. For FORM and SORM solutions the design point shall be documented to have a sound physical interpretation. About the best method to calculate marine structure reliability, the following methods is suggested:

- For linear failure limit function or the failure probability less than 0.05, the analytical FORM and SORM reliability estimates are suggested.
- Under 5 variables, the directly integrated method is suggested.
- The others except the above are calculated best by means of simulation methods (e.g. Monte Carlo Method)
- In general, the simulation methods shall be chosen first.
- For implicit limit state function, FORM ,SORM or response surface method could be selected.

For same kinds of structures, such as marine structures, reliability analysis should be done by the same reliability analysis method, i.e., selecting a kind of reliability method only, such as simulation method or FORM, etc. This means the same standard should be applied to same kind of structure. The following are the reasons:

- The analysis models of structural reliability are usually imperfect.
- The information about loads and resistance is usually incomplete.
- Reliability methods are based on analysis models for the structure in conjunction with available information about loads and resistances and their associated uncertainties.
- Reliability methods deal with the uncertainty nature of loads, resistance etc. and lead to assessment of the reliability.
- The reliability as assessed by reliability methods is therefore generally not a purely physical property of the structure in its environment of actions, but rather a nominal measure of the safety of the structure, given a certain analysis model and a certain amount and quality of information.
- Correspondingly, also the estimated failure probability is dependent on the analysis model and the level of information, and it can therefore usually not be interpreted as the frequency of occurrence of failure for the particular type of structure.

The reliability method used shall be capable of producing a full sensitivity analysis such as parametric sensitivities for changes in fixed variables and importance factors for uncertain variables. The sensitivity should be executed and documented as a part of the reliability analysis.

4.4.2 Reliability Methodology

The following introduces the basic reliability concept and illustrates aspects of the procedures of reliability analysis. A simple ship hull girder subjected to a load induced by the environment may be assumed. Traditionally, in the design process, practitioners and designers have used fixed deterministic values for loads acting on the girder and for its strength. In reality these values are not unique values but rather have probability distributions that reflect many uncertainties in the load and strength of the girder. Structural reliability theory deals mainly with the assessment of these uncertainties and the methods of quantifying and rationally including them in the design process. The load and strength are thus modeled as random variables. Figure 4.4.1 shows the frequency density functions of load and the strength of the girder in terms of applied bending moment and ultimate moment capacity of the girder, respectively. Both, the load L and strength R are assumed to follow the normal probability distribution.

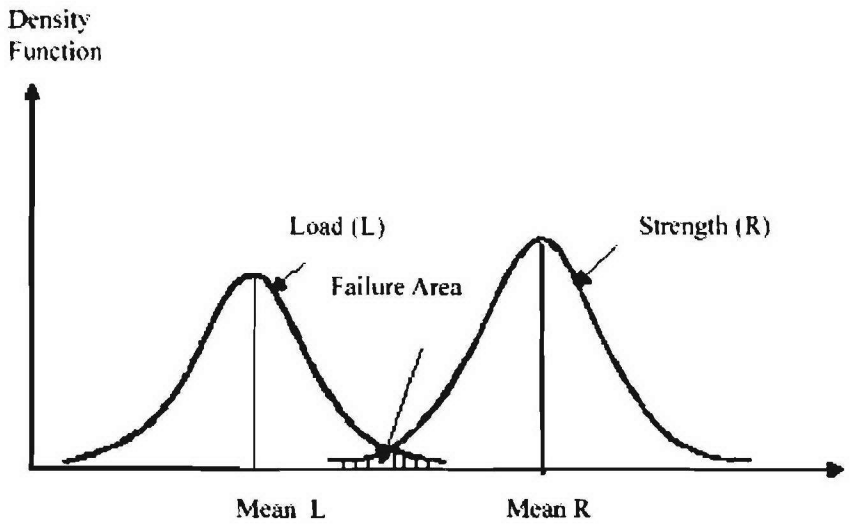

Figure 4.4.1: Frequency distribution of strength R and load L.

Now, a simple function g(R, L) can be constructed, the limit state function describes the safety margin M between the strength of the girder and the load acting on it.

$$M = g(R,L) = R - L \tag{4.4-1}$$

Both R and L are random variables and may assume several values. The following events or conditions describe the possible states of the structure.

Table 4.4-1: Possible values of the limit state function

Case 1: M=g(R, L)<0	Represents a failure state since this means that the load L exceeds the strength R
Case 2: M=g(R, L)>0	Represents the safe state
Case 3: M=g(R, L)=0	Represent the limit state surface or border surface between the safe and failure states

The probability of failure implied in case (1) can be computed from:

$$P_f = P[M = g(R,L) \le 0] = \iint_{g(R,L)\le 0} f_{R,L}(R,L)dRdL \tag{4.4-2}$$

In equation 4.4-2 $f_{R,L}(R,L)$ is the joint probability density function of R and L, and the domain of integration is over all values of R and L where the margin M is not positive, i.e. not in the safe state. If the applied load on the girder is statistically independent from the girder strength the above Eq. (4.4-2) can be simplified and interpreted as:

$$P_f = \int_0^\infty F_R(L) f_L(L) dL \tag{4.4-3}$$

Here $F_R(.)$ and $f_L(.)$ are the cumulative distribution function of R and the probability density function of L, respectively. Eq. (4.4-3) is the convolution integral to L. As mentioned above,

the R and L are both statistically independent and normally distributed. Eq. (4.4-3) can be thus shown to reduce to

$$P_f = \Phi(-\beta) \tag{4.4-4}$$

here $\Phi(.)$ is the standard normal cumulative distribution function and β is called the safety index and defined as:

$$\beta = \frac{\mu_R - \mu_L}{\sqrt{[\sigma_R^2 + \sigma_L^2]}} \tag{4.4-5}$$

Where μ, σ represent the mean value and standard deviation of the random variable, respectively. Notice that, as the safety index β increases, the probability of failure P_f as given by Eq. (4.4-4) decreases.

4.4.3 The calculation method of structural reliability

The structural reliability is evolved thoroughly so far and is currently categorized under three different levels (Level 1, Level 2 and Level 3) that depend mainly on the degree of sophistication of the analysis and the available input information. Level 3, which sometimes is referred to as the fully probabilistic approach, is the most demanding in terms of the required input information. However, even if the input information is available, the analytical or numerical evaluation of the resulting integrals for estimating the probabilities of structural failure is extremely difficult. The basic concept of Level 3 reliability analysis is that a probability of failure of a structure always exists and may be calculated by integrating the joint probability density function of variables involved in the load and strength of the structure. The domain of integration is over the unsafe region of variables. Because of the difficulties in connection with determining the joint probability density function of the variables and in evaluating the resulting multiple integrations, Level 2 reliability (semi-probabilistic approach) analysis was introduced. In this level, a reliability index, rather than a probability of failure, is introduced to assess the safety of the structure. The reliability index is connected to the probability of failure, and, under certain circumstances, the exact probability of failure may be directly obtained if the safety index is determined. For example, if the design variables are uncorrelated and normally distributed and the limit state function is linear, the probability of failure can be determined from safety index using tables of the standard normal distribution function. If the variables are correlated and not normally distributed, certain transformations can be made to obtain equivalent uncorrelated normal variables, and thus the approximate probability of failure may be determined. Similarly, certain approximations can be made for the nonlinear limit state function. There are several developed reliability analysis methods for Level 2, such as: Mean Value First Order Second Moment Analysis, The Generalized Safety Index, First Order Reliability Methods (FORM), Second Order Reliability Methods (SORM), and Advanced Mean Value (AMV) Method. Although Level 2 is easier to apply in practice, it is still of limited use to practitioners, normally a designer needs factors of safety to apply in the design process, such as those applied to the yield strength of the material and to the loads. This need resulted in the introduction of Level 1 reliability analysis. In this level, partial safety factors are determined, based on Level 2 reliability analysis. If these factors are used in the design, their cumulative effect is such that the resulting design will have a certain reliability level (i.e. a certain safety index). Thus, code development and classification societies may determine (and specify in their codes) these partial safety factors that ensure that the resulting design will have a specified reliability level. Besides the above-mentioned methods, there is

also a very efficient method, Monte Carlo Simulation, which is usually used for problems involving random variables of known or assumed probability distributions. Using statistical sampling techniques, a set of values of the random variables is generated in accordance with corresponding probability distributions. These values are treated similarly to a sample of experimental observations and are used to obtain a sample solution. By repeating the process and generating several sets of sample data, many sample solutions can be determined. Statistical analysis of the sample solution is then performed. As computer capabilities have increased and computer costs have decreased, Monte Carlo simulation for structural reliability analysis has gained new respectability. It has also helped that efficient methods, principally importance sampling, have been developed.

4.4.3.1 First Order Reliability Method (FORM)

First Order Reliability Method (FORM) was initially proposed by Hasofer /Lind (1974) for normal vector X and was later extended to arbitrary distribution by Rackwitz/Fiessler (1978). The limit state functions of common engineering problems can be either linear or non-linear functions of the basic variables. FORM can be used when the limit state function is a linear function of uncorrelated normal variables or when the non-linear limit state function is represented by the first-order (linear) approximation. It is based on the first order approximation (Taylor expansion) to the limit state surface. In this case where limit state function is linear (forming a hyper plane in the U-space), the projection of the origin onto the hyper plane is the most likely failure point. This geometrical property is approximated by a tangent hyper plane, and an iteration scheme is used to find the most likely failure point.

4.4.3.2 Second Order Reliability Method (SORM)

Second Order Reliability Method (SORM) includes the second order terms of the Taylor expansion of the limit-state surface. The second order reliability index is determined by a correction factor to the first order reliability index. The computations are based on asymptotic arguments regarding the curvature of the limit state surface at the design point. For SORM the failure surface must be twice differentiable, at least in the β -point. It is seen that second order results differs from first order result by a factor involving the curvatures of the failure, which generally is close to unity. Although SORM in general yields better estimates of the failure probability, it is computationally more intense than FORM.

4.4.3.3 Monte Carlo Method

Crude form:

The analytical methods (FORM/SORM) give approximate results, and should be applied for failure probability less than 0.05. For larger failure probability, direct integral method maybe can be used. But because the direct integral method is not suitable to a large numbers of variables, practitioner tried to develop other effective methods. Simulation methods are one of the effective methods and Monte Carlo Method is one of the most widely used simulation method.

Monte Carlo simulation is usually used for problems involving random variables of known or assumed probability distributions. Using statistical sampling techniques, a set of values of the random variables is generated in accordance with the corresponding probability distributions. These values are treated similar to a sample of experimental observations and are used to obtain a 'sample' solution. By repeating the process and generating several sets of sample data, many sample solutions can be determined. Statistical analysis of the sample solutions is then performed.
The Monte Carlo method thus consists of the following basic steps:

a) Simulation of the random variables and generation of several sample data using statistical sampling techniques
b) Solutions using the sampled data
c) Statistical analysis of the results

Since the results from the Monte Carlo technique depend on the number of samples used, they are not exact and are subject to sampling errors. Generally the accuracy increase as the sample size increases. Sampling from a particular probability distribution involves the use of random numbers. Random numbers are essentially random variables uniformly distributed over the unit interval [0, 1]. Many codes are available for computers for generating sequence of 'pseudo' random digits where each digit occurs with approximately equal probability. The generation of such random numbers plays a central role in the generation of a set of values (or realizations) of a random variable that has a probability distribution other than uniform probability law.
The Monte Carlo method is considered now as one of the most powerful techniques for analyzing complex problems. Since its chief constraint is computer capability, it is expected to become even more commonly used in the future as computer capacities increase and become less expensive to use.
The following are necessary to apply Monte Carlo techniques to structural reliability problems (Robert E. Melchers, 2001):

a) to develop systematic methods for numerical 'sampling' of the basic variables X;
b) to select an appropriate economical and reliable simulation technique or 'sampling strategy';
c) to consider the effect of the complexity of calculating $g(X)$ and the number of basic variables on the simulation technique used;
d) for a given simulation technique to be able to determine the amount of 'sampling' required to obtain a reasonable estimate of P_f;
e) to deal with dependence between all or some of the basic variables if necessary.

Monte Carlo Simulation (MCS) plays a very important role in different levels of reliability analysis. The high accuracy that the method produces is only dependent on the sampling number and is not affected by the distribution type and the number of basic variables. The method can be used in even those cases where the limit state function is not known implicitly and it is the only approach to highly non-linear problems. A number of variation reduction techniques have been proposed such as the Importance Sampling Method but as always the computation cost in large complex structural systems is still significantly high.

Variance reduction techniques

For a given level of confidence, the basic (crude) Monte Carlo method requires a large amount of samples in general. In order to look for a relative efficiency method, sample reduction

techniques are developed. This method reduce the error (or variance) without increasing the sample size and requires far fewer sample points than using the 'crude' Monte Carlo method. These techniques are known as variance reduction techniques, and the one that is used often in the structural failure problems is called 'antithetic variates'.

The following is an introduction of antithetic variates method.

Let Y_1 and Y_2 be two unbiased estimates of Y as determined from two separate sets of samples or simulation cycles. The average of these two unbiased estimations $Y_a=(Y_1+Y_2)/2$ is also an unbiased estimator since its expected value $E[Ya]$ is equal to Y. The variance σ_{ya}^2 of the new estimator Y_a is determined from the individual variances σ_{y1}^2 and σ_{y2}^2 as:

$$\sigma_{y_a}^2 = \frac{\sigma_{y_1}^2 + \sigma_{y_2}^2 + 2\mathrm{cov}(Y_1, Y_2)}{4} \qquad (4.4\text{-}6)$$

If Y_1 and Y_2 are negatively correlated, i.e., the cov $(Y_1, Y_2) < 0$, it is seen from Equation (4.4-6) that the third term becomes negative and

$$\sigma_{y_a}^2 < \frac{\sigma_{y_1}^2 \sigma_{y_2}^2}{4} \qquad (4.4\text{-}7)$$

That is, the accuracy of the estimator Y_a can be improved (or its variance can be reduced) if Y_1 and Y_2 are negatively correlated estimators. The antithetic variates method is thus a procedure that ensures a negative correlation between Y_1 and Y_2. This can be accomplished in structural reliability problems as follows.

If X is a random variable uniformly distributed between 0 and 1, then 1-X is also a uniformly distributed random variable between 0 and 1 and the two random variables X and 1-X are negatively correlated. Each of these random variables can be then used to generate the basic random variables Y_i, which have prescribed probability distributions as described earlier. This results in a pair of negatively correlated basic random variables. The procedure is repeated for all the random variables Y_i in the limit state equation. The limits state equation is then solved for each negatively correlated set of random variables separately and the results are averaged to estimate the population mean. Note that the error (or variance) of the result is reduced because of the negative correlation between the generated variables according to Equation (4.4-7).

5. A SAMPLE VESSEL

The sample vessel, which is called Hull 5415, was initially designed by NSWCCD. The principal dimensions of the vessel are shown in Table 5.1. The other details of Hull 5415 are presented in Appendix B. Division of the compartment of the vessel is presented in Figure 5.1.

Table 5.1: Principal dimensions of Hull 5415

Principal Dimensions	Values
Length Between Perpendiculars	142.04 metres (466 ft)
Overall Length	151.18 metres (496 ft)
Maximum Beam	21.15 metres (69.4 ft)
Beam at Water Line	20.03 metres (65.7 ft)
Depth of Hull	12.74 metres (41.8 ft)
Design Draught (moulded)	6.31 metres (20.7 ft)
Displacement at Load Draught	9032.24 tonnes (8890 L-tons)

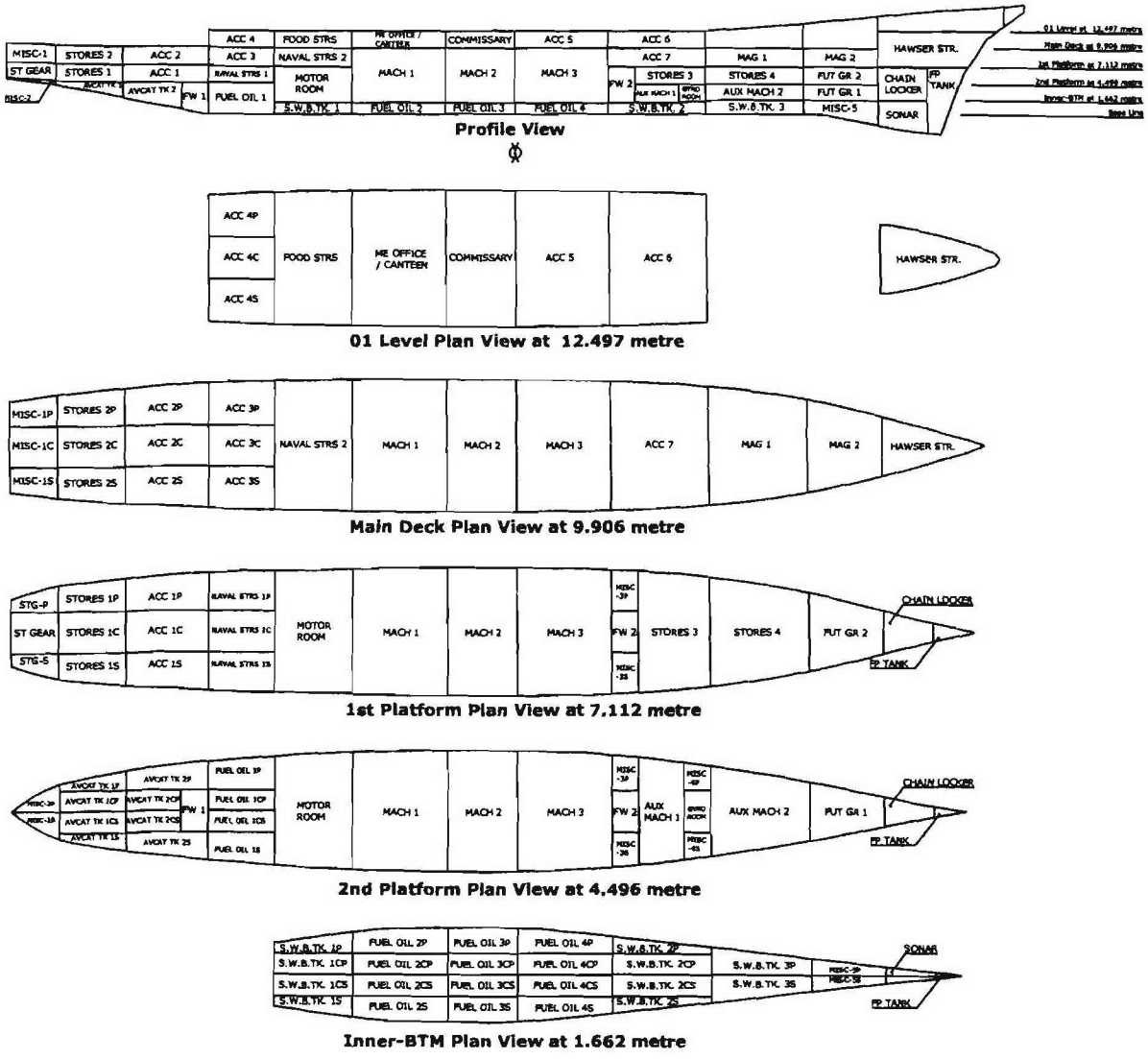

Figure 5.1: Division of the compartment of the vessel

6. DAMAGE SCENARIOS

6.1 Introduction

Damage in a ship may be caused by ship-ship collision, grounding, bottom slamming, bow flare slamming, green water, etc. The damage due to collision and grounding is the most common result of destruction of a ship structure. Ship-ship collision causes the bow of striking ship collapsed and the side of struck ship damaged. The ship-ship collision is the most destructive among all possible damages. In ship grounding on rock it will result in cutting or crushing of bow bottom. After collision or grounding has occurred, the damaged ship may settle down to a deeper draught and heel due to flooding. As a result, static water pressure on bottom structure may exceed design static pressure and dynamic wave induced loads may increase. When a ship rides in rough seas, she is inevitably subjected to severe motions. Relative large bow motion results in slamming impact on bow bottom and flare. In severe sea environment slamming on bow bottom and bow flare may damage local shell plating. When the bow becomes partially or fully submerged, green water may flow over the fore deck. A jet of water travels aft possibly damaging deck equipment and the front wall of the superstructure (Chan, 1998).

6.2 Determining Damage Scenarios for Model Tests and Numerical Computations

For considering most probable and severe conditions in the aspects of hydrostatic and hydrodynamic loadings, LR rules for naval vessels and recent incidents of navy ships were referred. Here collision damage to the side shell and raking damage to the bottom structure were considered. Table 6.1 explains the extent of damage in navy vessels that is recommended in Lloyd's Register Rules (Lloyd's Register of Shipping, 2002).

Table 6.2-1: Extent of damage in navy vessels

Military threats	The extent of damage due to military threats defined as the minimum of the shock or blast damage that is likely to result from a specified weapon threat.	
Collision damage to the side shell	Level A	- 5 m longitudinally between bulkheads - from the waterline up to the main deck - inboard for B/5 m
	Level B & C	- 5 m longitudinally anywhere including bulkheads - from the bilge keel up to the main deck - inboard B/5 m
Grounding or raking damage to the bottom structure	Level A	- length of 5 m anywhere forward of midships - upwards for 1 m or the underside of the inner bottom, whichever is less - breadth of 2.5 m
	Level B & C	- length of 0.1L anywhere forward of midships - upwards for 1 m or the underside of the inner bottom, whichever is less - breadth of 5 m

Figure 6.2-1 shows the outcome of a collision at sea between US navy destroyer and Saudi Arabian container vessel on 5 February 1999 (*http://www.shipstructure.org*). Figure 6.2-2 shows damage due to the apparent suicide attack against USS Cole destroyer blasted a 12 metres by 12 metres hole in the ship's side shell (*http://archives.cnn.com*). The damage of HMS Nottingham is provided in Figures 6.2-3 and 6.2-4. On 7 July 2002 Nottingham ran aground on the submerged but well-charted Wolf Rock near Lord Howe Island, 200 miles off

the coast of Australia. A 160 ft (50 m) hole was torn down the side of the vessel from bow to bridge, flooding five of her compartments and nearly causing her to sink (*http://pages.zdnet.com*, *http://en.wikipedia.org*).

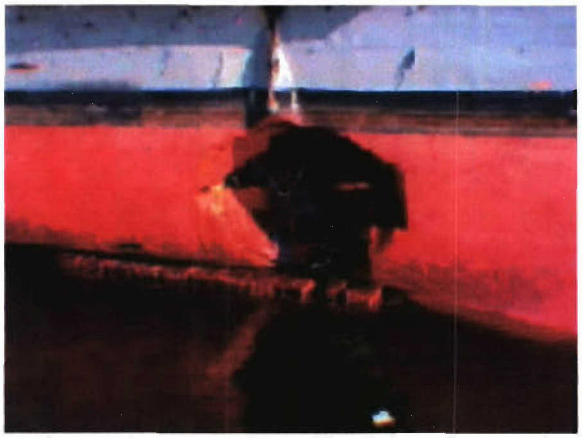

Figure 6.2-1: USS Radford (5 Feb. 1999)

Figure 6.2-2: USS Cole (12 Oct. 2000)

Figure 6.2-3: HMS Nottingham (7 Jul. 2002)

Figure 6.2-4: HMS Nottingham (7 Jul. 2002)

In this project, four damage scenarios are proposed and shown in Figures 6.2-5 ~ 6.2-8. Figure 6.2-5 presents damage scenario 1, which is at Level A. Figure 6.2-6 shows damage scenario 2, which is similar to the damage on USS Cole. Figure 6.2-7 shows a raking damage at Levels B & C. Shown in Figure 6.2-8 is a damage scenario that is similar to the accident of HMS Nottingham.

DEMAGE SCENARIO 1

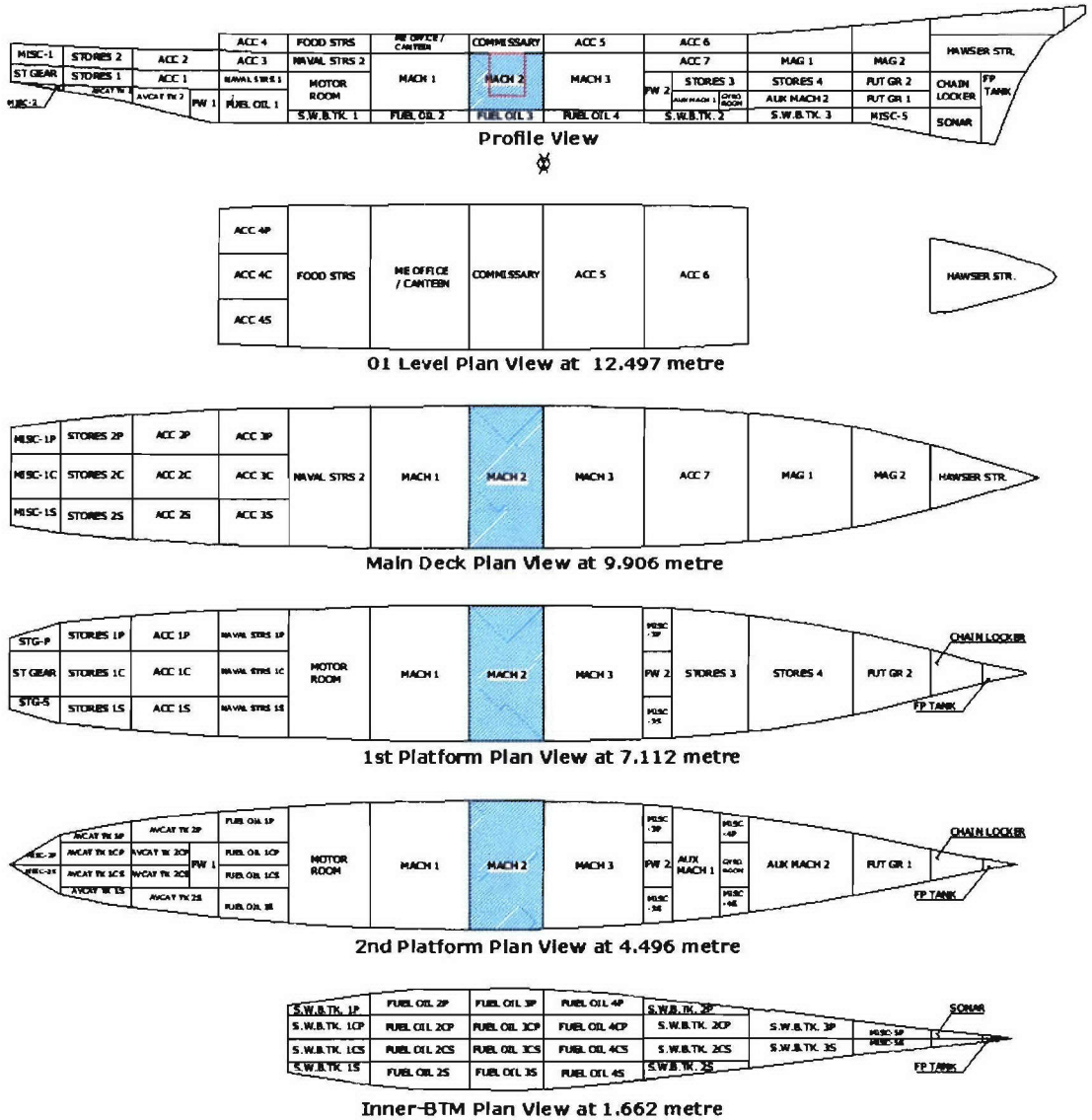

Figure 6.2-5: Damage scenario 1

DEMAGE SCENARIO 2

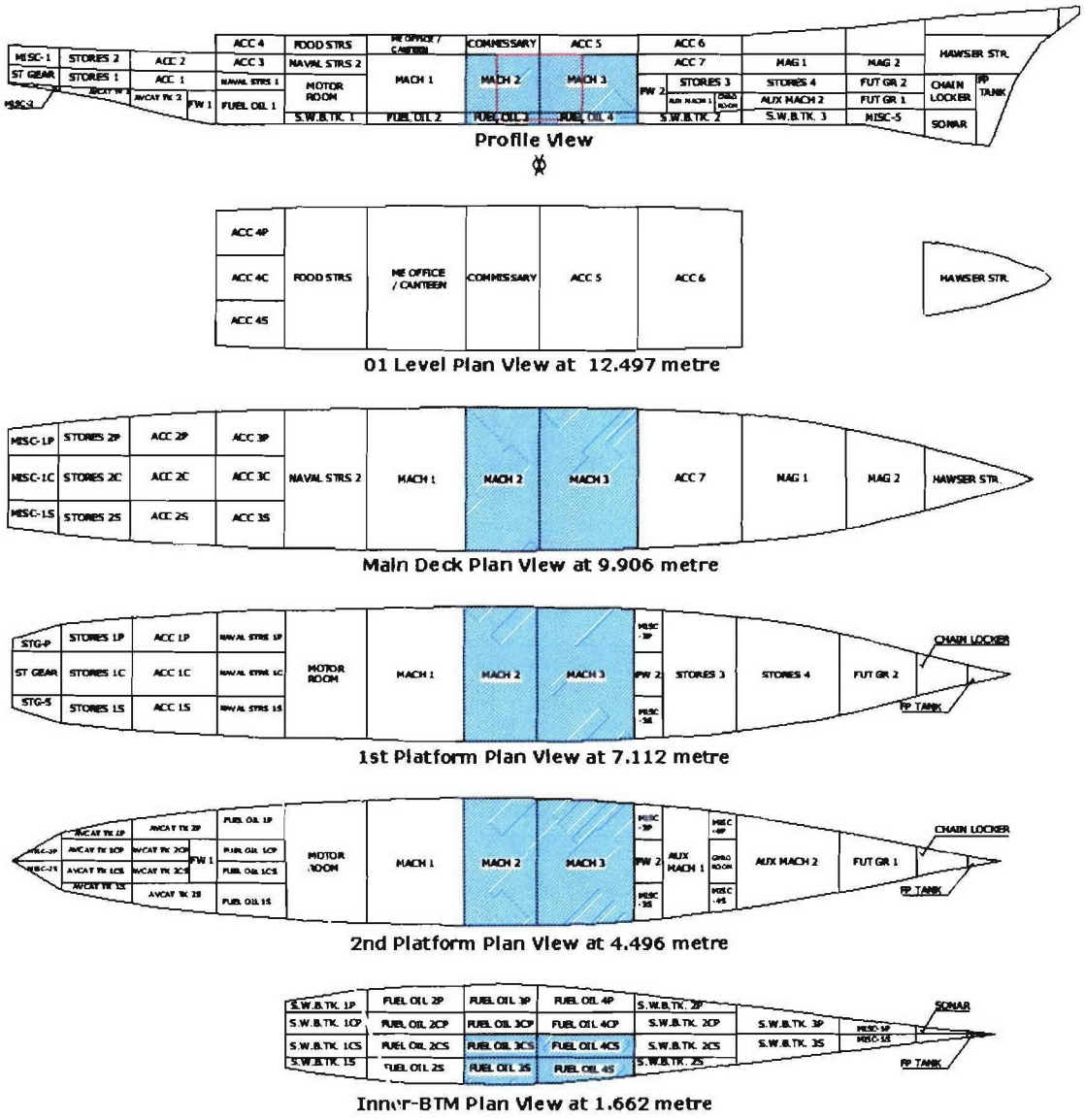

Figure 6.2-6: Damage scenario 2

DEMAGE SCENARIO 3

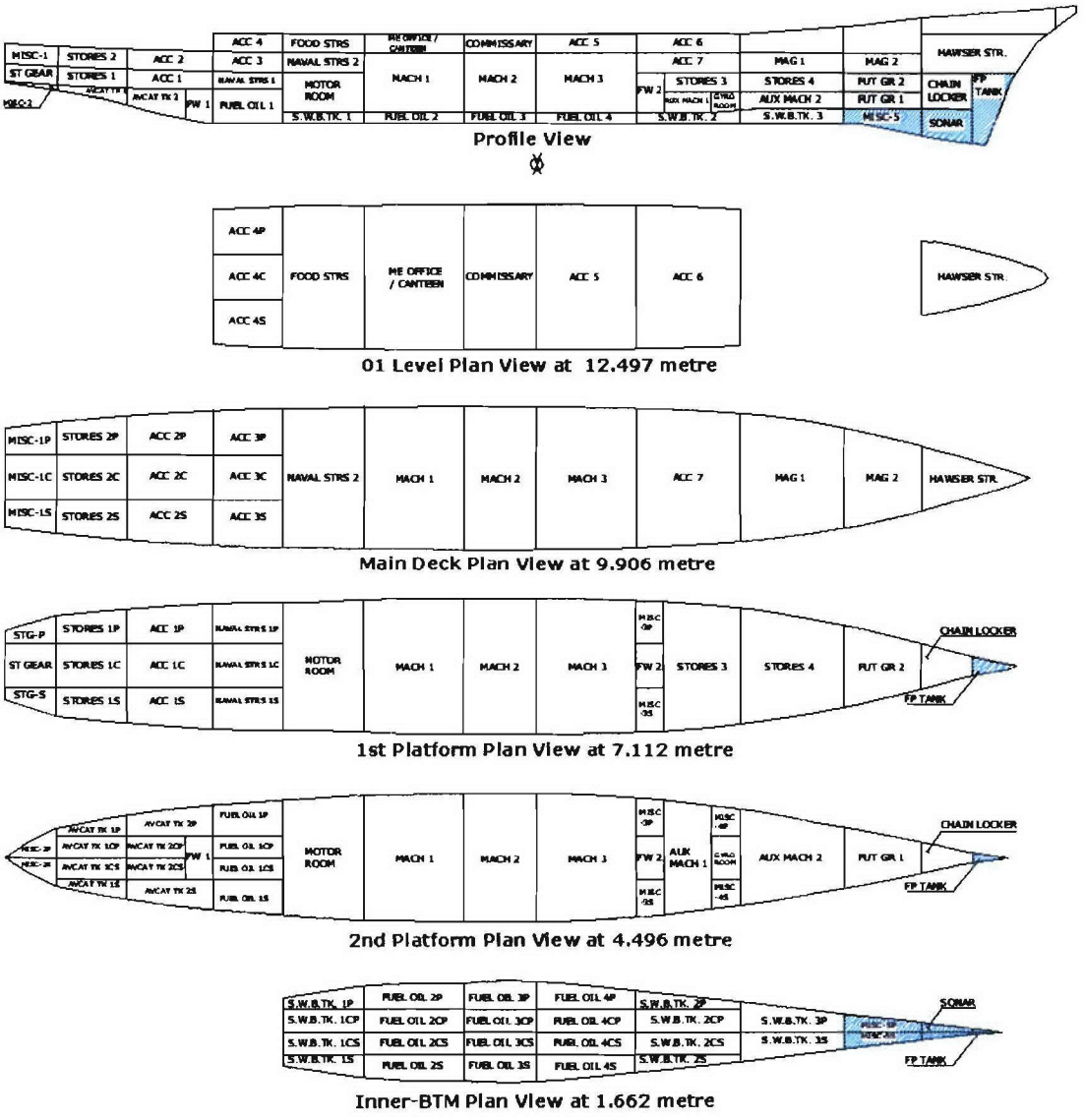

Figure 6.2-7: Damage scenario 3

DEMAGE SCENARIO 4

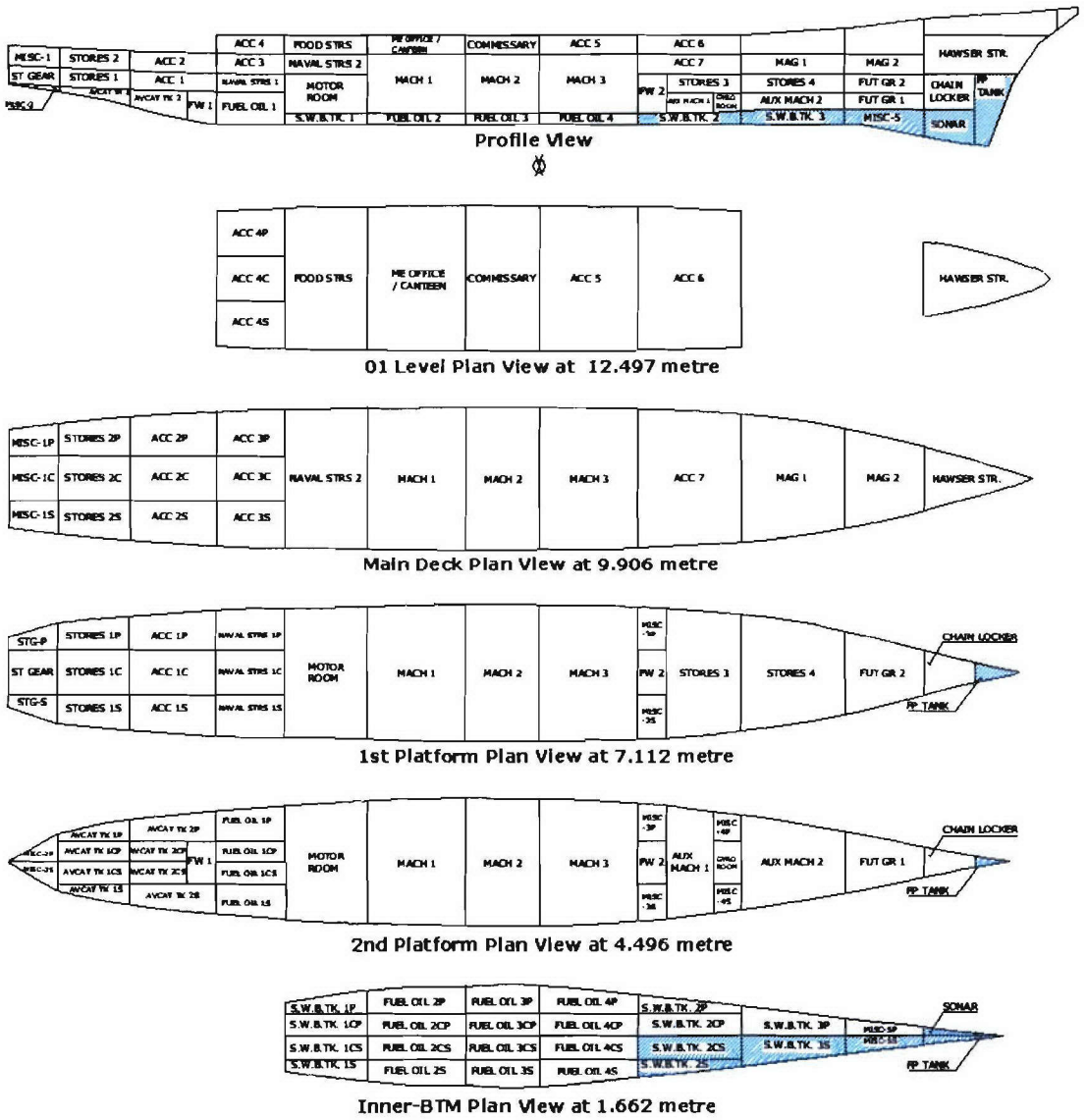

Figure 6.2-8: Damage scenario 4

7. DEMONSTRATION OF THE DEVELOPED PROCESS

7.1 Numerical Predictions of Motions and Loads

This section presents the prediction of ship motions and dynamic wave induced loads for a sample vessel in intact condition and damage conditions. The sample vessel was initially designed by NSWCCD. A general arrangement design and compartment modelling were conducted by UNEW. Details are presented in chapter 5. In this study the linear frequency domain analysis was carried out in several design conditions that are intended as examples of ship-ship collision and raking events as well as intact condition. The damage scenarios used in simulations were provided in chapter 6. In general the linear assumption is fairy good for most conventional ships, although it tends to produce better solution for motions than the loads. Linear techniques, especially linear strip theories, are the standard for the prediction of hydrodynamic responses in practical and design settings. In spite of practical success of linear theories, the applications are limited to small amplitude motions. Large amplitude motions and structural responses, which could not be accurately predicted by linear theory in some cases, are key issues for assessments of ultimate hull girder strength of intact ship and residual strength of damaged ship in extreme wave conditions. So far the time domain analysis for the prediction of large amplitude motions and structural responses was also carried out on the specified design conditions (Chan, 1998; Collette, 2005a). A series of internal sea-keeping and loading prediction programmes, UNEW Hydro Programme suite, has been developed using 2D linear and non-linear strip theory. The computation procedure of this study using UNEW Hydro Programme is provided in Figure 7.1-1. Also the detailed information on 2D linear programme is presented in Appendix A. The simulations were carried out with 19 cases in intact and damage conditions (see Table 7.1-5).

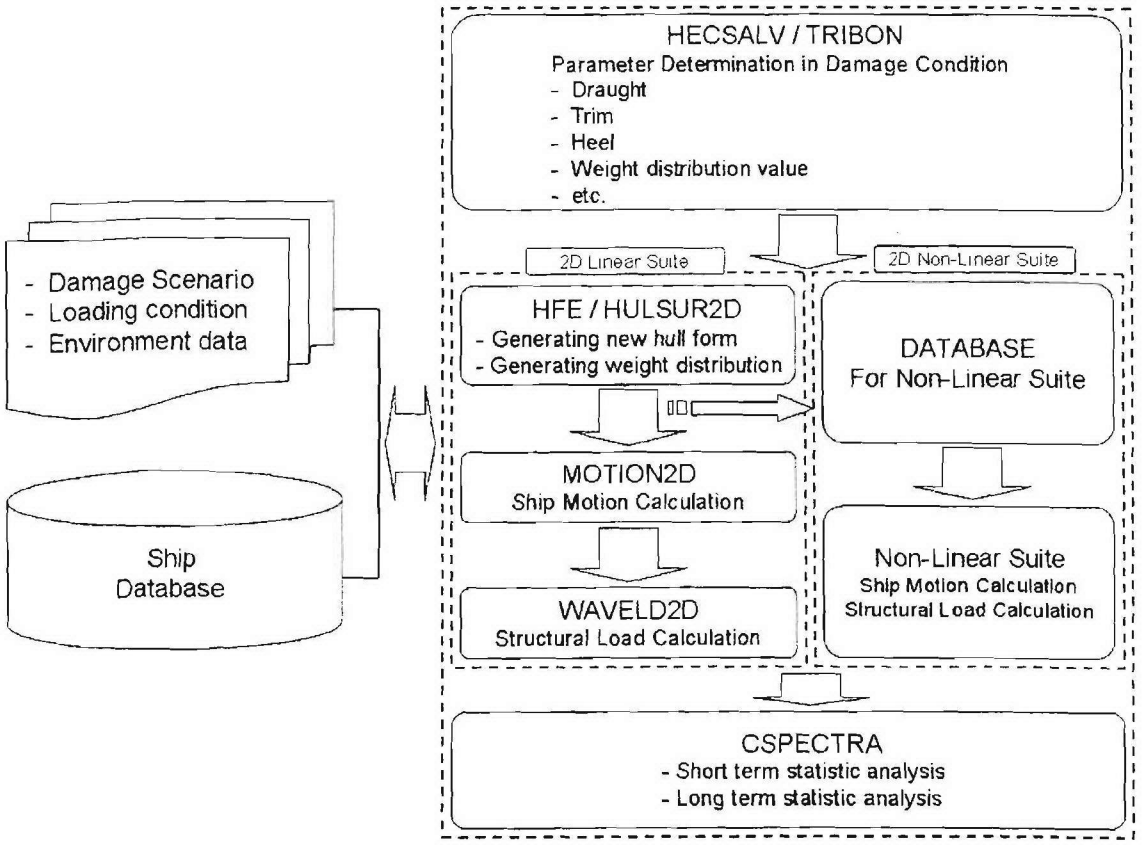

Figure 7.1-1: Computation procedure of UNEW Hydro Programme

7.1.1 Predictions of motions in intact and damage condition

The dynamic wave induced motion analysis of H5415 vessel was carried out in various design conditions in six degree of freedom. Figures 7.1-2 to 7.1-6 show the comparison of dynamic motion responses in head waves. The comparison of dynamic motion responses in stern quartering waves and beam waves are presented in Figures 7.1-7 to 7.1-11 and Figures 7.1-12 to 7.1-16 respectively.

In head waves heave and pitch motion response amplitudes of the damaged ship are less than that of the intact ship except case 15 (damage scenario 4) as shown in Figures 7.1-3 and 7.1-5. This phenomenon may be due to loss of buoyancy and the draught of the damaged ship is deeper than that of the intact ship. The other components of motion response amplitudes were small values compared to heave and pitch motion responses. The response amplitudes of horizontal motion components under asymmetric damaged conditions are larger than those of the intact and symmetrical damaged conditions. However the values are still small (see Figures 7.1-2, 7.1-4 and 7.1-6).

In general motion response amplitudes under the damaged conditions are less than that of the intact condition as shown in Figures 7.1-7 to 7.1-11 under stern quartering waves. Roll and pitch motion response amplitudes of the ship with damage at fore body are slightly larger than that of the intact ship. In yaw motions the amplitude of the intact ship are less than those of the ship with damage amidships.

Figures 7.1-12 and 7.1-14 show that sway and roll response amplitudes of damage conditions are less than that of the intact condition. Vertical component response values in the intact ship larger than that of the damaged ship, as shown in Figures 7.1-13 and 7.1-15. Response amplitudes of the ship with damage at fore body are less than that of the intact ship. The results of the ship with damage amidships show the other way (see Figures 7.1-16).

7.1.1.1 Head waves

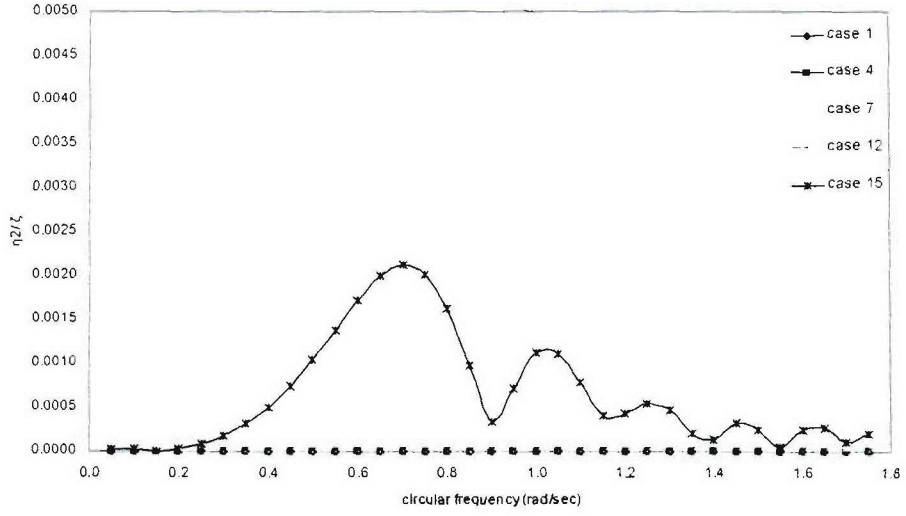

Figure 7.1-2: Sway RAO comparison at head waves

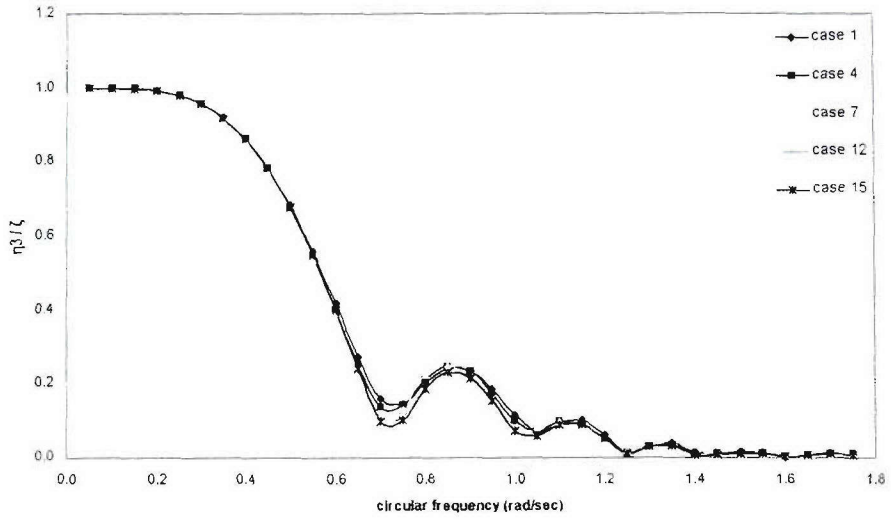

Figure 7.1-3: Heave RAO comparison at head waves

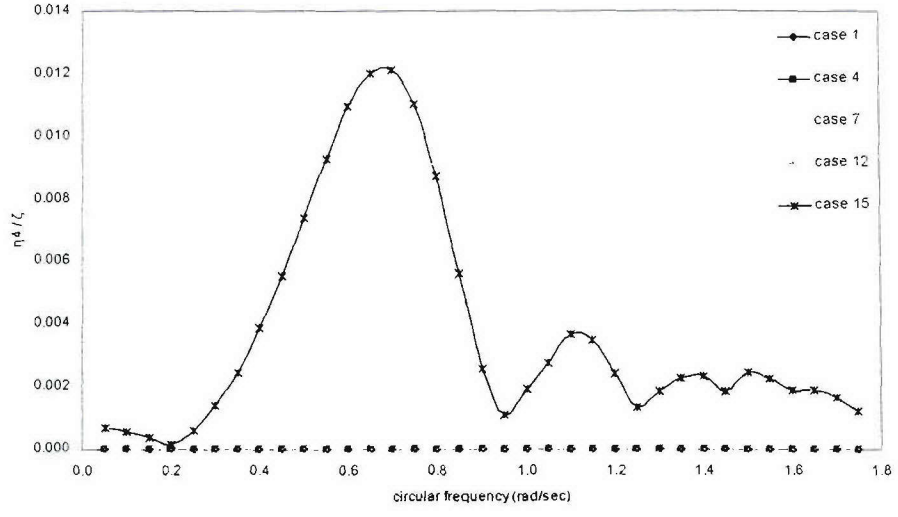

Figure 7.1-4: Roll RAO comparison at head waves

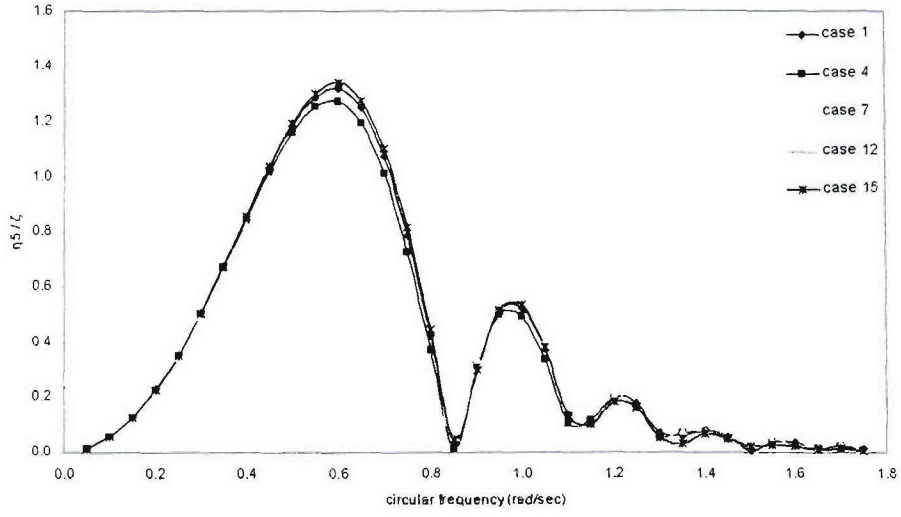

Figure 7.1-5: Pitch RAO comparison at head waves

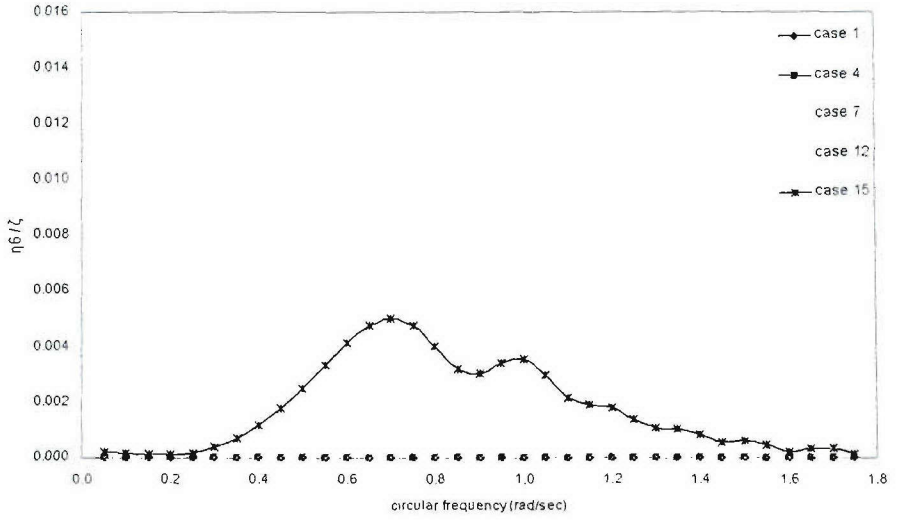

Figure 7.1-6: Yaw RAO comparison at head waves

7.1.1.2 Stern quartering waves

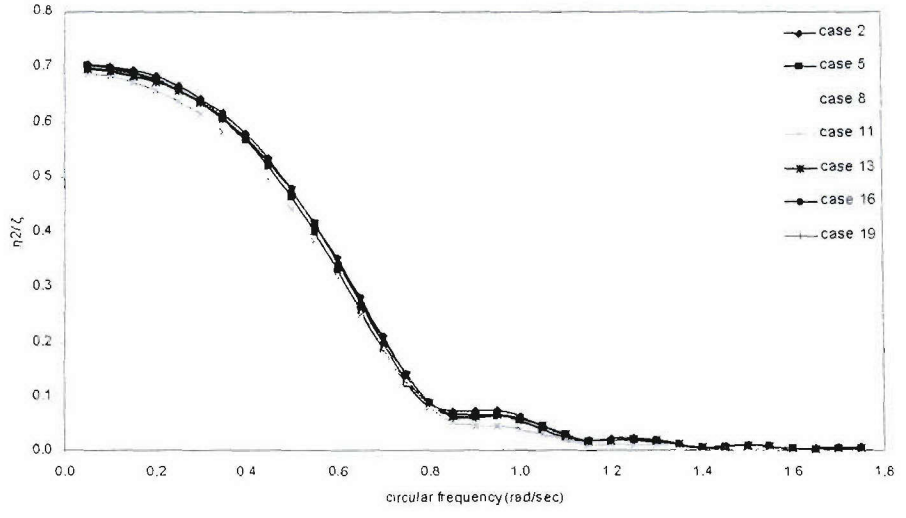

Figure 7.1-7: Sway RAO comparison at stern quartering waves

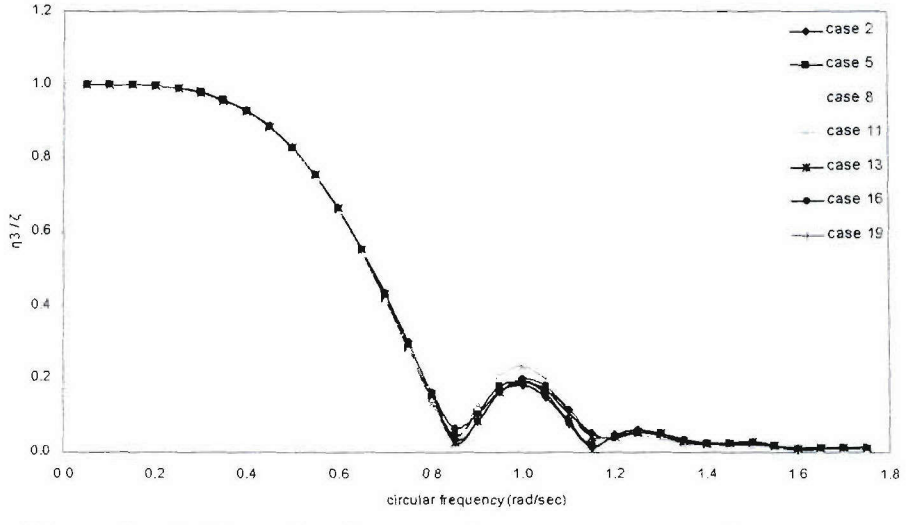

Figure 7.1-8: Heave RAO comparison at stern quartering waves

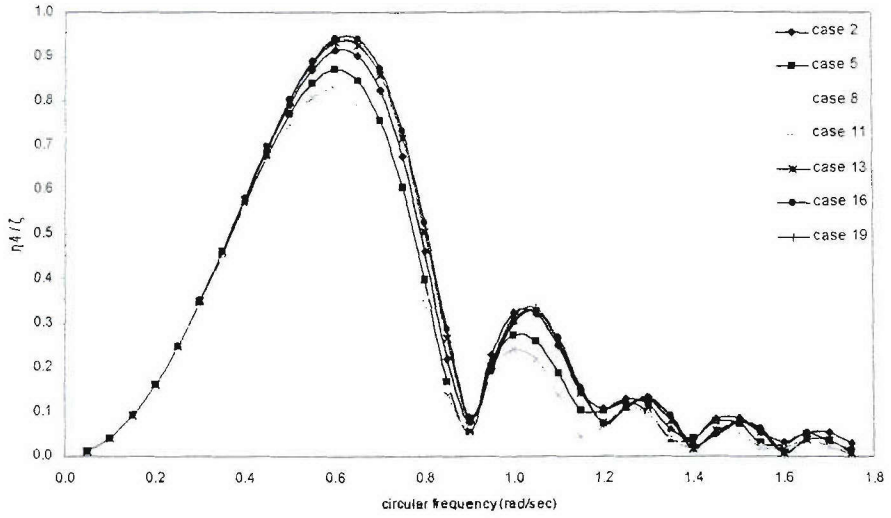

Figure 7.1-9: Roll RAO comparison at stern quartering waves

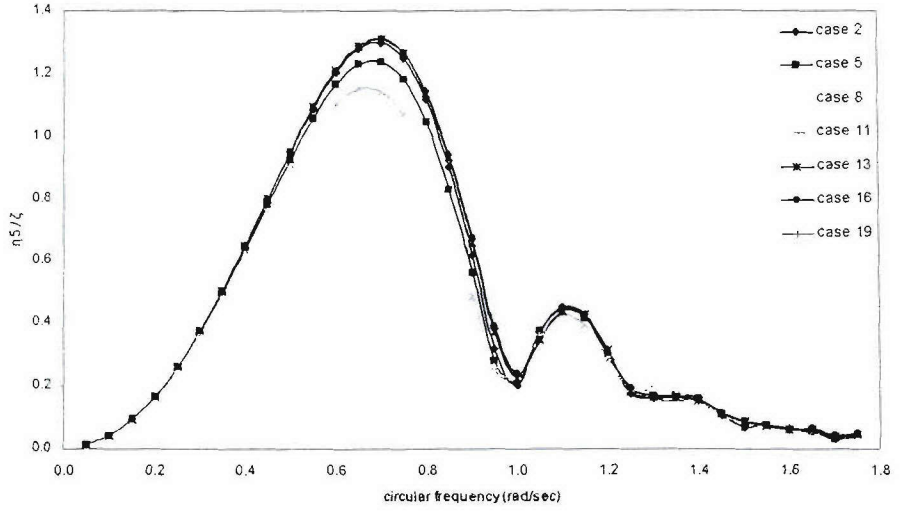

Figure 7.1-10: Pitch RAO comparison at stern quartering waves

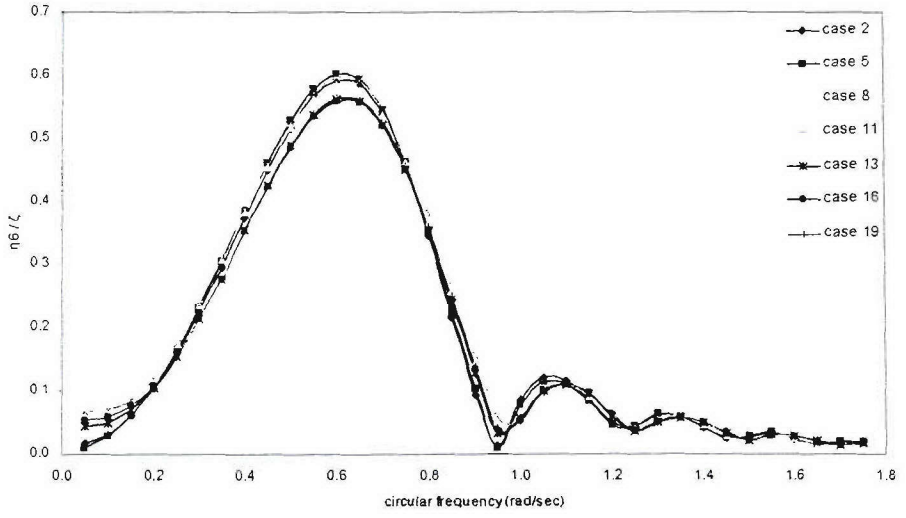

Figure 7.1-11: Yaw RAO comparison at stern quartering waves

7.1.1.3 Beam waves

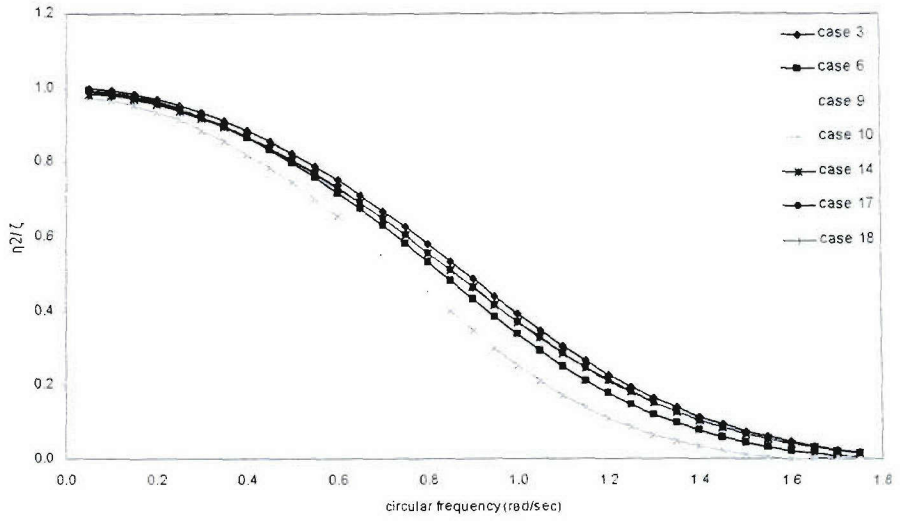

Figure 7.1-12: Sway RAO comparison at beam waves

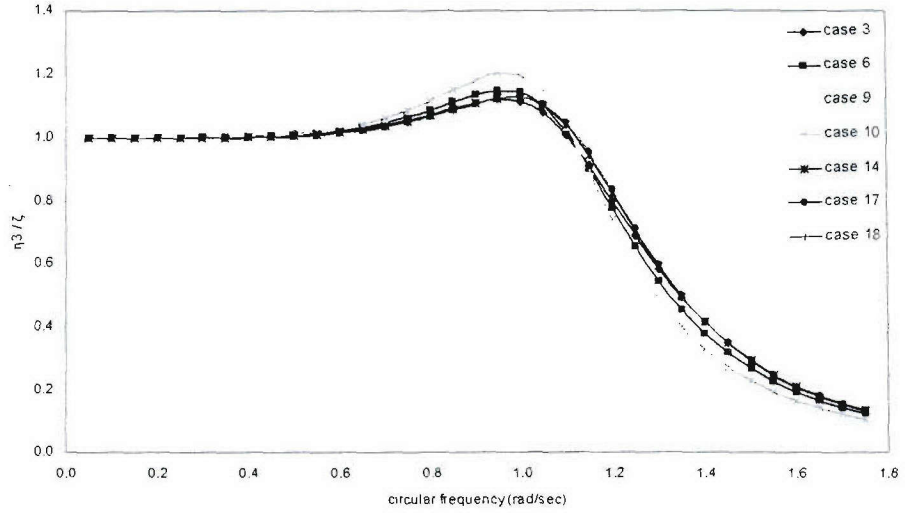

Figure 7.1-13: Heave RAO comparison at beam waves

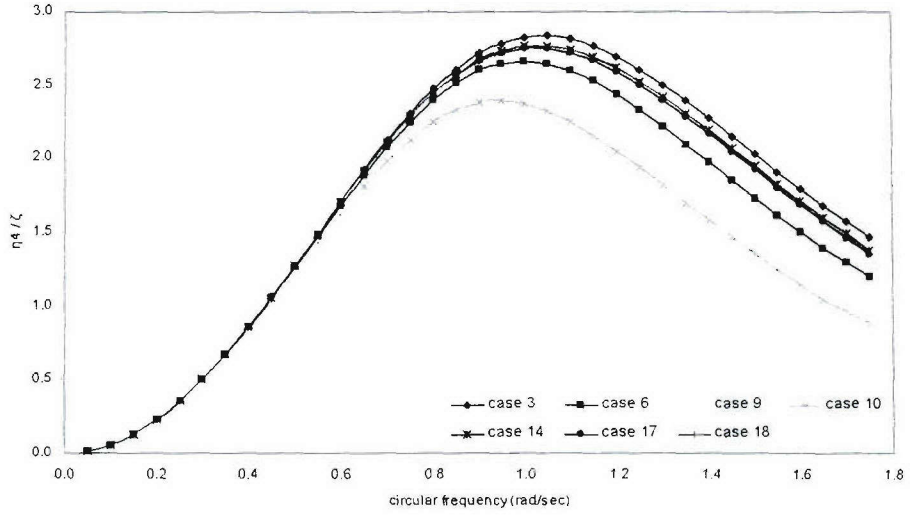

Figure 7.1-14: Roll RAO comparison at beam waves

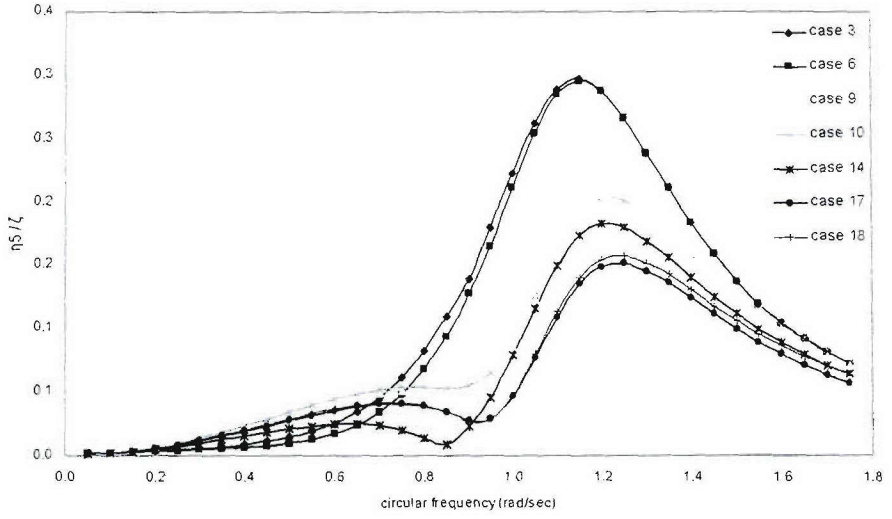

Figure 7.1-15: Pitch RAO comparison at beam waves

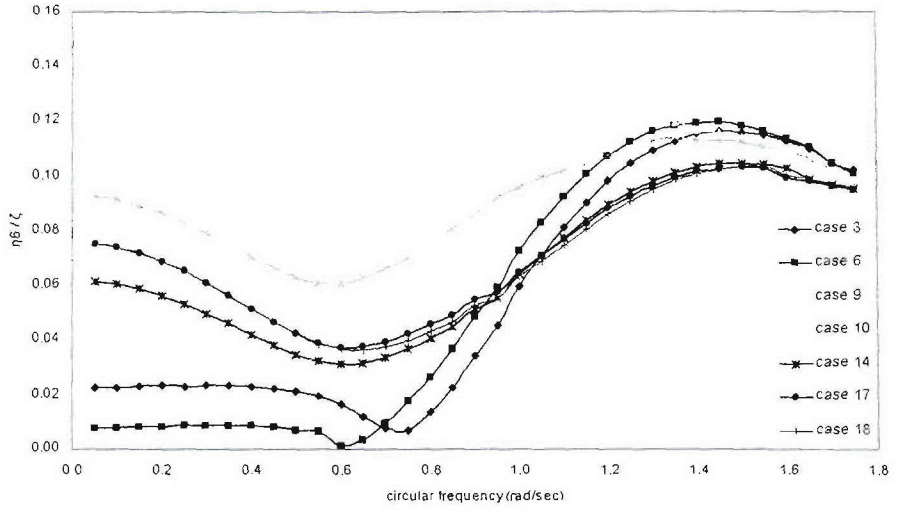

Figure 7.1-16: Yaw RAO comparison at beam waves

7.1.2 Weight distribution and global static loads

This section provides weight distribution, hydrostatic information for predicting motions and hydrodynamic loadings on the sample vessel 'H5415' using UNEW hydro suite as well as global static loads. The data in this part serves as the basis for all the numerical calculations so that the comparison would be made on the same ground.

Figure 7.1-17 shows H5415 vessel modelled for initial hydrostatic information of UNEW Hydro programme using HECSALV. Weight distribution used in numerical computations for this study in intact H5415 vessel is shown in Figures 7.1-18 and 7.1-19. The weight distribution of H5415 in full loading departure is used. So far the fuel oil to reflect burn off prior to the incident was not considered in modeling and computations. Tables 7.1-1 to 7.1-4 describe flooding summaries on different damage scenarios. The details of intact and damaged conditions investigated are shown in Table 7.1-5. More details on the sample vessel and damage scenarios can be found in chapters 5 and 6. Table 7.1-7 shows information of draught and hydrostatics at equilibrium in intact and damaged conditions. And intact stability and trim summary are given in Table 7.1-6.

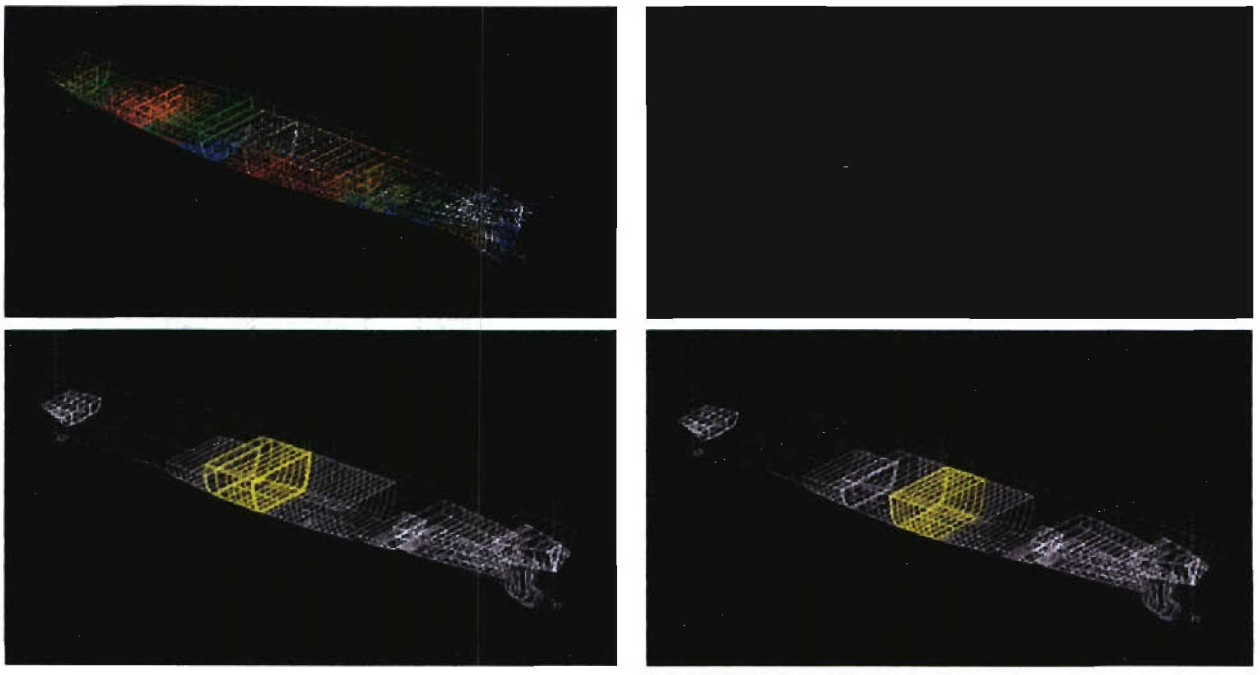

Figure 7.1-17: H5415 vessel modelled for initial hydrostatic information of UNEW Hydro programme using HECSALV

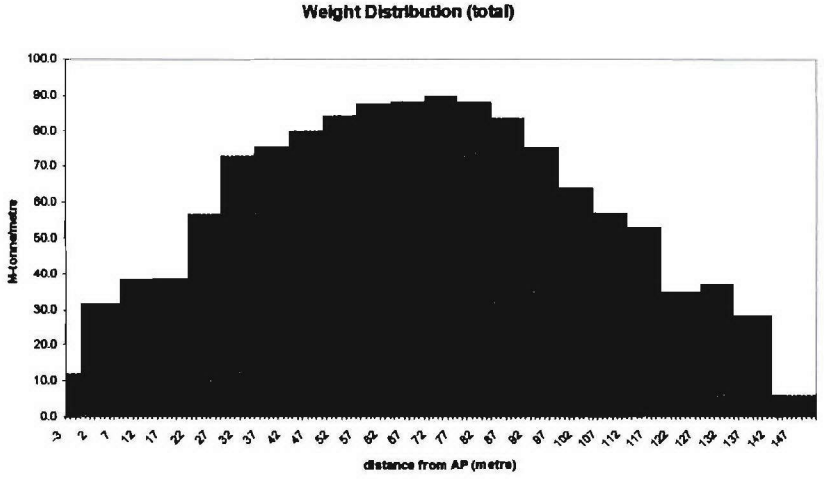

Figure 7.1-18: Weight distribution of intact 'H5415' vessel (I)

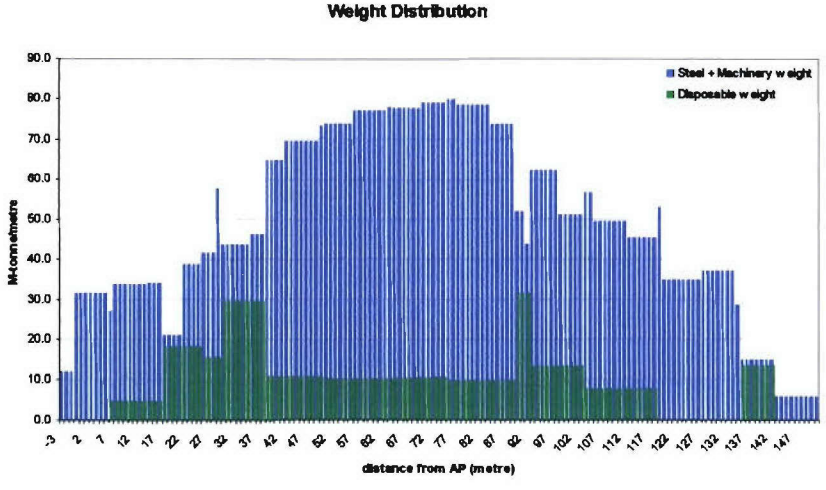

Figure 7.1-19: Weight distribution of intact 'H5415' vessel (II)

Table 7.1-1: Flooding summary on damage scenario 1

For equilibrium at 0.0 deg.

Compartment	Seawater MT	Oil MT	Perm.	Density MT/m3	VCG m	LCG m-AP	TCG m-CL	FSc m	Sounding m	Specified % Full	Pressure barG
MACH-2	797	----	0.850	1.0250	4.264	69.793F	0.000S	0.001	----	58.000	----
Totals	797	0			4.264	69.793F	0.000S	0.001			

Table 7.1-2: Flooding summary on damage scenario 2

For equilibrium at 1.1 deg. S

Compartment	Seawater MT	Oil MT	Perm.	Density MT/m3	VCG m	LCG m-AP	TCG m-CL	FSc m	Sounding m	Specified % Full	Pressure barG
MACH-2	921	----	0.850	1.0250	4.635	69.809F	0.117S	0.001	----	67.000	----
MACH-3	1,227	----	0.850	1.0250	4.741	81.929F	0.116S	0.001	----	68.000	----
FO-3CS	52	----	0.990	1.0250	0.883	69.793F	1.534S	0.000	----	100.000	----
FO-3S	37	----	0.990	1.0250	1.141	69.740F	4.671S	0.000	----	100.000	----
FO-4CS	67	----	0.990	1.0250	0.910	81.895F	1.511S	0.000	----	100.000	----
FO-4S	37	----	0.990	1.0250	1.187	81.221F	4.407S	0.000	----	100.000	----
Totals	2,342	0			4.390	76.686F	0.329S	0.001			

Table 7.1-3: Flooding summary on damage scenario 3

For equilibrium at 0.0 deg.

Compartment	Seawater MT	Oil MT	Perm.	Density MT/m3	VCG m	LCG m-AP	TCG m-CL	FSc m	Sounding m	Specified % Full	Pressure barG
MISC-5P	25	----	0.850	1.0250	1.099	123.590F	0.636P	0.000	----	100.000	----
MISC-5S	25	----	0.850	1.0250	1.099	123.590F	0.636S	0.000	----	100.000	----
SONAR	79	----	0.850	1.0250	-0.437	133.522F	0.000S	0.000	----	100.000	----
FOREPEAK-TK	95	----	0.990	1.0250	1.544	138.469F	0.000S	0.000	----	98.000	----
Totals	223	0			0.745	133.424F	0.000P	0.000			

Table 7.1-4: Flooding summary on damage scenario 4

For equilibrium at 0.4 deg. S

Compartment	Seawater MT	Oil MT	Perm.	Density MT/m3	VCG m	LCG m-AP	TCG m-CL	FSc m	Sounding m	Specified % Full	Pressure barG
SW-2CS	62	----	0.990	1.0250	1.017	96.161F	1.403S	0.000	----	100.000	----
SW-2S	12	----	0.990	1.0250	1.359	94.111F	3.834S	0.000	----	100.000	----
SW-3S	58	----	0.990	1.0250	1.337	110.293F	1.217S	0.000	----	100.000	----
MISC-5S	25	----	0.850	1.0250	1.099	123.590F	0.636S	0.000	----	100.000	----
SONAR	79	----	0.850	1.0250	-0.437	133.522F	0.000S	0.000	----	100.000	----
FOREPEAK-TK	97	----	0.990	1.0250	1.653	138.478F	0.000S	0.000	----	100.000	----
Totals	332	0			0.932	121.805F	0.659S	0.000			

Still water shear forces and bending moments are calculated by results of the difference between buoyancy and mass intensity along the ship length. In sign convention of vertical shear force and bending moment upward force on the cut of aft portion and sagging are positive. Maximum bending moment in the intact condition is hogging and occurs amidships while two peaks of vertical shear force have opposite sign and take place at the end of parallel middle body. The results of maximum bending moments and vertical shear forces in damage scenarios 3 and 4 show same trends. The values in damage scenarios 3 and 4 are greater than those of the intact ship. On the other hand, four peak points of vertical shear force and three peak points of vertical bending moment are shown in damage conditions amidships (damage scenarios 1 and 2). The second and third peak of vertical shear forces occur at the ends of the damaged compartment with upward shear at the aft end and downward shear at the fore end because buoyancy is larger than weight at stern and flooding water is in the damaged compartment. In addition the magnitude of the maximum shear force in damage scenario 2 is larger than that in the intact condition and other damaged conditions. And also the ship in

damage condition 2 suffers from sagging bending moment amidships and hogging bending moment in the rest of the ship.

Table 7.1-5: Intact and damage conditions investigated

Intact and Damaged Conditions to be Investigated								
Case	Condition	Displ. (tonne)	Mean draught (m)	Trim (m)	Heel (deg.)	Heading angle (deg.)	M. Test	Computation
1	Intact	9032.2400	6.3094	0.0000	0.0000	180.0000	N/A	OK
2	Intact	9032.2400	6.3094	0.0000	0.0000	45.0000	N/A	OK
3	Intact	9032.2400	6.3094	0.0000	0.0000	90.0000	N/A	OK
4	Damage Scenario 1	9905.0000	6.6830	0.2260F	0.0000	180.0000	N/A	OK
5	Damage Scenario 1	9905.0000	6.6830	0.2260F	0.0000	45.0000	N/A	OK
6	Damage Scenario 1	9905.0000	6.6830	0.2260F	0.0000	90.0000	N/A	OK
7	Damage Scenario 2	11450.0000	7.4175	1.4330F	1.100S	180.0000	OK	OK
8	Damage Scenario 2	11450.0000	7.4175	1.4330F	1.100S	45.0000	OK	OK
9	Damage Scenario 2	11450.0000	7.4175	1.4330F	1.100S	90.0000	OK	OK
10	Damage Scenario 2	11450.0000	7.4175	1.4330F	1.100S	270.0000	OK	OK
11	Damage Scenario 2	11450.0000	7.4175	1.4330F	1.100S	315.0000	OK	OK
12	Damage Scenario 3	9331.0000	6.4485	0.8370F	0.0000	180.0000	OK	OK
13	Damage Scenario 3	9331.0000	6.4485	0.8370F	0.0000	45.0000	OK	OK
14	Damage Scenario 3	9331.0000	6.4485	0.8370F	0.0000	90.0000	OK	OK
15	Damage Scenario 4	9439.0000	6.5055	1.0320F	0.400S	180.0000	N/A	OK
16	Damage Scenario 4	9439.0000	6.5055	1.0320F	0.400S	45.0000	N/A	OK
17	Damage Scenario 4	9439.0000	6.5055	1.0320F	0.400S	90.0000	N/A	OK
18	Damage Scenario 4	9439.0000	6.5055	1.0320F	0.400S	270.0000	N/A	OK
19	Damage Scenario 4	9439.0000	6.5055	1.0320F	0.400S	315.0000	N/A	OK

Table 7.1-6: Intact stability and trim summary

Stability Calculation			**Trim Calculation**		
KMt	9.470	metres	LCF Draft	6.310	metres
VCG	6.283	metres	LCB	70.078F	m-AP
GMt (Solid)	3.188	metres	LCF	64.482F	m-AP
FSc	0.061	metres	MT1cm	182.000	m-MT/cm
GMt (Corrected)	3.126	metres	Trim	0.000	m-F
			List	0.000	deg
Specific Gravity	1.025	MT/cu.m			
Drafts					
Draft at A.P.	6.310	metres			
Draft at M.S.	6.310	metres			
Draft at F.P.	6.310	metres			
Draft at Aft Marks	6.310	metres			
Draft at Mid Marks	6.310	metres			
Draft at Fwd Marks	6.310	metres			

Table 7.1-7: Draught and hydrostatics at equilibrium

	Intact condition	Damage scenario 1	Damage scenario 2	Damage scenario 3	Damage scenario 4	Unit
Draft at AP	6.310	6.570	6.701	6.030	5.990	metres
Draft at FP	6.310	6.796	8.134	6.867	7.021	metres
Trim	0.000	0.226F	1.433F	0.837F	1.032F	metres
Draft at Aft Marks	6.310	6.570	6.701	6.030	5.990	metres
Draft at Fwd Marks	6.310	6.796	8.134	6.867	7.021	metres
Static Heel Angle	0.000	0.000	1.1S	0.000	0.4S	deg
Total Weight	9032.240	9905.000	11450.000	9331.000	9439.000	MT
VCG	6.283	6.120	5.895	6.150	6.095	metres
LCG	70.078F	70.055F	71.429F	71.590F	71.895F	m-AP
TCG	0.000S	0.000S	0.067S	0.000P	0.023S	m-CL
Buoyancy	9032.240	9905.000	11450.000	9331.000	9439.000	MT
KB	3.743	3.963	4.386	3.809	3.842	metres
LCB	70.117F	70.057F	71.449F	71.604F	71.912F	m-AP
TCB	0.000S	0.000S	0.098S	0.000	0.040S	m-CL
KMt	9.470	9.431	9.409	9.434	9.426	metres
FSc	0.061	0.596	1.164	0.060	0.059	metres
GMt	3.126	2.675	2.314	3.181	3.229	metres

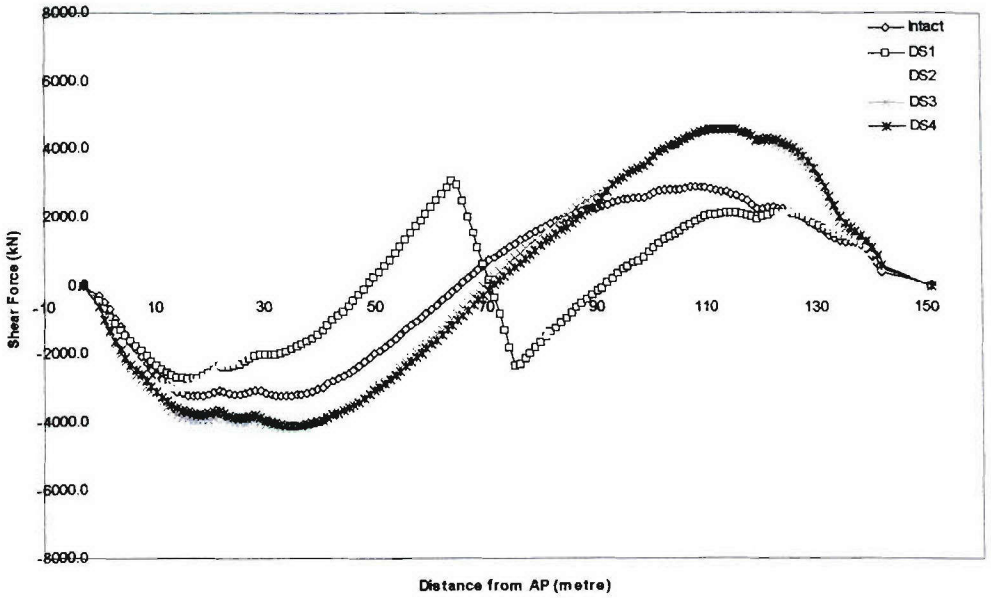

Figure 7.1-20: Distribution of static vertical shear force on H5415

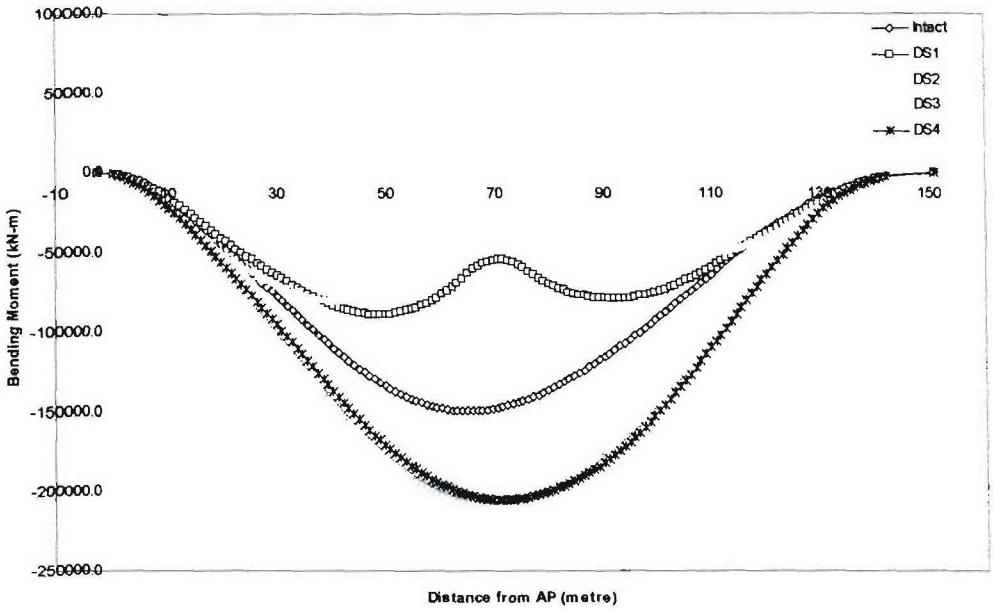

Figure 7.1-21: Distribution of static vertical bending moment on H5415

7.1.3 Predictions for global dynamic wave loads using 2D linear method

The results of global dynamic wave induced loads acting on HULL5415 in various design conditions using a 2D linear method are presented in this section. Design conditions investigated are shown in Table 7.1-5. The correlations between numerical calculations and experiments are described in section 7.2. In section 7.2 five global dynamic load components were considered for the purpose of validation. Here dynamic vertical bending moment, dynamic horizontal bending moment and torsion moment in an intact condition and four damaged conditions are displayed.

Figures 7.1-22 to 7.1-36 show dynamic vertical bending moments, dynamic horizontal bending moments and torsion moments in head waves. Global dynamic wave induced loads response amplitudes in stern quartering waves and beam waves are presented in Figures 7.1-37 to 7.1-57 and Figures 7.1-58 to 7.1-78 respectively. Base on the results of this section comparison and discussions of global dynamic wave loads in intact and damage conditions are presented in section 7.1.3.4.

7.1.3.1 Head waves

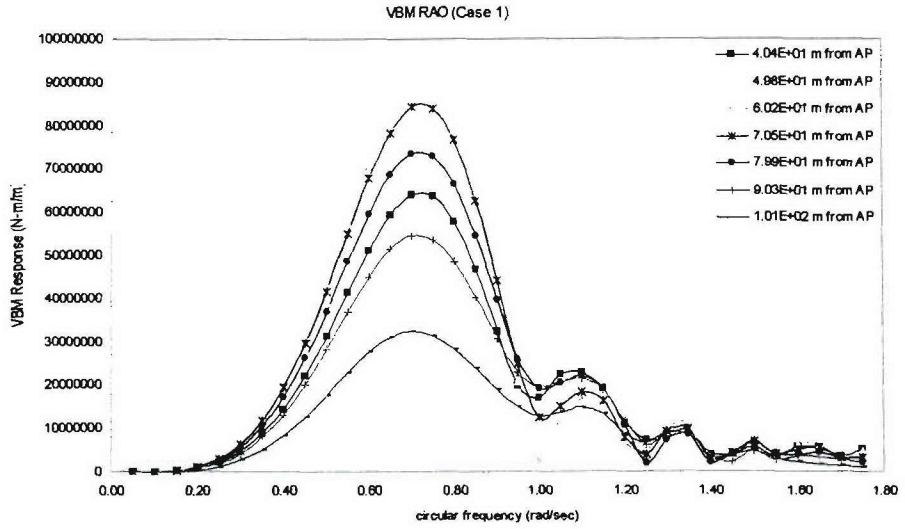

Figure 7.1-22: Vertical bending moment RAO at head waves

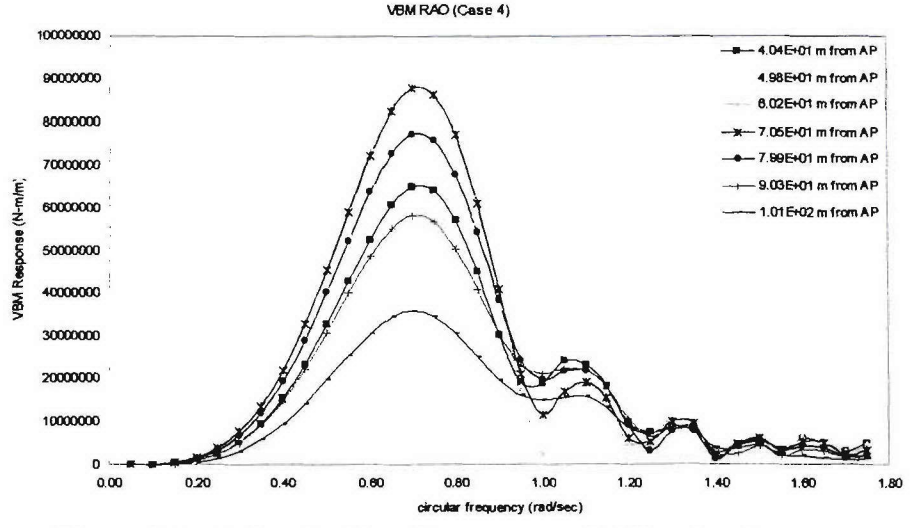

Figure 7.1-23: Vertical bending moment RAO at head waves

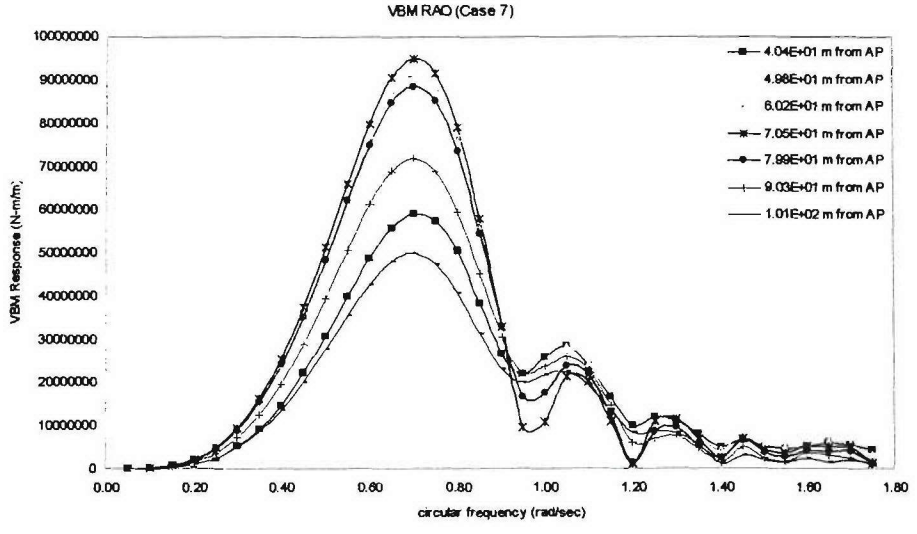

Figure 7.1-24: Vertical bending moment RAO at head waves

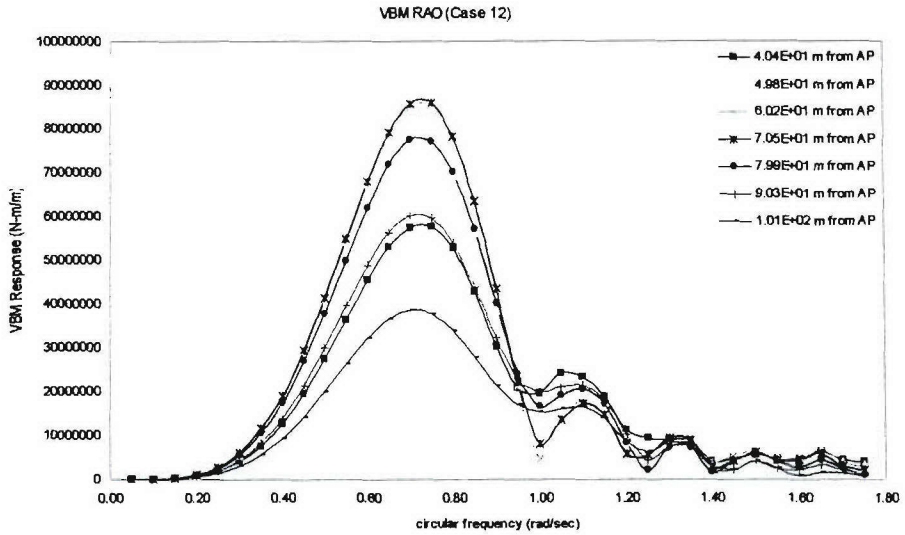

Figure 7.1-25: Vertical bending moment RAO at head waves

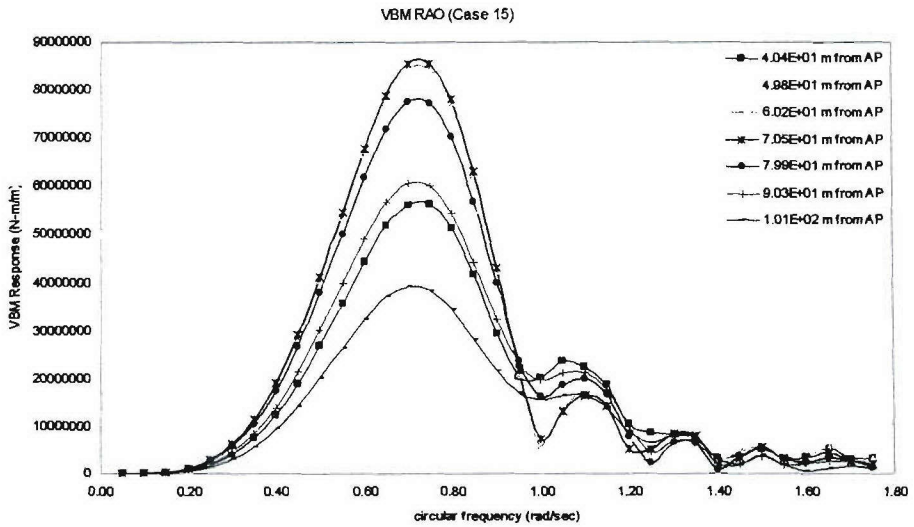

Figure 7.1-26: Vertical bending moment RAO at head waves

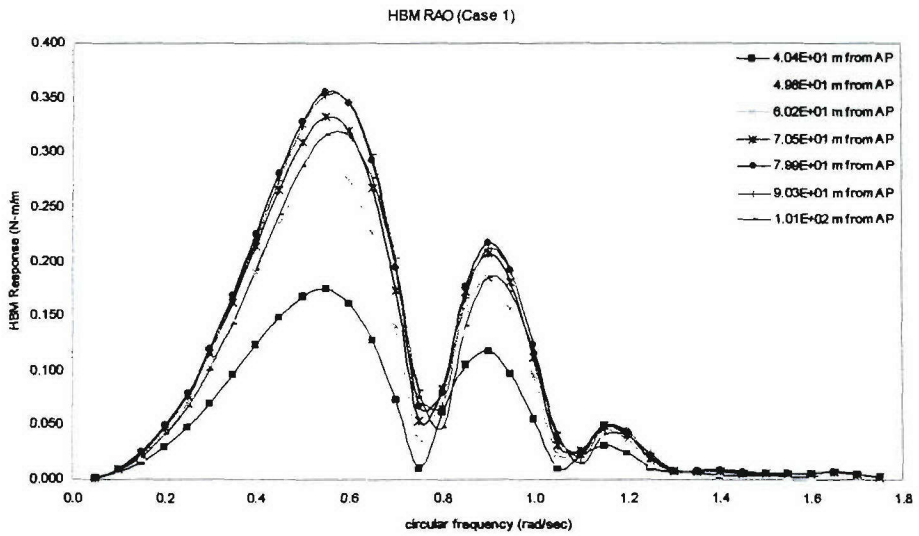

Figure 7.1-27: Horizontal bending moment RAO at head waves

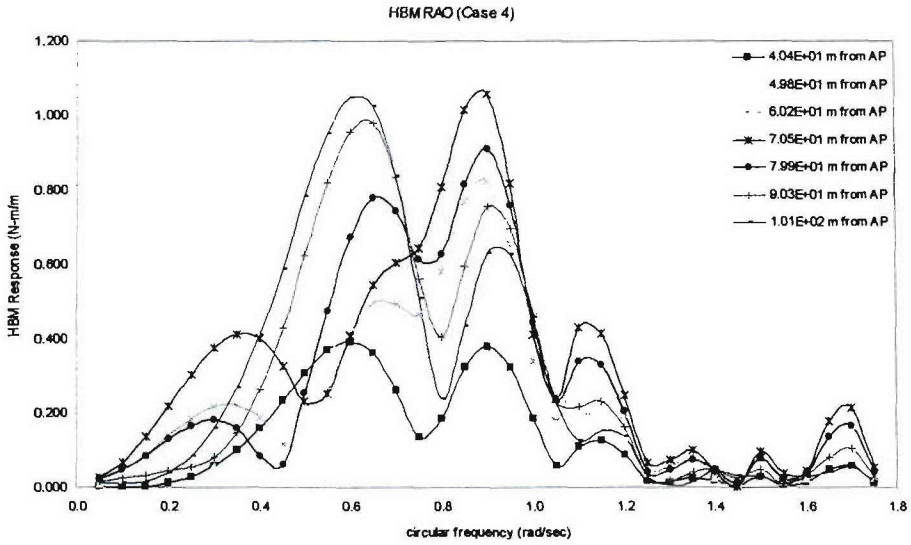

Figure 7.1-28: Horizontal bending moment RAO at head waves

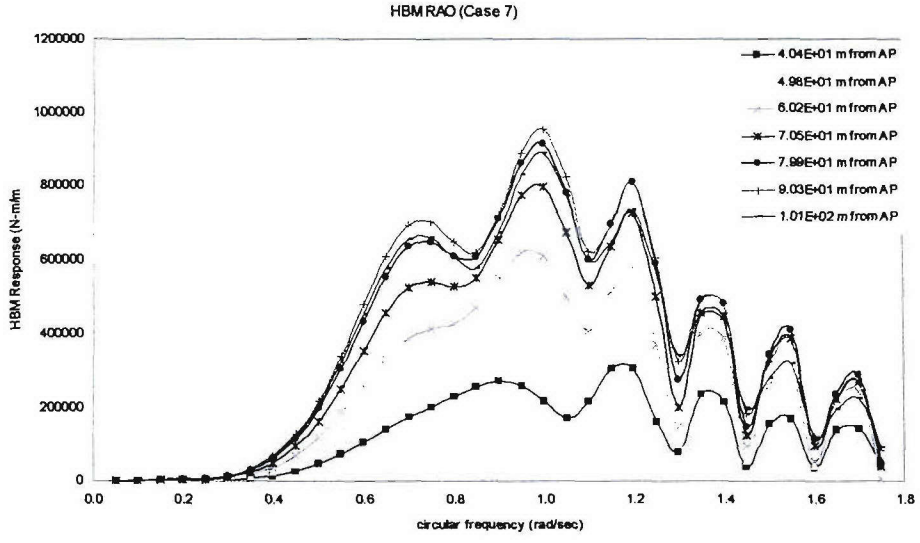

Figure 7.1-29: Horizontal bending moment RAO at head waves

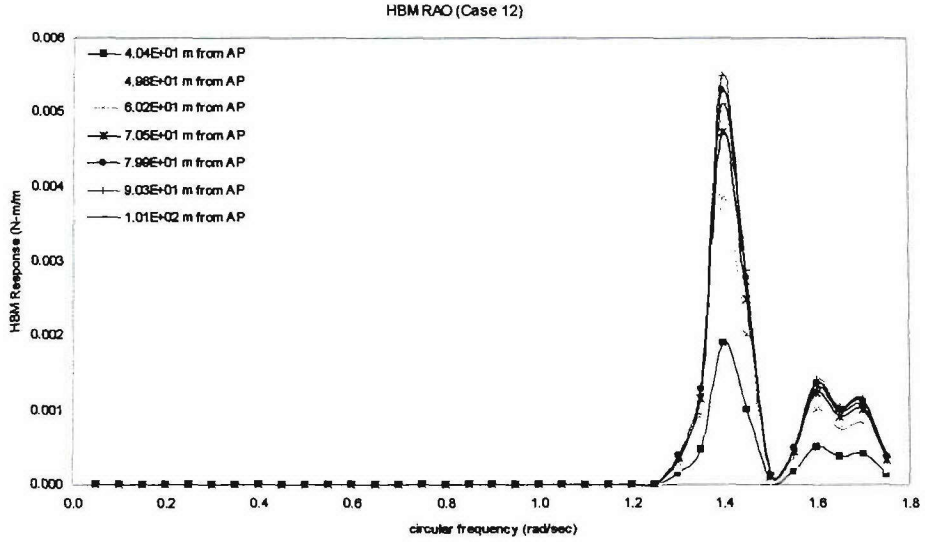

Figure 7.1-30: Horizontal bending moment RAO at head waves

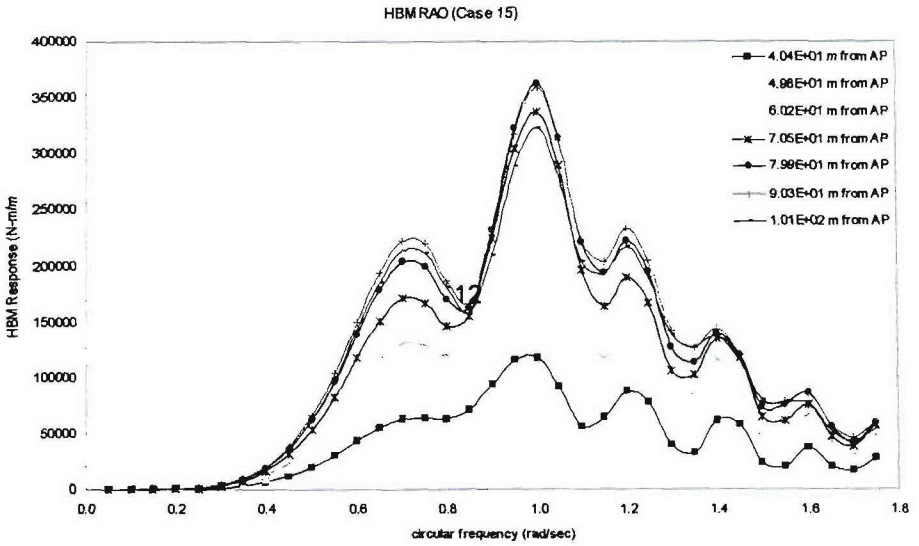

Figure 7.1-31: Horizontal bending moment RAO at head waves

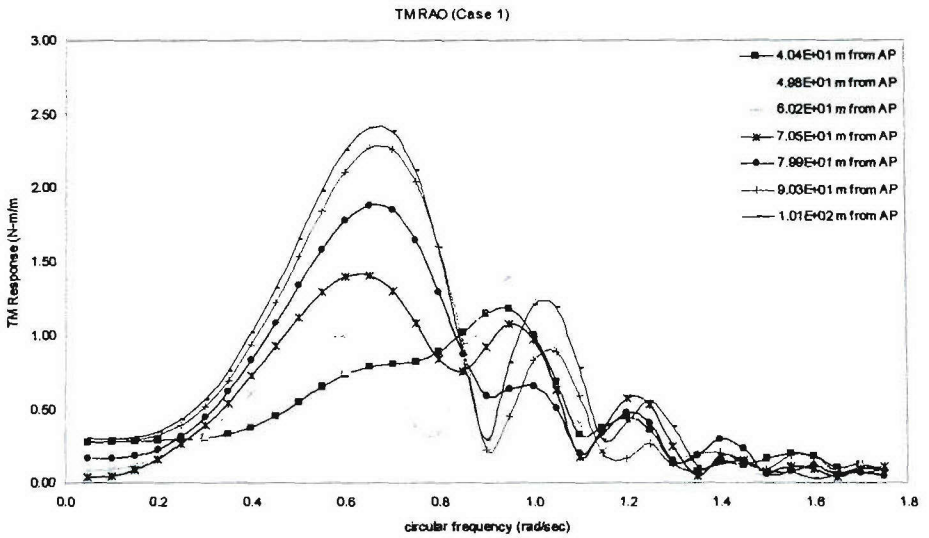

Figure 7.1-32: Torsion moment RAO at head waves

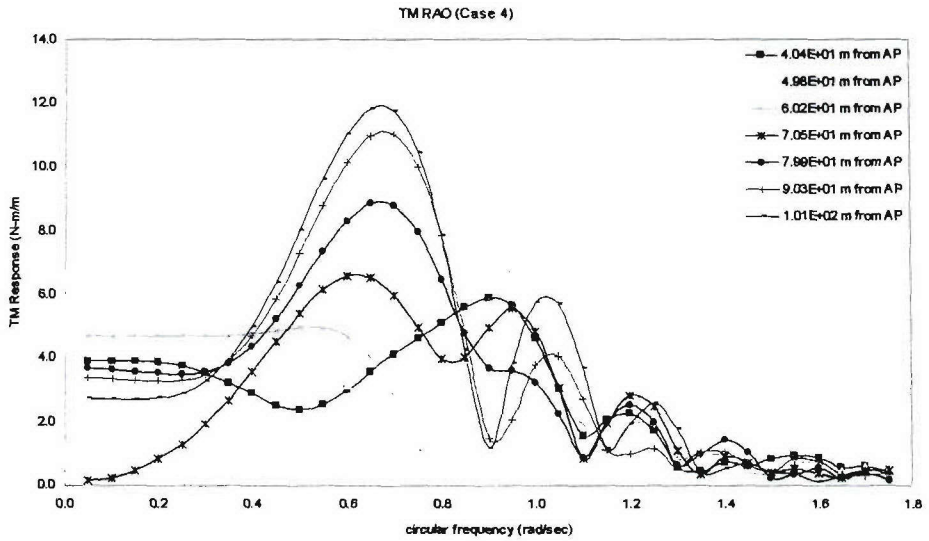

Figure 7.1-33: Torsion moment RAO at head waves

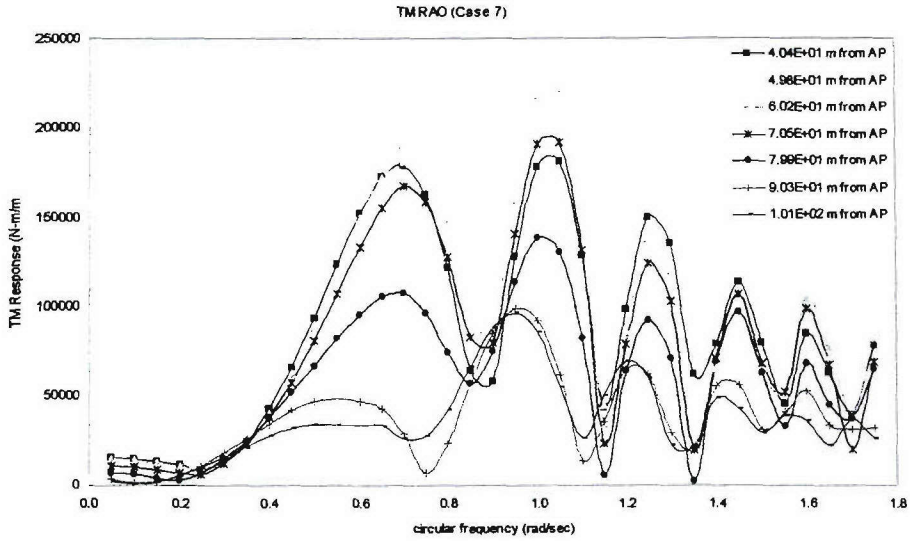

Figure 7.1-34: Torsion moment RAO at head waves

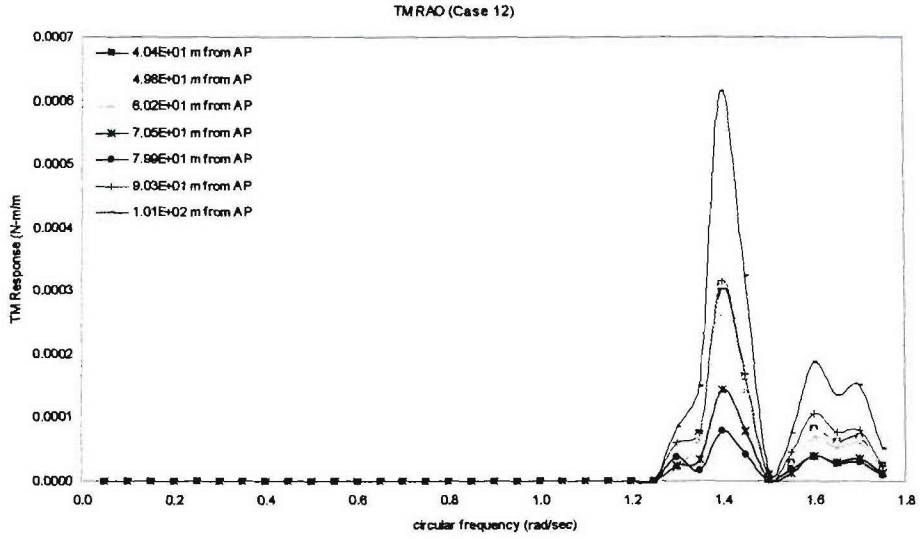

Figure 7.1-35: Torsion moment RAO at head waves

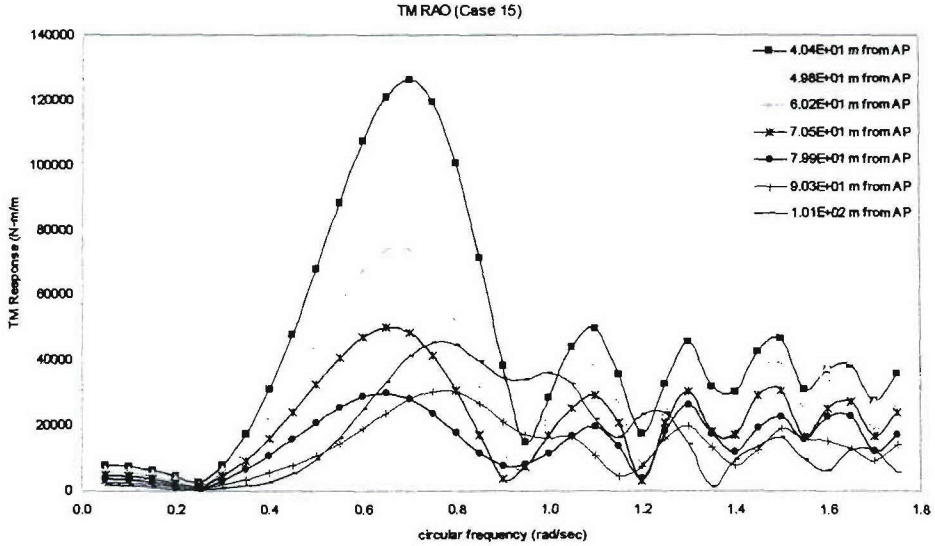

Figure 7.1-36: Torsion moment RAO at head waves

7.1.3.2 Stern quartering waves

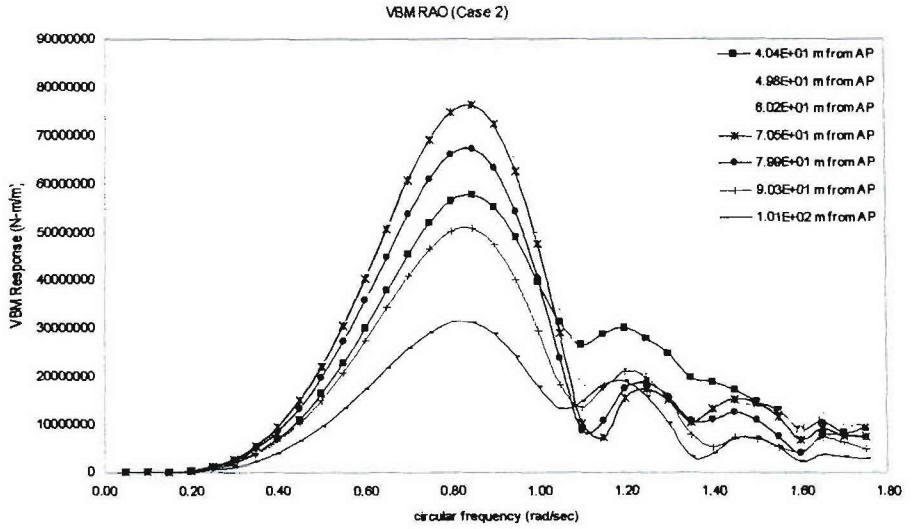

Figure 7.1-37: Vertical bending moment RAO at stern quartering waves

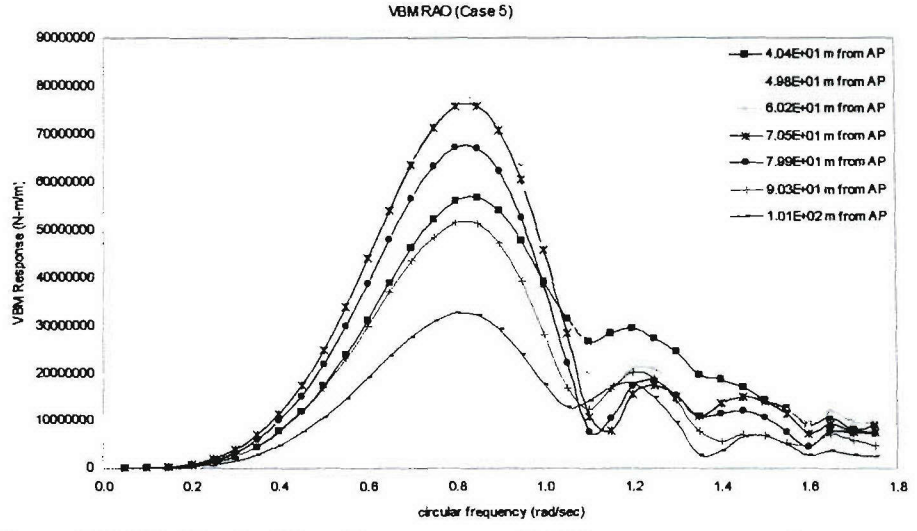

Figure 7.1-38: Vertical bending moment RAO at stern quartering waves

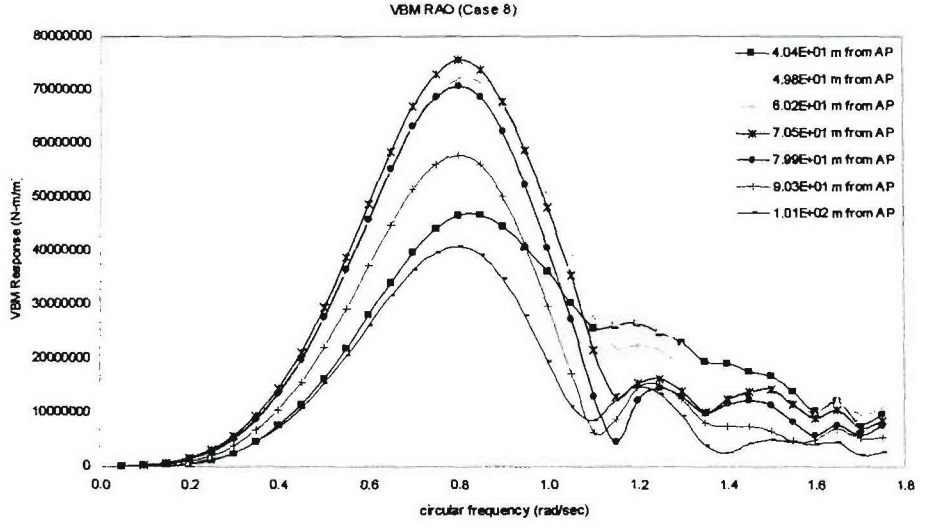

Figure 7.1-39: Vertical bending moment RAO at stern quartering waves

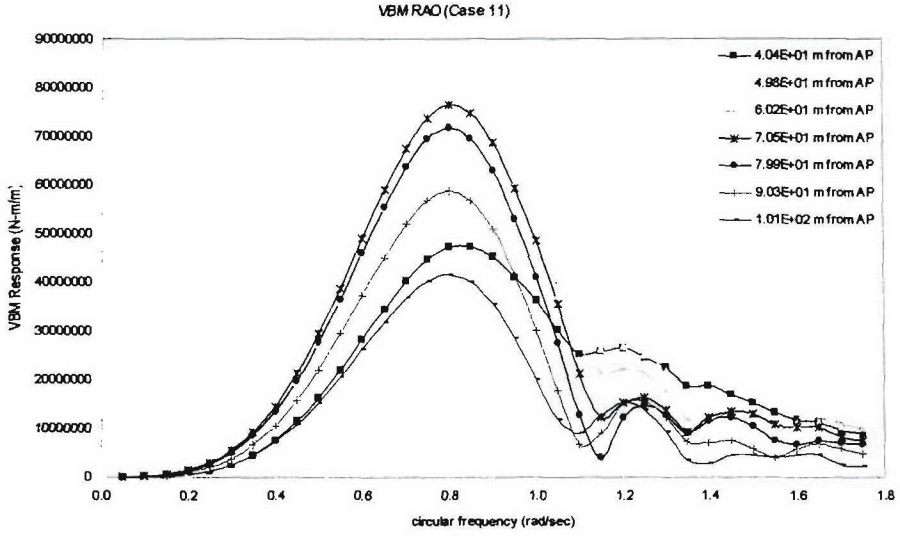

Figure 7.1-40: Vertical bending moment RAO at stern quartering waves

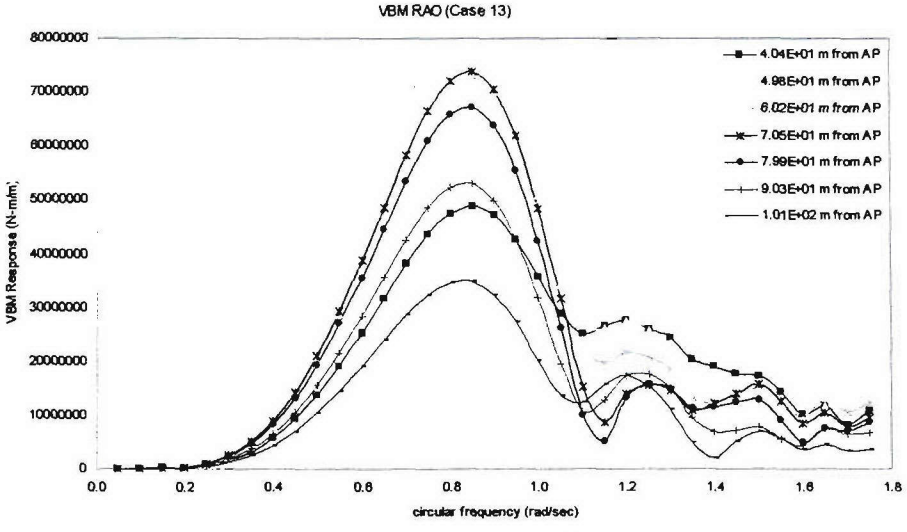

Figure 7.1-41: Vertical bending moment RAO at stern quartering waves

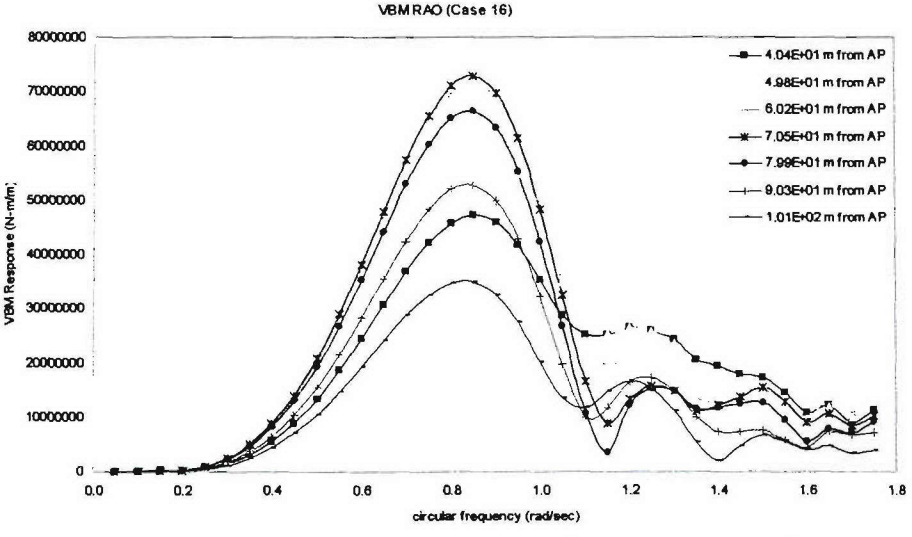

Figure 7.1-42: Vertical bending moment RAO at stern quartering waves

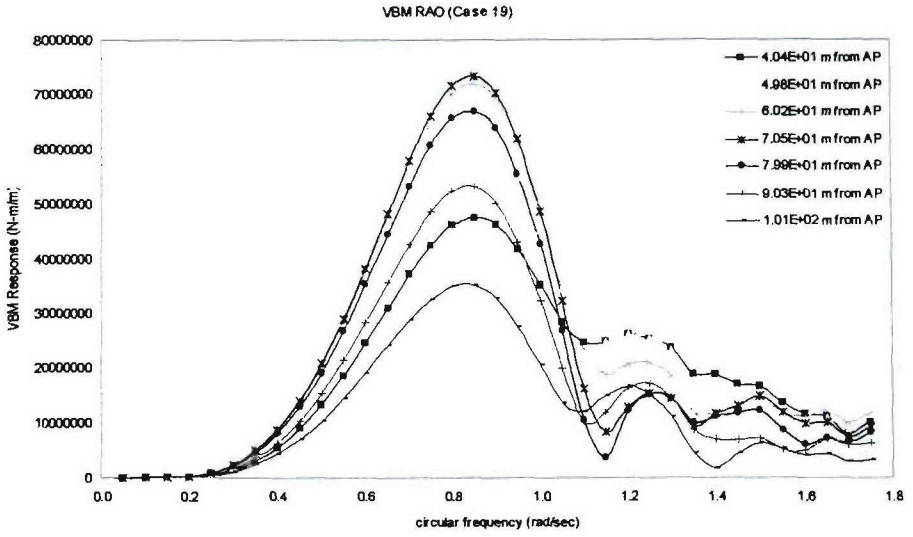

Figure 7.1-43: Vertical bending moment RAO at stern quartering waves

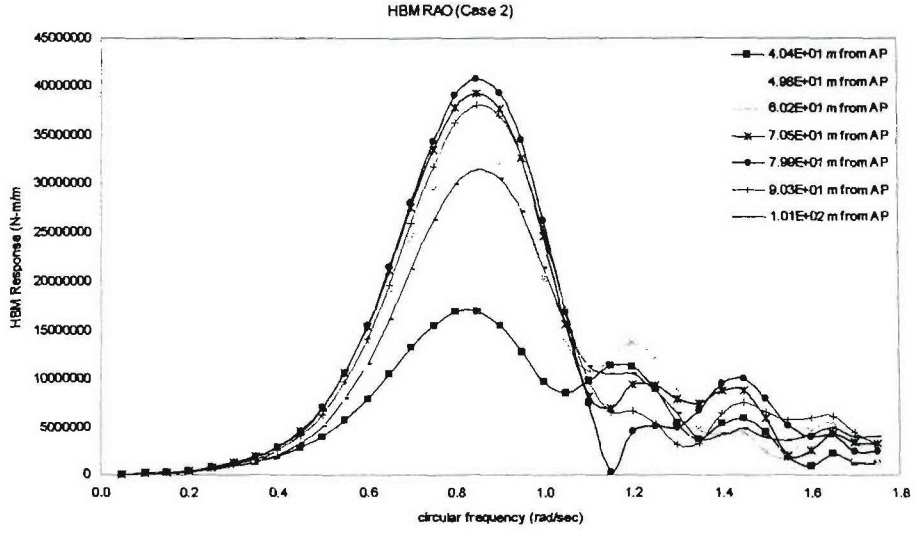

Figure 7.1-44: Horizontal bending moment RAO at stern quartering waves

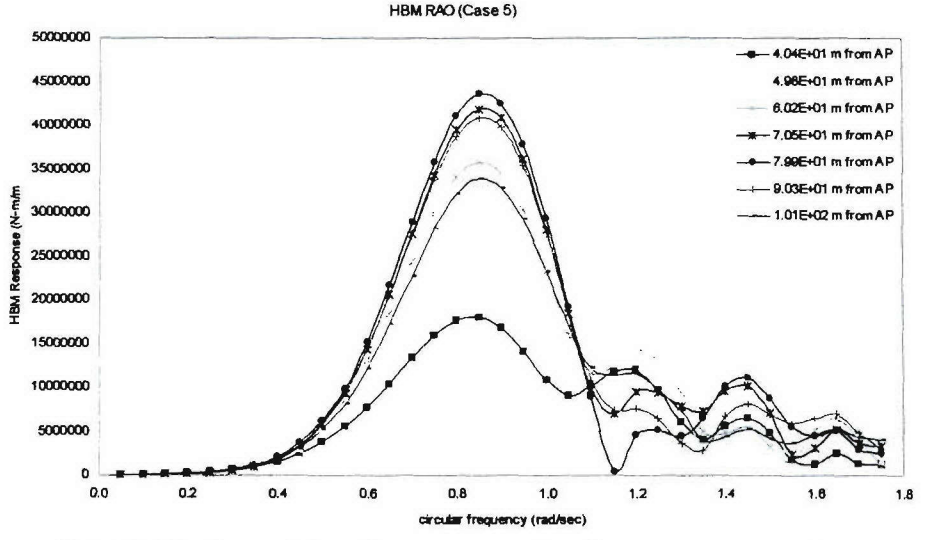

Figure 7.1-45: Horizontal bending moment RAO at stern quartering waves

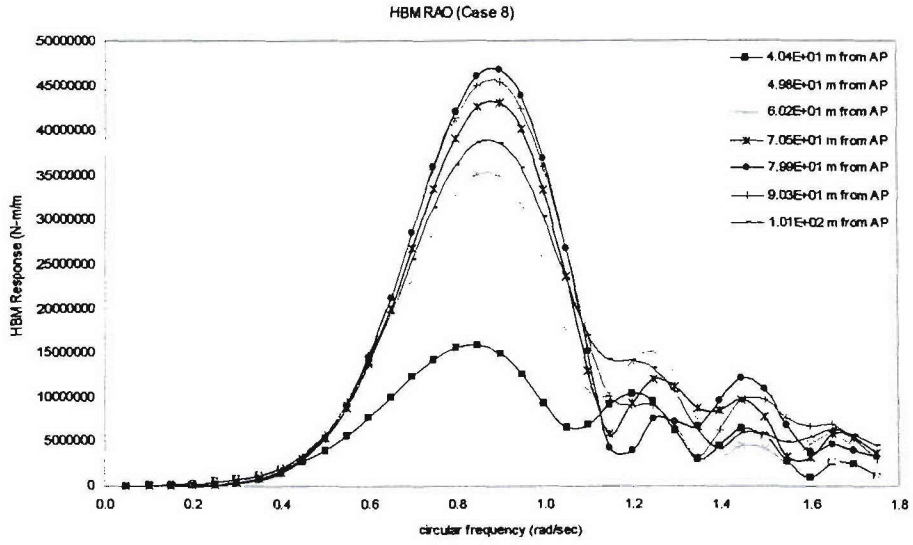

Figure 7.1-46: Horizontal bending moment RAO at stern quartering waves

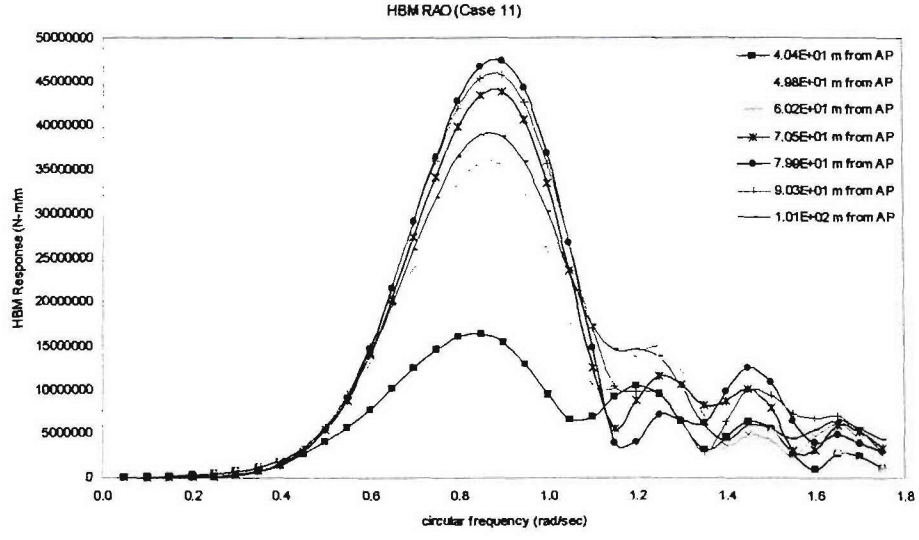

Figure 7.1-47: Horizontal bending moment RAO at stern quartering waves

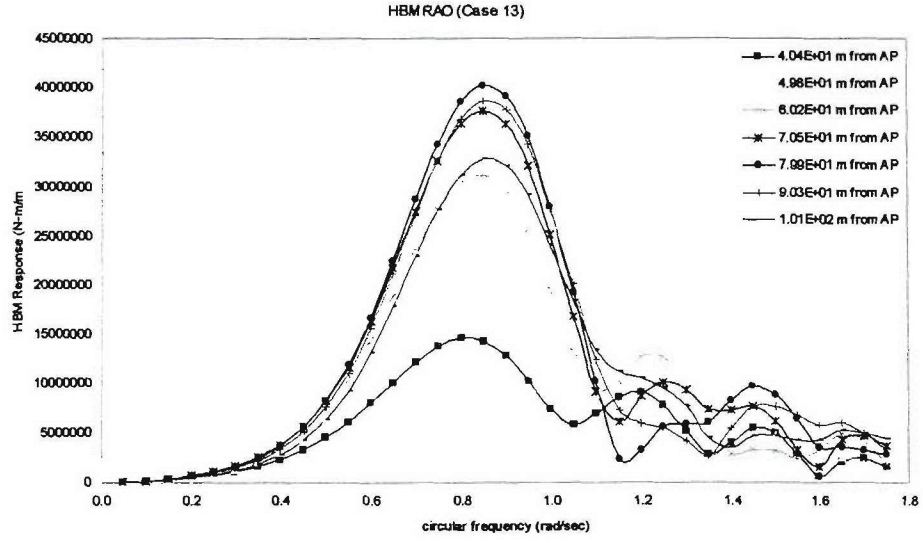

Figure 7.1-48: Horizontal bending moment RAO at stern quartering waves

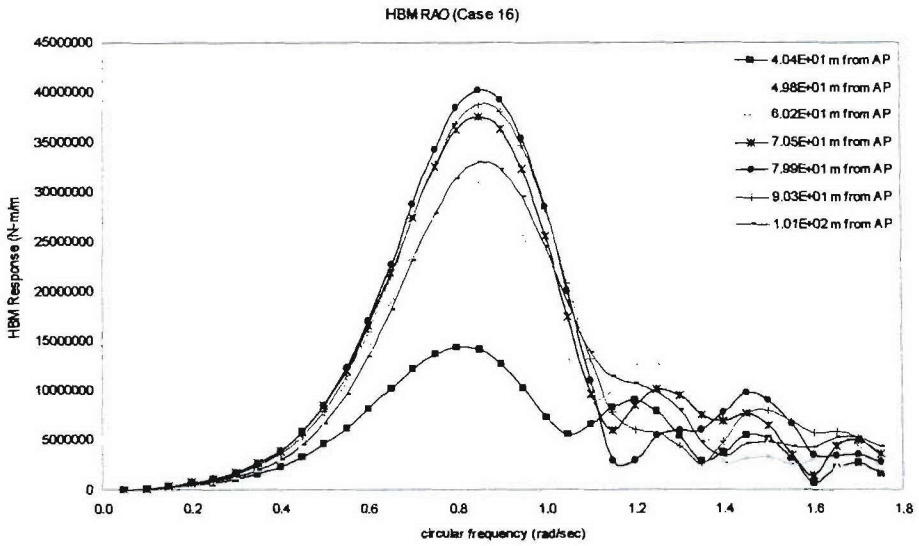

Figure 7.1-49: Horizontal bending moment RAO at stern quartering waves

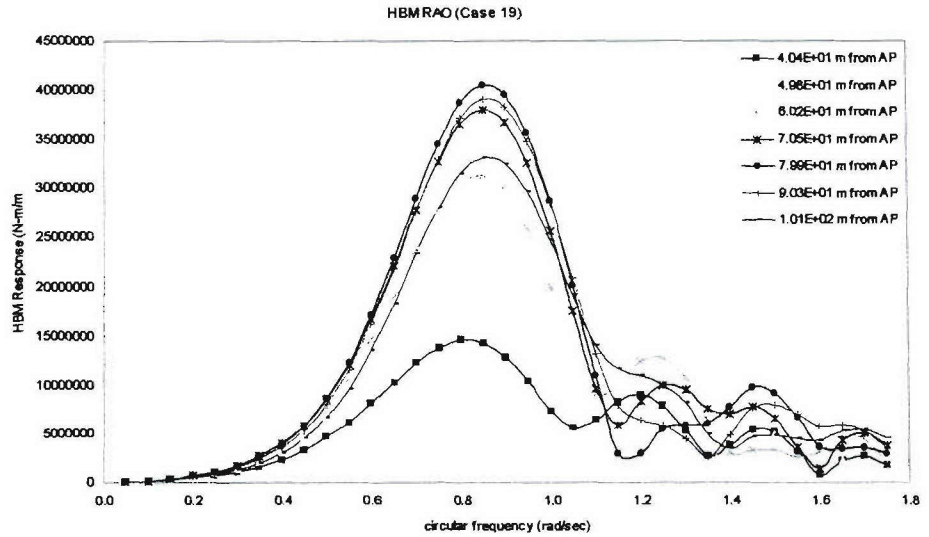

Figure 7.1-50: Horizontal bending moment RAO at stern quartering waves

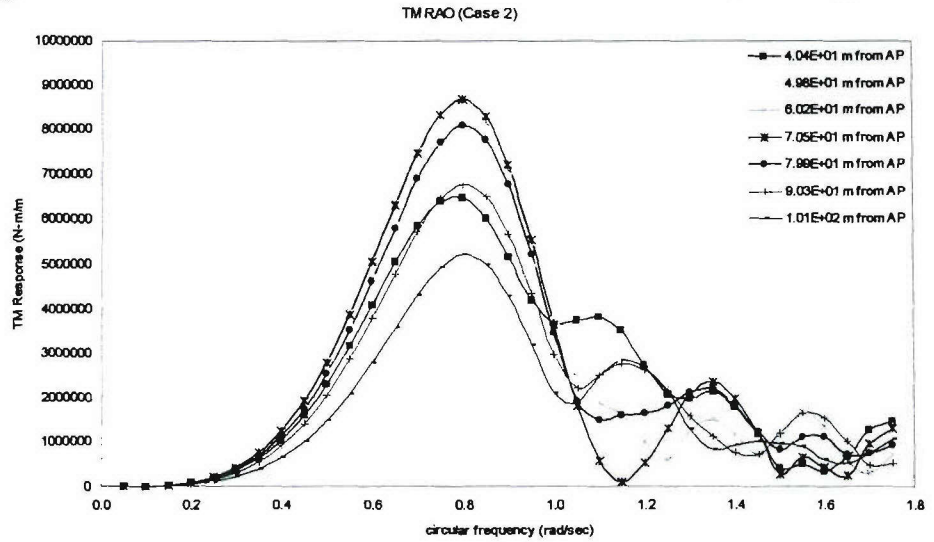

Figure 7.1-51: Torsion moment RAO at stern quartering waves

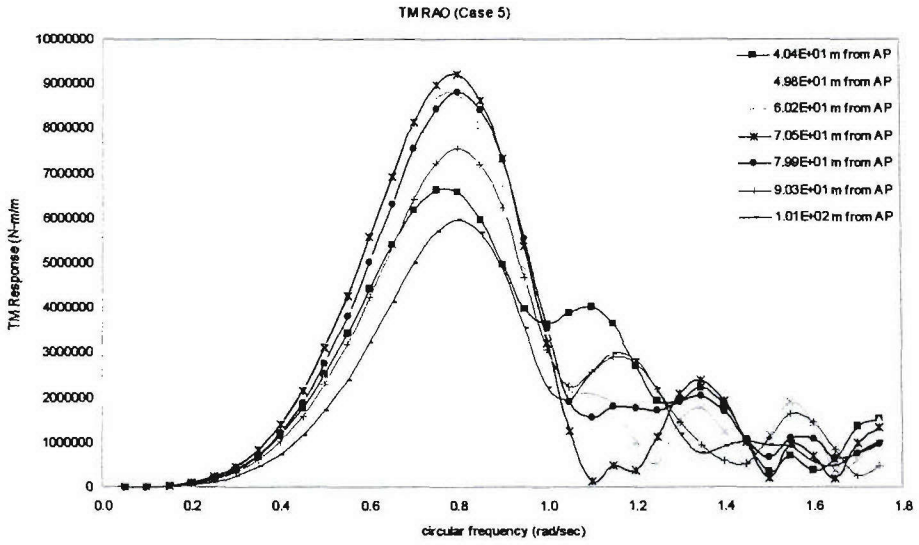

Figure 7.1-52: Torsion moment RAO at stern quartering waves

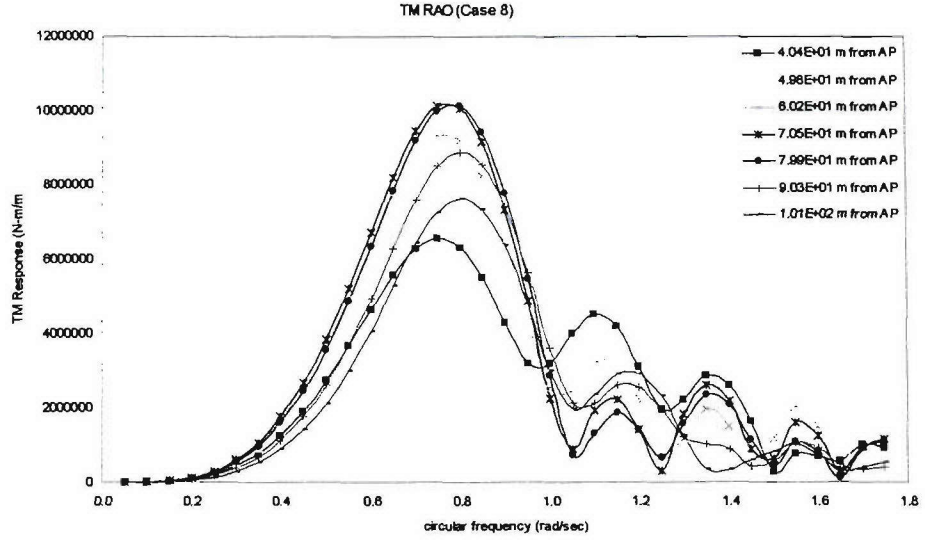

Figure 7.1-53: Torsion moment RAO at stern quartering waves

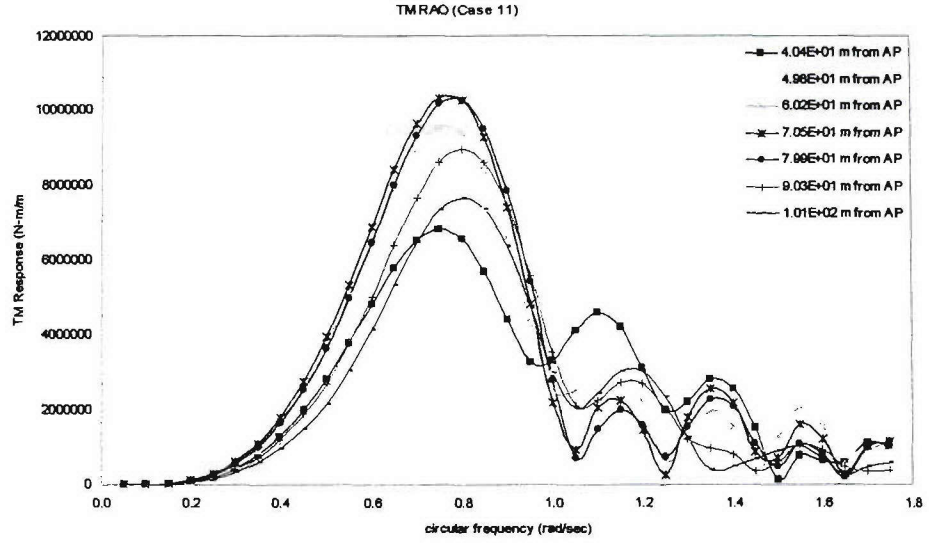

Figure 7.1-54: Torsion moment RAO at stern quartering waves

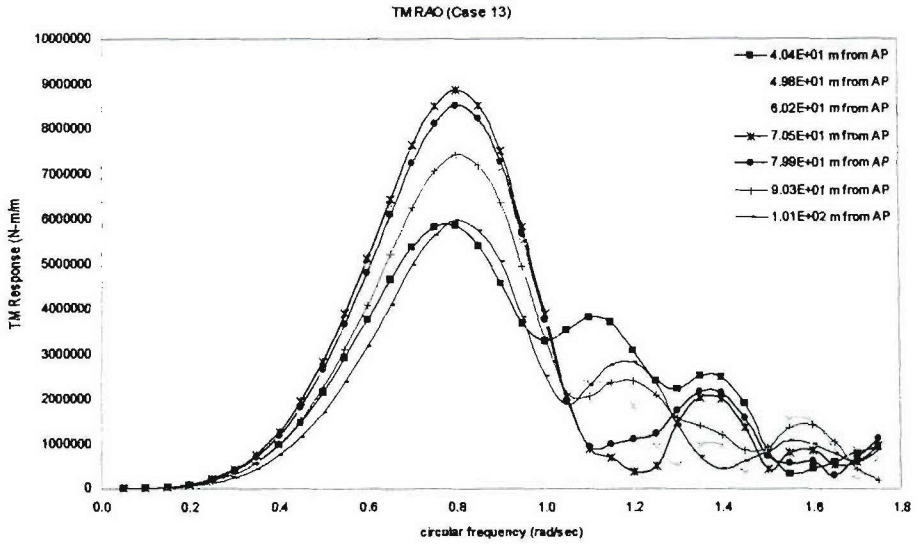

Figure 7.1-55: Torsion moment RAO at stern quartering waves

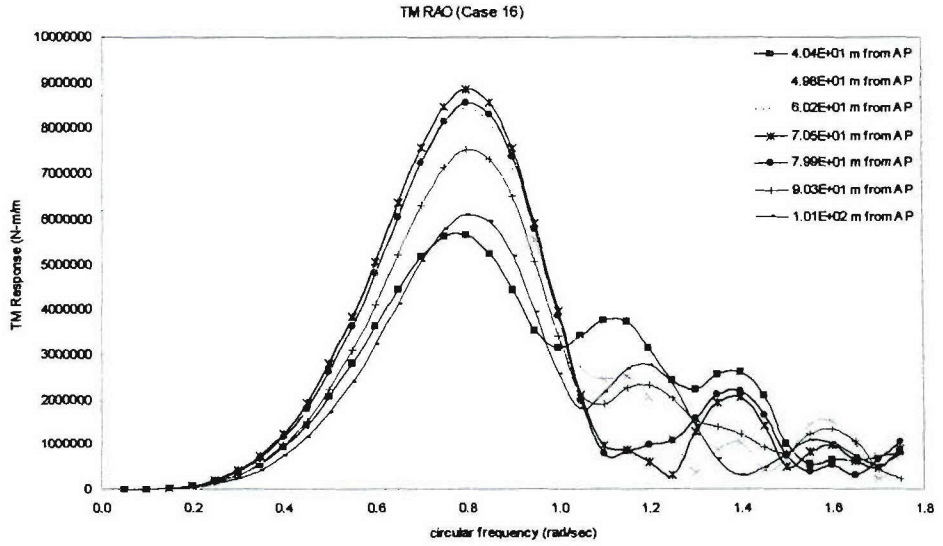

Figure 7.1-56: Torsion moment RAO at stern quartering waves

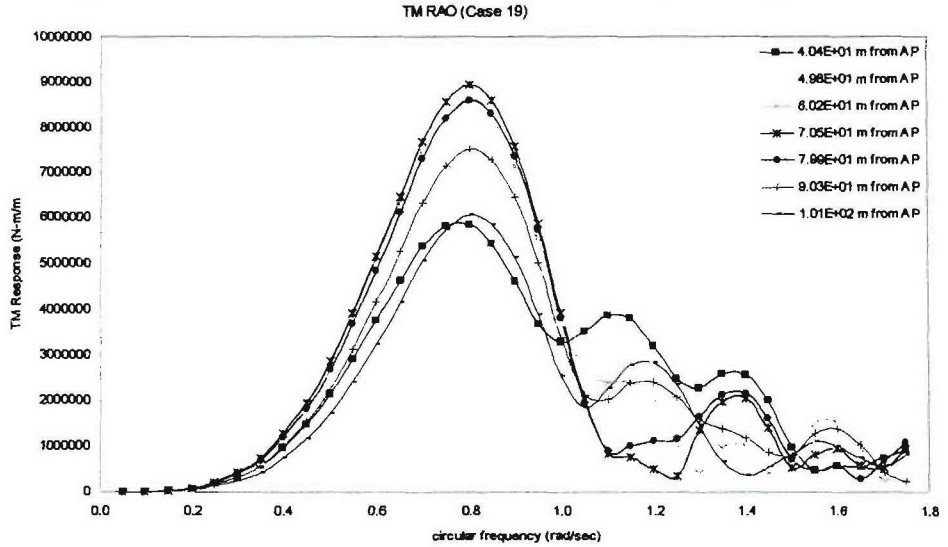

Figure 7.1-57: Torsion moment RAO at stern quartering waves

7.1.3.3 Beam waves

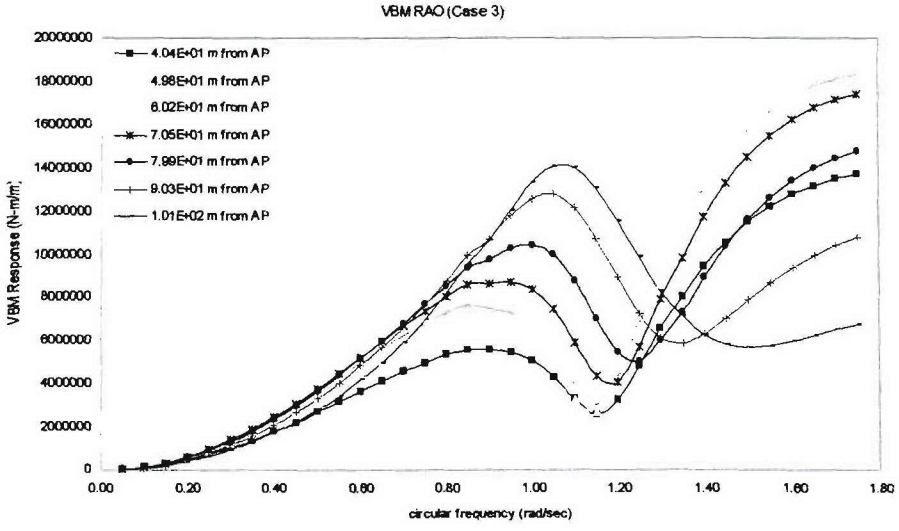

Figure 7.1-58: Vertical bending moment RAO at beam waves

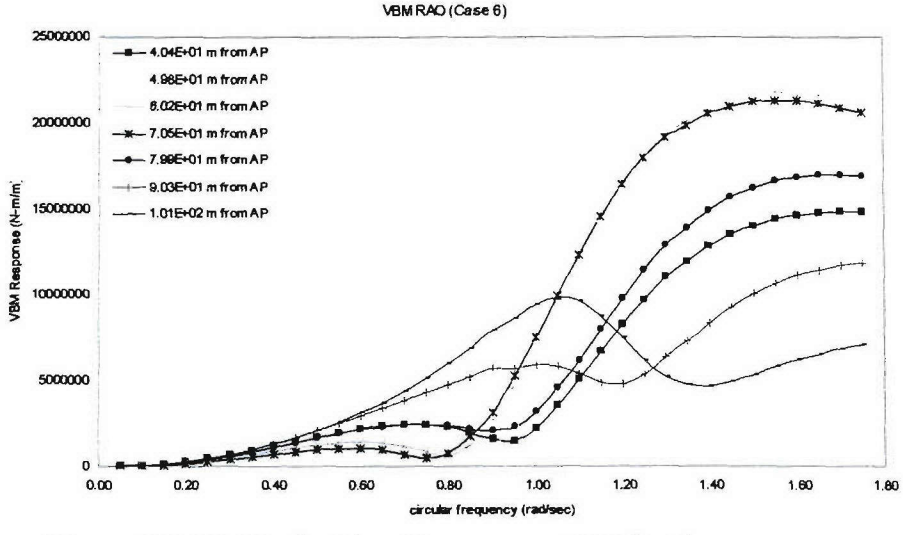

Figure 7.1-59: Vertical bending moment RAO at beam waves

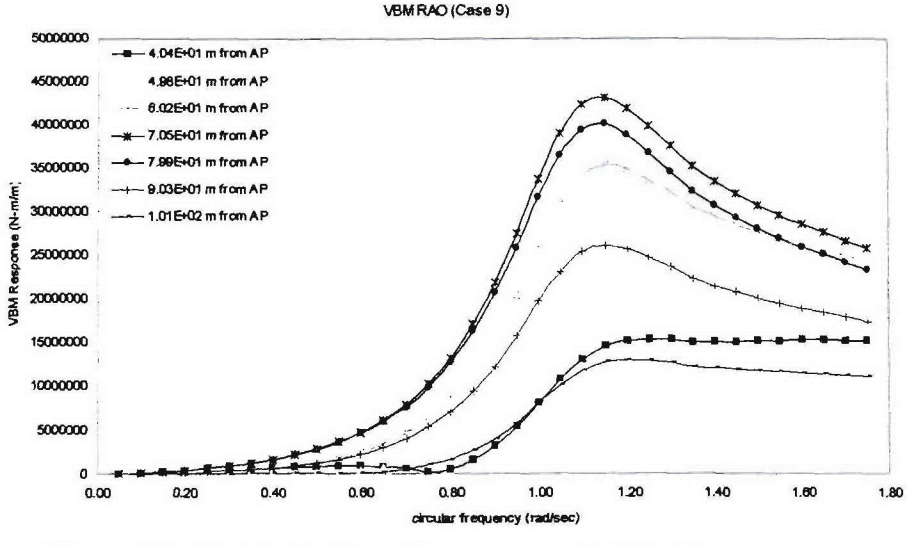

Figure 7.1-60: Vertical bending moment RAO at beam waves

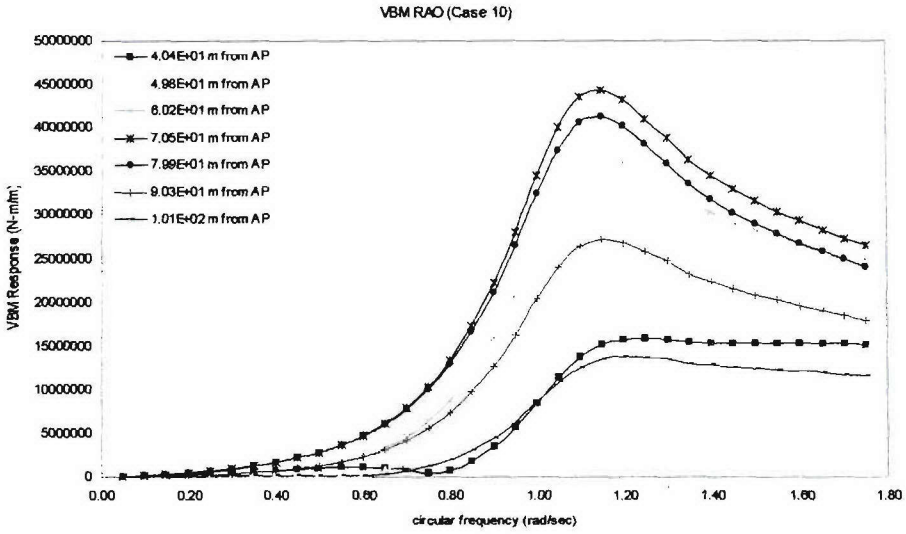

Figure 7.1-61: Vertical bending moment RAO at beam waves

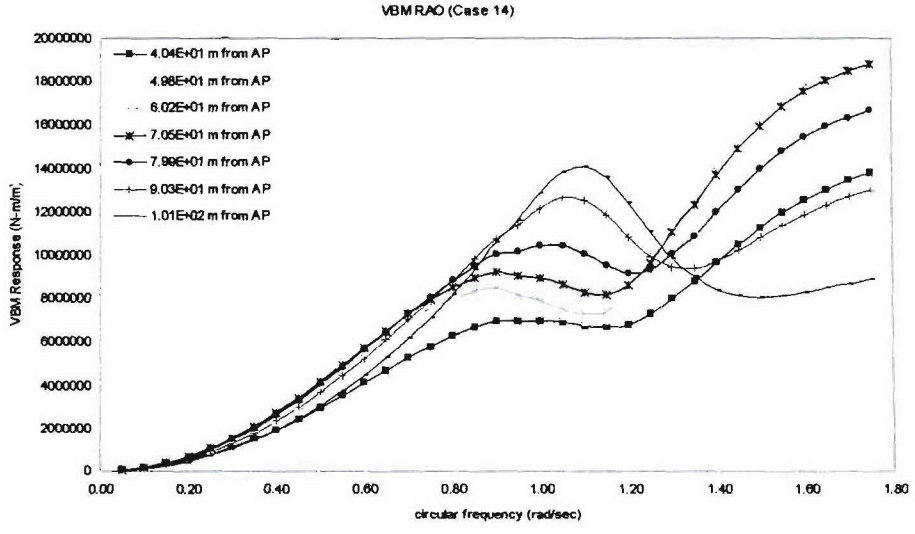

Figure 7.1-62: Vertical bending moment RAO at beam waves

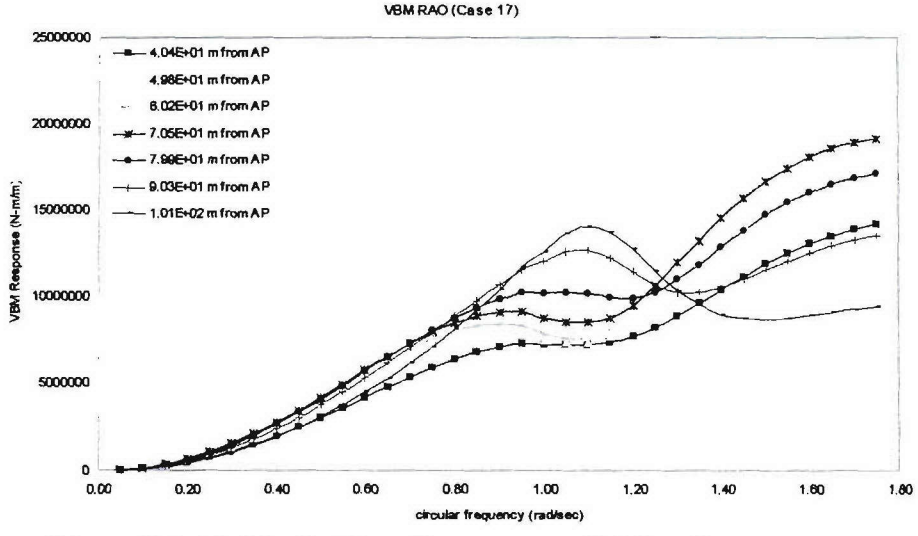

Figure 7.1-63: Vertical bending moment RAO at beam waves

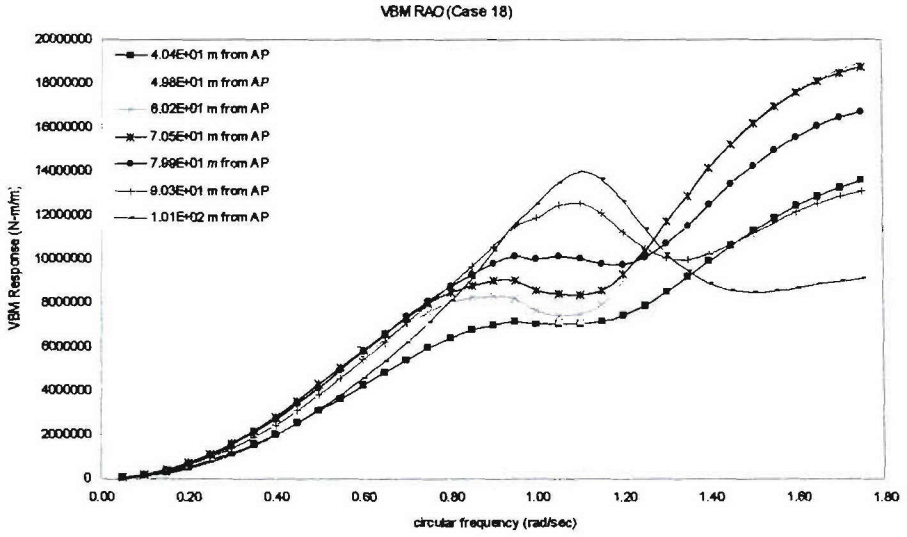

Figure 7.1-64: Vertical bending moment RAO at beam waves

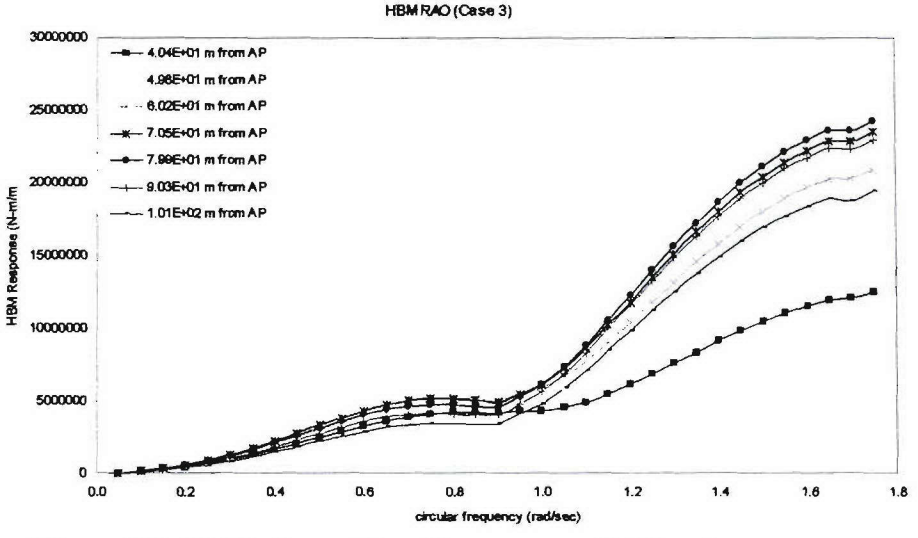

Figure 7.1-65: Horizontal bending moment RAO at beam waves

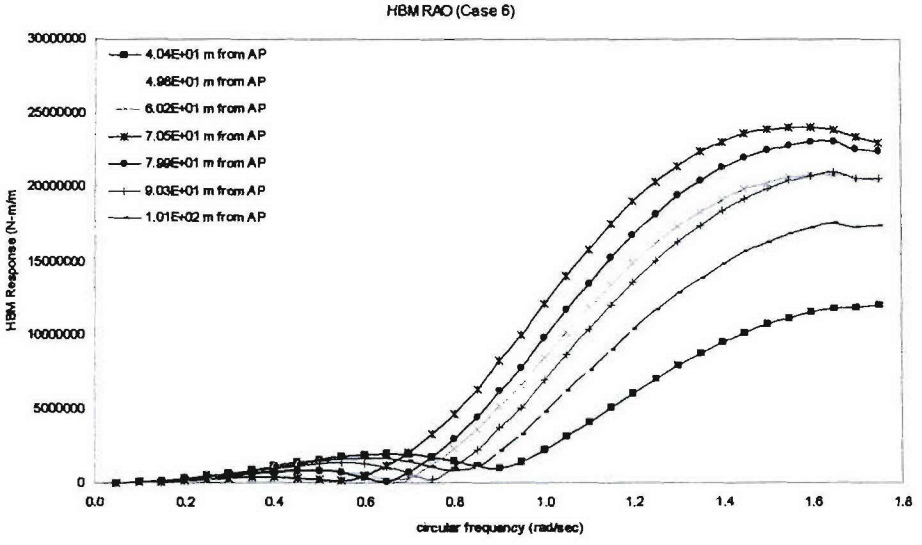

Figure 7.1-66: Horizontal bending moment RAO at beam waves

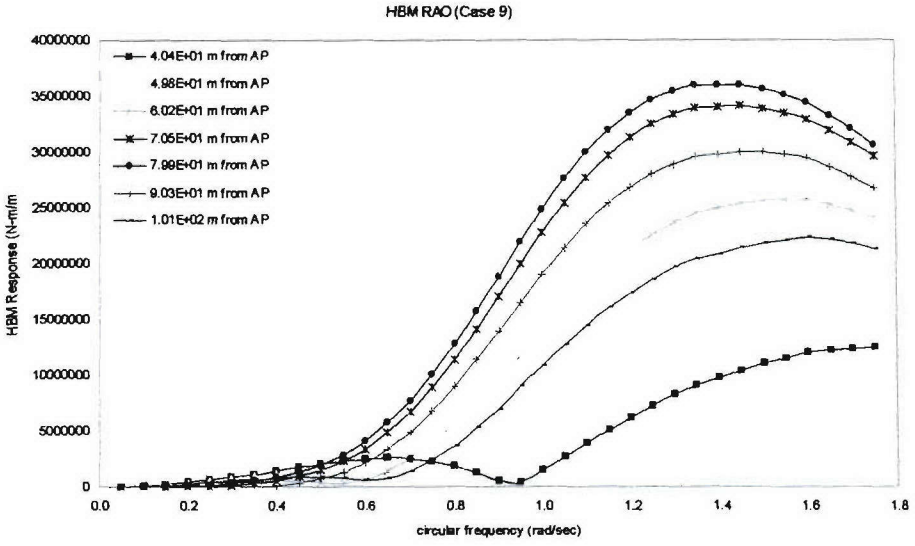

Figure 7.1-67: Horizontal bending moment RAO at beam waves

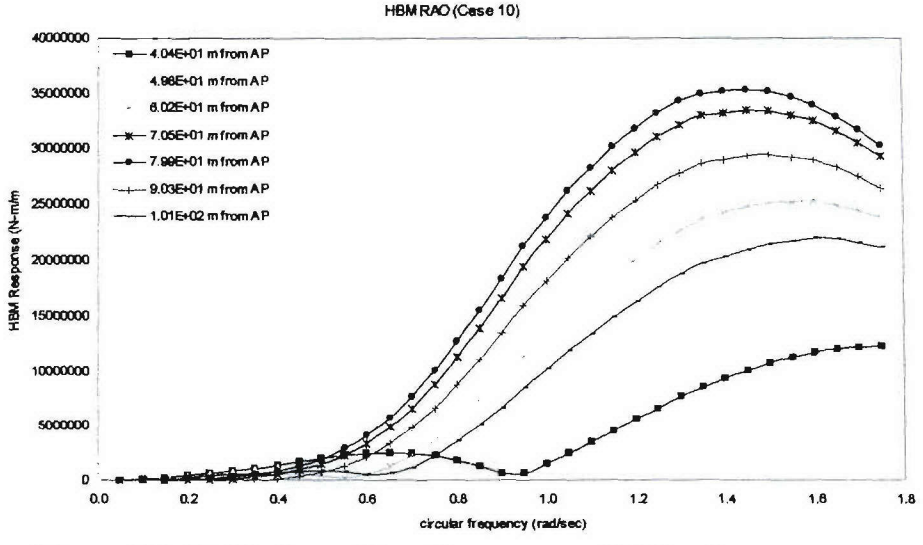

Figure 7.1-68: Horizontal bending moment RAO at beam waves

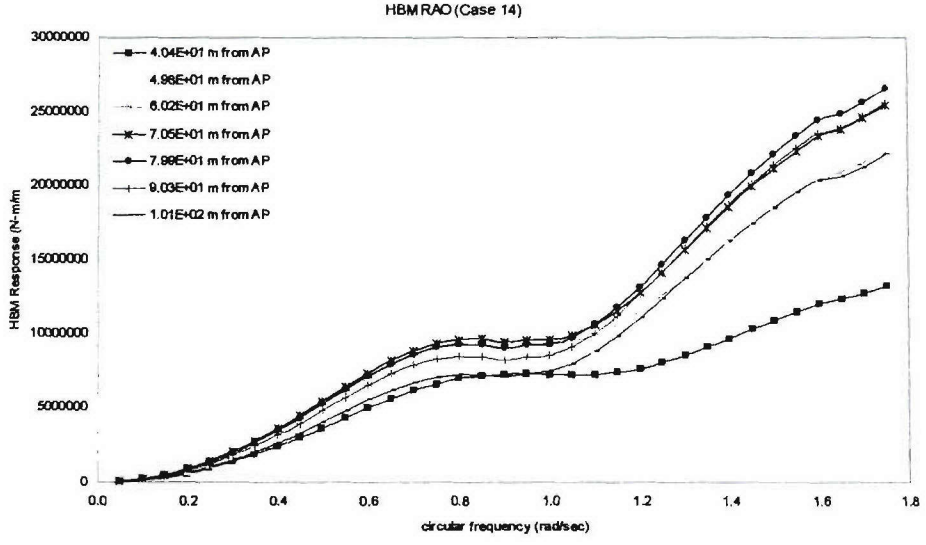

Figure 7.1-69: Horizontal bending moment RAO at beam waves

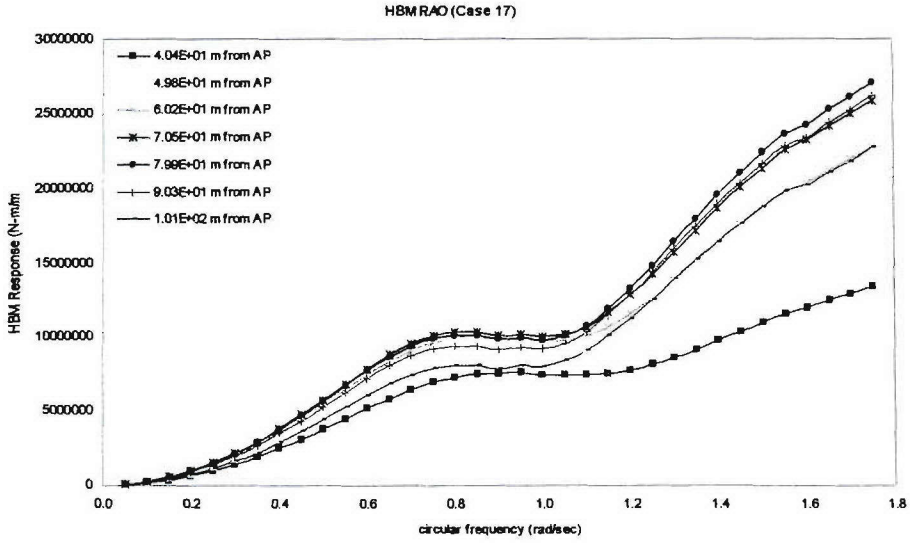

Figure 7.1-70: Horizontal bending moment RAO at beam waves

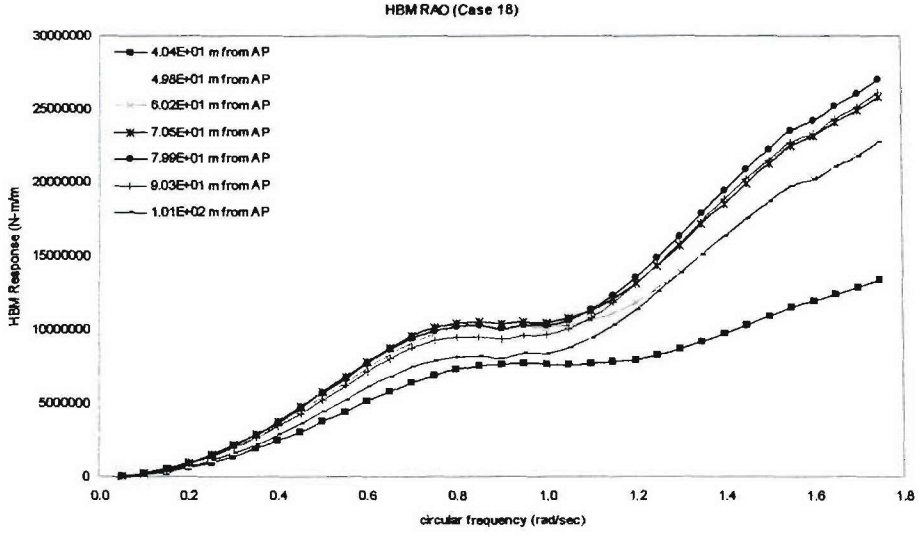

Figure 7.1-71: Horizontal bending moment RAO at beam waves

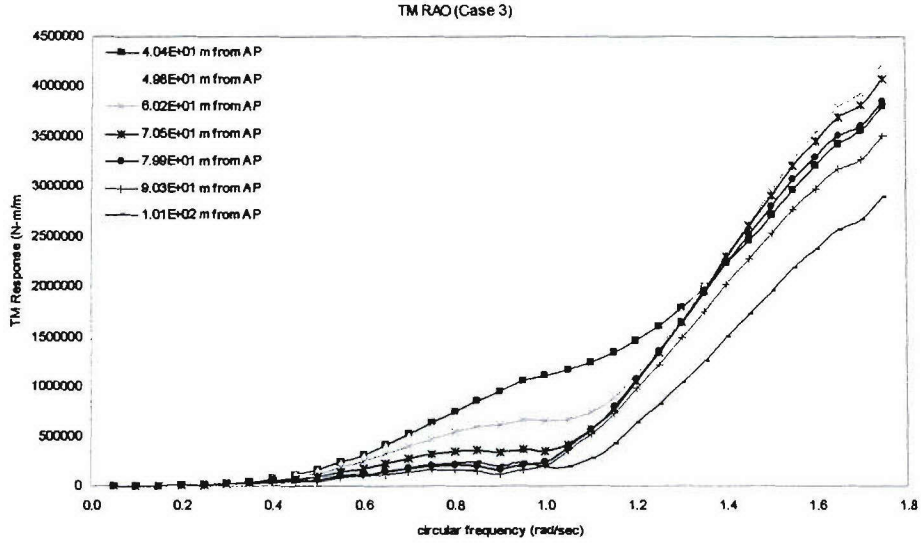

Figure 7.1-72: Torsion moment RAO at beam waves

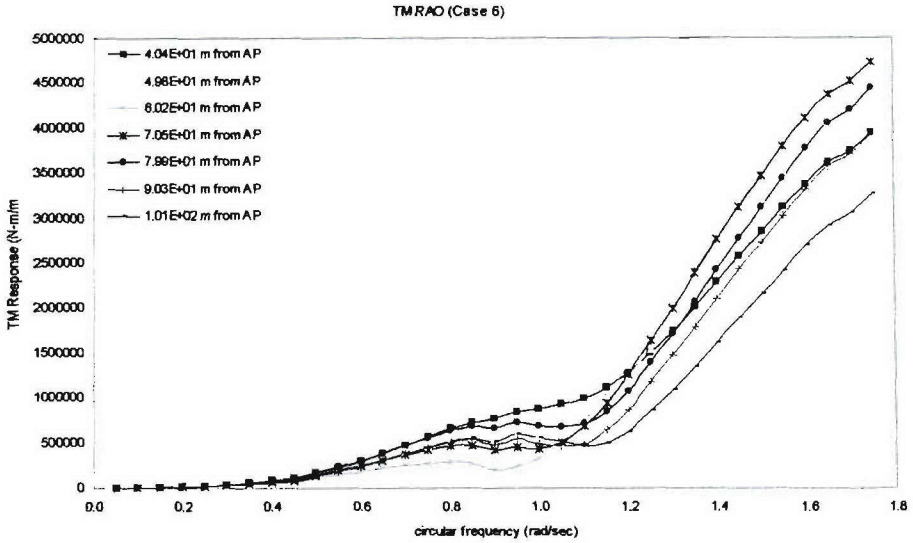

Figure 7.1-73: Torsion moment RAO at beam waves

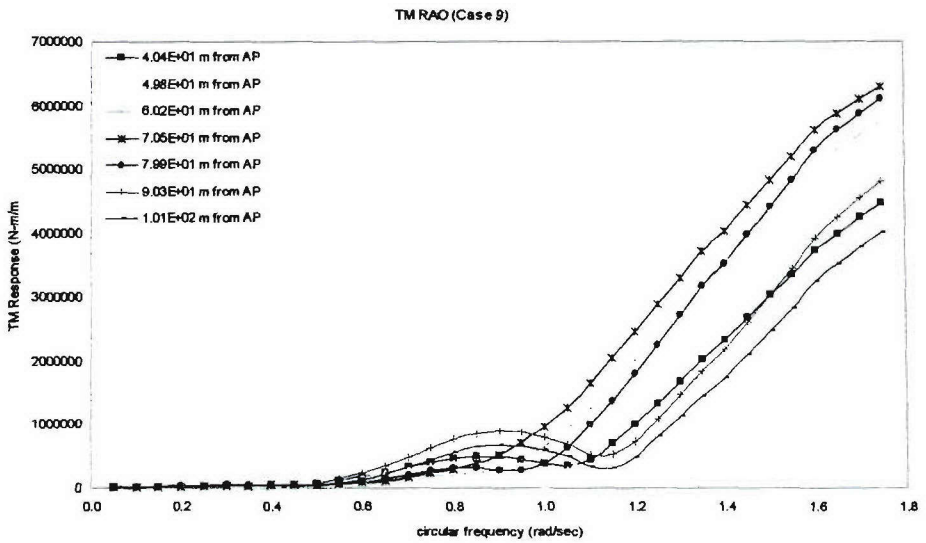

Figure 7.1-74: Torsion moment RAO at beam waves

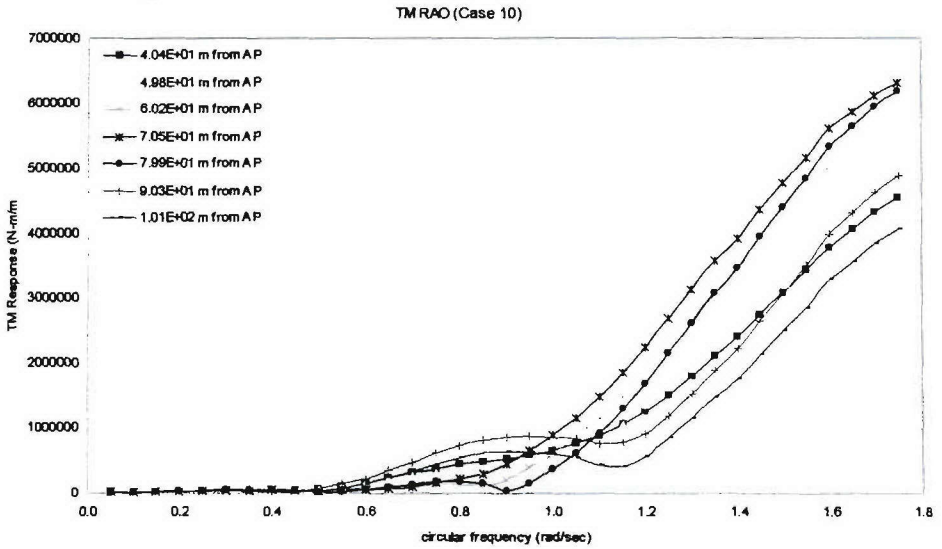

Figure 7.1-75: Torsion moment RAO at beam waves

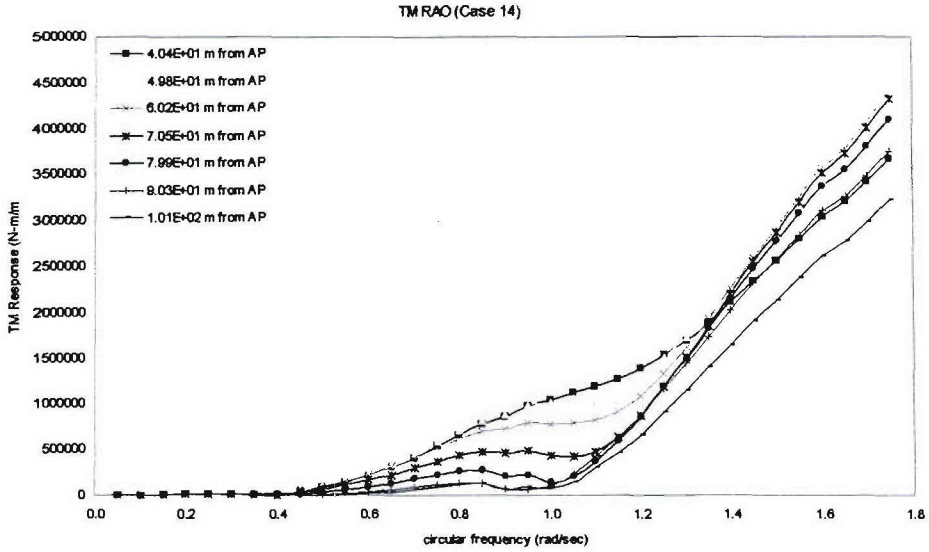

Figure 7.1-76: Torsion moment RAO at beam waves

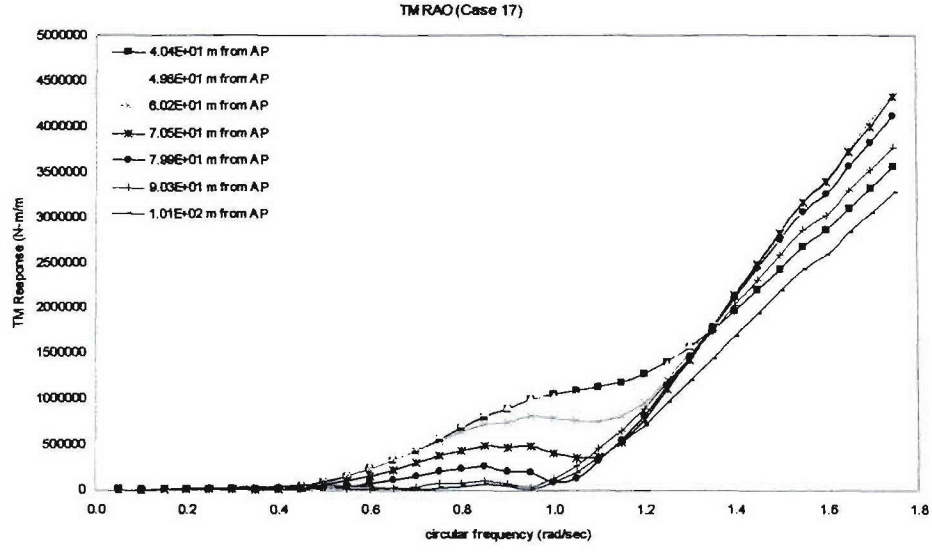

Figure 7.1-77: Torsion moment RAO at beam waves

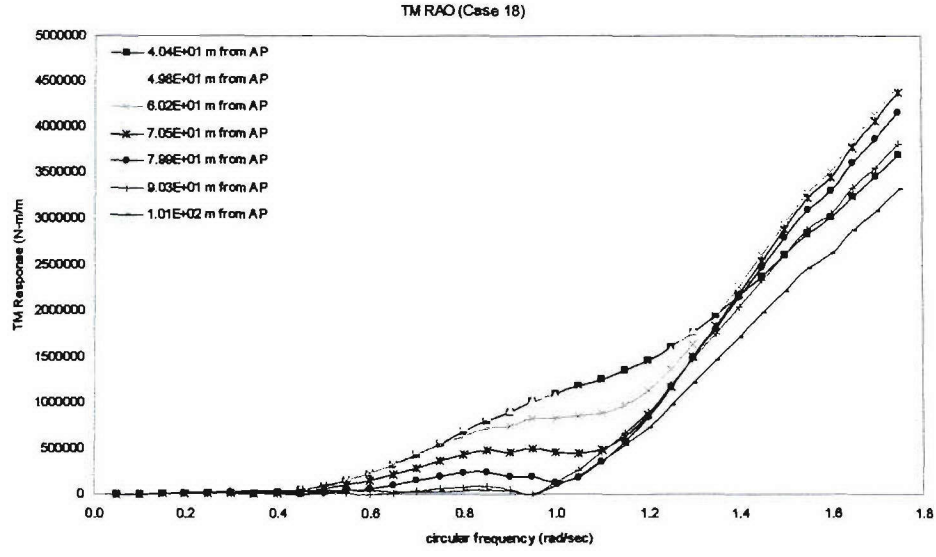

Figure 7.1-78: Torsion moment RAO at beam waves

7.1.3.4 Comparison of global dynamic wave induced loads in intact and damage conditions

Comparison of global dynamic wave induced loads in different design conditions are shown in this section to examine the damage effects on the sample vessel 'H5415' along the vessel length from Aft Perpendicular to Fore Perpendicular based on the results of the previous subsections 7.1.3.1 to 7.1.3.3. Figures 7.1-79 to 7.1-82 show the correlations of the computation results of vertical bending moments, horizontal bending moments and torsion moments in intact and damage conditions. Here damage scenario 1 (cases 4 and 5) and damage scenario 2 (cases 7, 8 and 11) stand for one and two compartment flooding damage conditions amidships respectively. Damage scenario 3 (cases 12 and 13) and damage scenario 4 (cases 15, 16 and 19) are related to the compartment flooding damages at fore body in the ship.

Figures 7.1-79 shows that in head waves the maximum vertical bending moment RAO in cases 4 and 7 (damage scenarios 1 & 2) is larger than that of intact condition, while the results in cases 12 and 15 (damage scenarios 3 & 4) show opposite. In addition case 7 (damage scenario 2) is the worst condition because its maximum vertical bending moment RAO is increased the most, and occurs amidships, where damage is imposed. This is probably due to the fact that the draught is increased the most (by 1.1 meters) in damage scenario 2.

Comparison of vertical bending moments at stern quartering waves is shown in Figure 7.1-80. This figure shows that the vertical bending moment in intact condition is larger than those in damaged conditions. In Figure 7.1-81 it can be seen that the horizontal bending moment RAOs in damage scenario 2 (cases 8 & 11) are the largest, and followed by damage scenario 1 (case 5), intact condition (case 2) and others. Figure 7.1-82 shows comparison of torsion moment at stern quartering waves. The torsional moment in the intact ship is the least amongst all the conditions, while damage scenario 2 (cases 8 & 11) has the largest torsional moment. Bearing in mind that damage scenario 2 has the largest opening, its torsional strength could be a concern. Of course this will be assessed in section 7.8.

7.1.3.4.1 Head waves

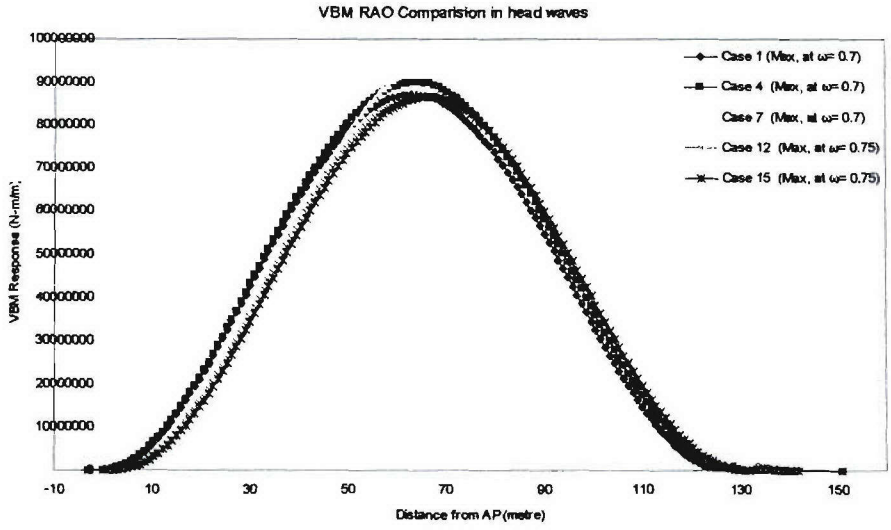

Figure 7.1-79: Vertical bending moment RAO comparison at head waves

7.1.3.4.2 Stern quartering waves

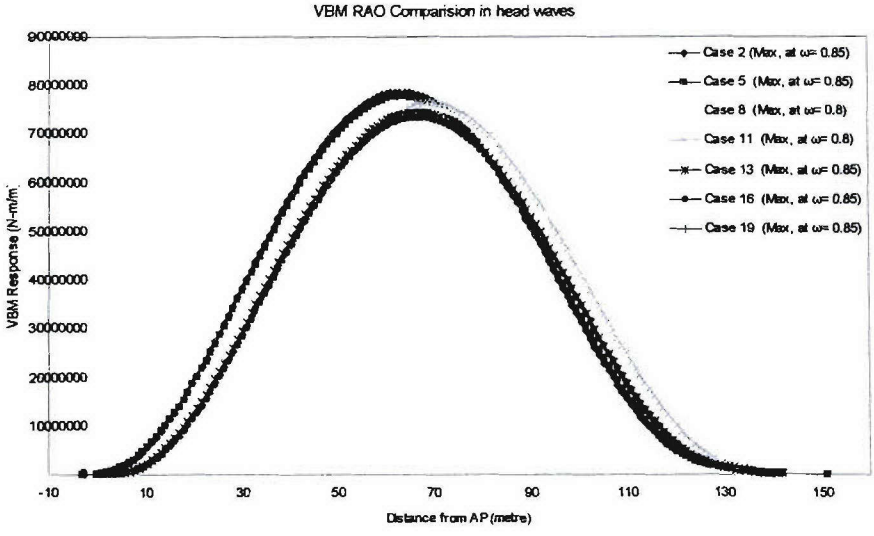

Figure 7.1-80: Vertical bending moment RAO comparison at stern quartering waves

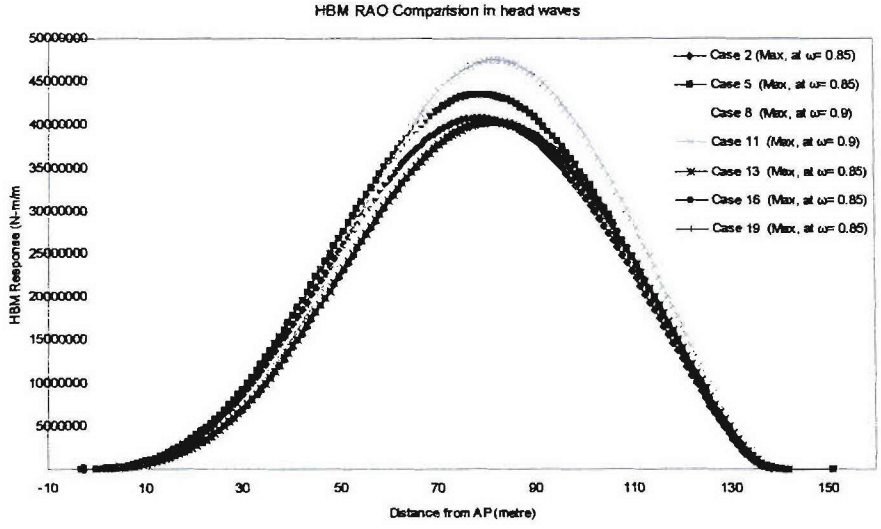

Figure 7.1-81: Horizontal bending moment RAO comparison at stern quartering waves

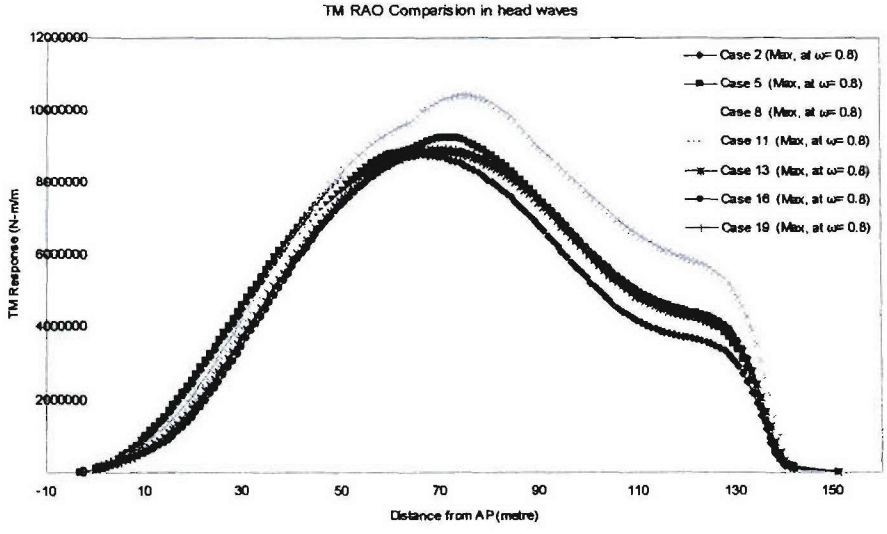

Figure 7.1-82: Torsion moment RAO comparison at stern quartering waves

7.2 Comparative Study in Hydrodynamic Aspects

The time history data of the incoming waves, motion responses and load responses were monitored in online. A Fast Fourier Transform (FTT) was used for analysing the measurements. The rates of sampling for the data acquisition were 60 samples/sec for motion tests and 100 samples/sec for loading tests. The initial transient condition was disregarded in FFT analysis. Typical time history records and FFT analysis results of an incoming wave and resulting heave motion of intact H5415 at the full scale $\omega=0.645$ and *Hw=small* are shown in Figure 7.2-1.

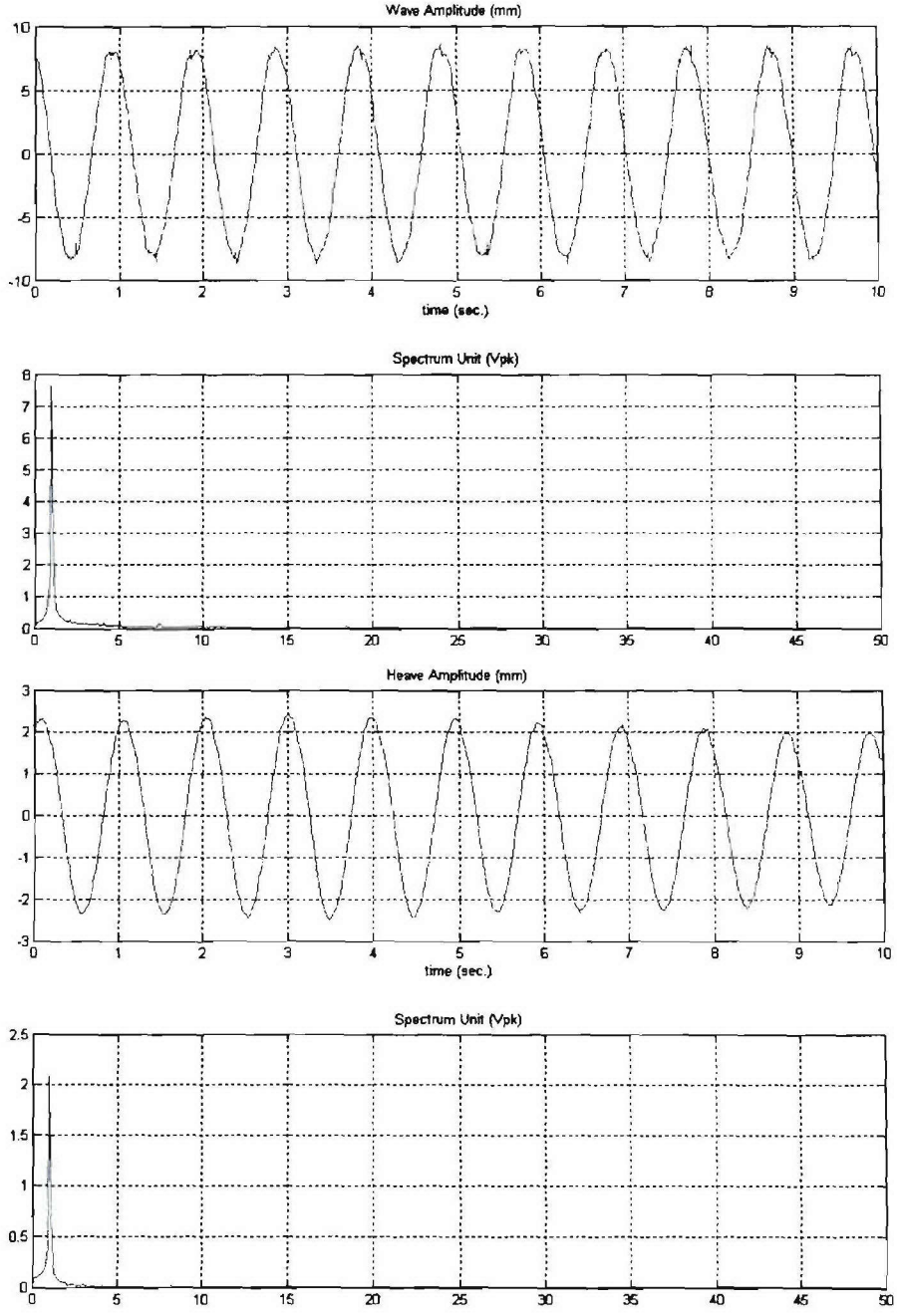

Figure 7.2-1: Typical time history and FFT analysis results of an incoming wave and resulting heave motion of intact H5415 at the full scale $\omega=0.645$ and *Hw=small*

Typical time history and FFT analysis results of an incoming wave and resulting vertical bending moment of intact H5415 at the full scale $\omega=0.698$ and *Hw=large* are shown in Figure 7.2-2.

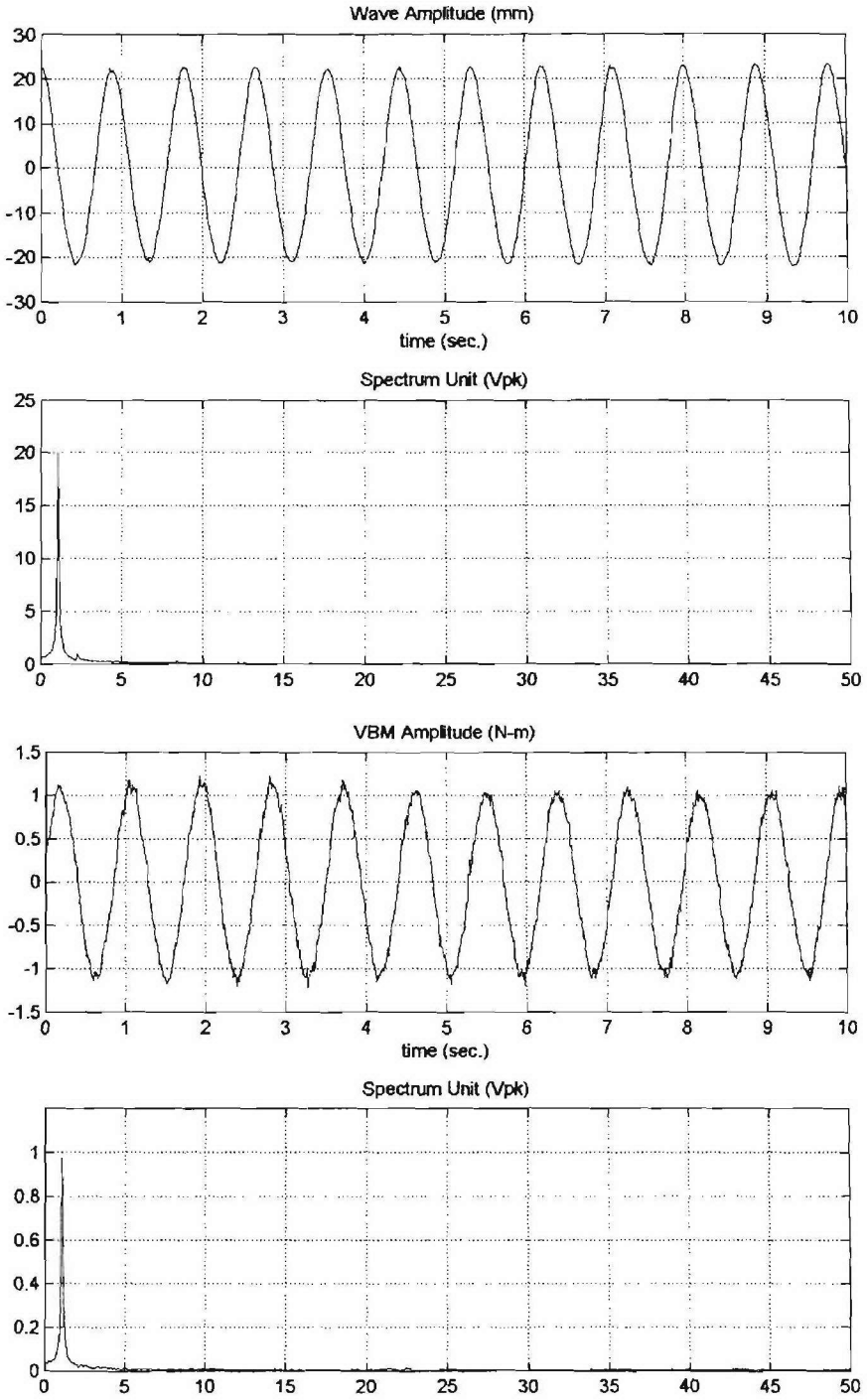

Figure 7.2-2: Typical time history and FFT analysis results of an incoming wave and resulting vertical bending moment of intact H5415 at the full scale $\omega=0.698$ and *Hw=large*

7.2.1 Comparison of predictions and measurements for motions

7.2.1.1 Comparison in intact condition

Experimental wave conditions and other information with respect to experiment investigations are provided in section 4.1.4. The comparison between predictions and measurements for motion responses in intact condition are shown in the following figures.

- Figures 7.2-3 to 7.2-7 for intact ship in head waves.
- Figures 7.2-8 to 7.2-12 for intact ship in stern quartering waves.
- Figures 7.2-13 to 7.2-17 for intact ship in beam waves.

The correlation between the predictions and measurements of motion response amplitudes of intact ship is satisfactory for head and stern quartering waves and reasonable for beam waves. For the roll motion responses of intact H5415 in three wave headings, the 2D linear strip method presents good agreement compared to the measurements except for the last three measurements which are in resonant frequency regions. Figure 7.2-12 shows the yaw motion response RAO of the intact ship at stern quartering waves. This figure presents the discrepancy between predictions and measurements due to drift motions and changed wave angles. At the moment the present linear solution can not consider viscous effects. The pitch motion response RAO of intact H5415 at beam waves are shown in Figure 7.2-16. The trends of the results from experiments give good agreements with respect to those of the results from numerical computations. On the other hand there are slightly big differences between the measured and predicted values. The small scale of the model could cause this problem, but the pitch motion response amplitudes in beam waves are much less than those in head and stern quartering waves. So they are insignificant.

7.2.1.1.1 Head waves

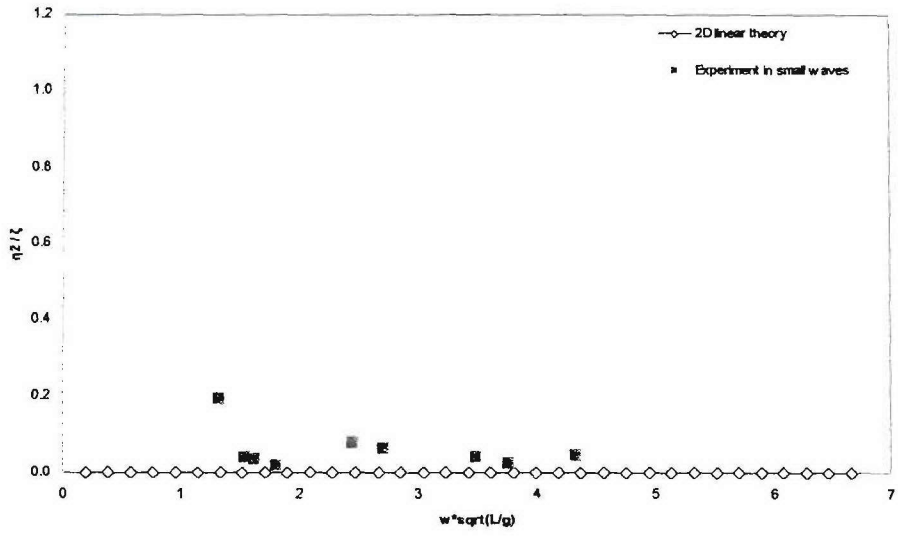

Figure 7.2-3: Sway RAO of intact H5415 at head waves

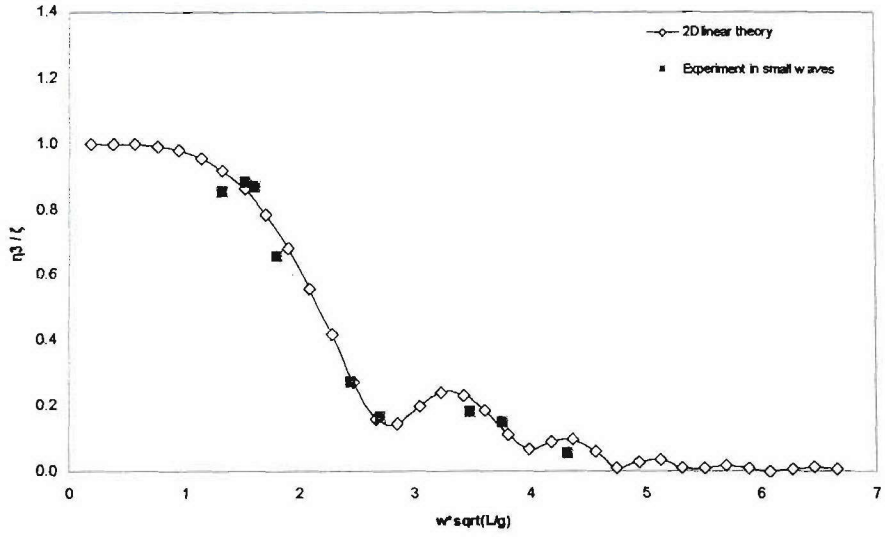

Figure 7.2-4: Heave RAO of intact H5415 at head waves

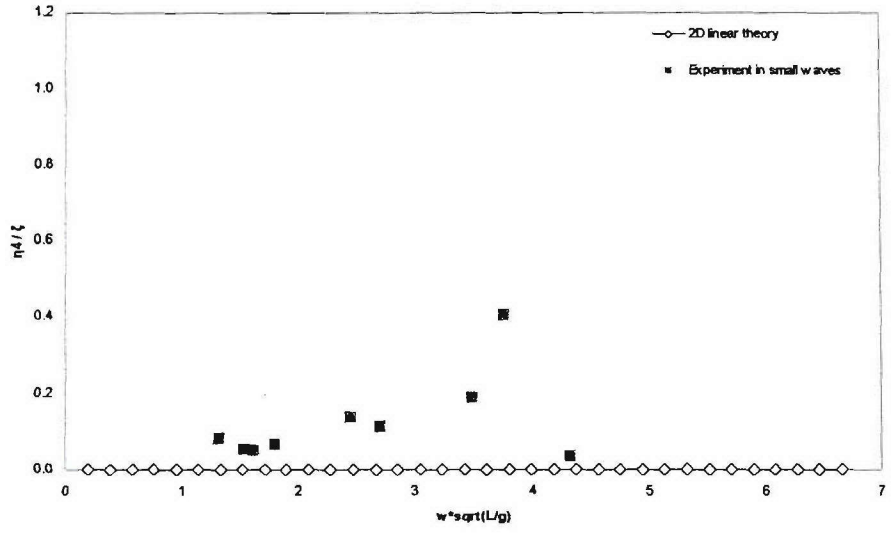

Figure 7.2-5: Roll RAO of intact H5415 at head waves

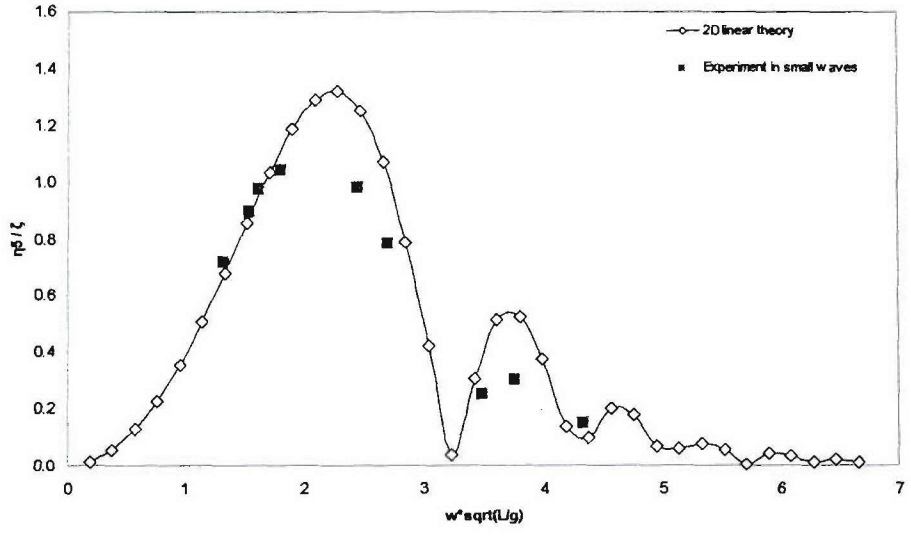

Figure 7.2-6: Pitch RAO of intact H5415 at head waves

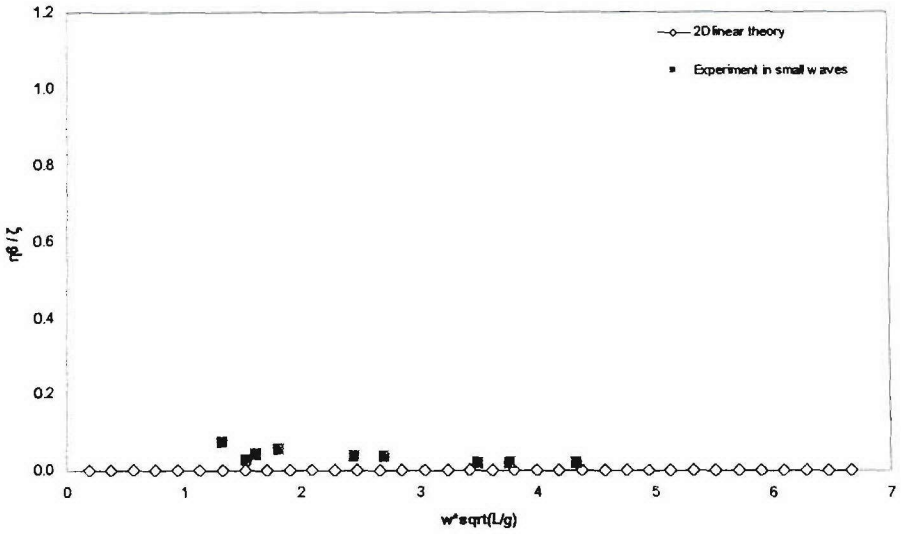

Figure 7.2-7: Yaw RAO of intact H5415 at head waves

7.2.1.1.2 Stern quartering waves

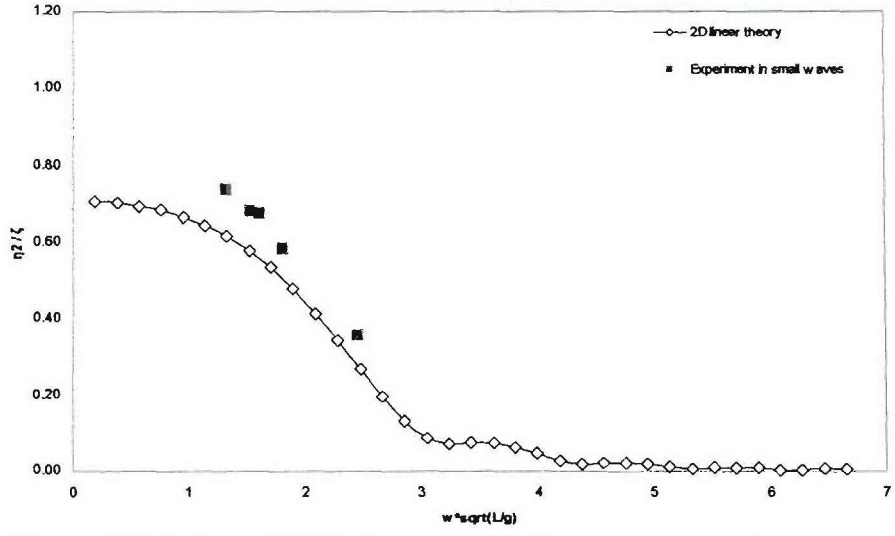

Figure 7.2-8: Sway RAO of intact H5415 at stern quartering waves

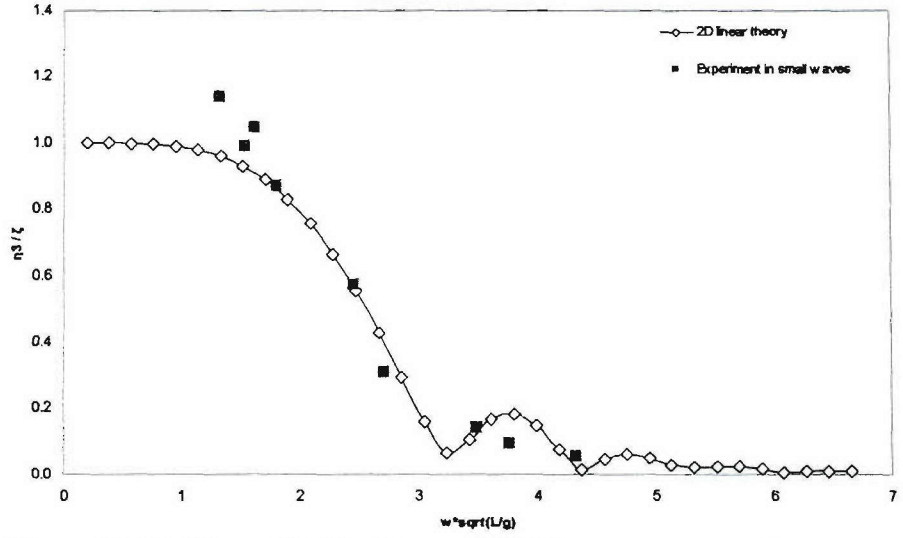

Figure 7.2-9: Heave RAO of intact H5415 at stern quartering waves

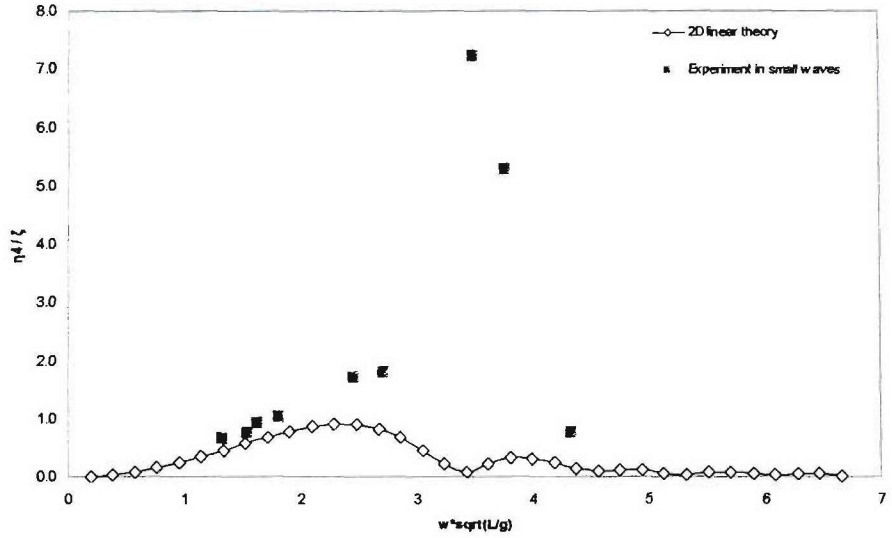

Figure 7.2-10: Roll RAO of intact H5415 at stern quartering waves

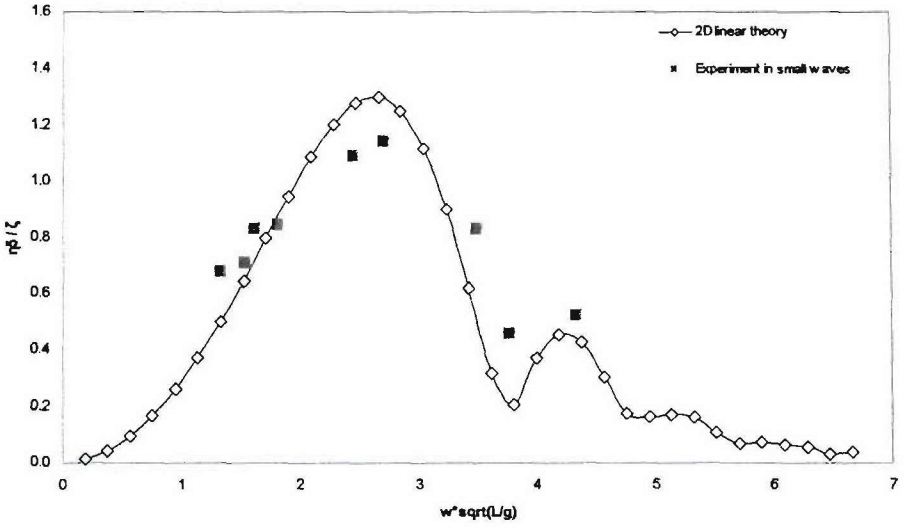

Figure 7.2-11: Pitch RAO of intact H5415 at stern quartering waves

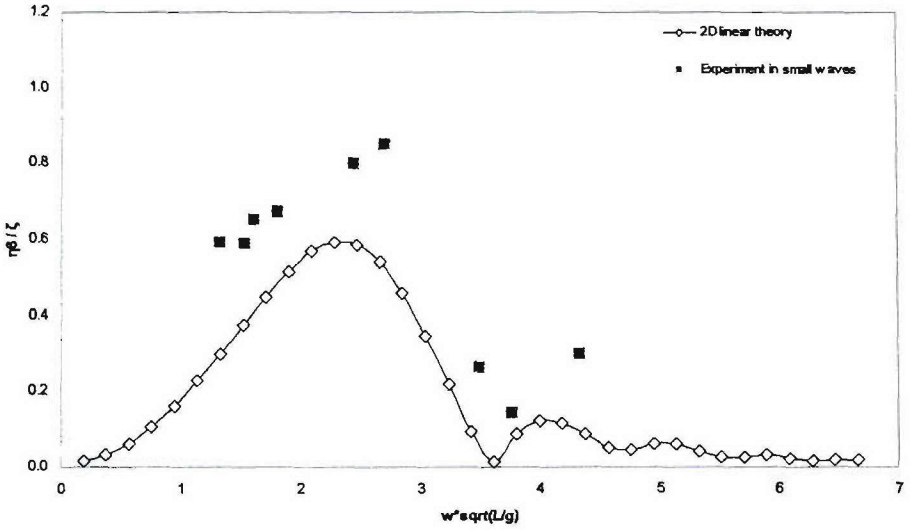

Figure 7.2-12: Yaw RAO of intact H5415 at stern quartering waves

7.2.1.1.3 Beam waves

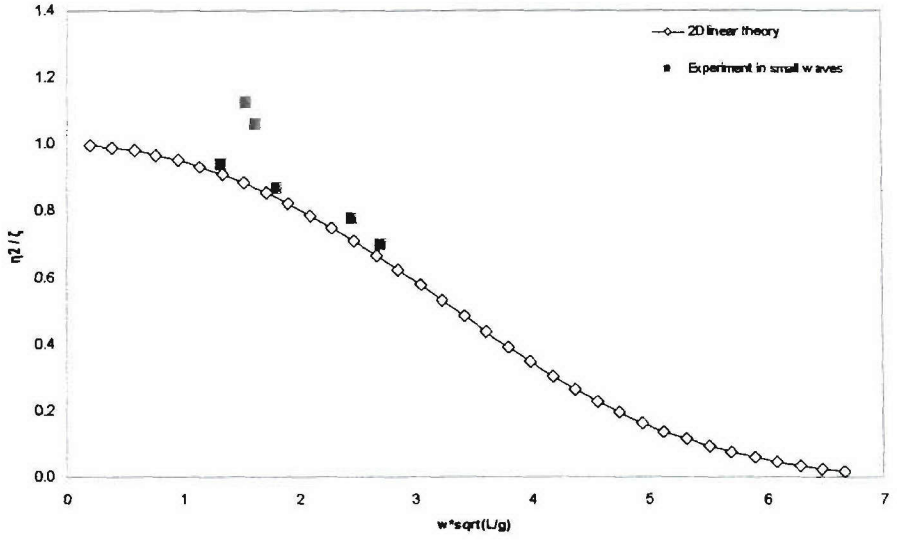

Figure 7.2-13: Sway RAO of intact H5415 at beam waves

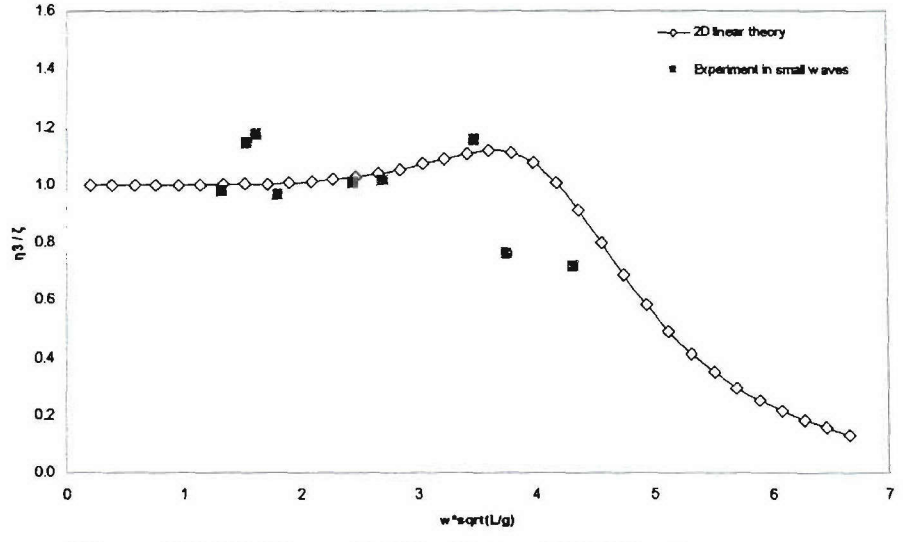

Figure 7.2-14: Heave RAO of intact H5415 at beam waves

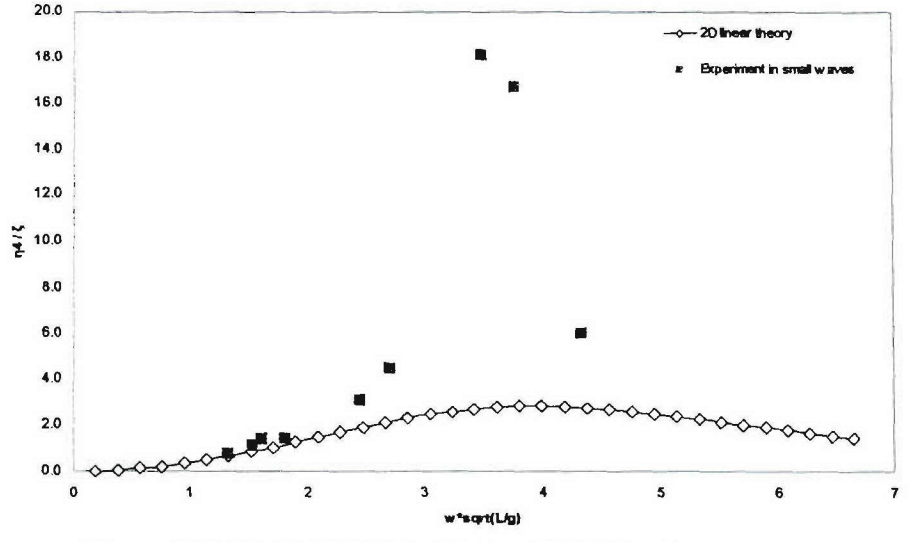

Figure 7.2-15: Roll RAO of intact H5415 at beam waves

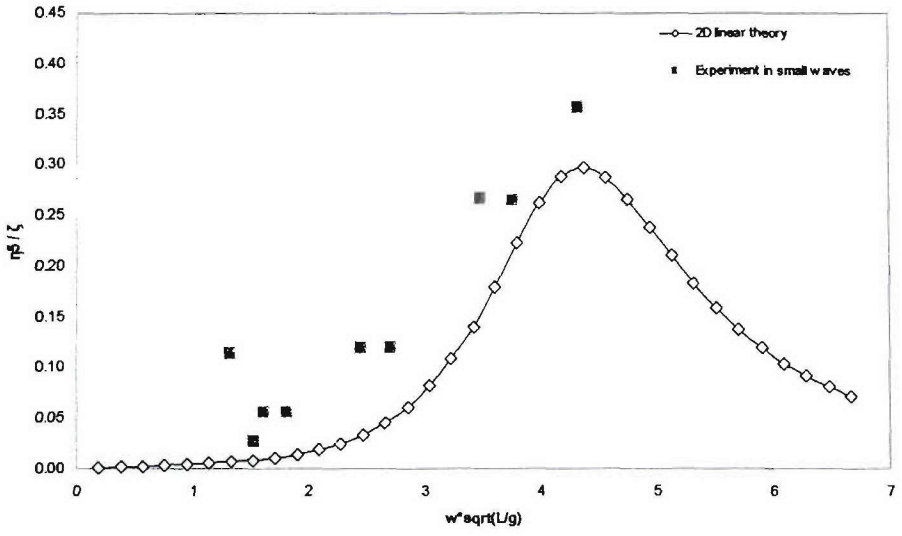

Figure 7.2-16: Pitch RAO of intact H5415 at beam waves

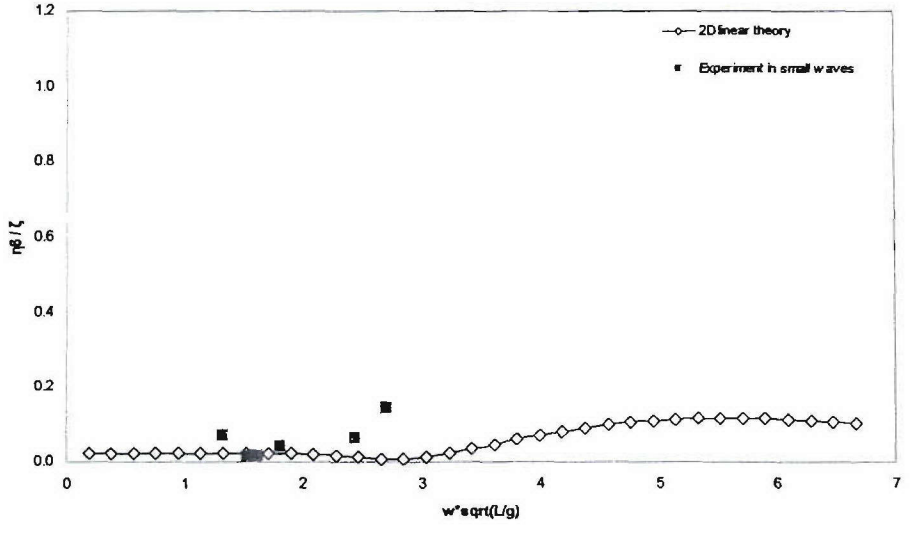

Figure 7.2-17: Yaw RAO of intact H5415 at beam waves

7.2.1.2 Comparison in damage scenario 2

The comparison between predictions and measurements for motion responses in damage scenario 2 are shown in the following figures.

- Figures 7.2-18 to 7.2-22 for DS2 ship in head waves.
- Figures 7.2-23 to 7.2-27 for DS2 ship in stern quartering waves.
- Figures 7.2-28 to 7.2-32 for DS2 ship in beam waves.

The correlation between the predictions and measurements of the motion response amplitudes of DS2 ship is satisfactory for head and stern quartering waves and acceptable for beam waves. For the roll motion responses of HULL5415 in three wave headings, the 2D linear strip method

presents acceptable agreements compared to the measurements except the last three measurements which are in resonant frequency regions. However the differences between calculated and measured values are larger than those of the other measured motion response amplitudes. Figure 7.2-27 describes the yaw motion response RAO of DS2 ship at stern quartering waves. This figure shows the differences between predictions and measurements due to drift motions and changed wave angles as well as some effects caused by the flooding compartment. The correlation between the numerical computations and experimental measurements in damage scenario 2 show lager differences than those in the intact condition. The reasons might be that the present linear solution can not consider viscous effects and phenomena of sloshing and slamming. And also the small scale of the model could cause this problem.

7.2.1.2.1 Head waves

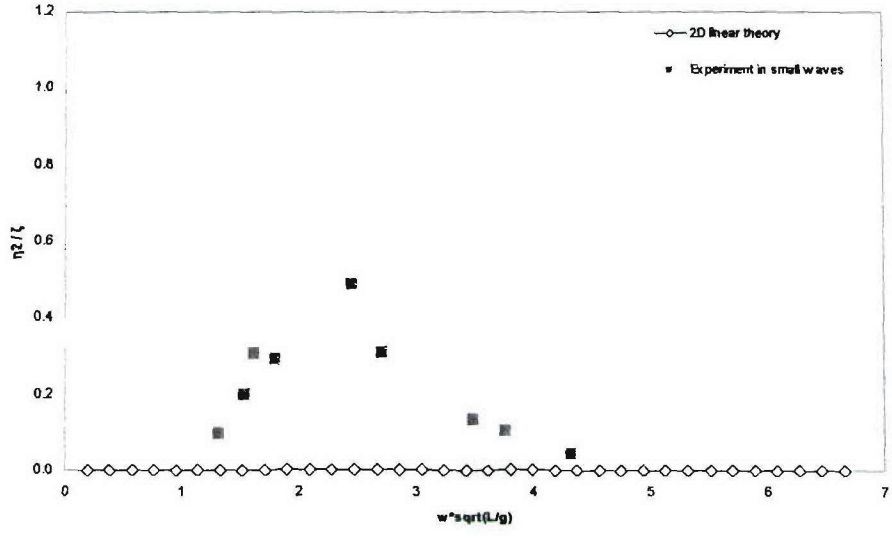

Figure 7.2-18: Sway RAO of DS2 H5415 at head waves

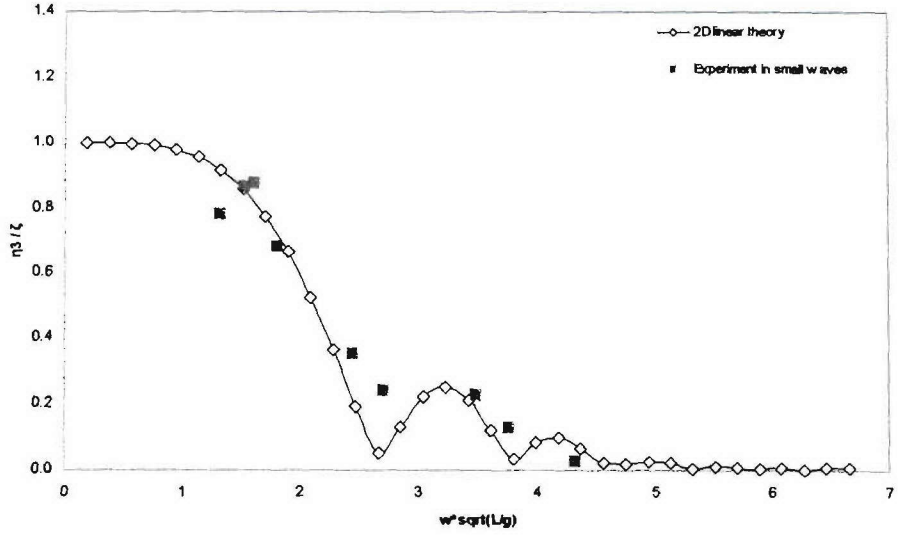

Figure 7.2-19: Heave RAO of DS2 H5415 at head waves

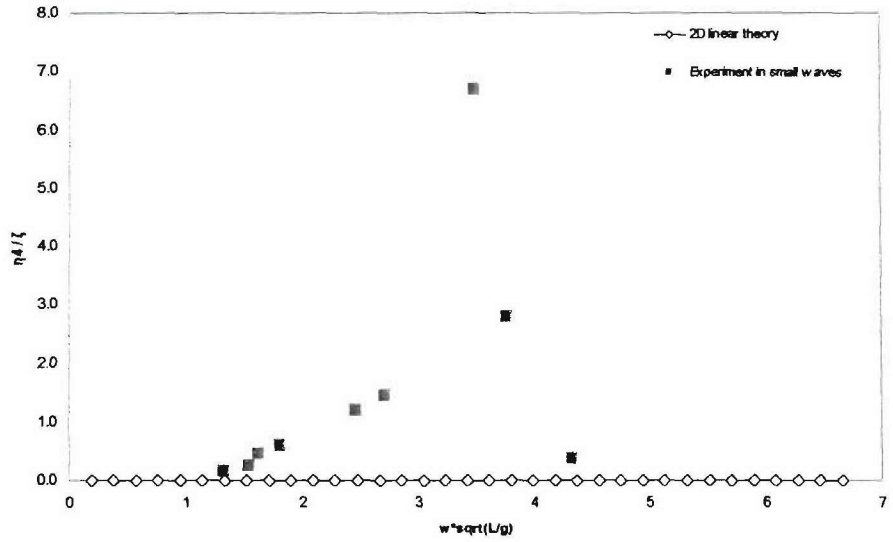

Figure 7.2-20: Roll RAO of DS2 H5415 at head waves

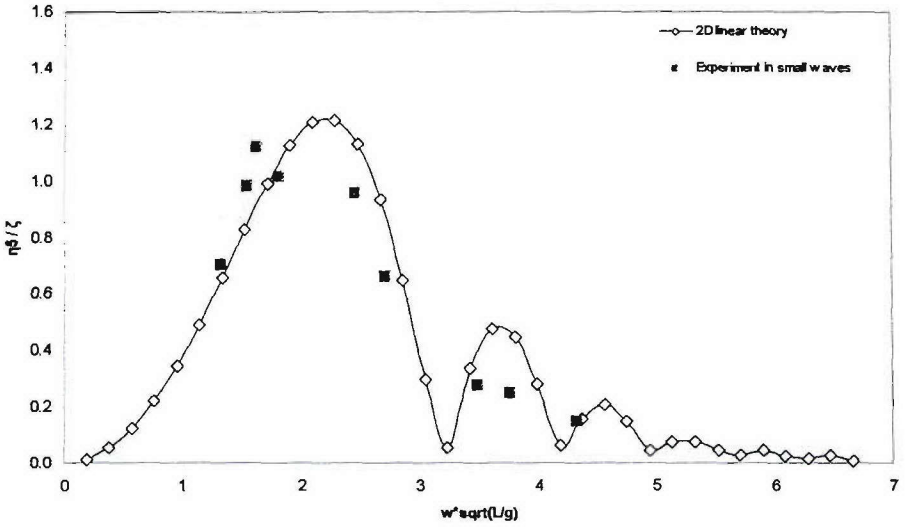

Figure 7.2-21: Pitch RAO of DS2 H5415 at head waves

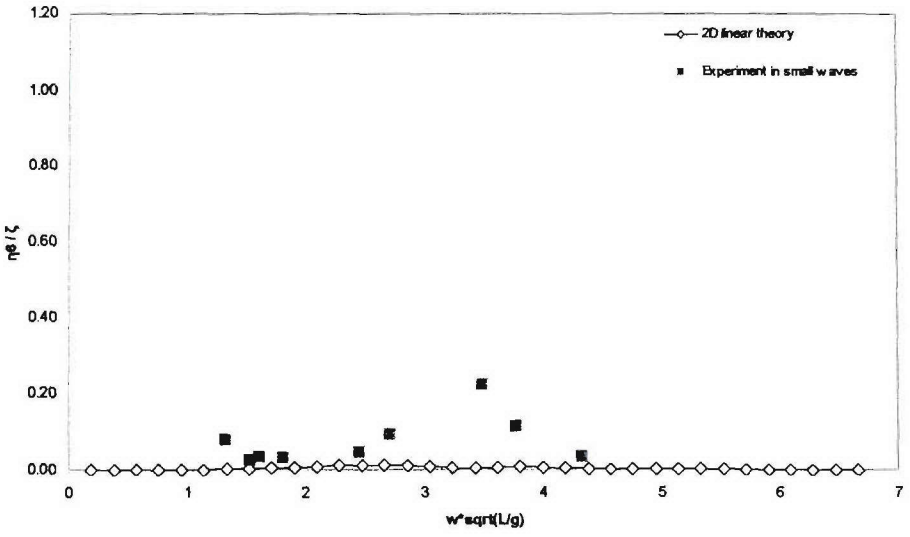

Figure 7.2-22: Yaw RAO of DS2 H5415 at head waves

7.2.1.2.2 Stern quartering waves

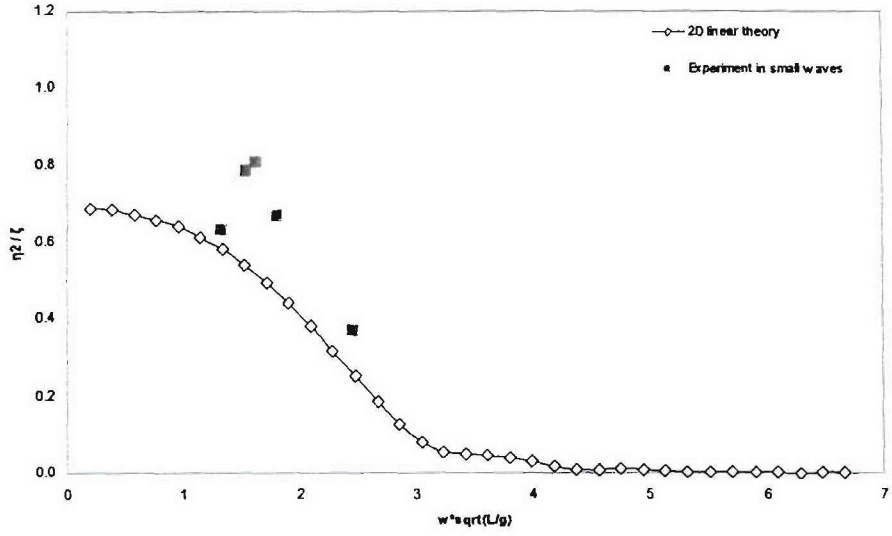

Figure 7.2-23: Sway RAO of DS2 H5415 at stern quartering waves

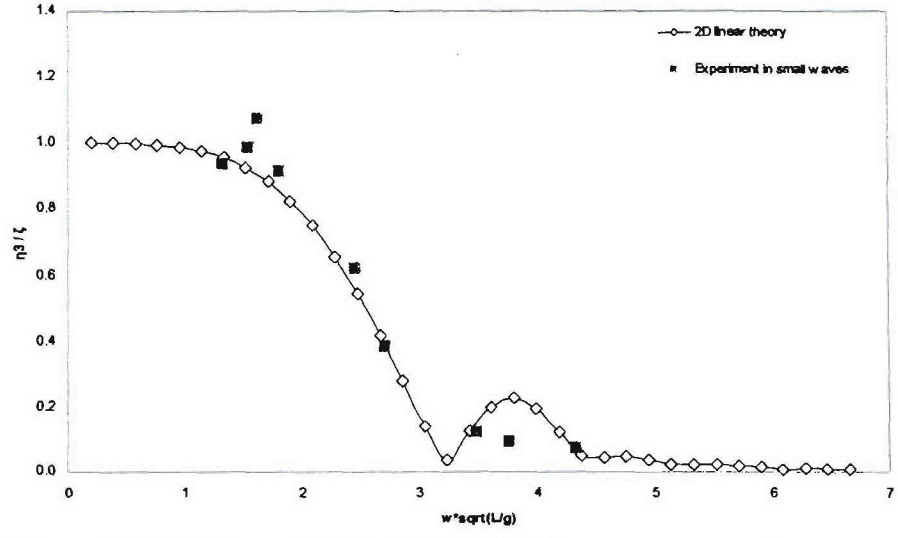

Figure 7.2-24: Heave RAO of DS2 H5415 at stern quartering waves

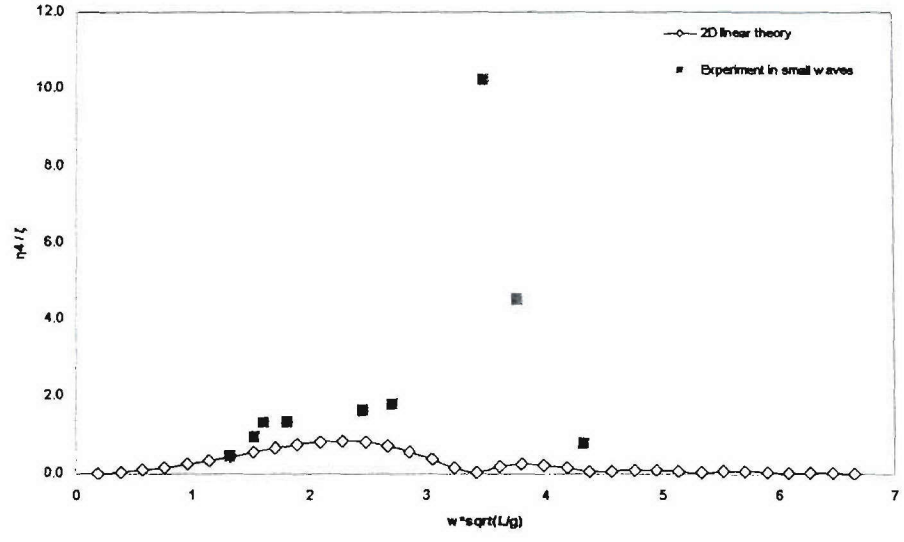

Figure 7.2-25: Roll RAO of DS2 H5415 at stern quartering waves

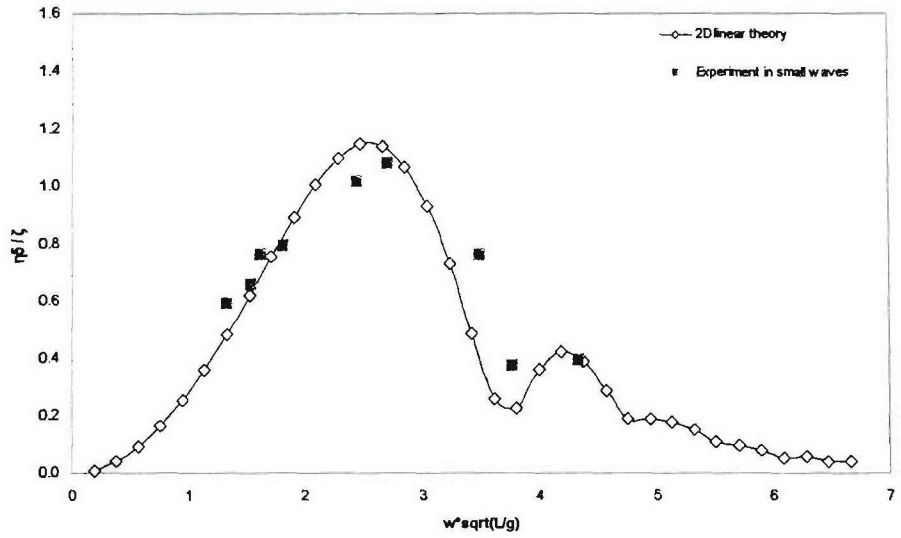

Figure 7.2-26: Pitch RAO of DS2 H5415 at stern quartering waves

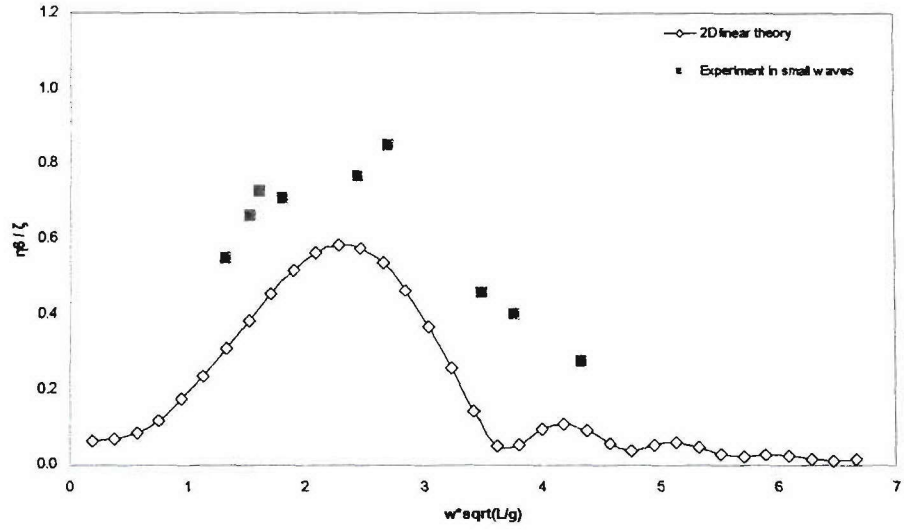

Figure 7.2-27: Yaw RAO of DS2 H5415 at stern quartering waves

7.2.1.2.3 Beam waves

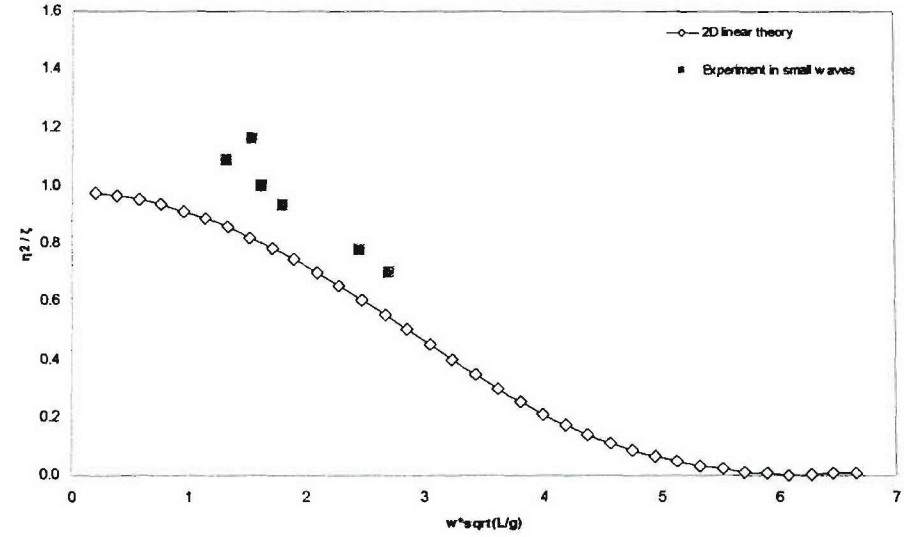

Figure 7.2-28: Sway RAO of DS2 H5415 at beam waves

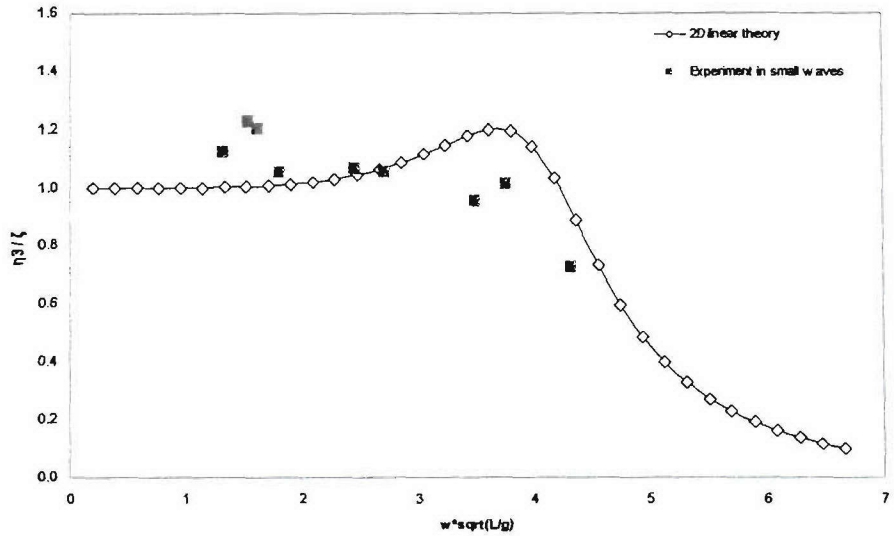

Figure 7.2-29: Heave RAO of DS2 H5415 at beam waves

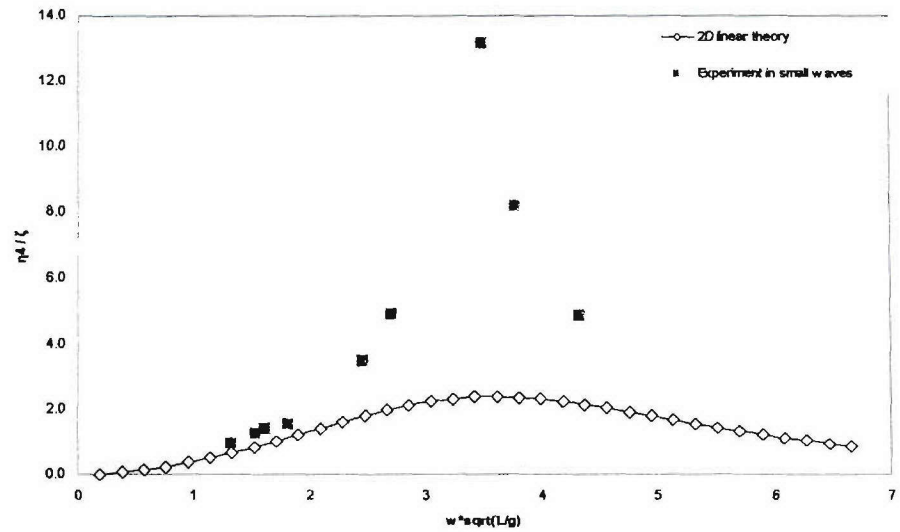

Figure 7.2-30: Roll RAO of DS2 H5415 at beam waves

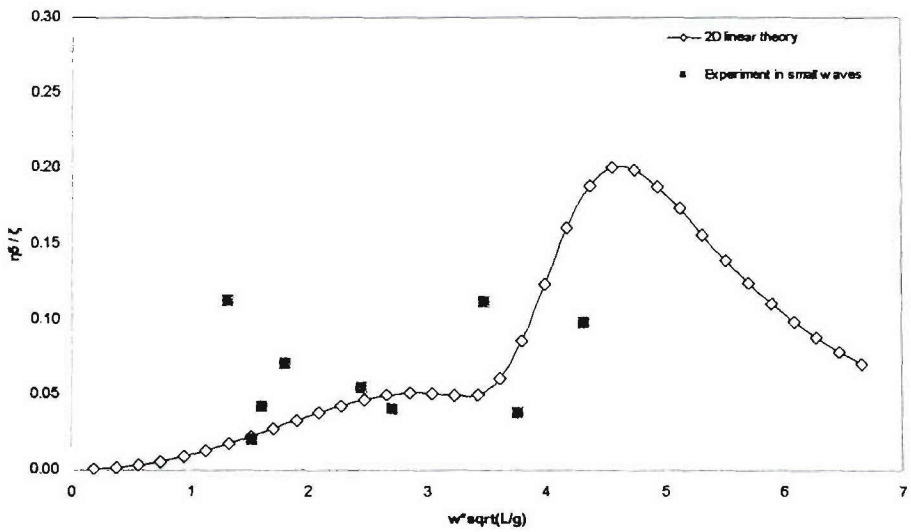

Figure 7.2-31: Pitch RAO of DS2 H5415 at beam waves

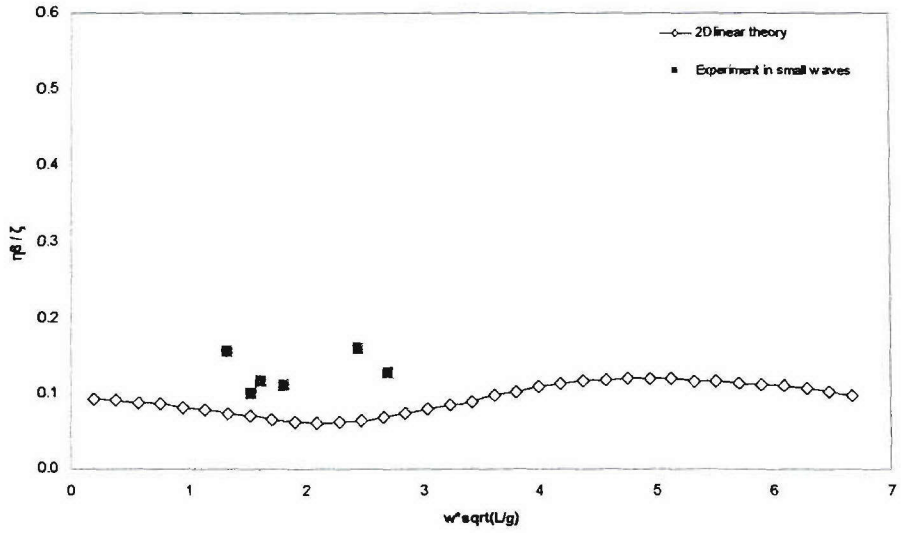

Figure 7.2-32: Yaw RAO of DS2 H5415 at beam waves

7.2.1.3 Comparison in damage scenario 3

The comparison between predictions and measurements for motion responses in damage scenario 3 are shown in the following figures.

- Figures 7.2-33 to 7.2-37 for DS3 ship in head waves.
- Figures 7.2-38 to 7.2-42 for DS3 ship in stern quartering waves.
- Figures 7.2-43 to 7.2-47 for DS3 ship in beam waves.

The correlation between the computations and measurements of motion response amplitudes of DS3 ship is satisfactory for head and stern quartering waves and reasonable for beam waves. This fore body flooding damage model shows similar trends compared to the comparative study in the previous section 7.2.1.1.

7.2.1.3.1 Head waves

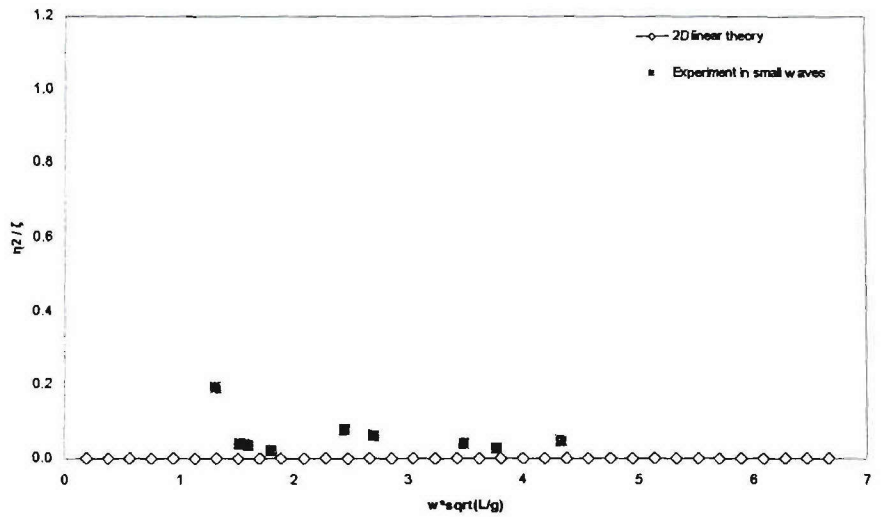

Figure 7.2-33: Sway RAO of DS3 H5415 at head waves

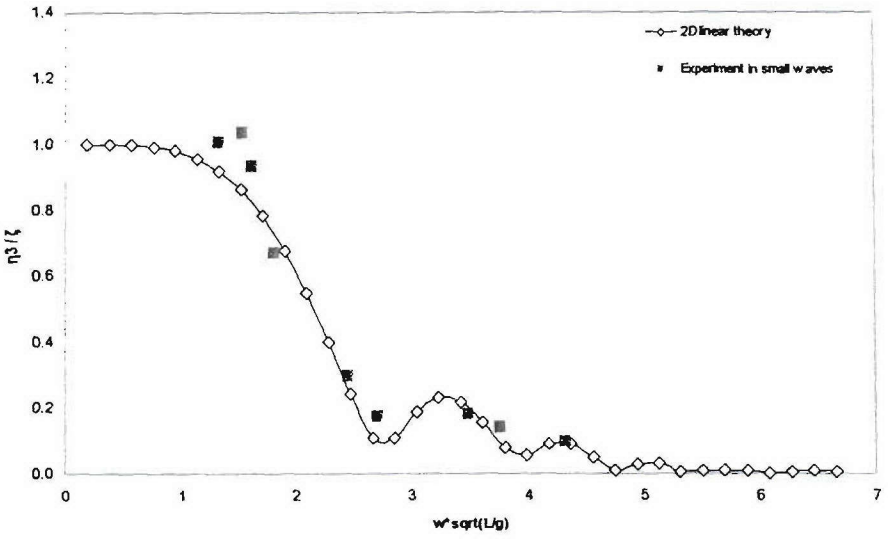

Figure 7.2-34: Heave RAO of DS3 H5415 at head waves

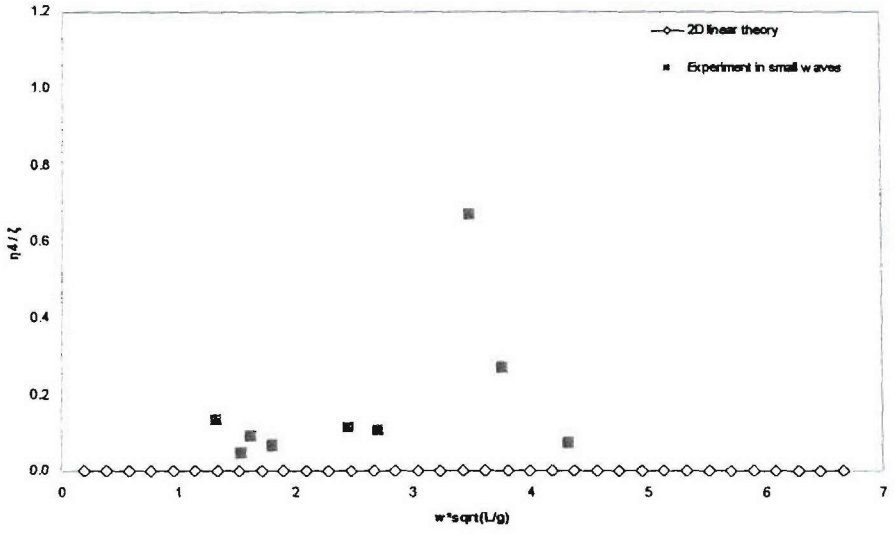

Figure 7.2-35: Roll RAO of DS3 H5415 at head waves

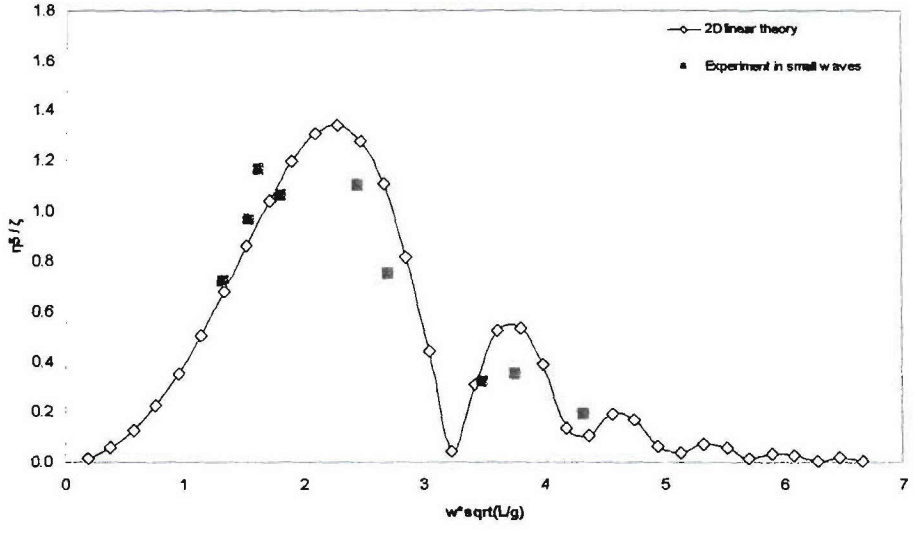

Figure 7.2-36: Pitch RAO of DS3 H5415 at head waves

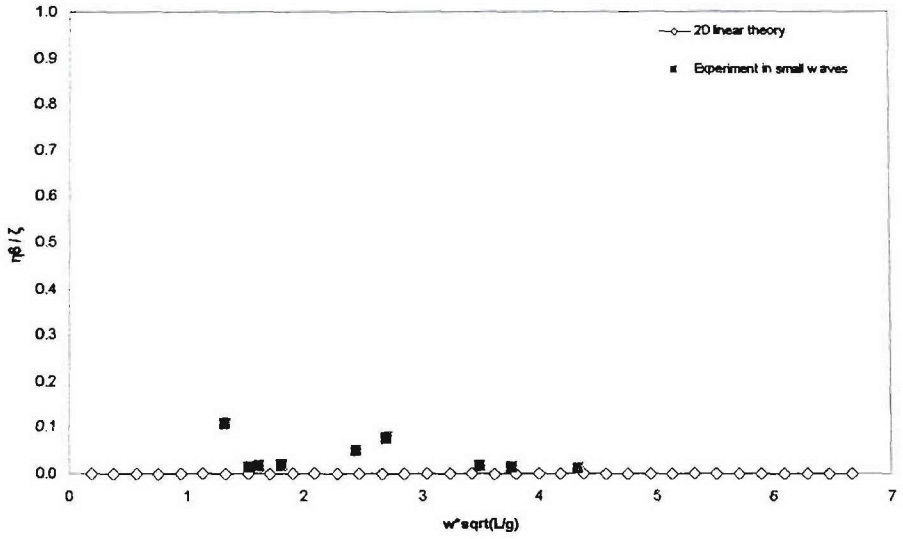

Figure 7.2-37: Yaw RAO of DS3 H5415 at head waves

7.2.1.3.2 Stern quartering waves

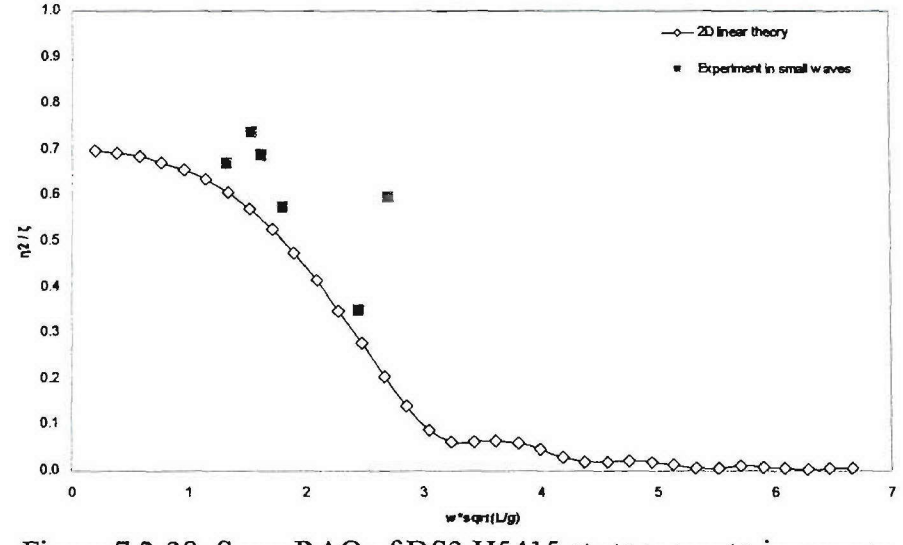

Figure 7.2-38: Sway RAO of DS3 H5415 at stern quartering waves

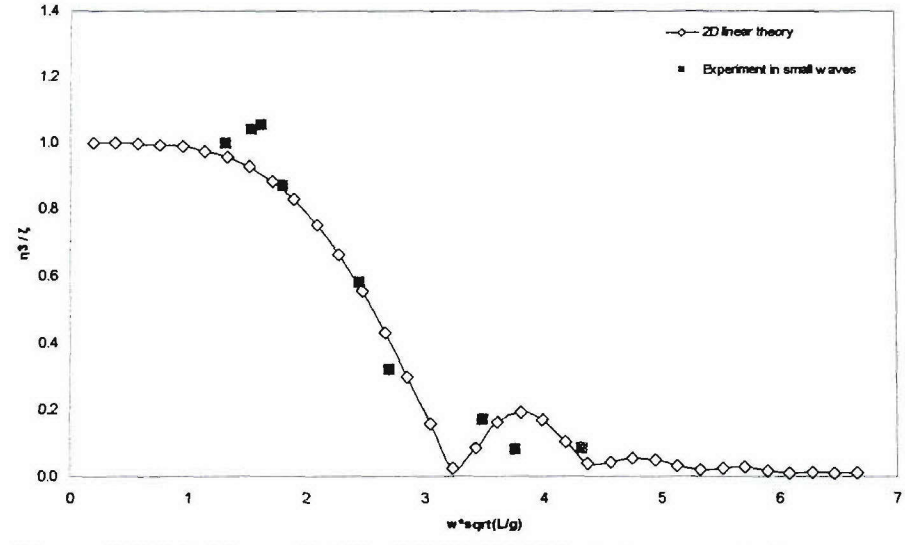

Figure 7.2-39: Heave RAO of DS3 H5415 at stern quartering waves

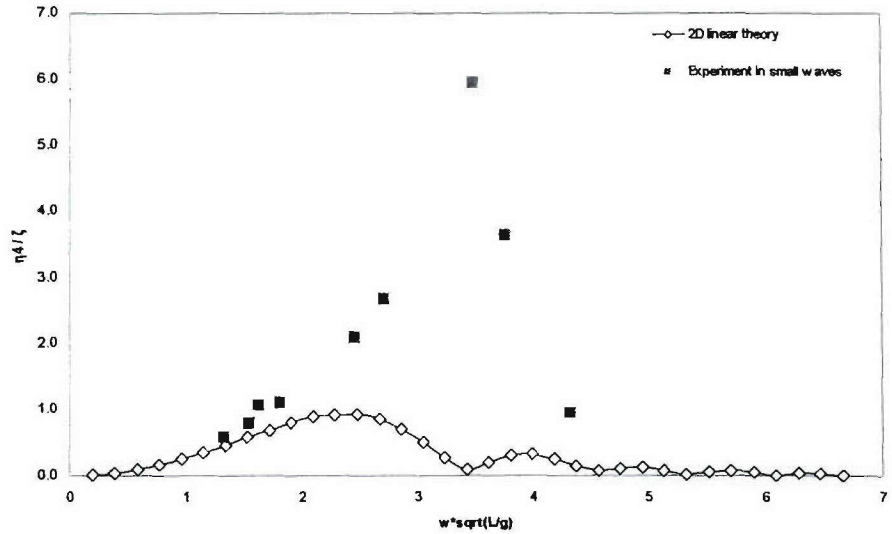

Figure 7.2-40: Roll RAO of DS3 H5415 at stern quartering waves

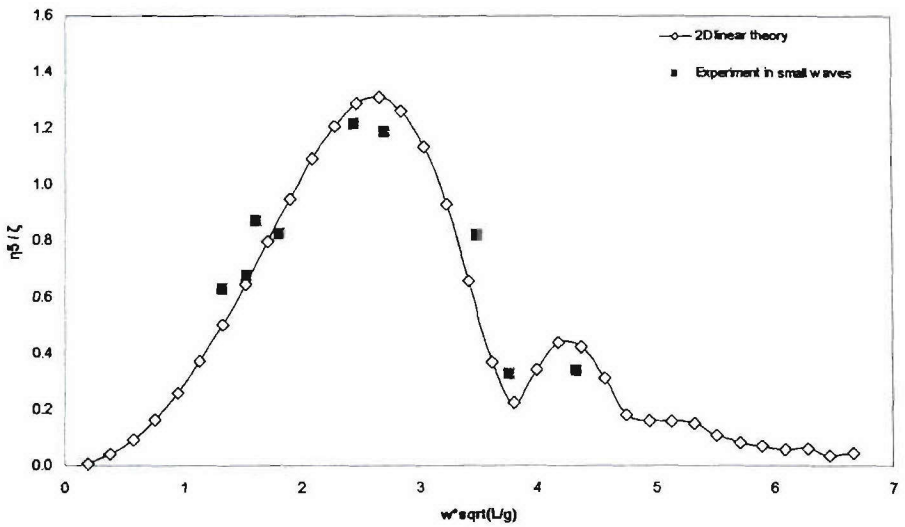

Figure 7.2-41: Pitch RAO of DS3 H5415 at stern quartering waves

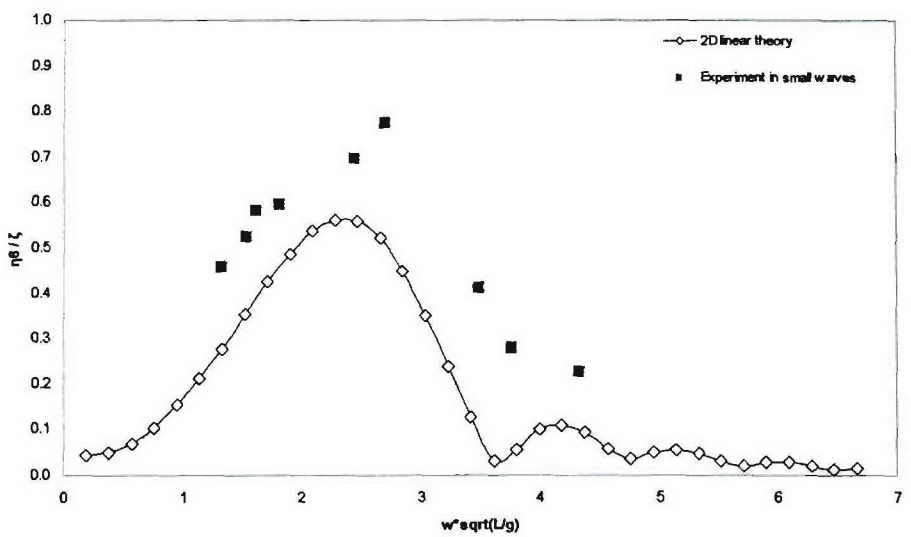

Figure 7.2-42: Yaw RAO of DS3 H5415 at stern quartering waves

7.2.1.3.3 Beam waves

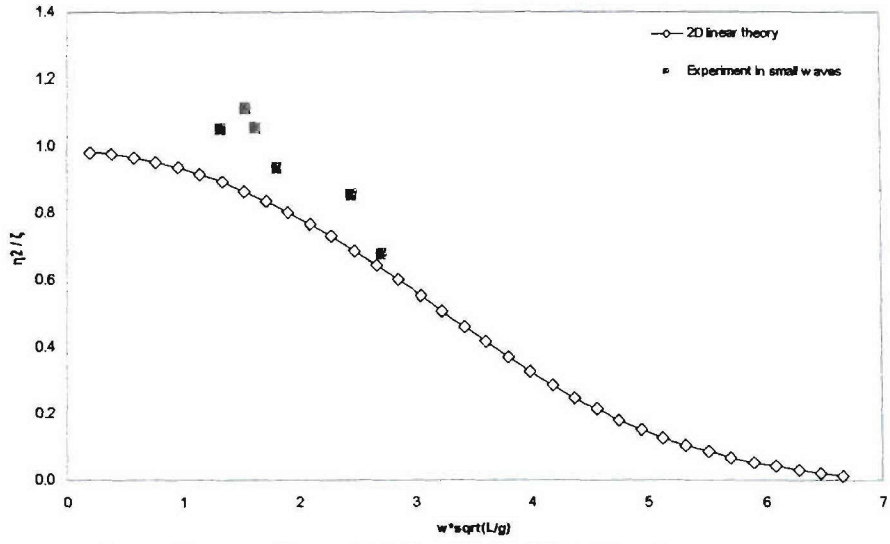

Figure 7.2-43: Sway RAO of DS3 H5415 at beam waves

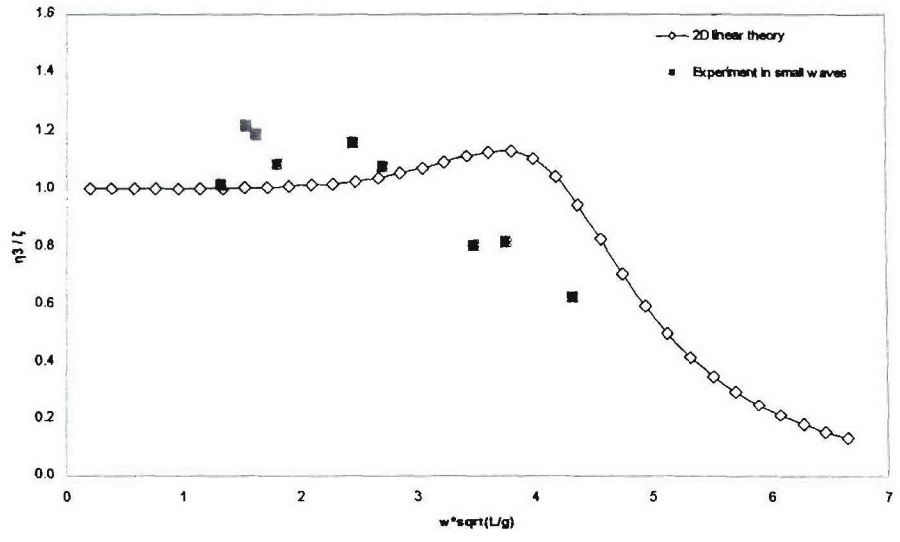

Figure 7.2-44: Heave RAO of DS3 H5415 at beam waves

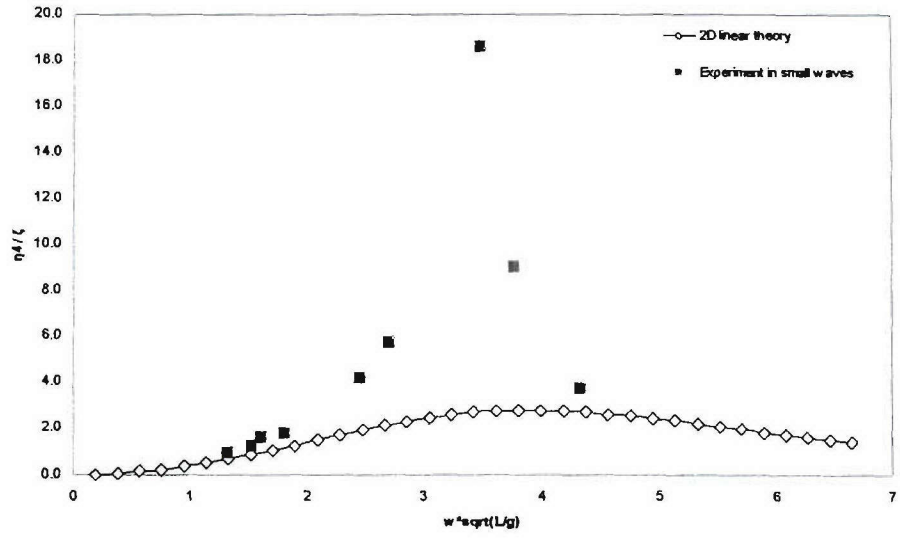

Figure 7.2-45: Roll RAO of DS3 H5415 at beam waves

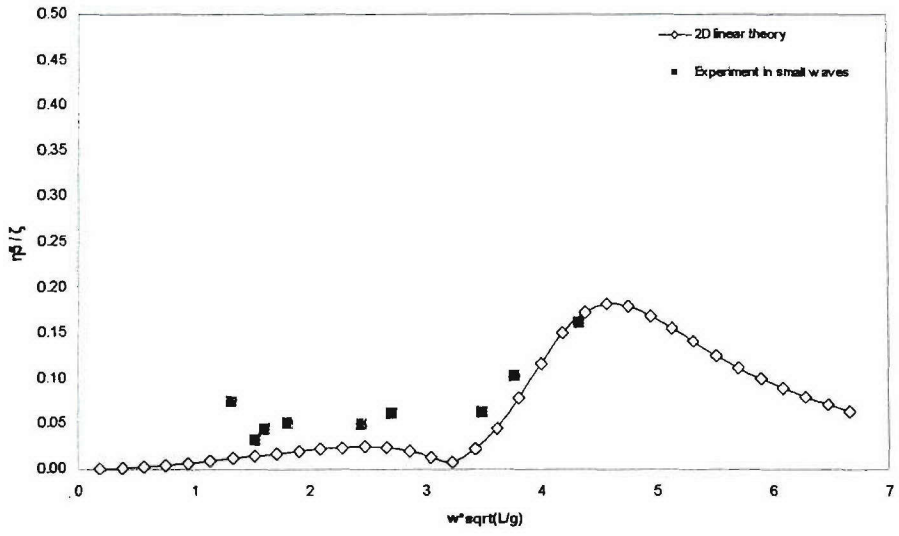

Figure 7.2-46: Pitch RAO of DS3 H5415 at beam waves

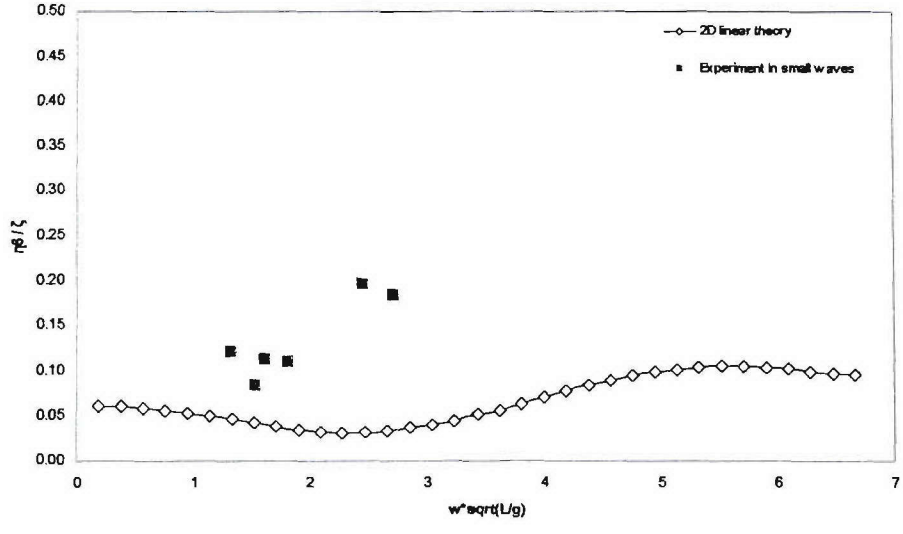

Figure 7.2-47: Yaw RAO of DS3 H5415 at beam waves

7.2.2 Comparison of predictions and measurements for global dynamic wave loads using 2D linear theory

7.2.2.1 Comparison in intact condition

The global dynamic wave induced loads calculated using 2D linear method and measurements of intact H5415 vessel in three different wave angles are presented in the following figures.

- Figures 7.2-48 to 7.2-52 for intact ship in head waves.
- Figures 7.2-53 to 7.2-57 for intact ship in stern quartering waves.
- Figures 7.2-58 to 7.2-62 for intact ship in beam waves.

In the measurements of model tests, the global dynamic wave induced loads in two different wave amplitudes were investigated. Experimental wave conditions used in model tests are shown in Table 4.1-5. The correlation between the predicted and measured values shows that the agreement in large waves is slightly better than those in small waves. But the differences in the experiment values according to wave amplitudes are small. The correlation between the computations and measurements of global dynamic wave induced load response amplitudes of the intact ship is reasonable for head and stern quartering waves while the differences of the results in beam waves are significant. Nevertheless the magnitude of loads in beam waves is usually very small, so the large difference in numerical prediction would not cause much concern in the strength assessment of hull girders. Overall the 2D linear strip method presents acceptable agreements with the measurements. This will be further examined by calculating the model uncertainty of the 2D linear method in section 7.3.

7.2.2.1.1 Head waves

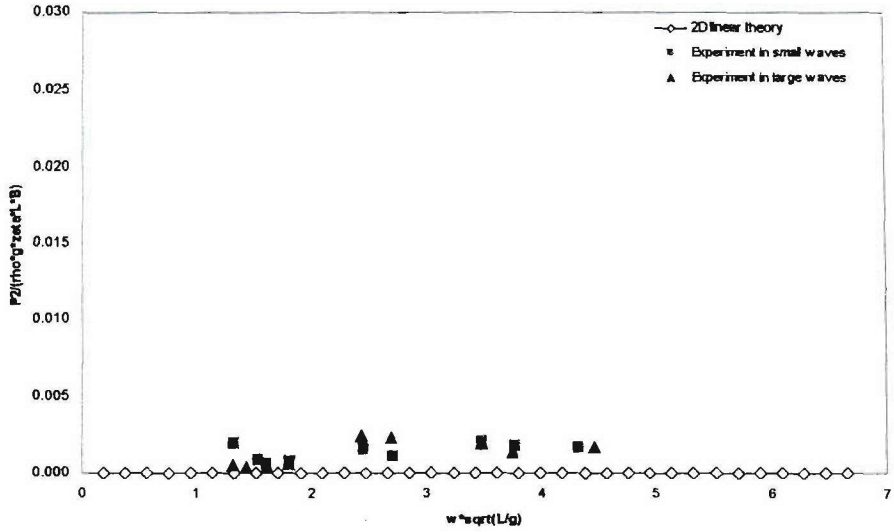

Figure 7.2-48: Dynamic horizontal shear force RAO of intact H5415 at head waves

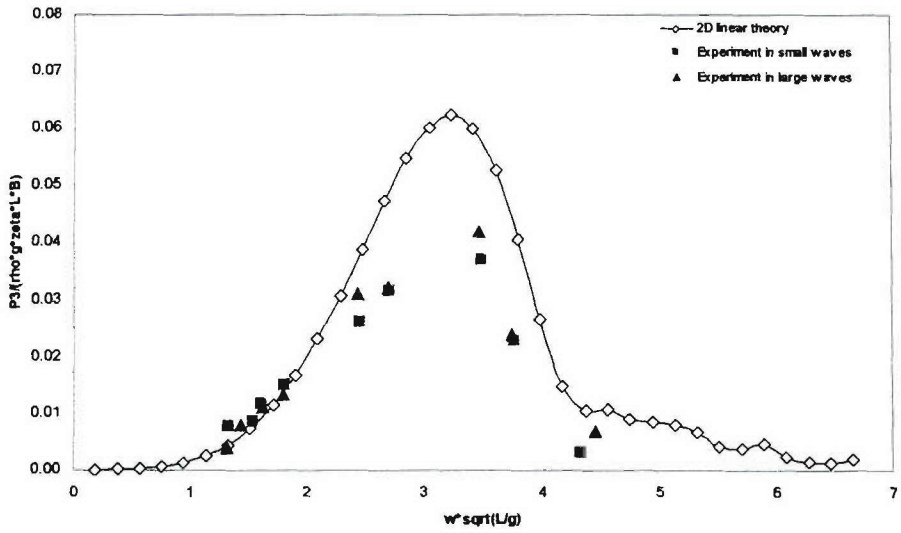

Figure 7.2-49: Dynamic vertical shear force RAO of intact H5415 at head waves

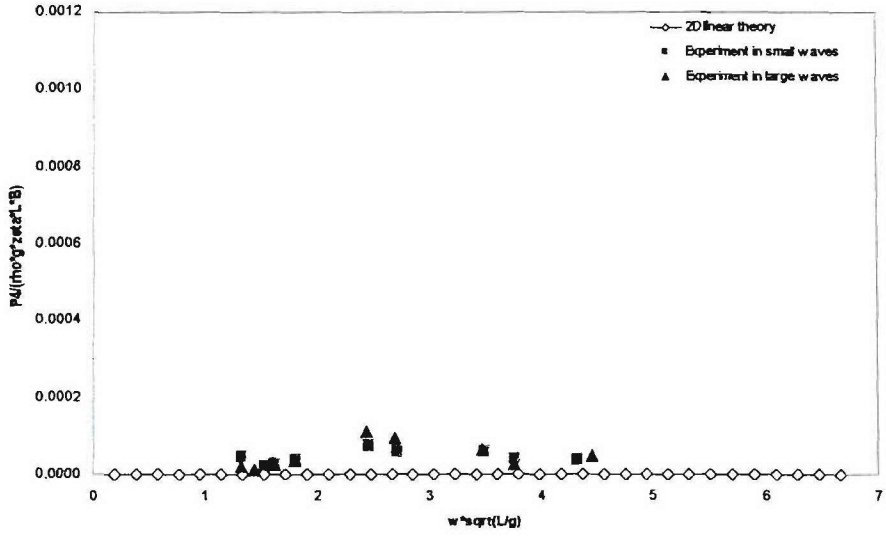

Figure 7.2-50: Dynamic torsion moment RAO of intact H5415 at head waves

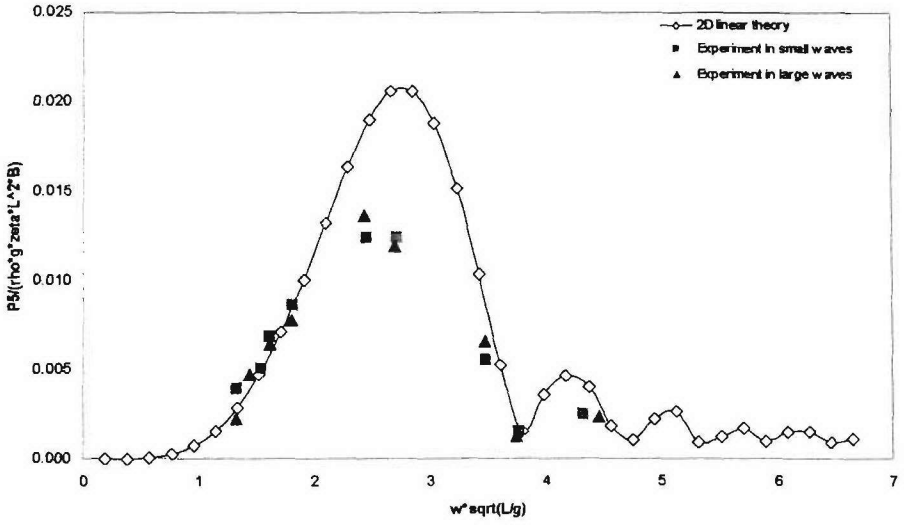

Figure 7.2-51: Dynamic vertical bending moment force RAO of intact H5415 at head waves

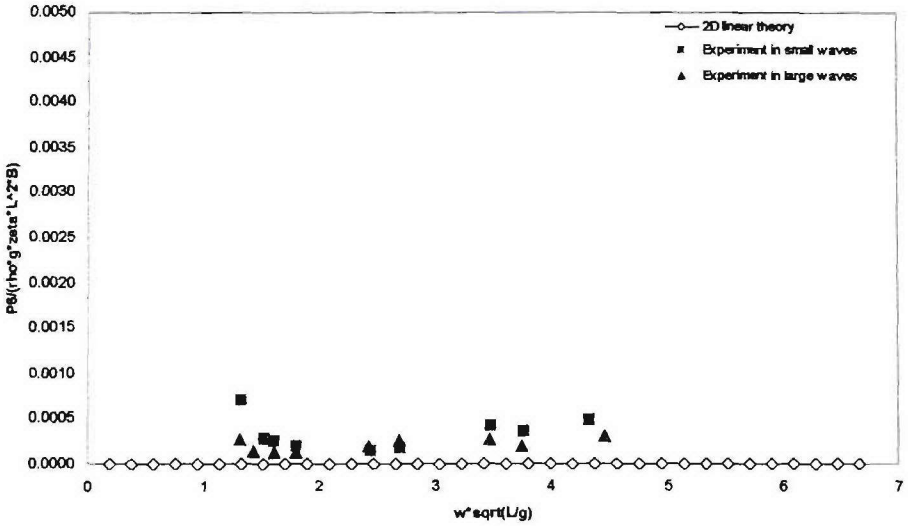

Figure 7.2-52: Dynamic horizontal bending moment RAO of intact H5415 at head waves

7.2.2.1.2 Stern quartering waves

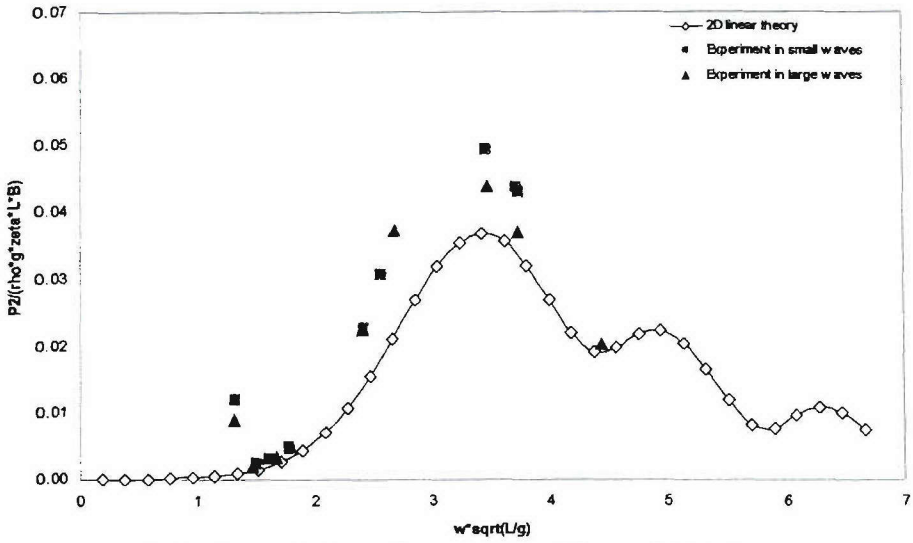

Figure 7.2-53: Dynamic horizontal shear force RAO of intact H5415 at stern quartering waves

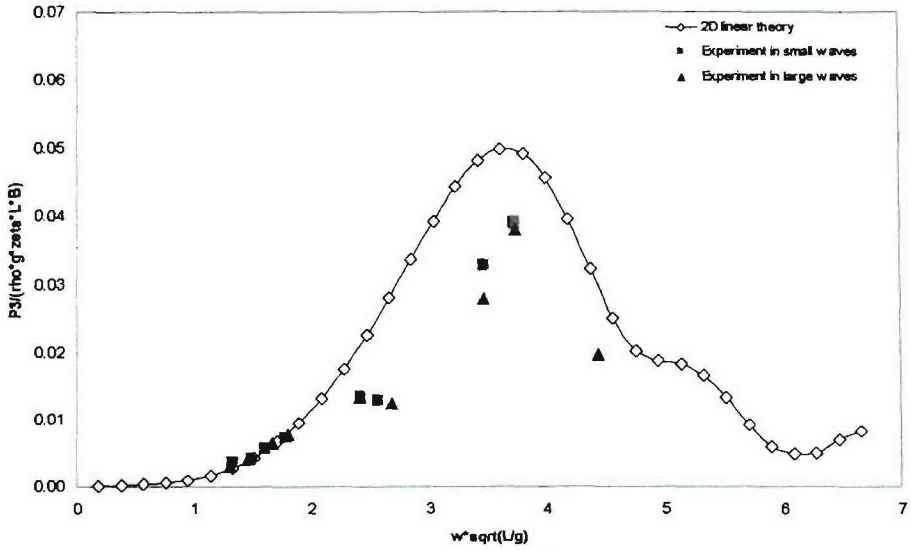

Figure 7.2-54: Dynamic vertical shear force RAO of intact H5415 at stern quartering waves

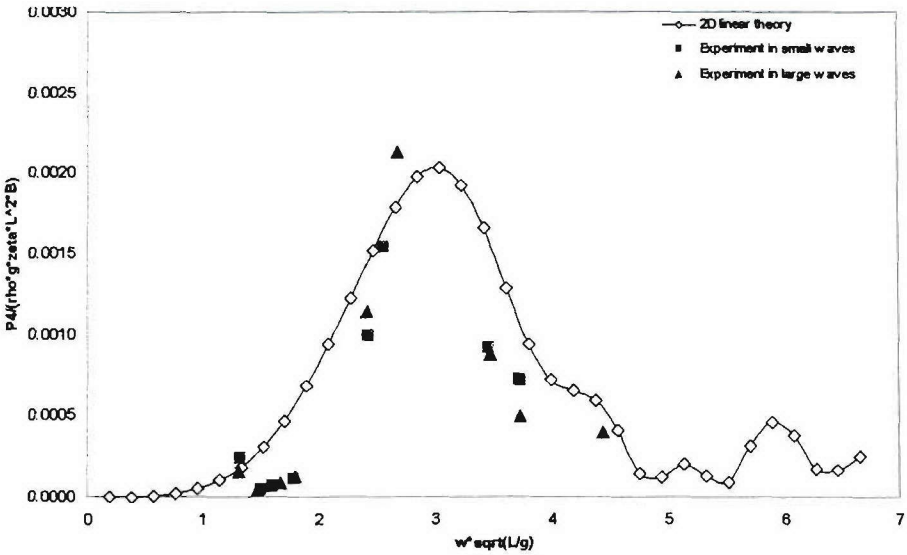

Figure 7.2-55: Dynamic torsion moment RAO of intact H5415 at stern quartering waves

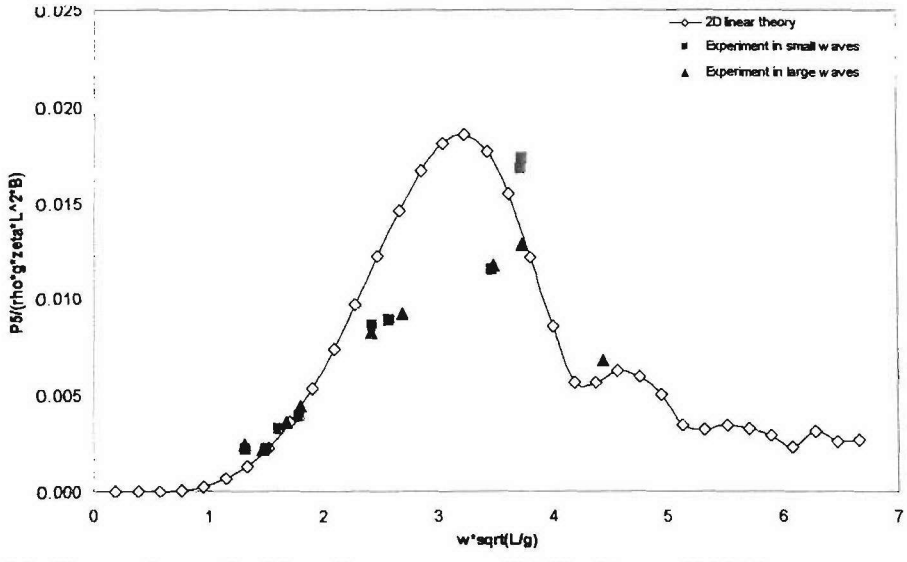

Figure 7.2-56: Dynamic vertical bending moment RAO of intact H5415 at stern quartering waves

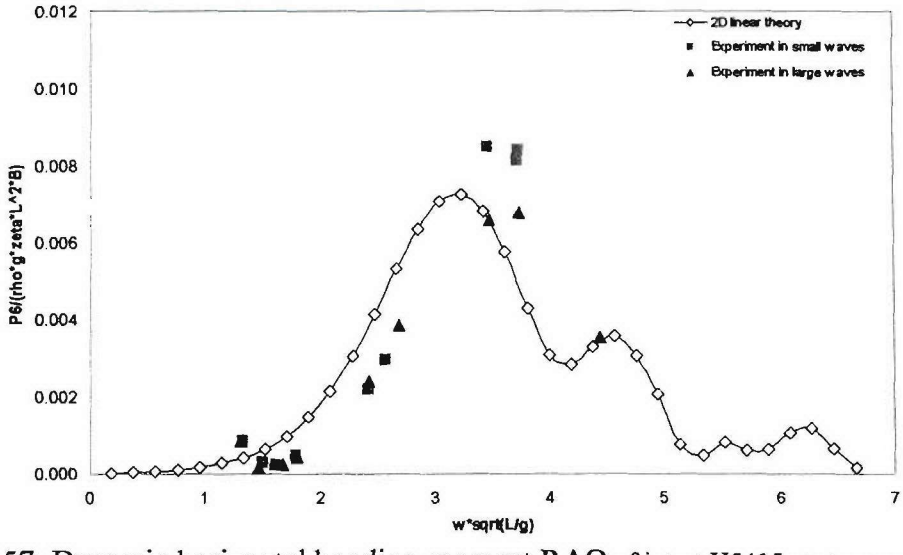

Figure 7.2-57: Dynamic horizontal bending moment RAO of intact H5415 at stern quartering waves

7.2.2.1.3 Beam waves

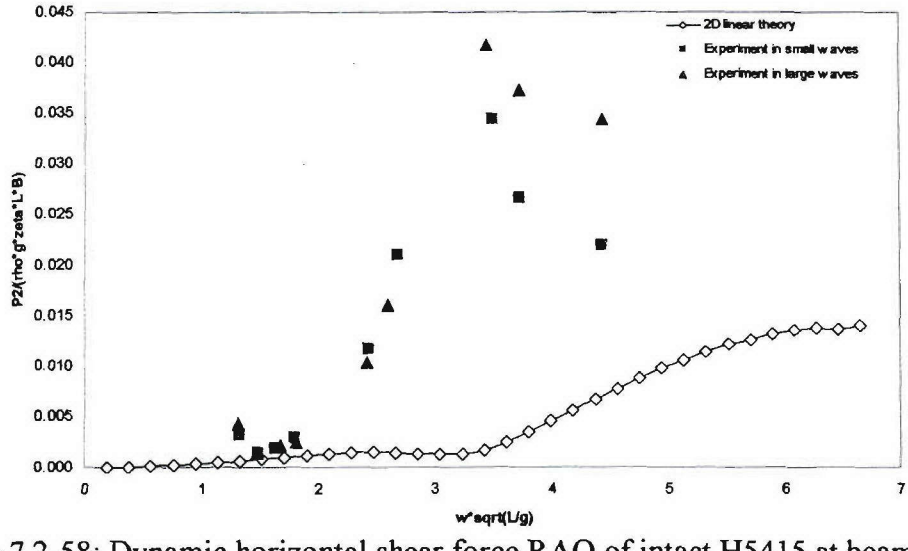

Figure 7.2-58: Dynamic horizontal shear force RAO of intact H5415 at beam waves

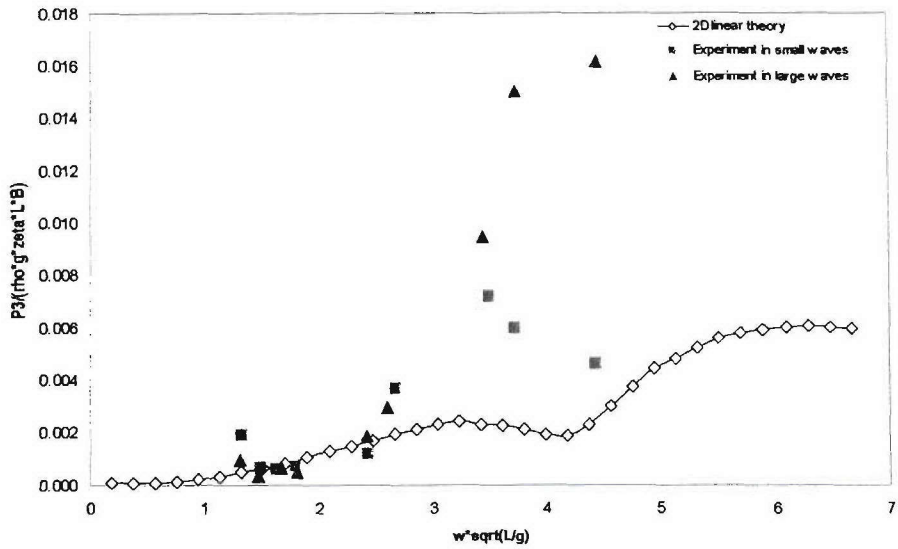

Figure 7.2-59: Dynamic vertical shear force RAO of intact H5415 at beam waves

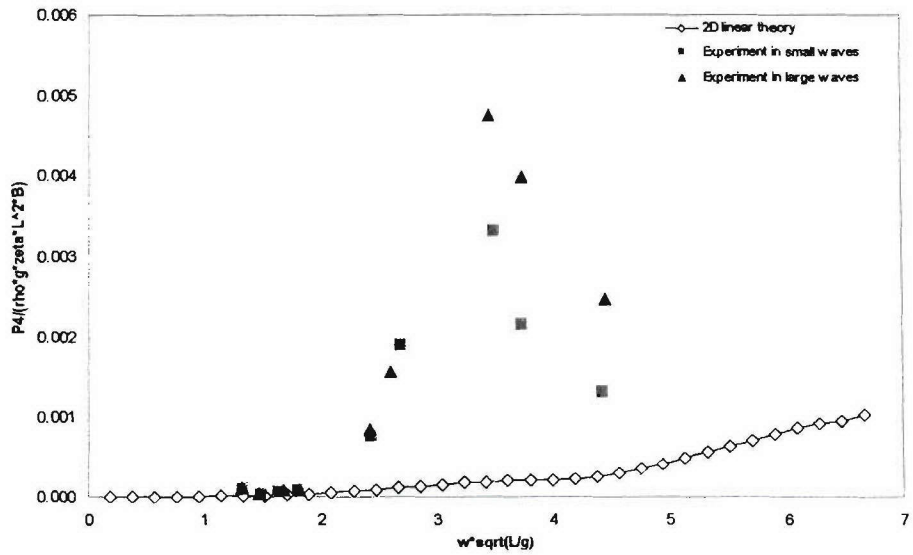

Figure 7.2-60: Dynamic torsion moment RAO of intact H5415 at beam waves

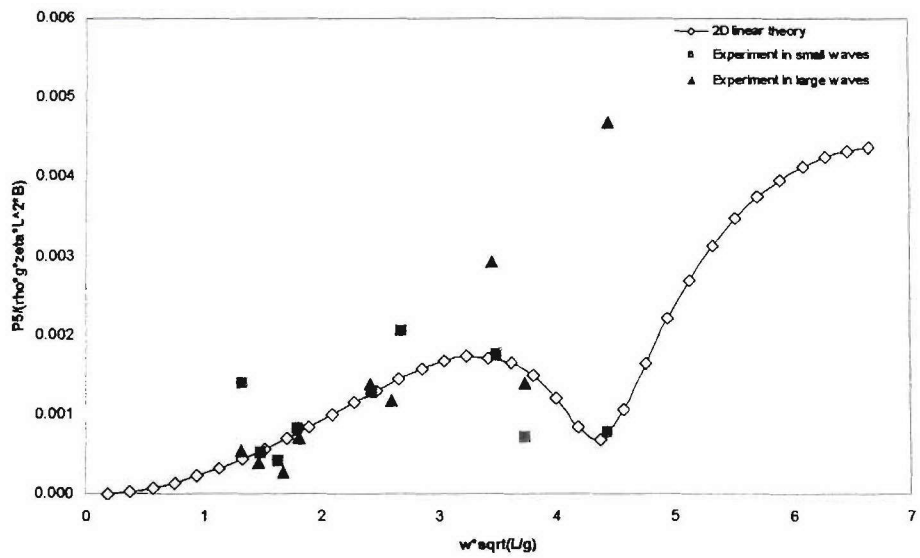

Figure 7.2-61: Dynamic vertical bending moment RAO of intact H5415 at beam waves

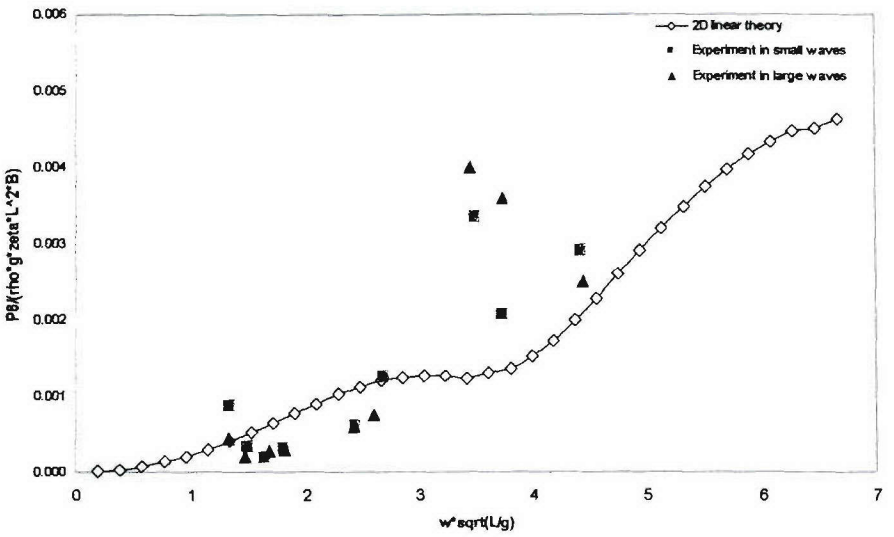

Figure 7.2-62: Dynamic horizontal bending moment RAO of intact H5415 at beam waves

7.2.2.2 Comparison in damage scenario 2

The global dynamic wave induced loads calculated using 2D linear method and measurements of DS2 H5415 vessel in five different wave angles are presented in the following figures.

- Figures 7.2-63 to 7.2-67 for DS2 ship in head waves.
- Figures 7.2-68 to 7.2-72 for DS2 ship in stern quartering waves *(β=45)*.
- Figures 7.2-73 to 7.2-77 for DS2 ship in stern quartering waves *(β=315)*.
- Figures 7.2-78 to 7.2-82 for DS2 ship in beam waves *(β=90)*.
- Figures 7.2-83 to 7.2-87 for DS2 ship in beam waves *(β=270)*.

In the experiments the global dynamic wave induced loads with two different wave amplitudes were investigated. The correlation between the predicted and measured values shows that the measurements under large waves and small waves are not significantly different.

In head and stern quartering waves, the differences between the computations and measurements of global dynamic wave induced load response amplitudes of DS2 ship with different wave amplitudes are reasonable. The 2D linear method presents acceptable agreements with the measurements. However the differences between the predictions and measurements of dynamic torsion moments are significant. And these phenomena could be caused by the effects of sloshing and slamming within the damaged compartments, which could reduce the global dynamic wave load components.

The measured and predicted dynamic wave induced loads in beam waves are in good agreements for vertical shear forces and vertical bending moments while there are significant differences in the results of horizontal dynamic wave induced load components. The possible reasons for this difference are the sloshing and slamming effects within the damaged compartment. In addition the drift of model may also be attributed to this difference.

7.2.2.2.1 Head waves

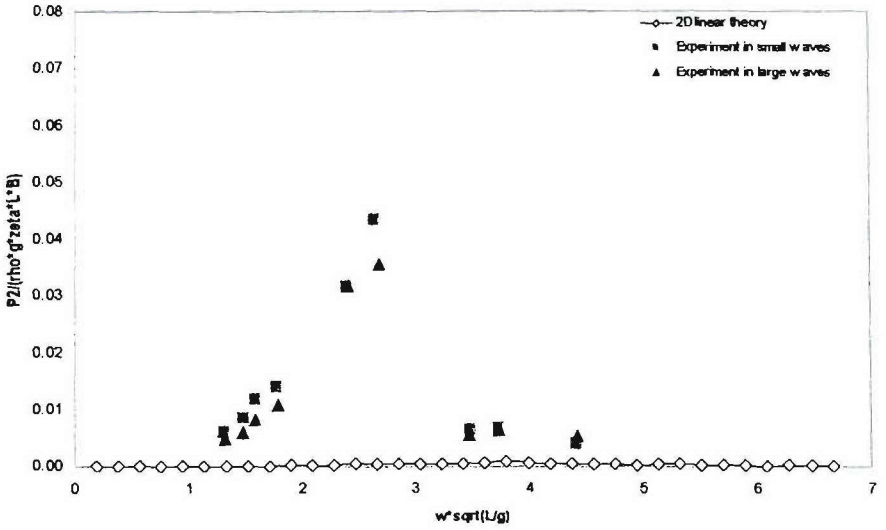

Figure 7.2-63: Dynamic horizontal shear force RAO of DS2 H5415 at head waves

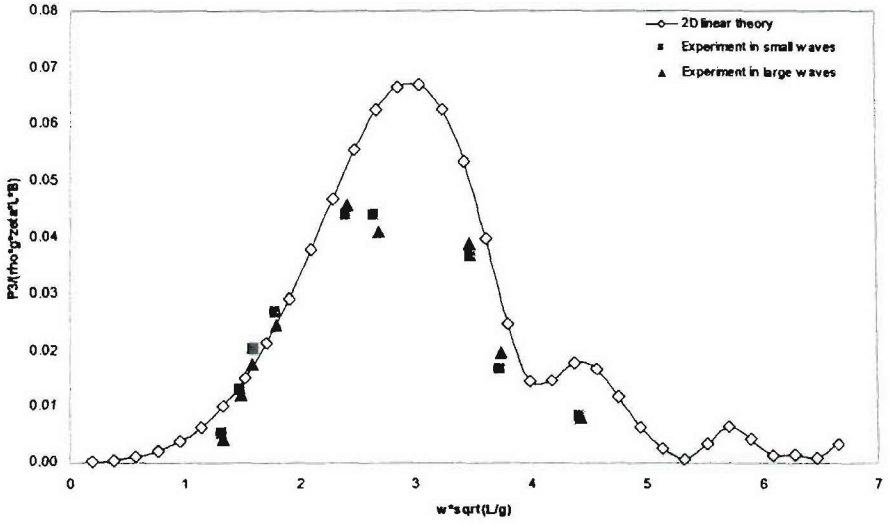

Figure 7.2-64: Dynamic vertical shear force RAO of DS2 H5415 at head waves

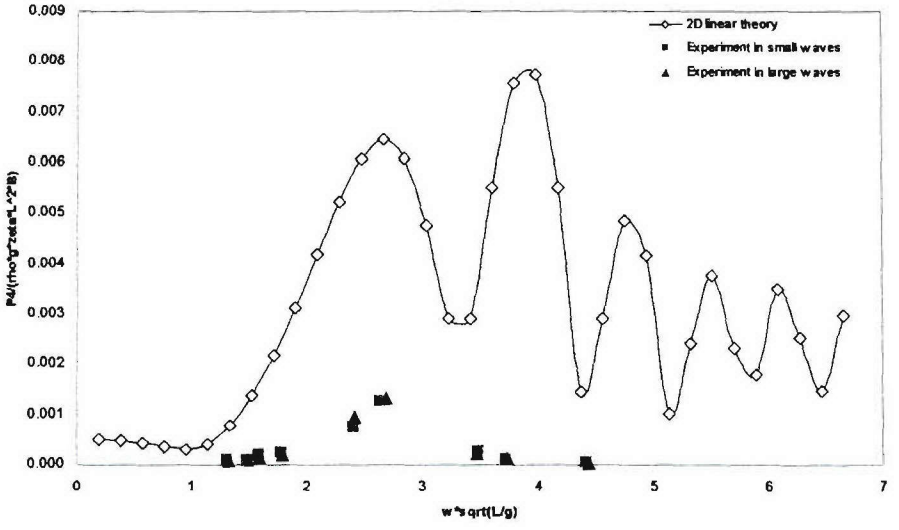

Figure 7.2-65: Dynamic torsion moment RAO of DS2 H5415 at head waves

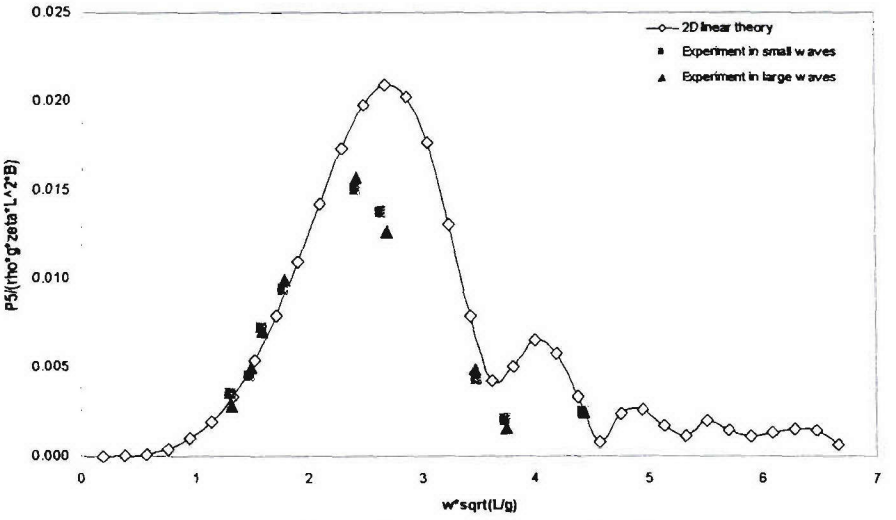

Figure 7.2-66: Dynamic vertical bending moment RAO of DS2 H5415 at head waves

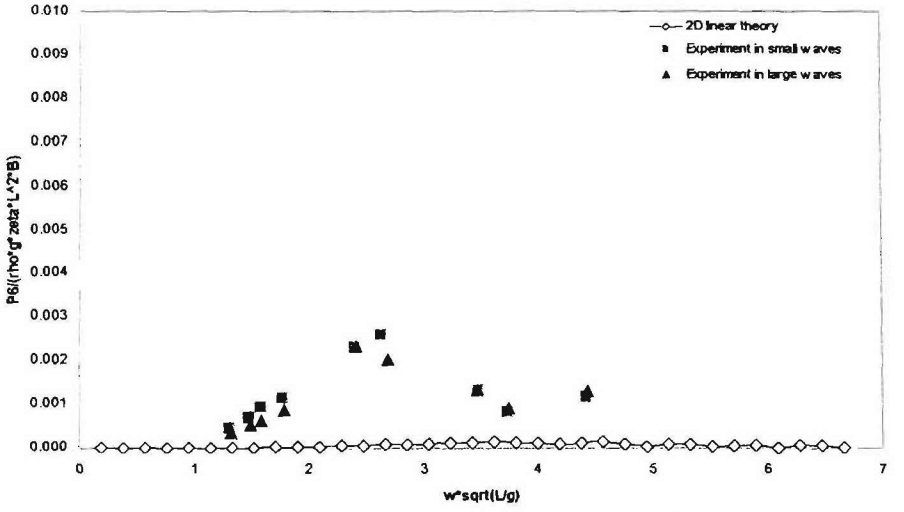

Figure 7.2-67: Dynamic horizontal bending moment RAO of DS2 H5415 at head waves

7.2.2.2.2 Stern quartering waves (heading 45)

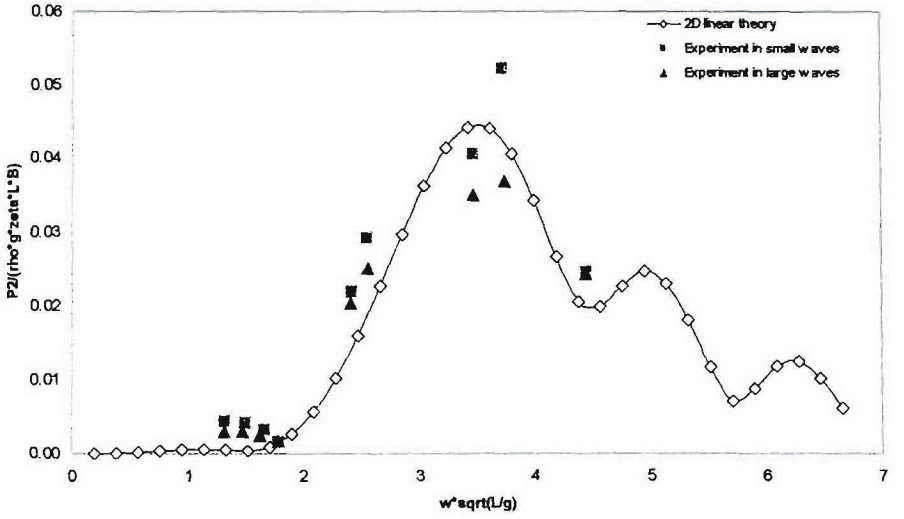

Figure 7.2-68: Dynamic horizontal shear force RAO of DS2 H5415 at stern quartering waves (heading 45)

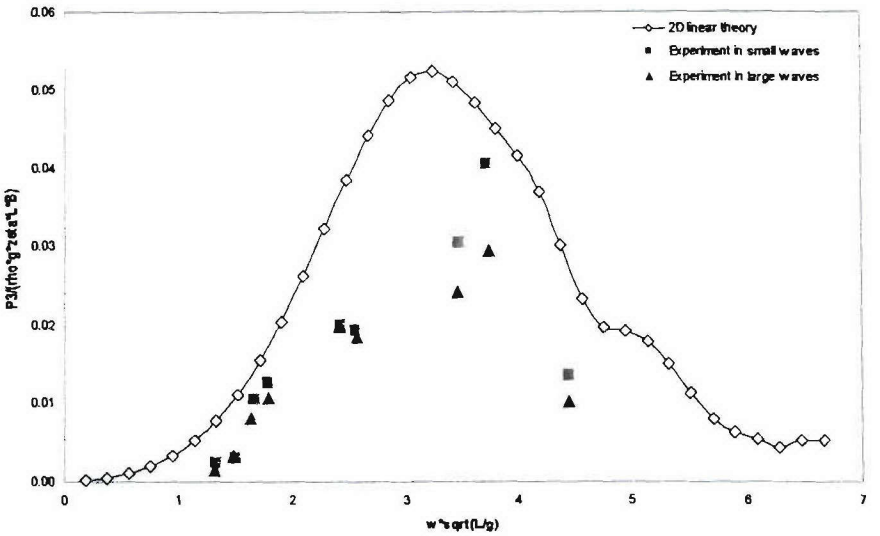

Figure 7.2-69: Dynamic vertical shear force RAO of DS2 H5415 at stern quartering waves (heading 45)

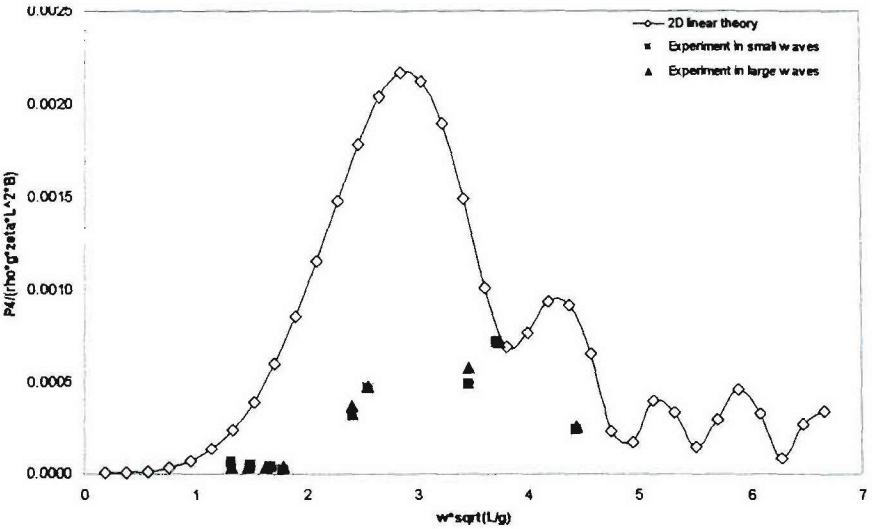

Figure 7.2-70: Dynamic torsion RAO of DS2 H5415 at stern quartering waves (heading 45)

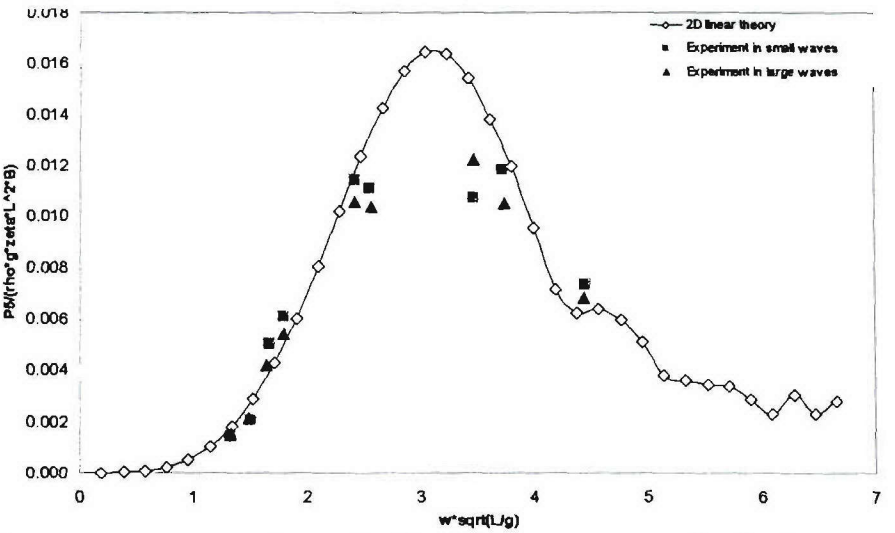

Figure 7.2-71: Dynamic vertical bending moment RAO of DS2 H5415 at stern quartering waves (heading 45)

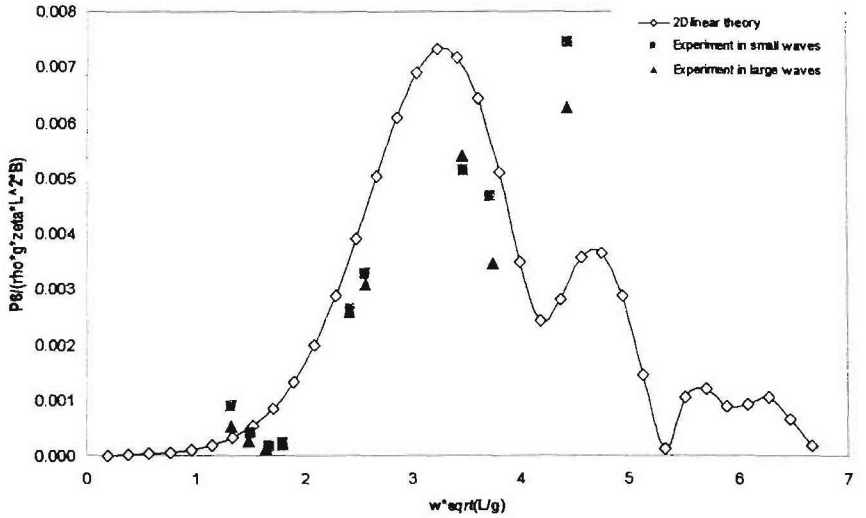

Figure 7.2-72: Dynamic horizontal bending moment RAO of DS2 H5415 at stern quartering waves (heading 45)

7.2.2.2.3 Stern quartering waves (heading 315)

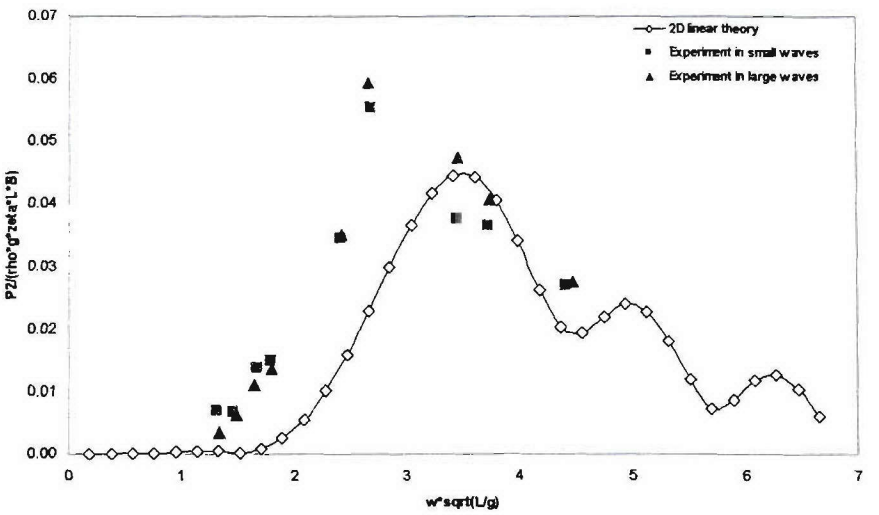

Figure 7.2-73: Dynamic horizontal shear force RAO of DS2 H5415 at stern quartering waves (heading 315)

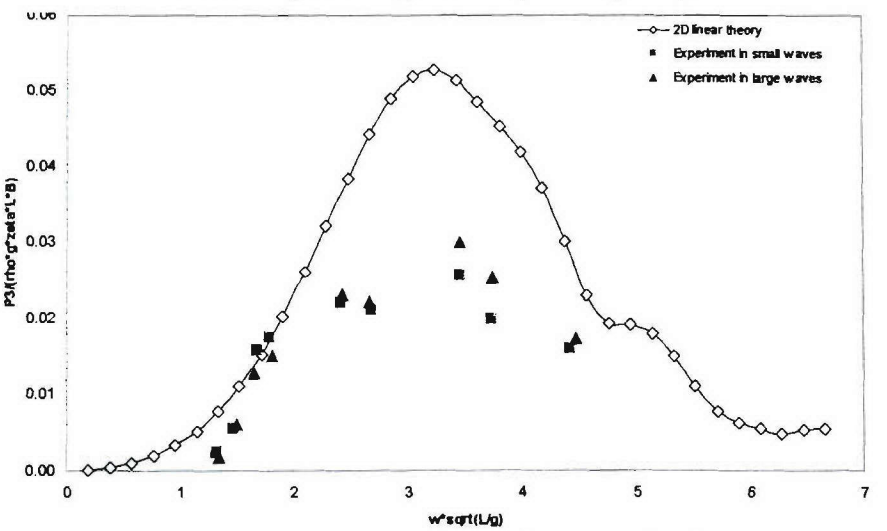

Figure 7.2-74: Dynamic vertical shear force RAO of DS2 H5415 at stern quartering waves (heading 315)

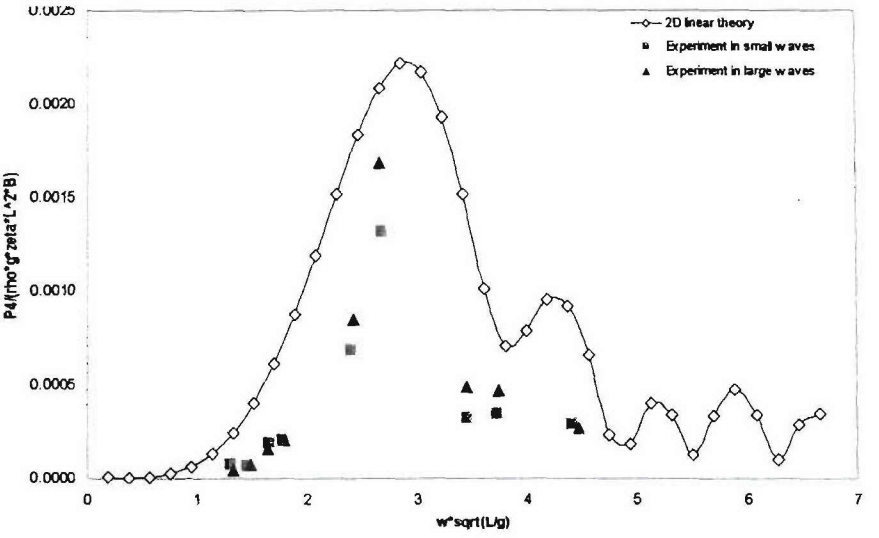

Figure 7.2-75: Dynamic torsion moment RAO of DS2 H5415 at stern quartering waves (heading 315)

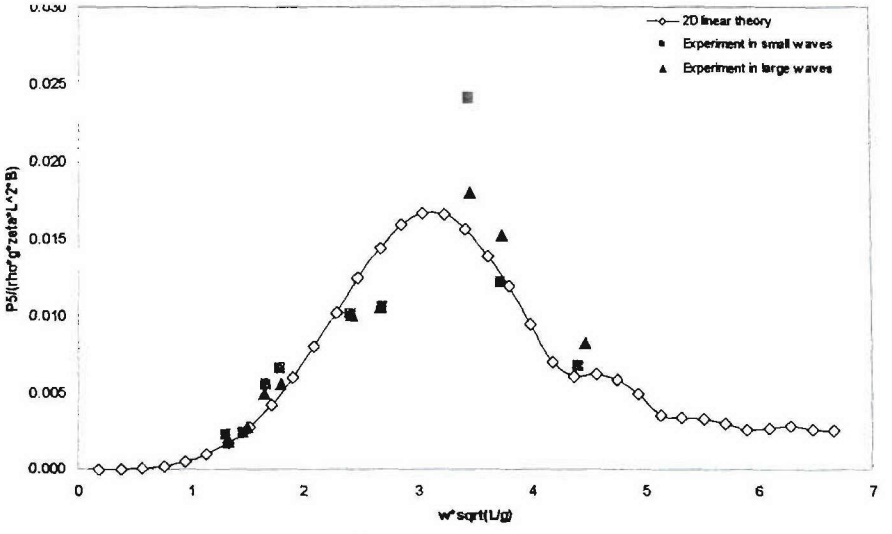

Figure 7.2-76: Dynamic vertical bending moment RAO of DS2 H5415 at stern quartering waves (heading 315)

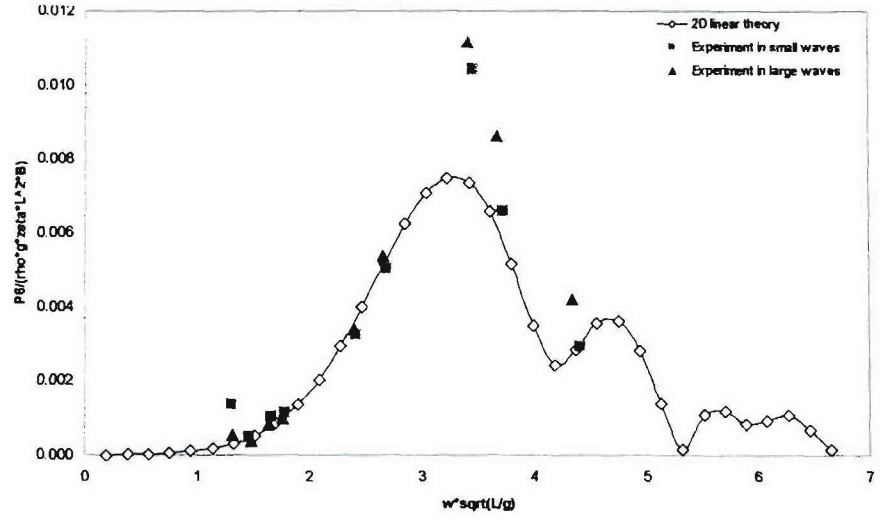

Figure 7.2-77: Dynamic horizontal bending moment RAO of DS2 H5415 at stern quartering waves (heading 315)

7.2.2.2.4 Beam waves (heading 90)

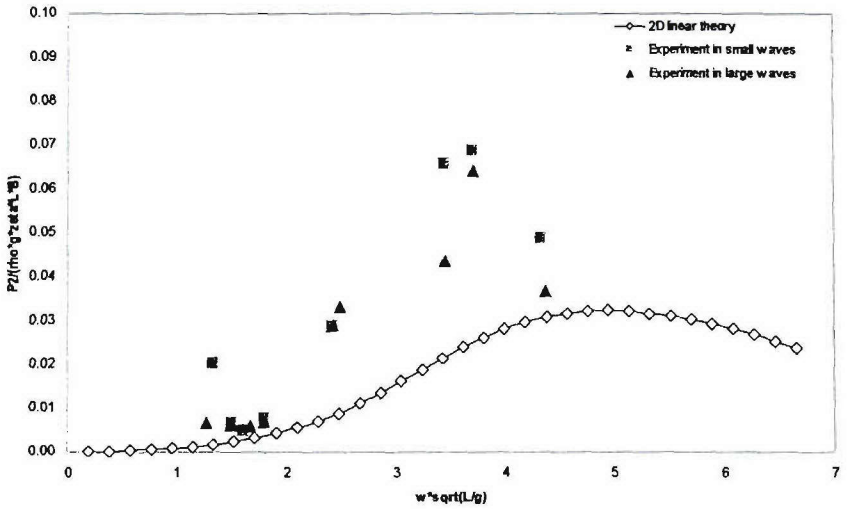

Figure 7.2-78: Dynamic horizontal shear force RAO of DS2 H5415 at beam waves (heading 90)

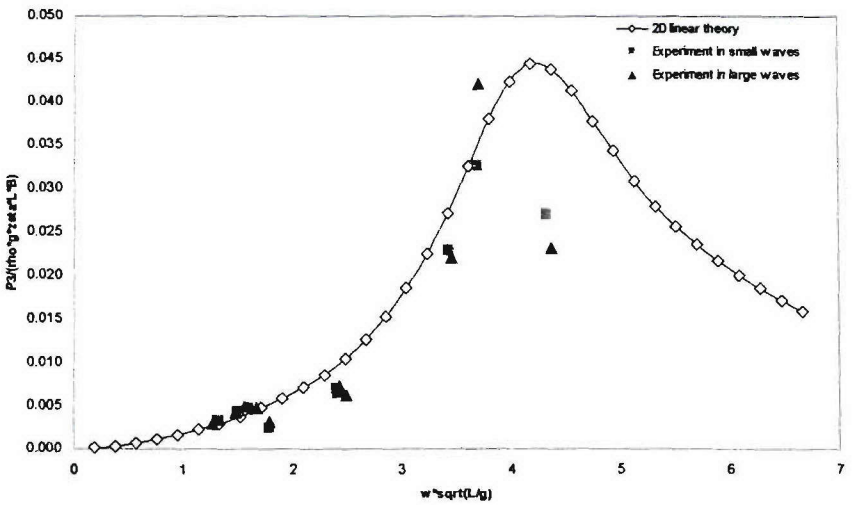

Figure 7.2-79: Dynamic vertical shear force RAO of DS2 H5415 at beam waves (heading 90)

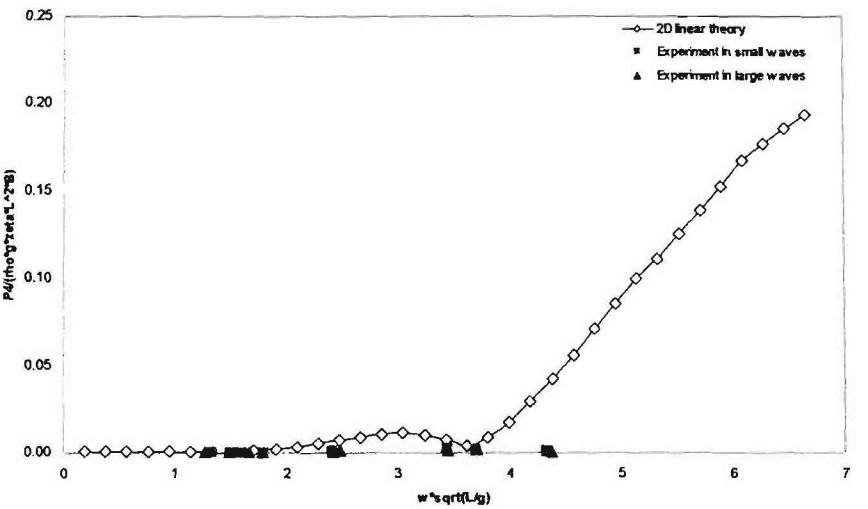

Figure 7.2-80: Dynamic torsion moment RAO of DS2 H5415 at beam waves (heading 90)

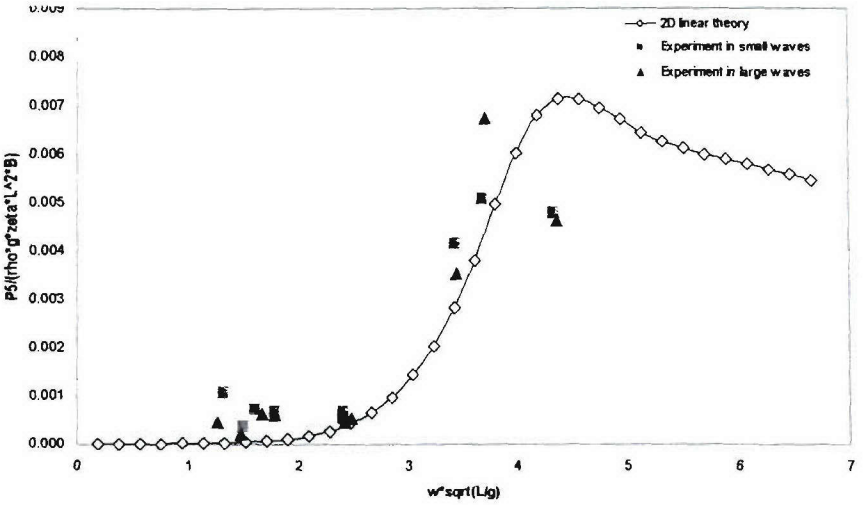

Figure 7.2-81: Dynamic vertical bending moment RAO of DS2 H5415 at beam waves (heading 90)

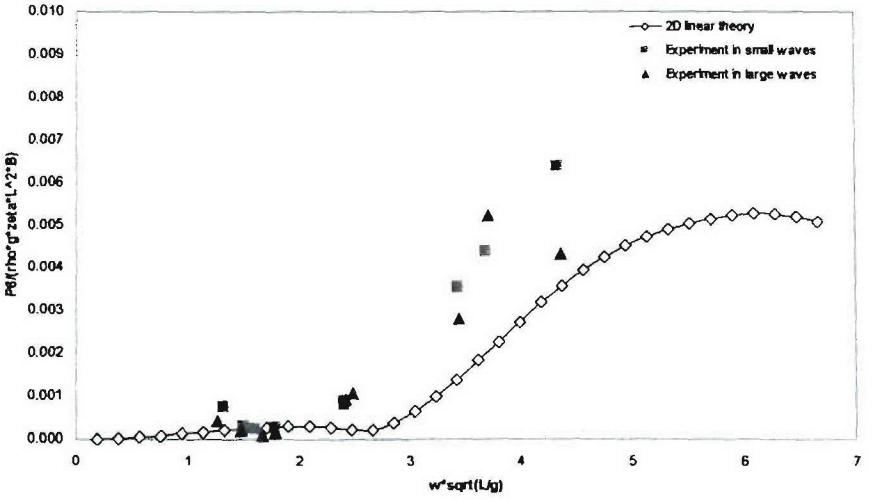

Figure 7.2-82: Dynamic horizontal bending moment RAO of DS2 H5415 at beam waves (heading 90)

7.2.2.2.5 Beam waves (heading 270)

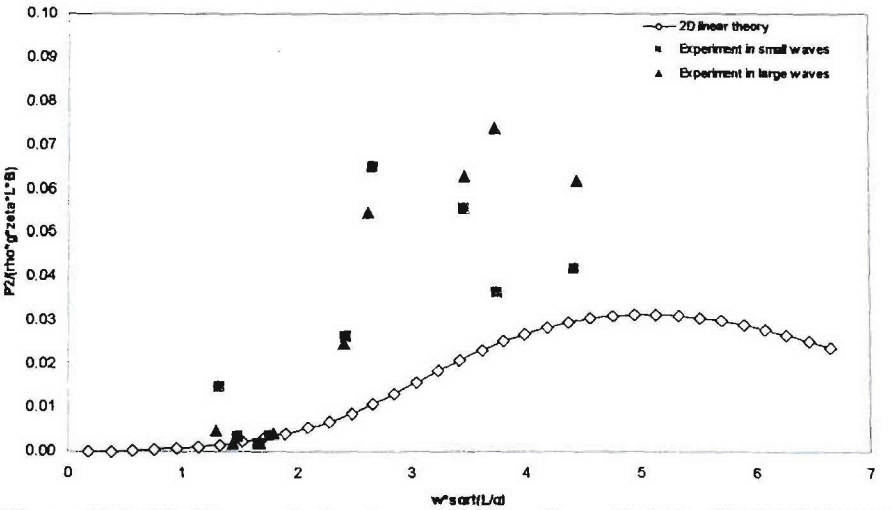

Figure 7.2-83: Dynamic horizontal shear force RAO of DS2 H5415 at beam waves (heading 270)

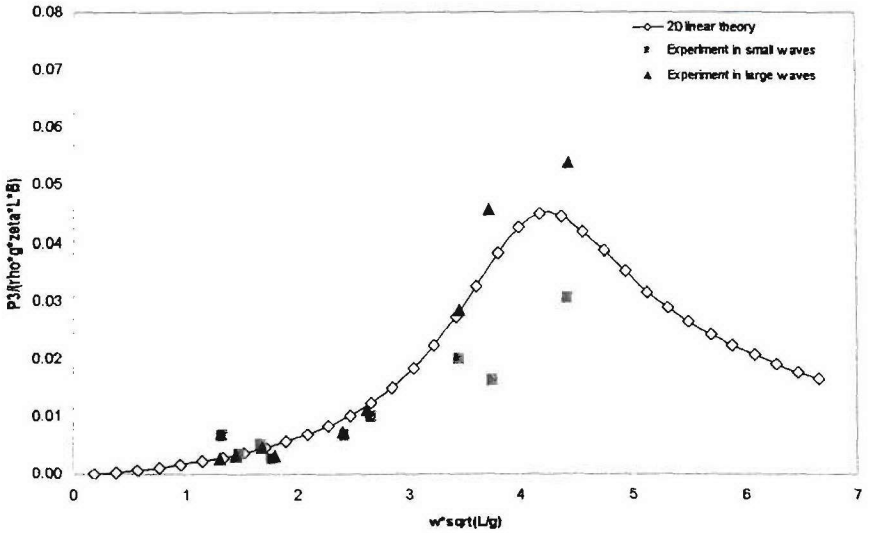

Figure 7.2-84: Dynamic vertical shear force RAO of DS2 H5415 at beam waves (heading 270)

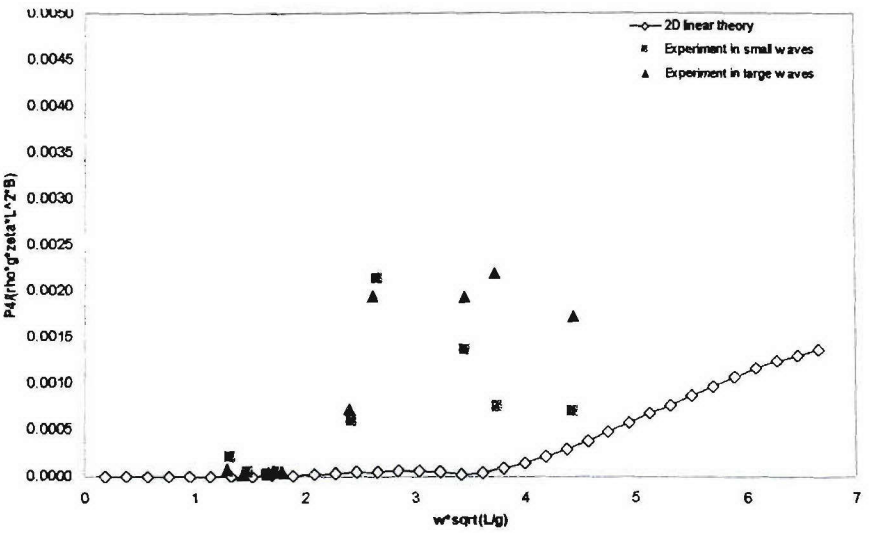

Figure 7.2-85: Dynamic torsion moment RAO of DS2 H5415 at beam waves (heading 270)

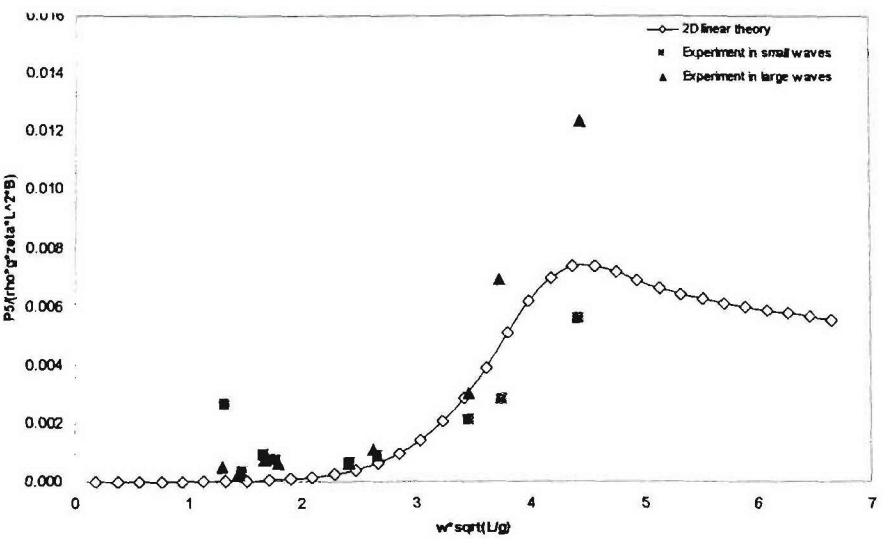

Figure 7.2-86: Dynamic vertical bending moment RAO of DS2 H5415 at beam waves (heading 270)

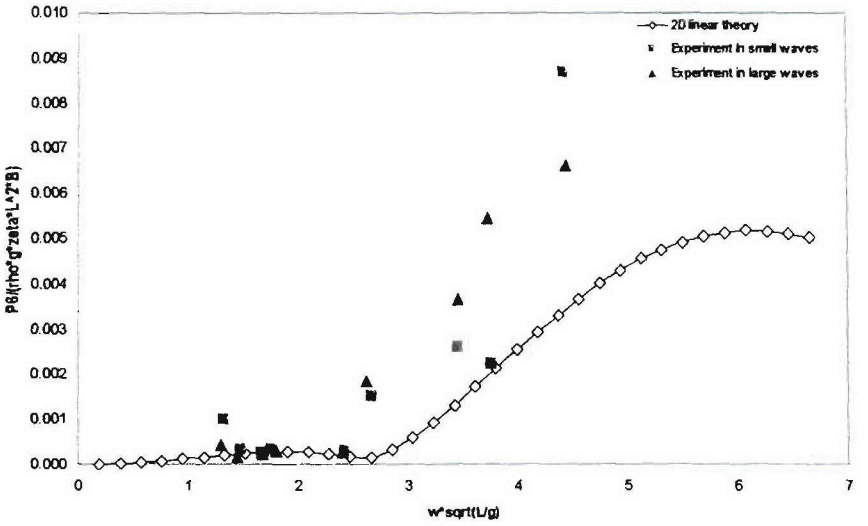

Figure 7.2-87: Dynamic horizontal bending moment RAO of DS2 H5415 at beam waves (heading 270)

7.2.2.3 Comparison in damage scenario 3

The calculated global dynamic wave induced loads and measurements of DS3 H5415 in three different wave angles are shown in the following figures.

- Figures 7.2-88 to 7.2-92 for DS3 ship in head waves.
- Figures 7.2-93 to 7.2-97 for DS3 ship in stern quartering waves.
- Figures 7.2-98 to 7.2-102 for DS3 ship in beam waves.

For experimental wave conditions investigated in model tests, see Table 4.1-5. The global dynamic wave induced loads with two different wave amplitudes were investigated in the tests. The measurements in large waves produce slightly better agreements with numerical results than those in small waves. In head and stern quartering waves, the correlation between the computations and measurements of dynamic load response amplitudes for DS3 ship is satisfactory. In the computations some predicted values are underestimated while some others are overestimated depending on the measured values. But reasonable agreements were obtained. The global dynamic wave induced loads in beam waves are not important because they are small values compared to the other load components.

7.2.2.3.1 Head waves

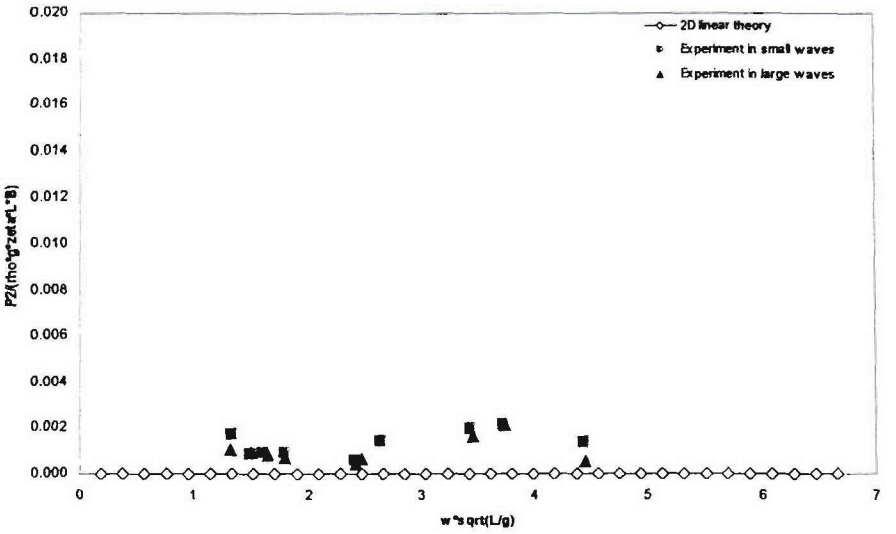

Figure 7.2-88: Dynamic horizontal shear force RAO of DS3 H5415 at head waves

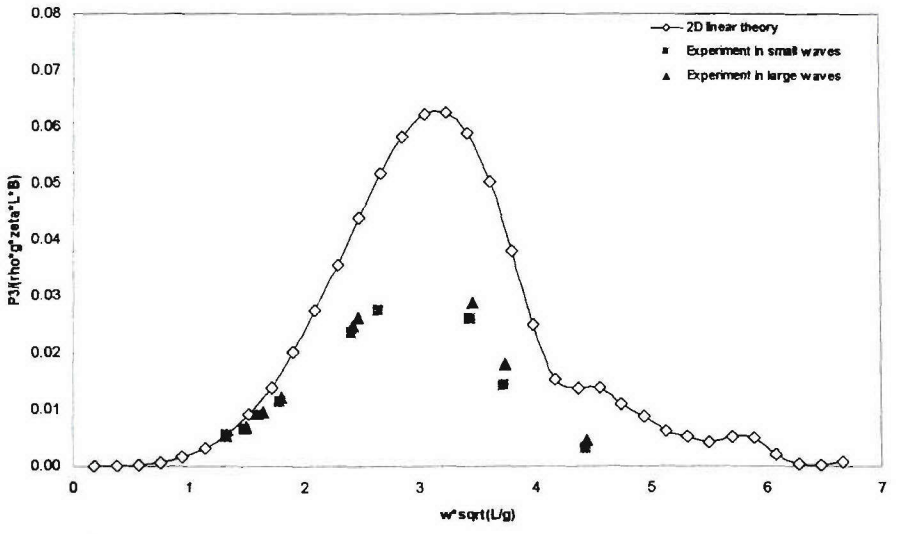

Figure 7.2-89: Dynamic vertical shear force RAO of DS3 H5415 at head waves

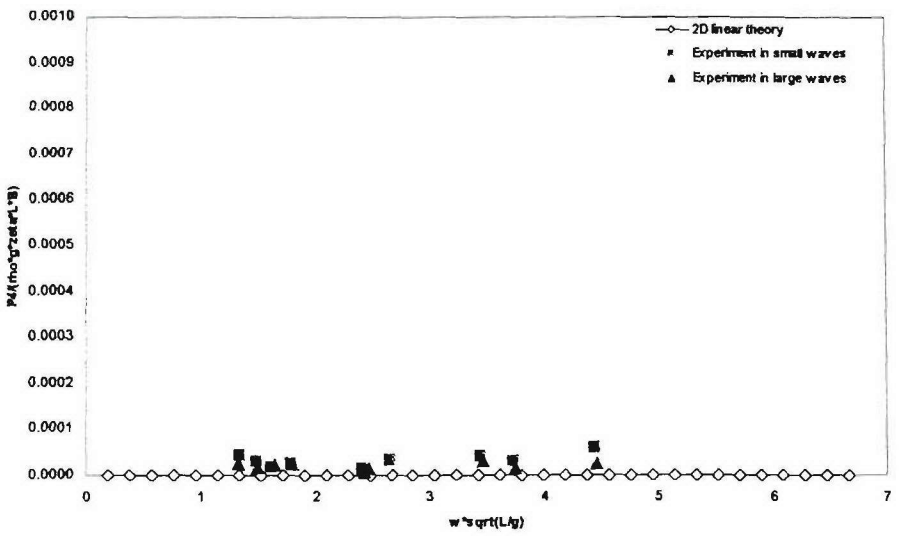

Figure 7.2-90: Dynamic torsion moment RAO of DS3 H5415 at head waves

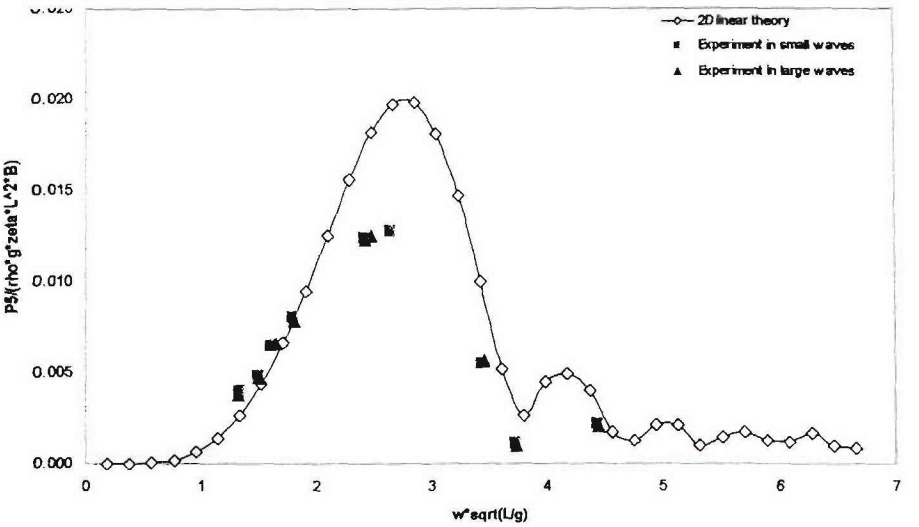

Figure 7.2-91: Dynamic vertical bending moment RAO of DS3 H5415 at head waves

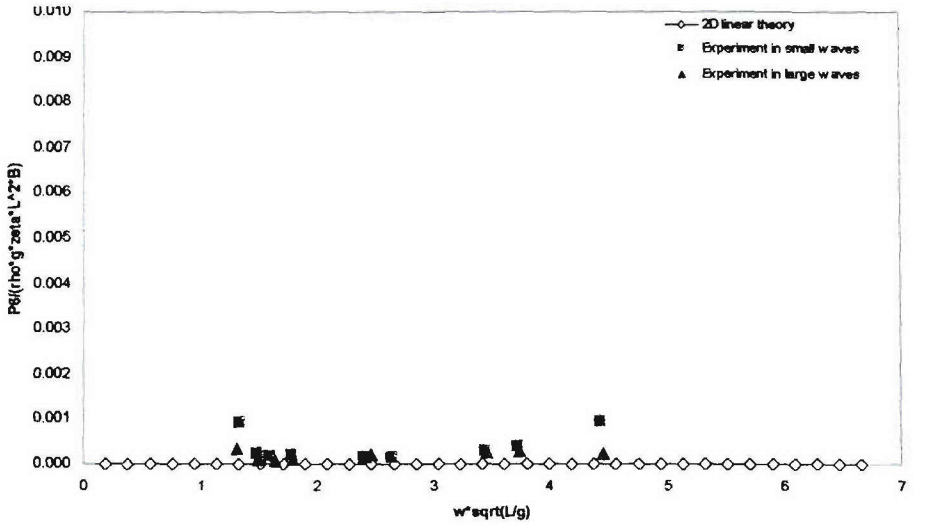

Figure 7.2-92: Dynamic horizontal bending moment RAO of DS3 H5415 at head waves

7.2.2.3.2 Stern quartering waves

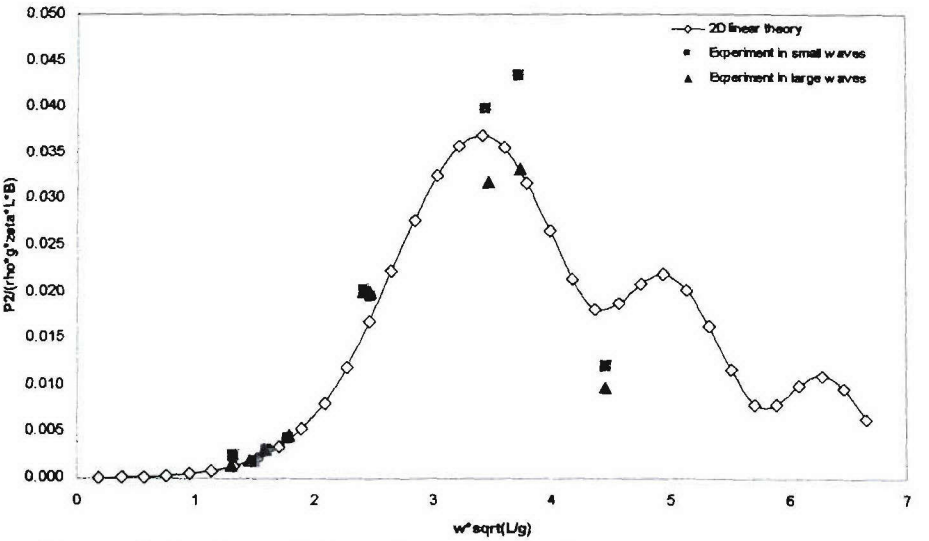

Figure 7.2-93: Dynamic horizontal shear force RAO of DS3 H5415 at stern quartering waves

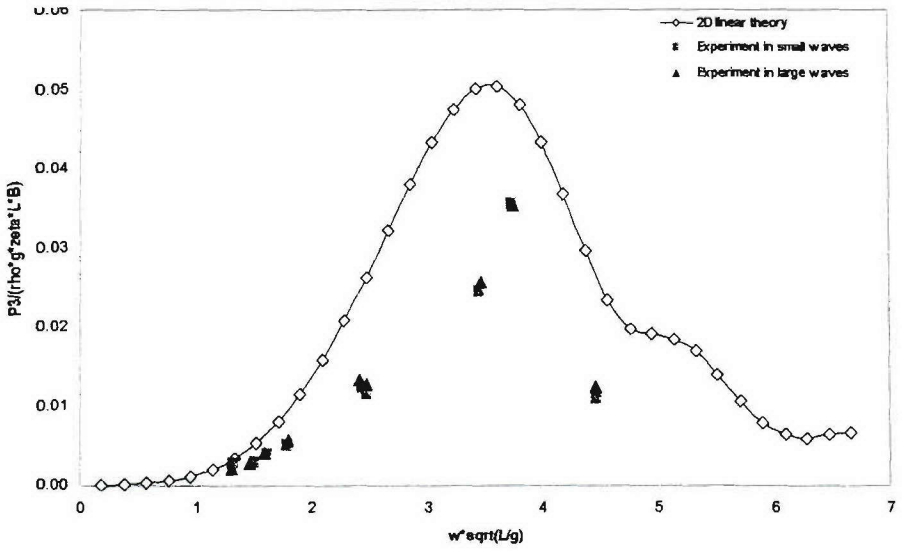

Figure 7.2-94: Dynamic vertical shear force RAO of DS3 H5415 at stern quartering waves

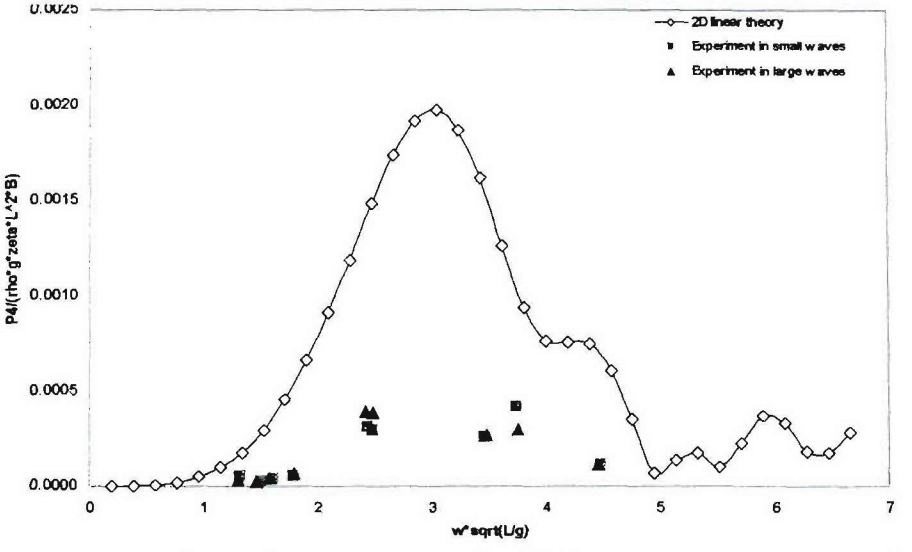

Figure 7.2-95: Dynamic torsion moment RAO of DS3 H5415 at stern quartering waves

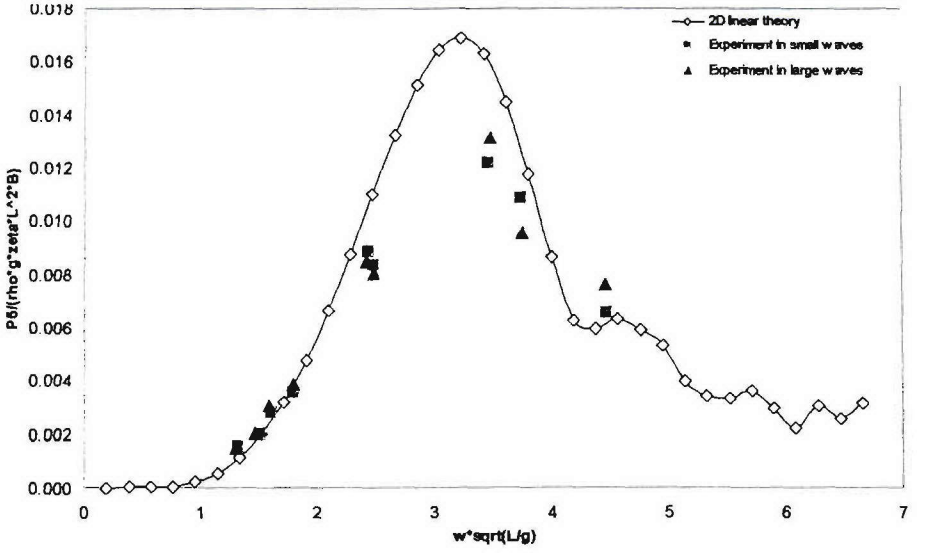

Figure 7.2-96: Dynamic vertical bending moment RAO of DS3 H5415 at stern quartering waves

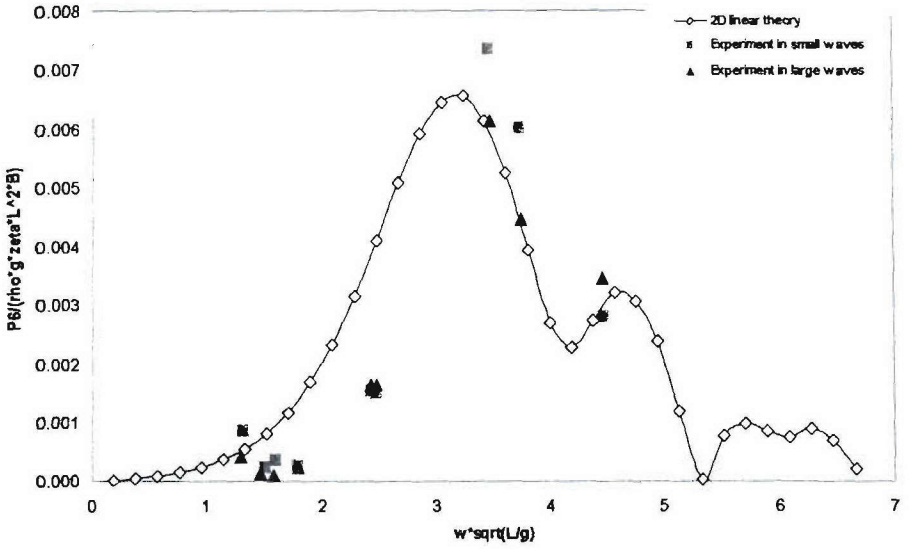

Figure 7.2-97: Dynamic horizontal bending moment RAO of DS3 H5415 at stern quartering waves

7.2.2.3.3 Beam waves

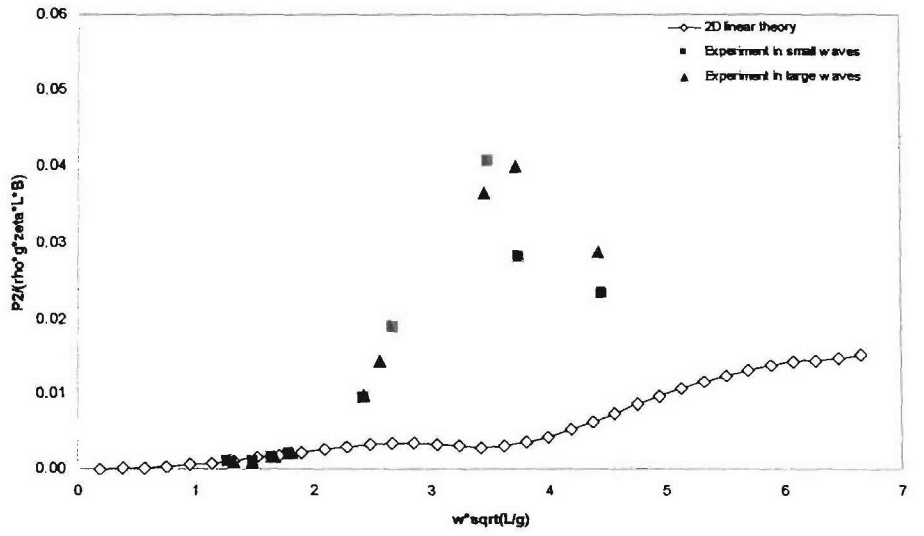

Figure 7.2-98: Dynamic horizontal shear force RAO of DS3 H5415 at beam waves

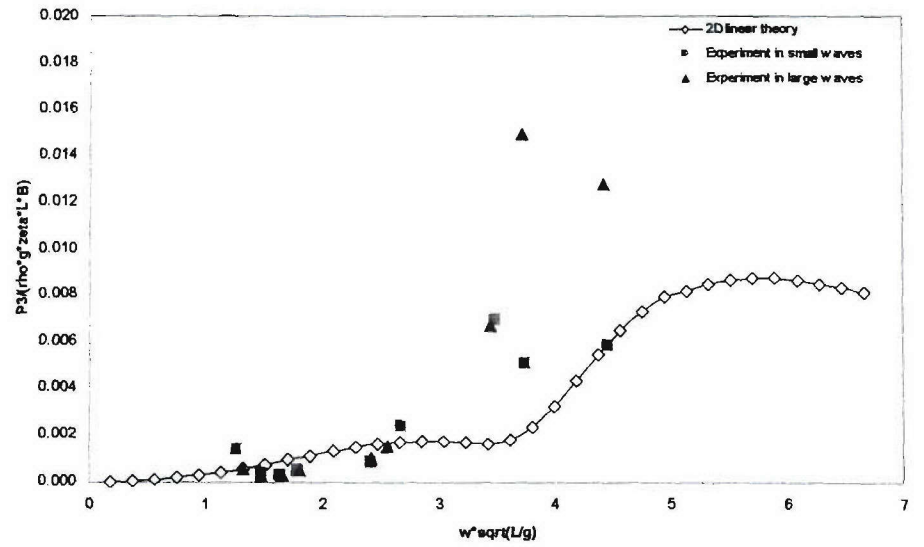

Figure 7.2-99: Dynamic vertical shear force RAO of DS3 H5415 at beam waves

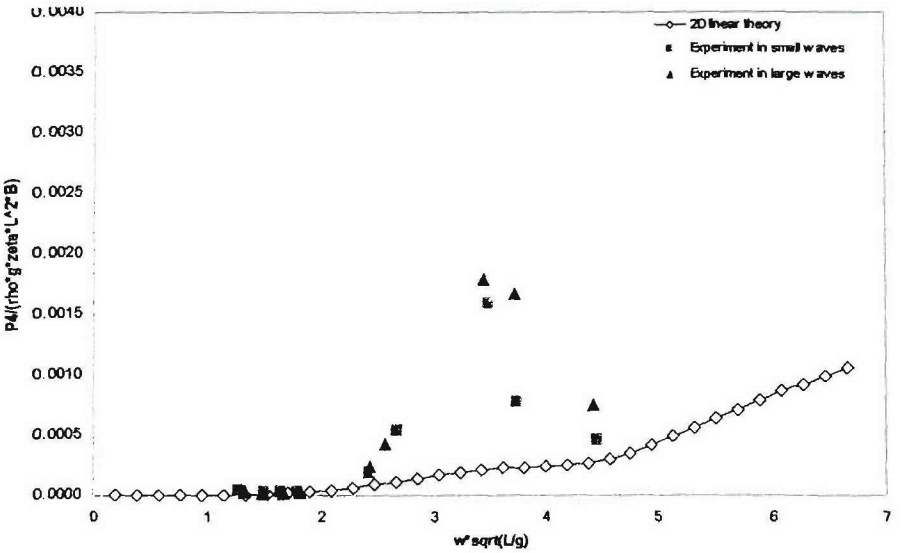

Figure 7.2-100: Dynamic torsion moment RAO of DS3 H5415 at beam waves

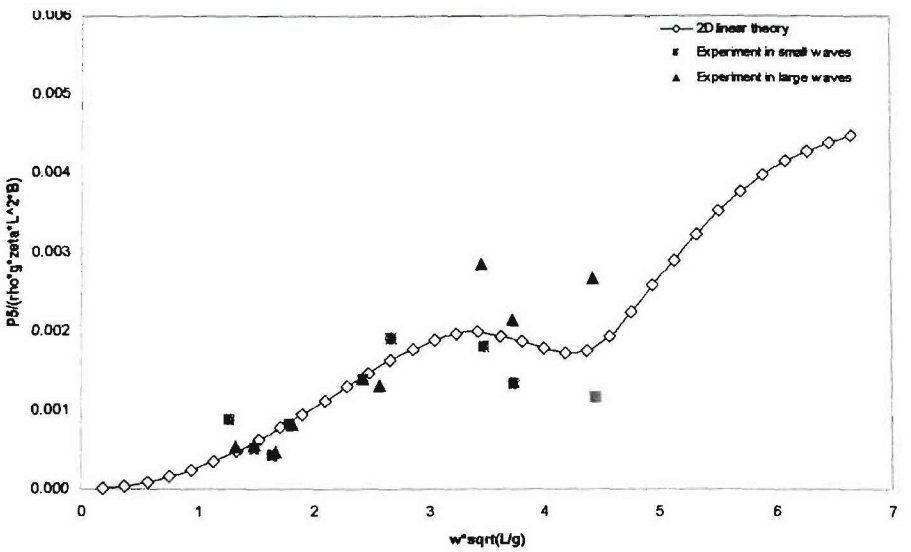

Figure 7.2-101: Dynamic vertical bending moment RAO of DS3 H5415 at beam waves

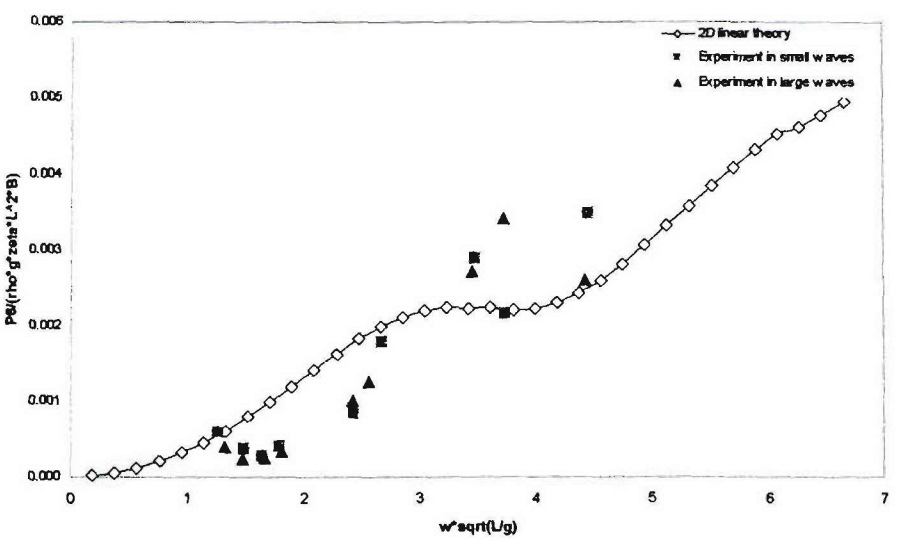

Figure 7.2-102: Dynamic horizontal bending moment RAO of DS3 H5415 at beam waves

7.3 Model Uncertainties of 2D Linear Method

As mentioned in section 4.1.5 model uncertainty is a very important source of uncertainties in structural design process. Since a coefficient of variation (COV) of a typical strength prediction could be about 10 to 15% while a COV of wave-induced load prediction could be well above 30%, model uncertainties of wave-induced load prediction is a major uncertainty in structural strength assessment.

Hence the model uncertainties of the 2D linear method are calculated by using Eq. (4.1-33) in this section. Based on the observation in previous sections, the accuracies of the 2D linear method are different for different load components. It would be interesting to quantitatively demonstrate this difference. So model uncertainties are calculated for different load components. However it is a normal practice to use a combined model uncertainty in reliability analysis, so a combined model uncertainty including all the load components is also calculated. Conventionally model uncertainties were only predicted for intact condition, so it would be interesting to see how different the accuracy could be between intact condition and damaged conditions. Again a combined model uncertainty for different conditions is also computed. A summary of model uncertainties (X_{m1}) of the 2D linear method for vertical bending moment and horizontal bending moment are shown in Table 7.3-1, while the details of the model uncertainty calculations including the other load components are presented in Appendix C.

Table 7.3-1: Model uncertainties (X_{m1}) of numerical methods

design condition	load	heading	mean, L2	COV, L2	mean, L3	COV, L3	mean, L4	COV, L4	mean, L5	COV, L5
Intact	VBM	180	0.8637	0.2787						
		45	1.0370	0.3431	0.9503	0.3283				
	HBM	180	small values ≈ 0							
		45	0.9626	0.6986	0.9626	0.6986	0.9544	0.4794		
DS2	VBM	180	0.8503	0.2781						
		45	0.9473	0.1833						
		315	1.1212	0.2162	0.9729	0.2502				
	HBM	180	small values ≈ 0							
		45	0.9342	0.8108						
		315	1.3657	0.6062	1.1500	0.7061	1.0437	0.5267		
DS3	VBM	180	0.8797	0.4037						
		45	1.0025	0.2275	0.9411	0.3195				
	HBM	180	small values ≈ 0							
		45	0.7660	1.0118	0.7660	1.0118	0.8827	0.5769	0.9755	0.5299

In Table 7.3-1 mean, L2 and COV, L2 stand for mean and COV for each load component and each heading angle; mean, L3 and COV, L3 stand for mean and COV of each load component including all heading angles; mean, L4 and COV, L4 stand for mean and COV in each floating condition including all load components; mean, L5 and COV, L5 stand for the combined mean and COV for all load components and floating conditions. It is observed that the accuracy for vertical bending moment is generally better than that for horizontal bending moment, and the COV of horizontal bending moment is almost as twice as that of vertical bending moment. It may be logical to consider model uncertainties for vertical bending moment and horizontal bending moment separately in reliability analysis. However this could be the further research topic. The accuracies at different floating conditions (intact, DS2 and DS3) are slightly different, but are comparable.

7.4 Prediction of Extreme Design Loads

The distributions of the most probable extreme amplitudes of global dynamic wave induced vertical and horizontal bending moments on the sample vessel 'H5415' in intact and different damaged conditions were calculated using dynamic wave induced vertical and horizontal bending moment response amplitudes in stochastic analysis. Figure 7.4-1 shows modified Pierson-Moskowitz (ISSC) spectrum with two parameters and vertical bending moment response spectra (left column: at case 4 & sea state 3; right column: case 1 & sea state 5). The wave elevations in a space and time domain at sea states 3 and 5 are shown in Figures 7.4-2 and 7.4-3.

In order to predict the most probable extreme design loads for the intact condition, a 20 years wave condition were used in stochastic computations. The results are shown in Figures 7.4-4 to 7.4-7. Table 7.4-1 summarises the bending and torsion moments for intact H5415 with a still bending, dynamic wave induced bending and torsion moments in head and stern quartering waves.

Extreme design loads in damaged conditions were simulated with sea state 3 during 96 hours in short term predictions. Figures 7.4-8 to 7.4-11 describe distributions of the most probable extreme amplitudes of dynamic wave induced loads for different damage scenarios in head and stern quartering waves. The summaries of a still water, dynamic wave induced bending and torsion moments for damaged H5415 model are shown in Tables 7.4-2a and 7.4-2b. One and two compartment damaged conditions amidships are the worst conditions for the most probable extreme amplitudes of dynamic wave induced vertical and horizontal bending moments in head and stern quartering waves. Figure 7.4-11 shows that the differences of torsion moments between case 8 (heading 45) and case 11 (heading 315) are quite big as around 25% value differences amidships. Both Cases 8 and 11 are for damage scenario 2. This means that the effects caused by heading are important for torsion moments in stern quartering waves. The most extreme loads for damage scenarios 3 and 4 (Cases 13, 16 and 19) are less than those for damage scenarios 1 and 2 (cases 5, 8 and 11).

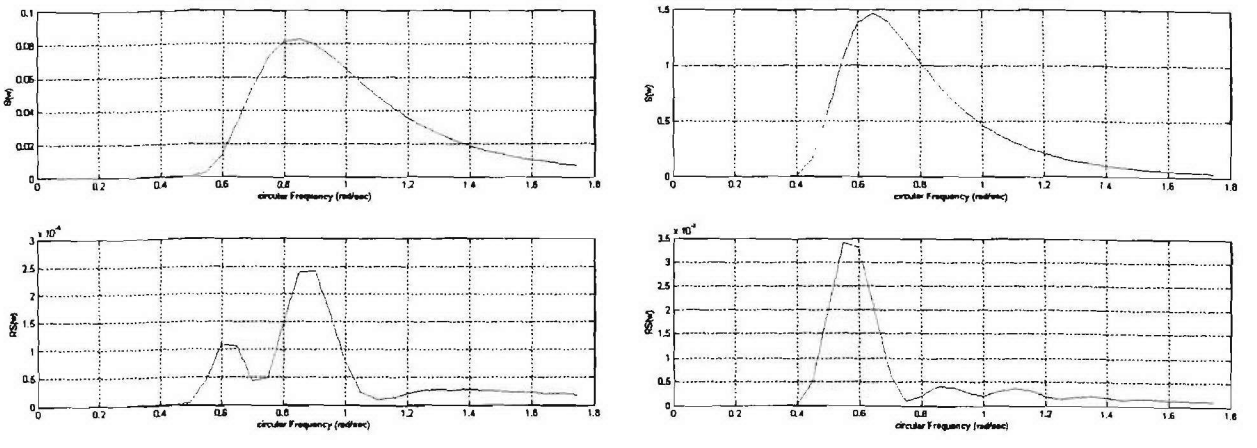

Figure 7.4-1: Modified Pierson-Moskowitz (ISSC) spectrum and vertical bending moment response spectrum (left column: at case 4, sea state 3 and right column: case 1, sea state 5)

The maximum values of the most probable extreme amplitudes of dynamic wave induced loads in damaged conditions are much less than those in intact condition, because the most probable extreme design load in intact condition is based on long term prediction with a

duration of 20 years, while the most probable extreme design load for damaged conditions is based on short term prediction (sea state 3 for 96 hours). However the loads in damage scenarios 1 and 2 are important to assess the residual strength of the damaged ship due to her loss of the most main structural members amidships.

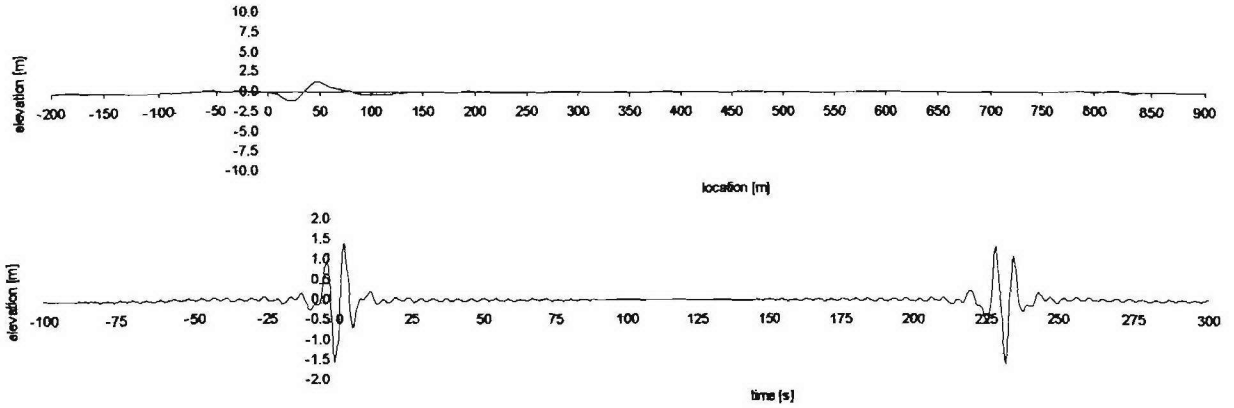

Figure 7.4-2: Wave elevation in a space at 7 sec and time domain (sea spectrum at sea state 3)

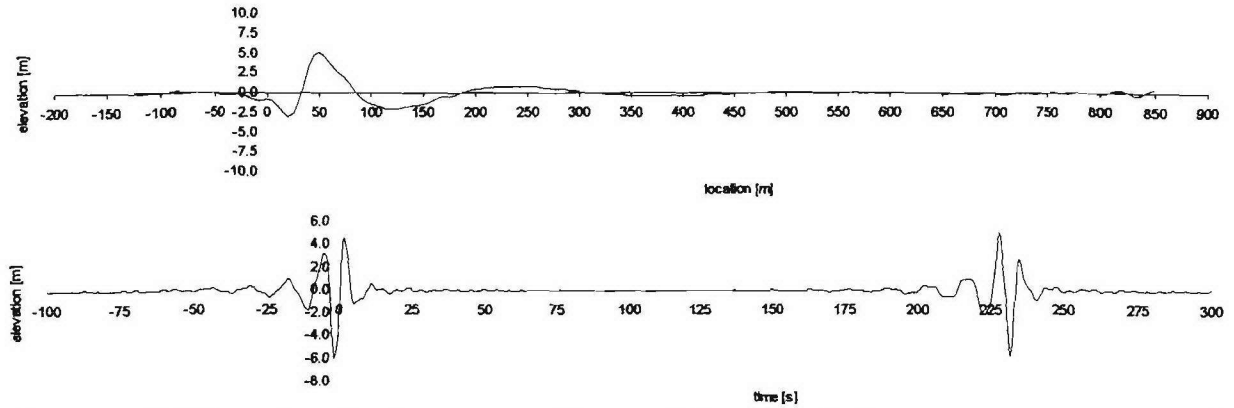

Figure 7.4-3: Wave elevation in a space at 7 sec and time domain (sea spectrum at sea state 5)

7.4.1 Responses in intact condition

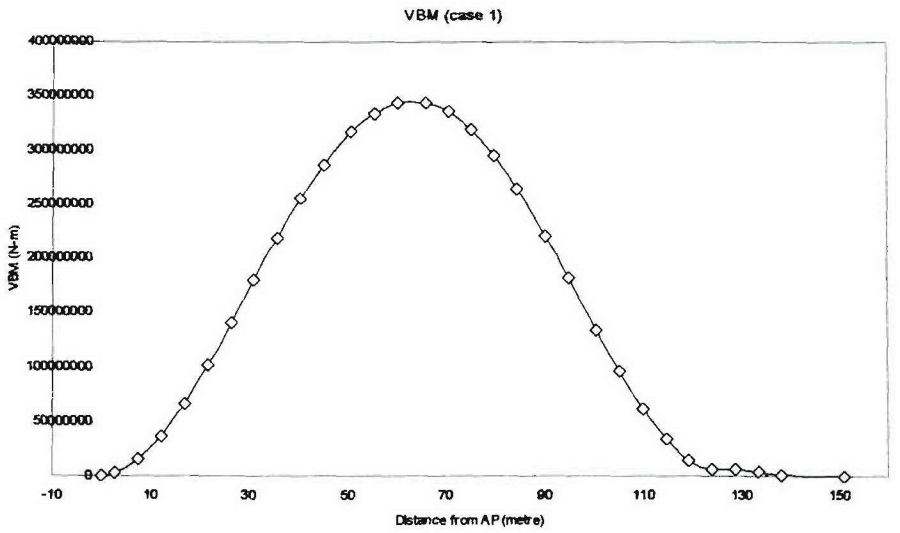

Figure 7.4-4: Distributions of most probable extreme amplitudes of dynamic wave induced vertical bending moments for intact conditions in head waves

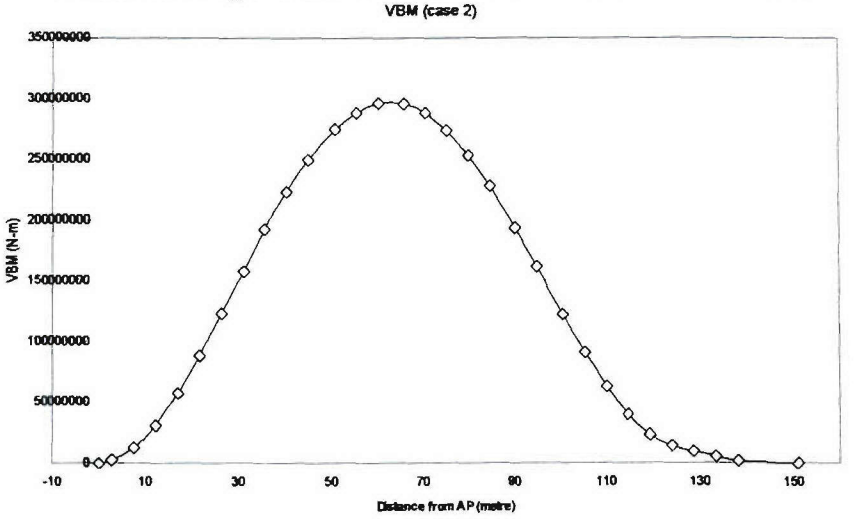

Figure 7.4-5: Distributions of most probable extreme amplitudes of dynamic wave induced vertical bending moments for intact conditions in stern quartering waves

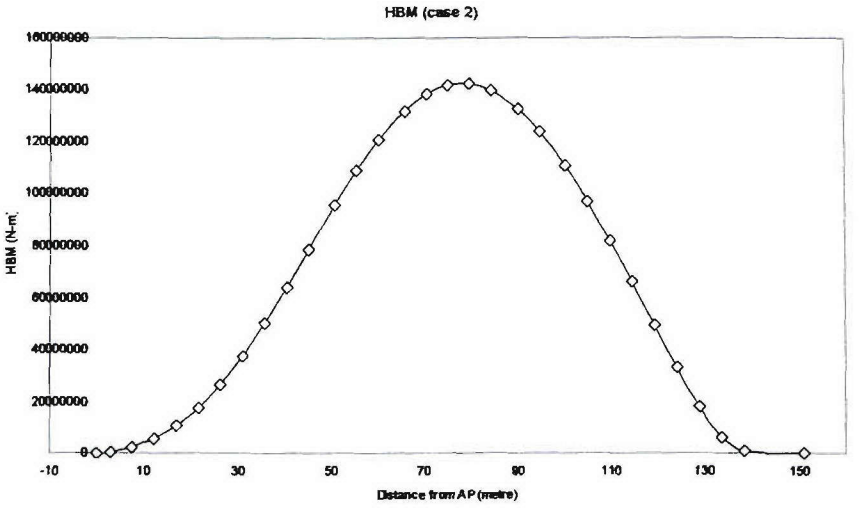

Figure 7.4-6: Distributions of most probable extreme amplitudes of dynamic wave induced horizontal bending moments for intact conditions in stern quartering waves

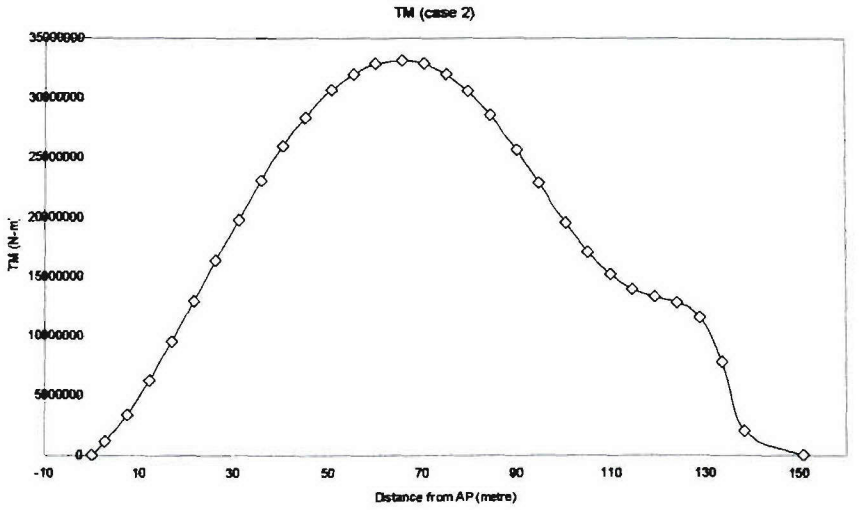

Figure 7.4-7: Distributions of most probable extreme amplitudes of dynamic wave induced torsion moments for intact conditions in stern quartering waves

Table 7.4-1: Bending and torsion moments (kN-m) for intact H5415 model (at 70.5m from AP)

SWMB	in head waves	in stern quartering waves		
	WVBM	WVBM	WHBM	WTM
	case1	case2	case2	case2
147610	335580	287740	138370	32860

7.4.2 Responses in damaged conditions

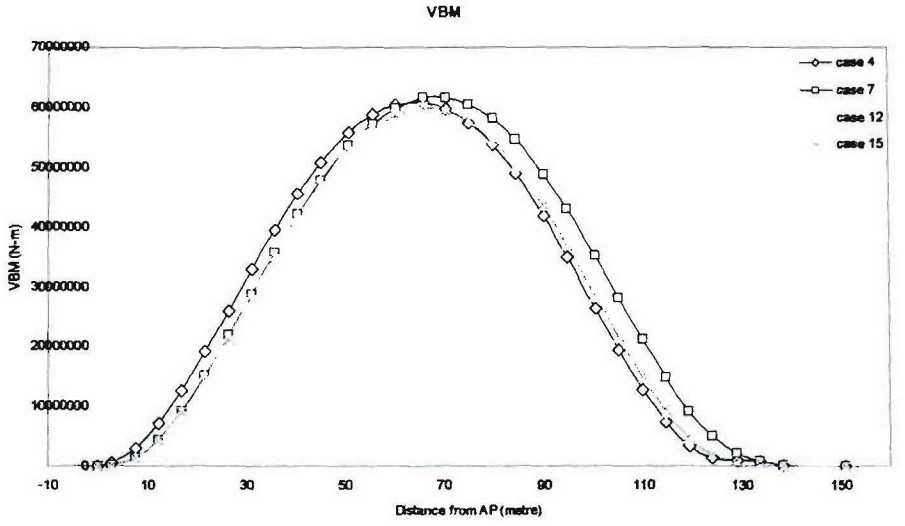

Figure 7.4-8: Distributions of most probable extreme amplitudes of dynamic wave induced vertical bending moments for different damage scenarios in head waves

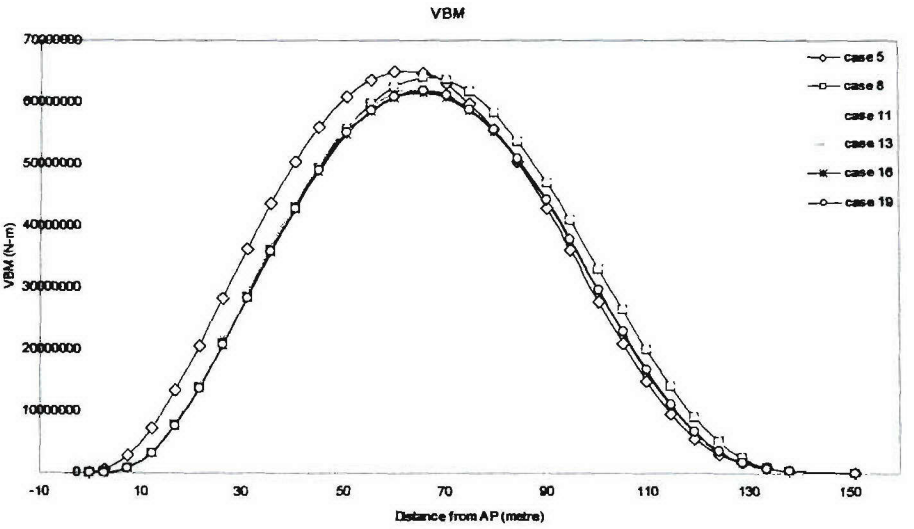

Figure 7.4-9: Distributions of most probable extreme amplitudes of dynamic wave induced vertical bending moments for different damage scenarios in stern quartering waves

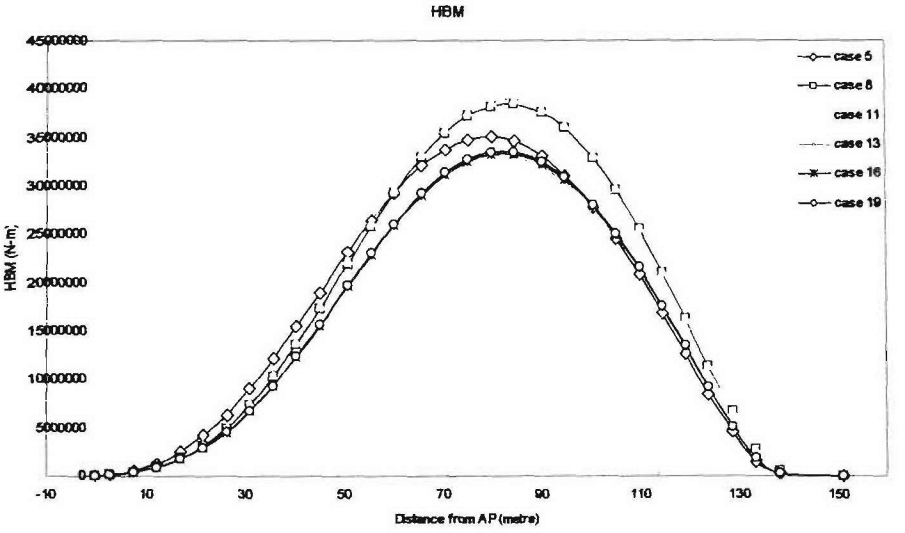

Figure 7.4-10: Distributions of most probable extreme amplitudes of dynamic wave induced horizontal bending moments for different damage scenarios in stern quartering waves

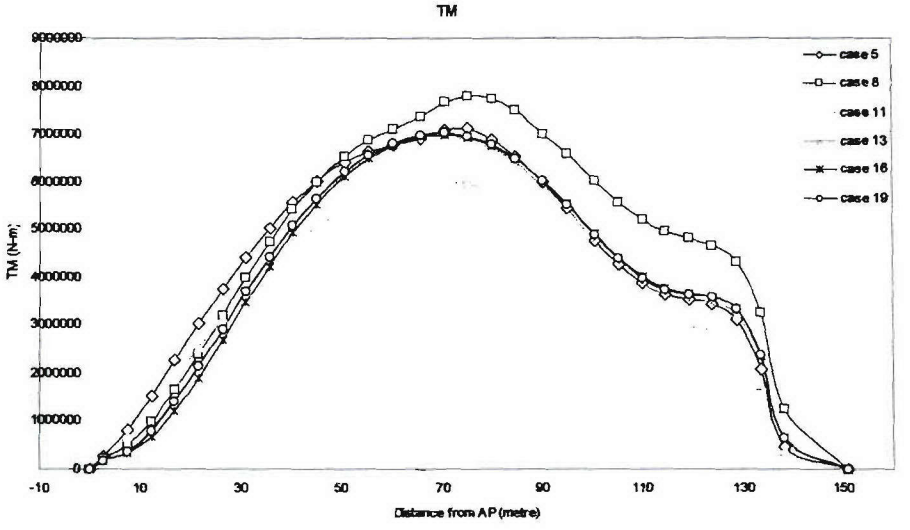

Figure 7.4-11: Distributions of most probable extreme amplitudes of dynamic wave induced torsion moments for different damage scenarios in stern quartering waves

Table 7.4-2a: Bending moments (kN-m) for damaged H5415 ship (at 70.5m from AP)

				in head waves				in stern quartering waves				
SWBM in DS1	SWBM in DS2	SWBM in DS3	SWBM in DS4	WVBM case4	WVBM case7	WVBM case12	WVBM case15	WVBM case5	WVBM case8	WVBM case11	WVBM case13	WVBM case16
54588	-30934	207161	205003	59822	61585	59809	59379	62986	63610	64275	61240	60734

where, case 5: damage scenario 1, cases 8 & 11: damage scenario 2, case 13: damage scenario 3 and cases 16 & 19: damage scenario 4

Table 7.4-2b: Bending and torsion moments (kN-m) for damaged ship (at 70.5m from AP)

in stern quartering waves												
WVBM case19	WHBM case5	WHBM case8	WHBM case11	WHBM case13	WHBM case16	WHBM case19	WTM case5	WTM case8	WTM case11	WTM case13	WTM case16	WTM case19
61066	33740	35400	35950	31019	31097	31313	7086	7668	7785	6955	6986	7016

where, case 5: damage scenario 1, cases 8 & 11: damage scenario 2, case 13: damage scenario 3 and cases 16 & 19: damage scenario 4

The distribution of the total loads including stillwater bending moment and wave-induced bending moment over the ship length has been plotted in Figures 7.4-12 to 7.4-16 to show how each damage changes the distribution of total loads and each load component. These curves could be used to identify the critical cross sections, which need strength assessment after damage, apart from the damaged cross sections. It is interesting to note that the total vertical bending moment over the whole length of the ship in intact condition is greater than that in damage scenarios 1 and 2. However in damage scenarios 3 and 4 in some cross sections the total vertical bending moment in the damaged condition is slightly greater than that in intact condition although it is opposite in majority of the areas.

In head waves

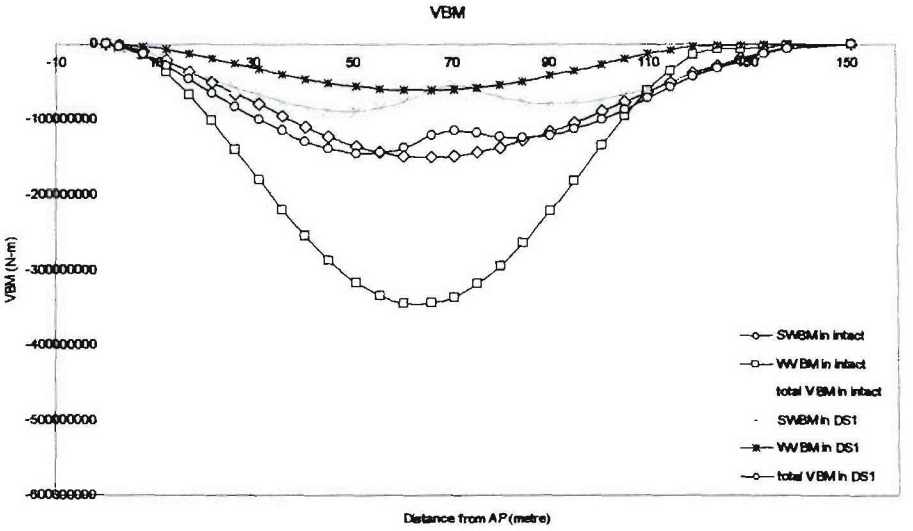

Figure 7.4-12: Comparison of the total loads in intact and damage scenario 1

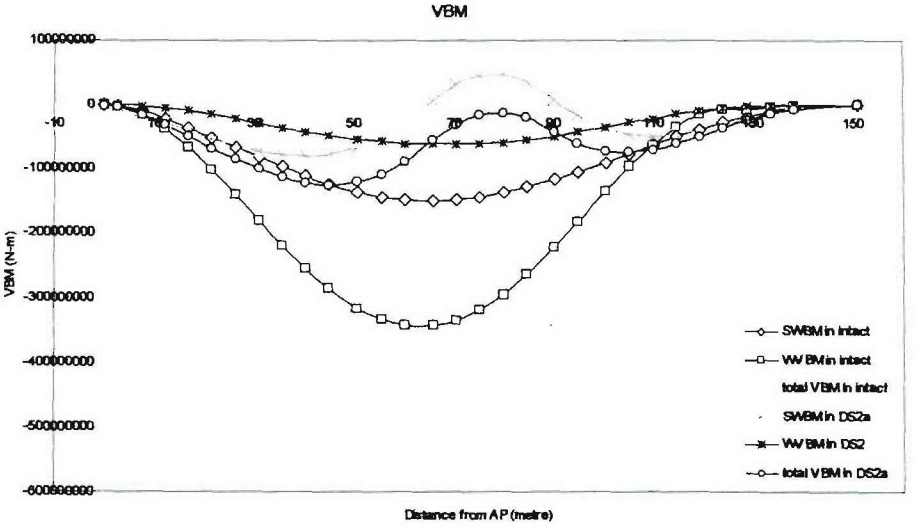

Figure 7.4-13: Comparison of the total loads in intact and damage scenario 2

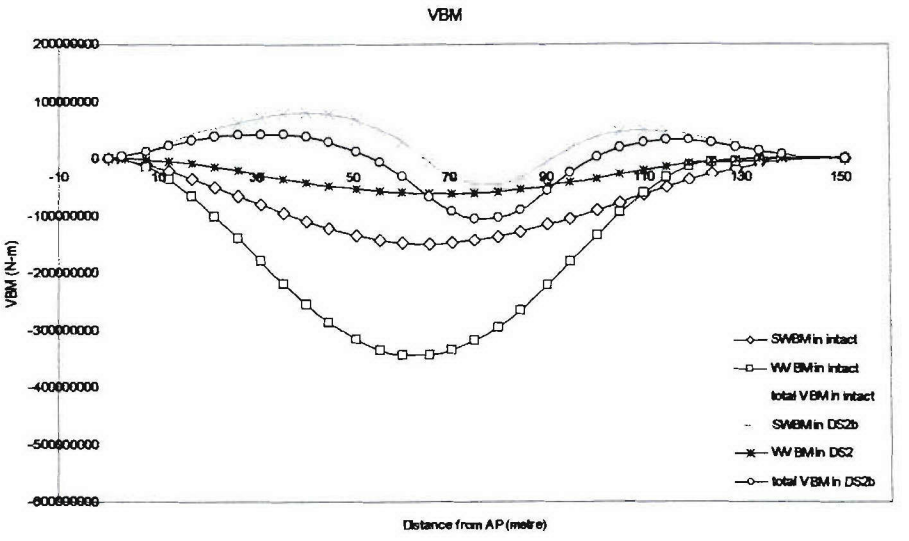

Figure 7.4-14: Comparison of the total loads in intact and damage scenario 2

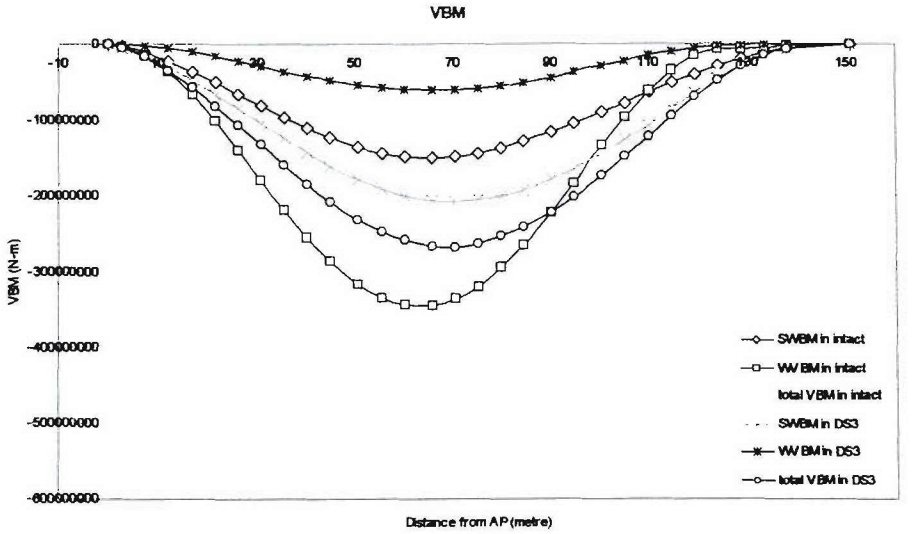

Figure 7.4-15: Comparison of the total loads in intact and damage scenario 3

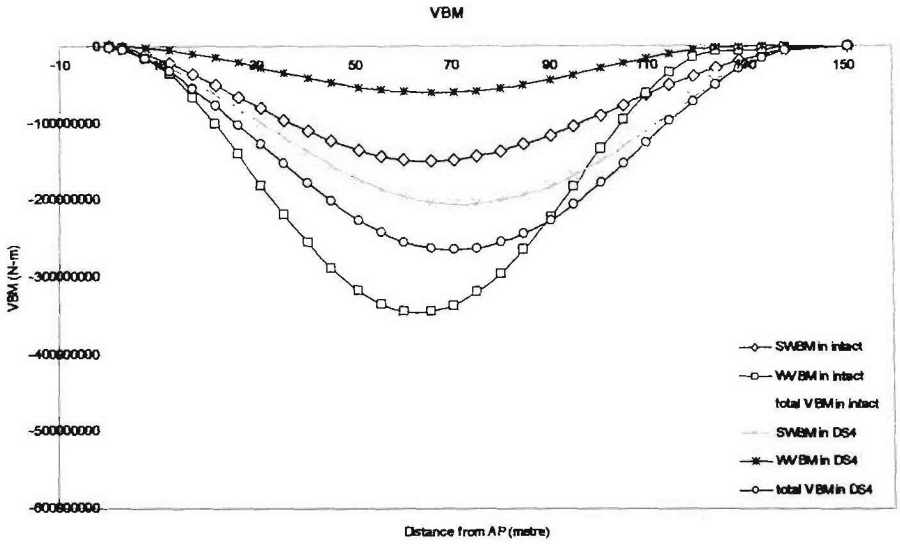

Figure 7.4-16: Comparison of the total loads in intact and damage scenario 4

7.6 Ultimate Strength of Hull Girders

7.6.1 Modelling of ship's cross-section

The modelling of the ship's cross-section consists of dividing the hull into stiffened plate elements, which are representative of panel behaviour. Most of the present day ships have longitudinally stiffened hulls. In this kind of hull, it is common practice to have large panels with similar and repetitive properties such as space between stiffeners and stiffener geometry. As the behaviour of these panels may be represented as the behaviour of n equally spaced stiffened plate elements, the hull section will be divided into small elements representing a plate between stiffeners and the corresponding stiffener. Apart from the validity of this model which influences the panel behaviour, some other points of the modelling present some problems or approximations, especially related to:

- The validity of the element's stress state as derived from the strain state at the centroid of the element,
- The modelling of side girders when web stiffeners aren't present,
- The modelling of the corners of the hull girder,
- The modelling of large and reinforced flanges of primary longitudinal girder system and the validity of this subdivision on the overall behaviour of main girders, especially relating to sideways flexural behaviour.

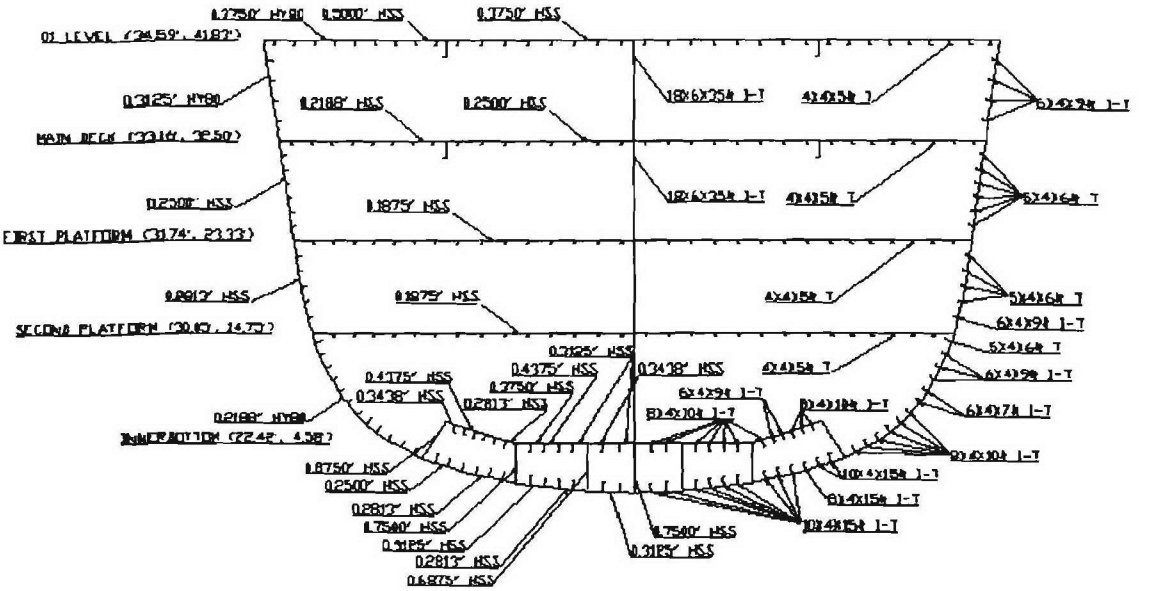

Figure 7.6-1: Mid-ship section of the hull 5415.

Table 7.6-1: Scantlings of the stiffeners

Designation	Area (mm^2)	Ctoe (mm)	I xx (mm^4)	h_w (mm)	t_w (mm)	b_f (mm)	tf (mm)
4X 4 X 5 T	929.03	75.69	0.8741	95.123	4.318	100.076	5.207
5X 4 X 6 T	1116.13	90.17	1.7898	120.142	4.826	100.584	5.334
6X 4 X 9I-T	1167.74	107.19	2.7055	144.399	4.318	100.076	5.461
6X 4 X 7 T	1316.13	105.92	3.1634	145.669	5.080	100.838	5.715
8X 4 X 10I-T	1361.29	135.89	5.9105	195.199	4.318	100.076	5.207
10 x 4 x 12# I-T	1722.58	161.80	11.7377	245.364	4.826	100.584	5.334
6X 4 X 9.5 T	1774.19	112.27	4.1623	145.542	5.969	101.854	8.890
8X 4 X 13I-T	1806.45	135.13	7.9916	196.469	5.842	101.600	6.477
8X 4 X 15I-T	2045.16	139.95	9.2403	197.993	6.223	102.108	8.001
7X 5 X 11 T	2051.61	129.03	6.1186	165.989	5.842	127.000	8.509
12 x 4 x 14# I-T	2083.87	190.25	20.6035	296.799	5.080	100.838	5.715
10X 4 X 15I-T	2141.93	164.85	14.9011	246.888	5.842	101.600	6.858
12 x 4 x 16# I-T	2348.38	193.29	23.5171	297.815	5.588	101.346	6.731
10X 4 X 17I-T	2367.74	170.43	16.7741	248.412	6.096	101.854	8.382
8X 51/2X 13 T	2432.25	145.54	9.7398	190.627	6.350	139.700	8.763
7X 5 X 13 T	2438.70	132.33	7.2008	166.116	6.477	127.762	10.668
10X 4 X 19I-T	2612.90	176.02	18.8137	250.063	6.350	102.108	10.033
10 x53/4 x 22#I-T	2851.61	184.91	19.7294	249.174	6.096	146.050	9.144
14 x 5 x 22# I-T	3070.96	231.65	40.5409	340.487	5.842	127.000	8.509
12 x61/2x 26# I-T	3348.38	224.03	33.3818	300.736	5.842	164.846	9.652
14 x 5 x 26# I-T	3580.64	238.51	48.0747	342.646	6.477	127.762	10.668
16 x51/2 x26# I-T	3696.77	260.86	63.8499	389.763	6.350	139.700	8.763
18X 6 X 35I-T	4987.09	293.62	109.3856	438.785	7.620	152.400	10.795
18 x 6 x 40# I-T	5567.73	303.78	124.1202	441.325	8.001	152.908	13.335
18 x71/2 x50# I-T	6748.37	314.71	150.2179	442.468	9.017	190.500	14.478
18x7 1/2 x60# I-T	8083.85	319.79	183.4332	445.643	10.541	192.024	17.653
27 x 10 x 94#I-T	13103.20	458.22	660.0598	664.210	12.446	253.746	19.050

The stress state of the components of the element (plate and stiffener) is computed considering the strain at the centroid. In this study the girders are modelled considering two main components: the stiffened plate with web and flange and the un-stiffened plate. The stiffened plates are modelled as beam-column in order to compute their higher rigidity. Equal breadths of the stiffeners have been considered between two adjacent decks. Figure 7.6-1 shows the cross section of the mid-ship section. The dimensions of the stiffeners are presented in Table 7.6-1. The half of the mid-ship section has been divided into 149 stiffened plates, plates and hard corner elements as shown in Figure 7.6-2.

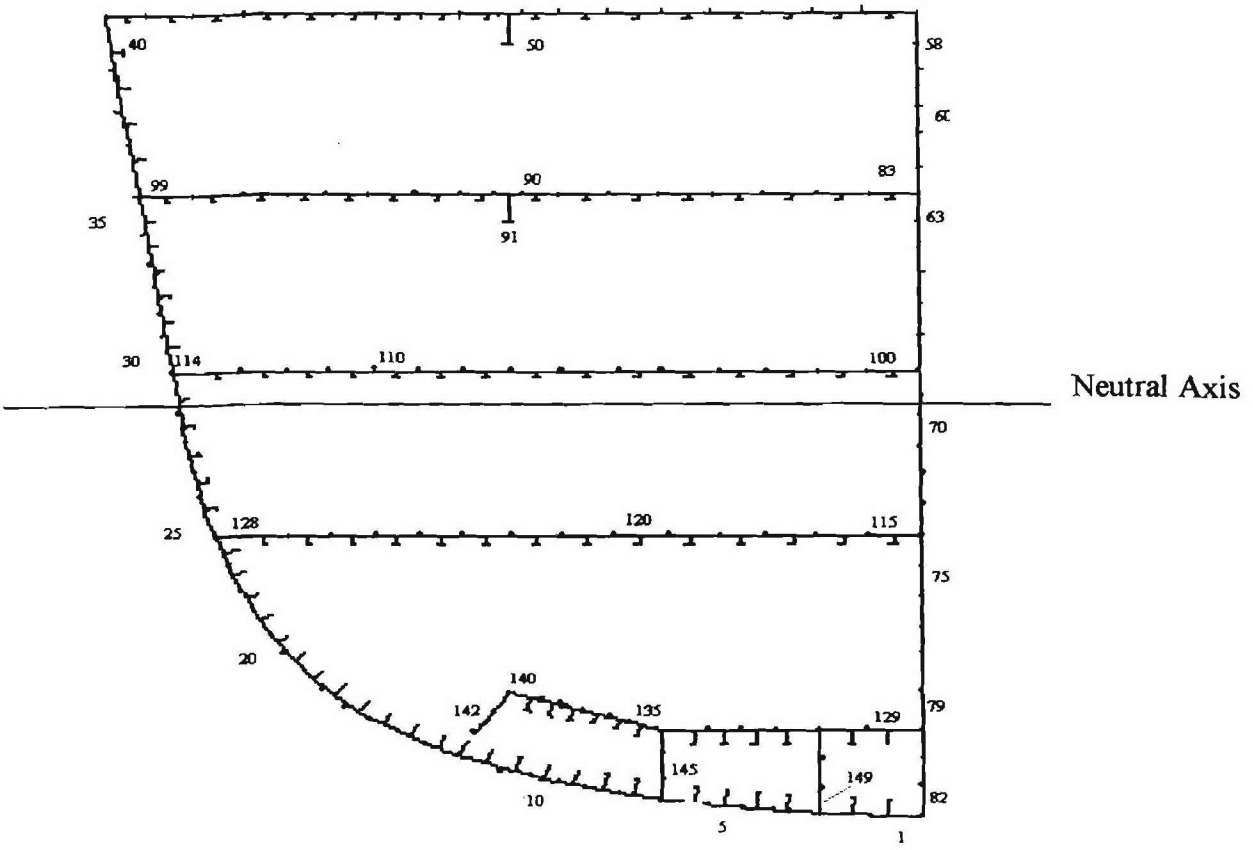

Figure 7.6-2: Half of mid-ship section of the Hull 5415 showing all the elements.

7.6.2. Results and discussion

The moment-curvature relationship depends on the individual contribution of the elements in the hull section. It varies due to different effective width formulation. The relationship between bending moment and curvature using the method described in chapter 4.3 is shown in Figure 7.6-3. It can be noticed from Figure 7.6-3 that the bending moment increases with the increment of curvature and during hogging, at the curvature of about 0.0004 m^{-1} the moment starts to decrease smoothly. The highest point in the M-Φ curve is called the ultimate strength of hull 5415 in intact scenario. Similarly during the sagging condition the M-Φ curve is smooth and the absolute value of moment starts decreasing at the curvature of 0.00035 m^{-1}. The ultimate strength is 1.77×10^6 kNm and -1.40×10^6 kNm for hogging and sagging conditions

respectively using the aforesaid formulations for stress-strain relationship of the individual elements.

The yield moment is calculated to be 2.066 x 10^9 Nm, as it can be noticed from Figure 7.6-3, the ultimate strength is lower than the yield moment of the hull 5415. So it demonstrates that the elements of the hull 5415 have undergone either flexural buckling or torsional buckling (tripping). It can be noticed that the ultimate strength in hogging condition is higher than that in sagging condition. The neutral axis is at 6.35m from the bilge and during sagging conditions the elements above the neutral axis has undergone compression and due to flexural buckling or tripping, the elements have lower local strength. Similarly during hogging condition the elements below the neutral axis are in compression and above it are in tension, so the ultimate strength in hogging is higher than that in sagging.

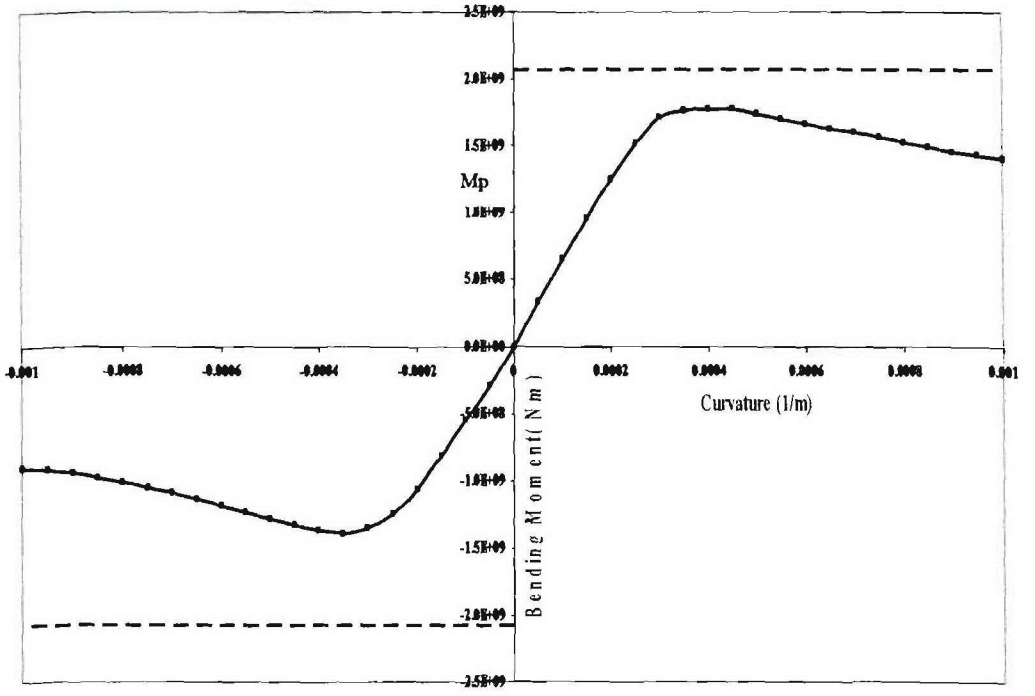

Figure 7.6-3: Moment-Curvature relationship of Hull5415 in intact scenario

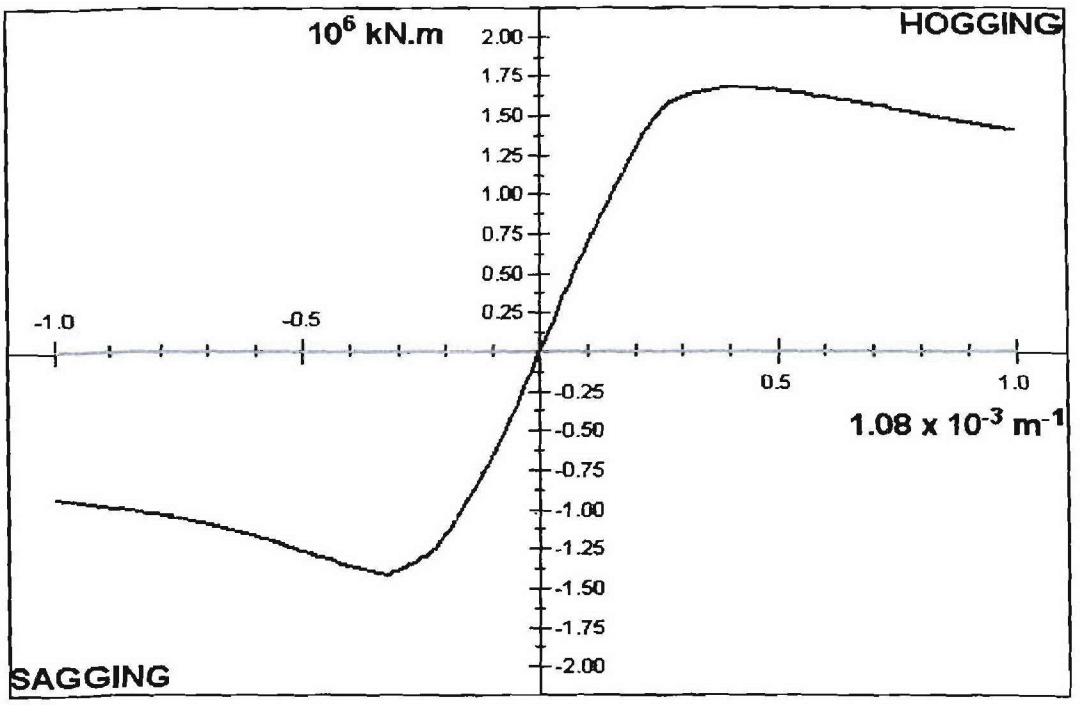

Figure 7.6-4: Moment-Curvature relationship of the Hull5415 using MARS (Bureau Veritas).

In order to validate the developed method, the method developed by Bureau Veritas (MARS) is also applied to the mid-ship section of the sample vessel to calculate the vertical ultimate strength. As it can be seen from Figure 7.6-5 & Table 7.6-2, the ultimate strength obtained using MARS is 1.69 x 10^9 Nm and 1.40 x 10^9 Nm for hogging and sagging conditions respectively. It can be observed from Table 7.6-2 that the ultimate strength calculated using the present method and MARS are very close with each other in intact condition. The ultimate strength using the present method is about 4.7 % higher in hogging and 1% less in sagging than that of MARS. It may be said that the accuracy of the present method is acceptable. So it is applied to other cases.

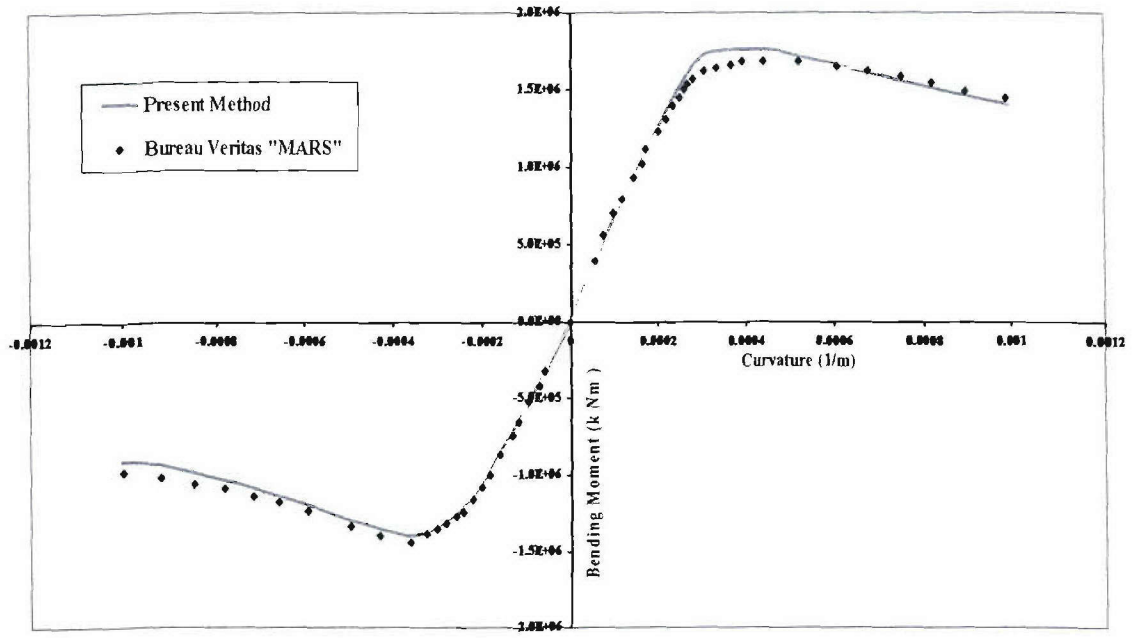

Figure 7.6-5: Comparison of Moment-Curvature relationship of the Hull5415 using the described formula for elements and MARS (Bureau Veritas) for the mid-ship section.

Table 7.6-2: Ultimate strength of mid-ship section of Hull 5415 in intact condition

Particular	***Values***	
Ultimate strength using present method (x 10^9 Nm)	**1.77**	**(hogging)**
	1.4	**(sagging)**
Ultimate strength using MARS (Bureau Veritas) (x 10^9 Nm)	**1.69**	**(hogging)**
	1.41	**(sagging)**
Ratio: Ultimate Strength (Present method/ MARS)	**1.047**	**(hogging)**
	0.993	**(sagging)**

Ultimate strength of hull 5415 in horizontal and vertical bending are presented in Table 7.6-4 considering intact, damage scenarios 1 and 2. It is observed from Figure 7.6-6, that the horizontal bending moment is maximum (2.17x 10^9 Nm) at a curvature of 0.0006 m^{-1} and it starts to decrease smoothly with the increment of curvature afterwards. Since the breadth of hull 5415 is larger than the depth, the horizontal bending moment is expected to be higher than the vertical bending moment (1.77 x 10^9 Nm).

The vertical residual strength in the damage scenarios 1 & 2 are also documented in Table 7.6-4 & Figures 7.6-9. The vertical residual strength is reduced in the damaged conditions as expected. But it can be said that the residual strength in damaged scenarios are dependent on the size and the location of the damage. In this case the damage location is close to the neutral axis, so the vertical residual strength is about 96.6% and 93% of the intact strength during hogging condition for damage scenarios 1 & 2 respectively.

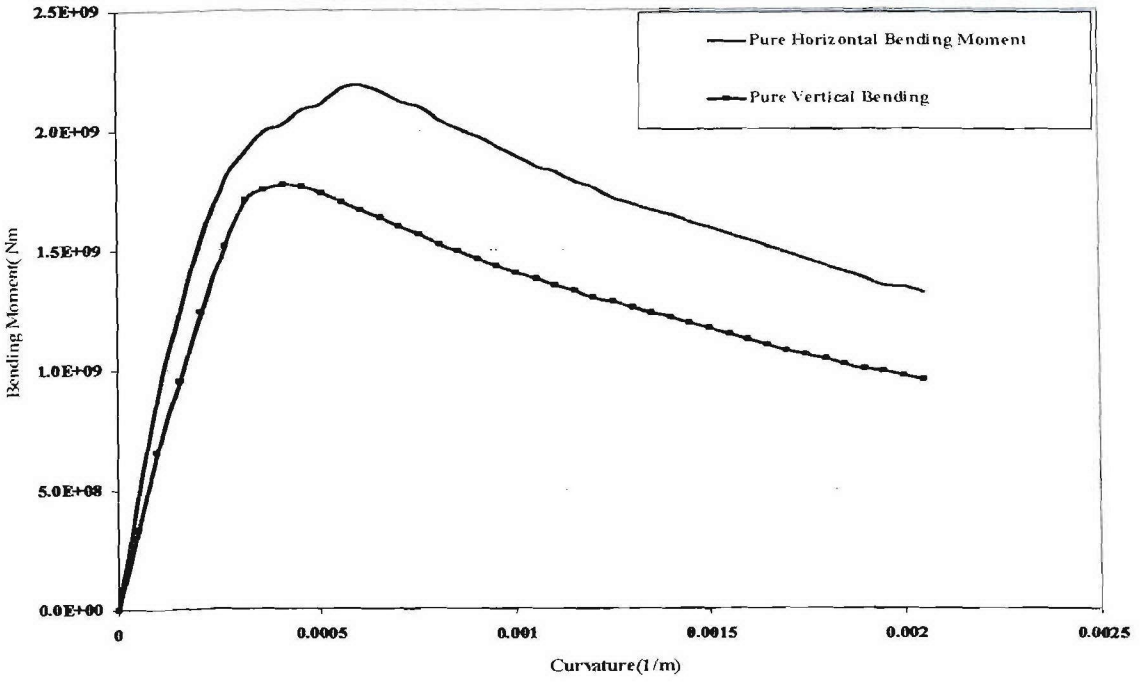

Figure 7.6-6: The moment-curvature relationship of horizontal and vertical bending (hogging) in intact scenario at the mid-ship section.

The damage scenarios are re-stated here for the purpose of residual strength assessment of some particular cross-sections shown in Table 7.6-3, Figures 7.6-7 and 7.6-8.

Table 7.6-3 : Damage Scenarios

Military threats	The extent of damage due to military threats defined as the minimum of the shock or blast damage that is likely to result from a specified weapon threat.	
Collision damage to the side shell	Damage Scenario 1 Level A	- 5 m longitudinally between bulkheads - from the waterline up to the main deck - inboard for B/5 m
	Damage Scenario 2 Level B & C	- 5 m longitudinally anywhere including bulkheads - from the bilge keel up to the main deck - inboard B/5 m
Grounding or raking damage to the bottom structure	Damage Scenario3 Level A	- length of 5 m anywhere forward of mid-ships - upwards for 1 m or the underside of the inner bottom, whichever is less - breadth of 2.5 m
	Damage Scenario 4 Level B & C	- length of 0.1L anywhere forward of mid-ships - upwards for 1 m or the underside of the inner bottom, whichever is less - breadth of 5 m

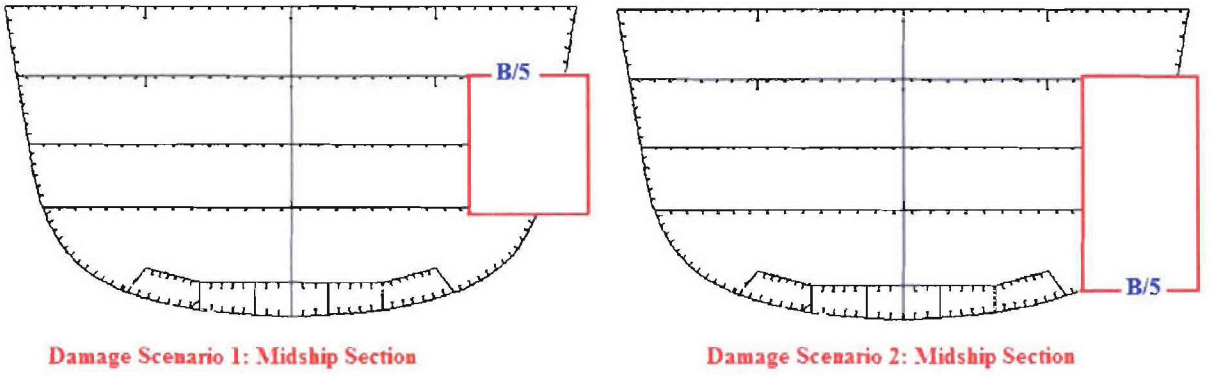

Figure 7.6-7: Damage scenarios 1 and 2 in the mid-ship section (the elements in the starboard side inside red colour box are damaged)

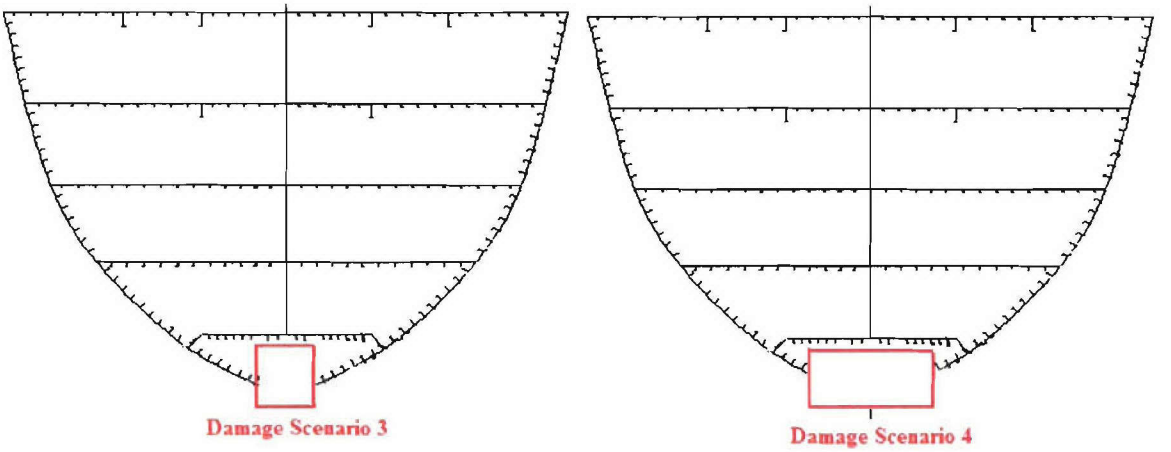

Figure 7.6-8: Damage scenarios 3 and 4 at station 5 (the elements inside the red coloured box are damaged)

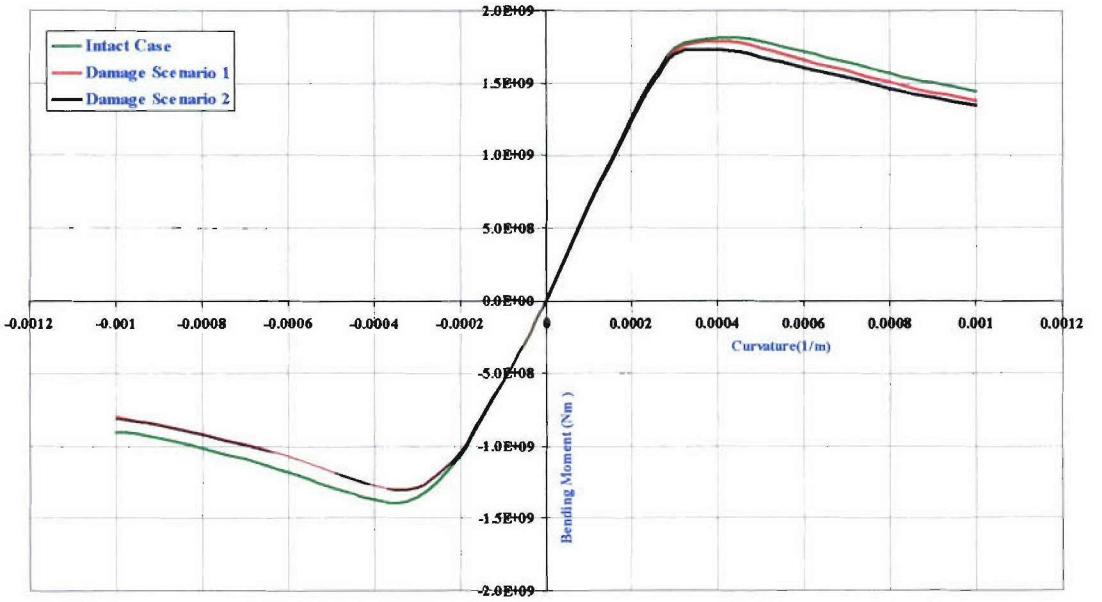

Figure 7.6-9: Comparison of vertical moment-curvature relationship in different scenarios in hogging and sagging conditions at the mid-ship section.

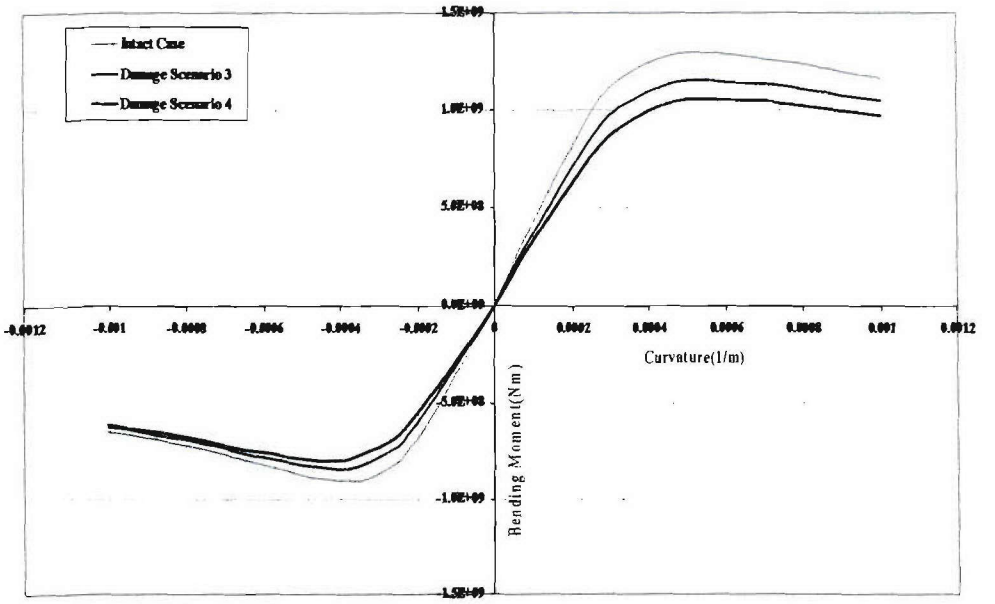

Figure 7.6-10: Vertical ultimate/residual strength of Station 5 in damage scenarios 3 and 4

The damage scenarios 3 and 4 are passing through the station-5, so the ultimate/residual strength of this cross-section has been calculated. The results are presented in Table 7.6-5 and Figure 7.6-10. The vertical ultimate strength at station 5 is 1.3 x 10^9 Nm and 9.1 x 10^8 Nm in hogging and sagging conditions respectively. Since the location of damage in this case is at the bottom, and the cross section at station 5 is symmetric after damage, the horizontal bending moment remain same if we consider compression either at the starboard or port side. The vertical bending moment at station 5 may be designated as the local strength of hull 5415 at station 5, since the ultimate strength of the ship as a whole (at the mid-ship section) during damage scenario 3 and 4 may be higher. So the residual strength calculated for damage scenarios 3 and 4, have been presented so as to compare it with the ultimate strength at station 5.

Table 7.6-4: The ultimate/residual strength of Hull 5415 in different scenarios

Ultimate/residual strength	My, Yield Moment	Intact Scenario	Damage Scenario 1	Damage Scenario 2
Vertical bending moment (hogging)	2.066 x10^9 Nm	1.77x10^9 Nm	1.74x10^9 Nm	1.66 x10^9 Nm
Vertical bending moment (sagging)	2.066 x10^9 Nm	1.40x10^9 Nm	1.31x10^9 Nm	1.29x10^9 Nm
Horizontal BM (Damaged starboard side is in Compression)	–	2.17x10^9 Nm (symmetric about central line)	1.94x10^9 Nm	1.86x10^9 Nm
Horizontal BM (Damaged starboard side is in Tension)	–		1.81x10^9 Nm	1.72x10^9 Nm

Table 7.6-5: Vertical ultimate/residual strength at station 5

	Intact Scenario	Damage Scenario 3	Damage Scenario 4
Hogging Condition(Vertical)	$1.3x10^9$ Nm	$1.154x10^9$ Nm	$1.05x10^9$ Nm
Sagging Condition(Vertical)	$9.1x10^8$ Nm	$8.5 x10^8$ Nm	$8.05x10^8$ Nm

When a ship is damaged in one side (see Fig. 7.6-7), the mid-ship section doesn't remain structurally symmetric along the central line. So the horizontal bending moment creates significant impact on the strength of the ship depending on from which side the ship is horizontally bending. The compressive stress of an element is generally less than the tensile stress, in which case the element behaves elastic- perfectly plastic. So when the port (undamaged in this case) side of the hull 5415 undergoes tension, the residual strength in horizontal bending is higher than that experienced when it undergoes compression. For the damage scenarios 1 and 2 the behaviour of hull 5415 during horizontal bending have been presented in Table 7.6-4 and Figures 7.6-11 and 7.6-12.

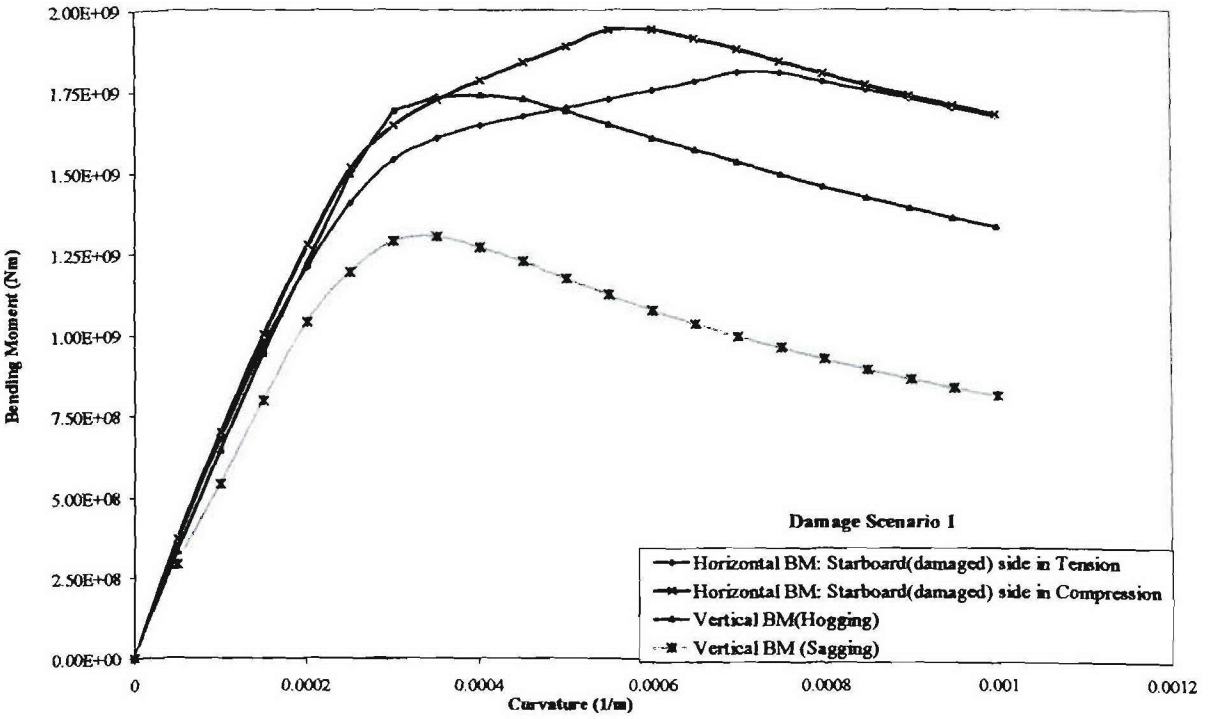

Figure 7.6-11: Comparison of moment-curvature relationship in Damage Scenario 1 in different bending conditions.

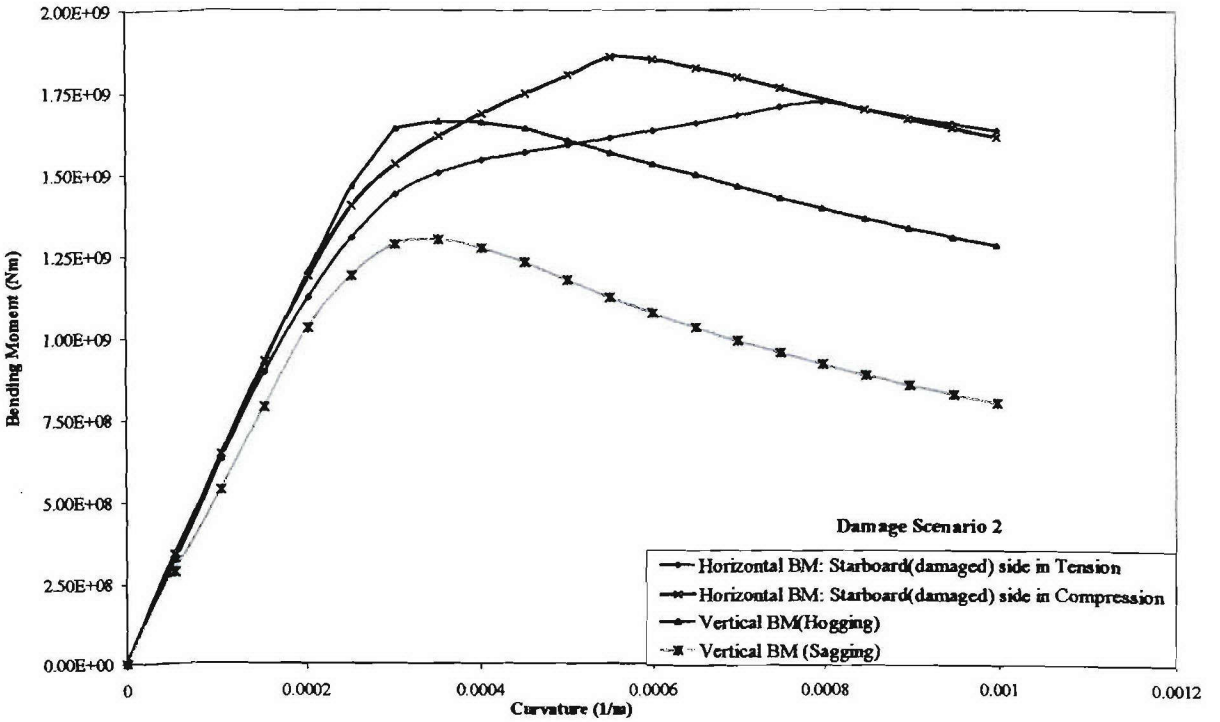

Figure 7.6-12: Comparison of moment-curvature relationship in Damage Scenario 2 in different bending conditions.

For the damage scenario 1 it is observed from Fig. 7.6-11 & Table 7.6-4, that when the starboard (damaged side) is in tension the horizontal residual strength of 1.81 x 10^9 Nm is experienced at a curvature of about 0.0007m^{-1}, where as when the starboard comes under compression the horizontal residual strength is expected to be 1.94 x 10^9 Nm at a curvature of about 0.0005m^{-1}. Similarly for damage scenario 2 (see Fig.7.6-12 and Table 7.6-4) the horizontal residual strength for starboard being under tension and compression is estimated to be 1.72 x 10^9 Nm and 1.86 x 10^9 Nm respectively. It can be observed that when the starboard side of hull 5415 undergoes tension, the horizontal residual strength is lower compared to that when it undergoes compression. In an asymmetric hull, since more number of undamaged elements are present in the port side and those elements contribute more towards the bending moment while it undergoes tension, this behaviour in horizontal bending is being experienced.

7.7 Comparison of Smith Method with US Navy Program – ULSTR

In this project, the Smith's method for predicting ultimate strength of hull girders is compared with 'ULSTR', a US Navy program for the same purpose as Smith's method. This comparison is very useful to US Navy to benchmark its existing tools with other tools. Basically, ULSTR is applied to predict the ultimate strength of the hull girder of a ro-ro ship, DEXTRA, to which Smith's method was applied in a EU project. The results of both methods are compared. Because this work was mainly carried out by NSWCCD with the assistance of UNEW, details of this work will not be presented in this report.

7.8 Deterministic Safety Assessment

In damaged conditions the critical condition may be in quartering seas in which wave-induced vertical and horizontal bending moments are coupled together. They achieve their maximum at different phase angles. Similarly torsion reaches maximum in quartering seas. Therefore to assess the structural safety of a damaged ship, the interaction of vertical bending moment, horizontal bending moment and torsion should ideally be considered. In this project only the interaction of vertical bending moment and horizontal bending moment will be taken into account due to the limit of time, while the effect of torsion will be considered in the following SSC + ONR project. For the deterministic analysis the interaction equation to combine the vertical and horizontal bending moment can be expressed as:

$$\left(\frac{M_V}{M_{UV}}\right)^m + \left(\frac{M_H}{M_{UH}}\right)^n = 1 \qquad (7.8\text{-}1)$$

In which
M_{UV} and M_{UH} are maximum capacities in vertical and horizontal bending moment
M_V and M_H are applied vertical and horizontal bending moments loads, and expressed as:

$$M_V = k_s M_S + k_w M_{wv} \qquad (7.8\text{-}2)$$

$$M_H = k_w M_{wh} \qquad (7.8\text{-}3)$$

Where

k_s and k_w are model uncertainty factors for still-water bending moment and wave-induced bending moment. M_s is still-water bending moment, M_{wv} and M_{wh} are wave-induced vertical and horizontal bending moment respectively.

When the left hand side of Eq. (7.8-1) is less than 1, the structure is viewed as safe, while if it is greater than 1, the structure would fail. Obviously the curve of Eq. 7.8-1 represents the border between safe and failure.

A few of points are noted here:

- The value of the coefficients *m* and *n* are dependent on the type of bending the ship has undergone, for example the value of *m* and *n* will be different during hogging and sagging condition in intact condition. In intact condition due to symmetry to the central plane the horizontal bending moment remains the same no matter which side the ship would be bent towards to (see Fig. 7.8-3).

- When a ship is damaged asymmetrically as what is in damage scenario 2 the values of *m* and *n* are different for different combinations of bending. For example, in hogging condition the value *m* and *n* will be different when the starboard is in compression from it being in tension in horizontal bending. Similarly in sagging condition the there will be two sets of values of *m* and *n* depending on which direction the hull is experiencing vertical bending (see Figure. 7.8-4)

- The values of *m* and *n* have been taken same for a particular scenario. The coefficients *m* and *n* for the interaction curve between the vertical and horizontal bending moment should be determined by performing the regression analysis.

- A load combination factor of 1 is implied in Eqs. (7.8-2) and (7.8-3) as discussed in section 4.2. k_s, k_w are taken as 1 when the IACS rule are followed to calculate the maximum still water and wave induced bending moments in intact condition.
- The target is to consider the interaction of not only vertical and horizontal bending moment but also torsion. Considering the effect of torsion in this case, equation (7.8-1) should be expanded to:

$$\left(\frac{M_V}{M_{UV}}\right)^m + \left(\frac{M_H}{M_{UH}}\right)^n + \left(\frac{T}{T_U}\right)^l = 1 \qquad (7.8\text{-}4)$$

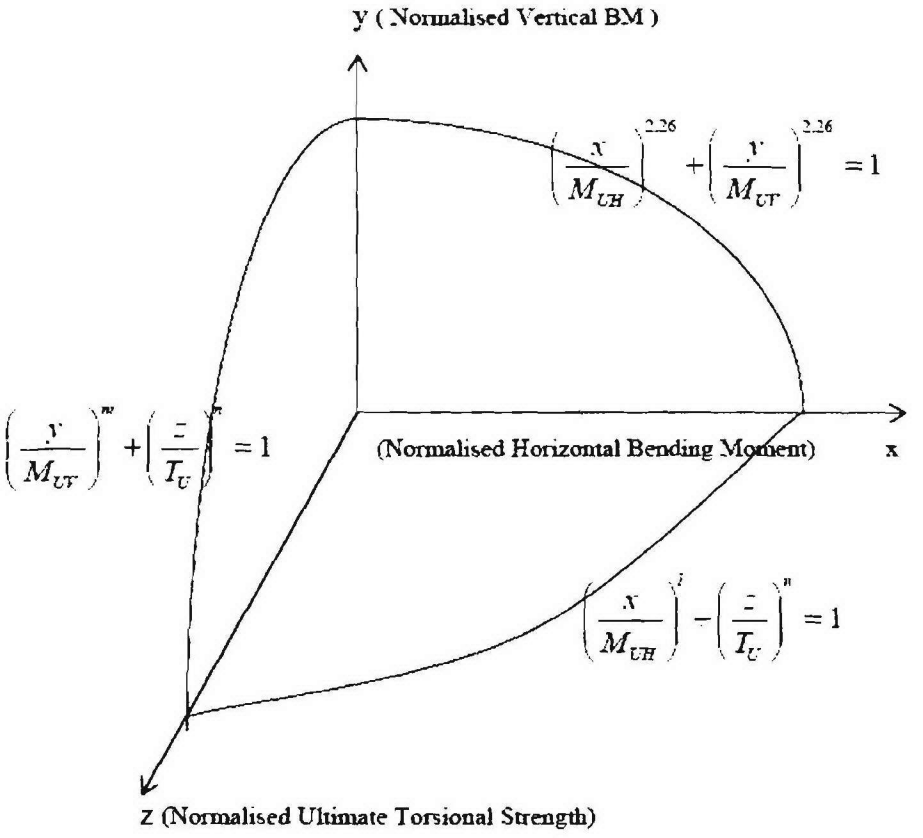

Figure 7.8-1: Schematic diagram for the interaction curve between vertical bending moment, horizon bending moment and the torsional strength in a 3D view.

Many authors including Paik *et al.* have studied the effect of torsion on the collapse behaviour of ships. But in most of the cases the contribution of torsion has been considered separately, in 2D way. Equation 7.8-4 represents the surface, which joins the xy, yz and zx plane as shown in Figure 7.8-1. More studies are required to find out the *l*, *m* and *n* coefficients of the surface representing the equation 7.8-4, since for torsional strength analysis the assumptions taken for progressive collapse analysis (plane sections are assumed to remain plane when curvature is increasing) doesn't remain same. So it is challenging to combine torsional moment with

vertical and horizontal bending moment in a 3D approach in analytical method. For that reason the reliability analysis of the hull 5415 has been performed considering only the vertical and horizontal bending moment in the section 7.9.

7.8.1 Wave induced bending moment

For a long term wave load the IACS ('95) unified formula for estimating the design wave–induced vertical bending moments (M_{wv}), wave induced horizontal bending moment (M_{wh}) and still water bending moment (M_s) are expected as

$$M_{wv} = \begin{cases} 110.C_1L^2B(C_b+0.7)\times10^{-3}\text{kNm} & \text{for sagging} \\ 190.C_1L^2BC_b\times10^{-3}\text{kNm} & \text{for hogging} \end{cases} \quad (7.8\text{-}5)$$

$$M_{wh} = 0.320.C_1.C_3L^2d_f\sqrt{\frac{L-35}{L}} \quad \text{kNm} \quad (7.8\text{-}6)$$

$$M_s = \begin{cases} -0.065*C_1*L^2*B*(C_b+0.7)\text{kNm} & \text{(sagging)} \\ C_1*L^2*B*(0.1225-0.015*C_b)\text{kNm} & \text{(hogging)} \end{cases} \quad (7.8\text{-}7)$$

Where L, B and C_b are ship length between perpendicular (in m), moulded breadth (m) and block coefficient, respectively, and C_1 is the wave height coefficient given by

$$C_1 = \begin{cases} 10.75-((300-L)/100)^{1.5} & 100<L\le300\text{(m)} \\ 10.75 & 300<L\le350\text{(m)} \\ 10.75-((L-350)/150)^{1.5} & L>350\text{(m)} \end{cases} \quad (7.8\text{-}8)$$

C_3: Distribution coefficient of the horizontal bending moment in the length direction of the ship, which is determined by linear interpolation using the equation given below according to the position of the considered cross section.

$$C_3 = \begin{cases} 0 & \text{at AP} \\ 1 & \text{at } 0.35L-0.65L \\ 0 & \text{at FP} \end{cases} \quad (7.8\text{-}9)$$

Using the above formula the wave induced bending moments and still water bending moments for long term are summarised in Table 7.8-1.

Table7.8-1: Ultimate strength and wave induced moments in long term loading condition for the mid-ship section.

Condition	M_{UV} (10^8 Nm)	M_{UH} (10^8 Nm)	M_S (10^8 Nm) (Long term loading)	M_{wv} (10^8 Nm) (Long term loading)	M_{wh} (10^8 Nm) (Long term loading)
Intact: Hogging	17.7	21.7	4.0781	3.3036	3.0996

Intact: Sagging	14.0	21.7	2.7418	4.6399	3.0996

(M_{UV}- ultimate vertical BM, M_{UH}= ultimate horizontal BM; M_{wv}-wave induced vertical BM; M_{wh}-wave induced horizontal BM; M_s- Still water BM; TM-tosional moment)

Table 7.8-2: Extreme design loads in mid-ship of hull 5415 in DS2 at sea state 3 for 96 hours

	M_{wv} (Nm)	M_{wh} (Nm)	TM (Nm)	M_S (Nm)
R_Max	1.4552×10^7	1.0007×10^7	1.4795×10^6	3.748×10^7
R_Design	1.7394×10^7	1.1961×10^7	1.7685×10^6	

(M_{wv}-wave induced vertical BM; M_{wh}-wave induced horizontal BM; M_s- Still water bending moment; TM-tosional moment)

Table 7.8-3: Model uncertainties of wave induced loads

	Mean	St. Dev	COV
Intact (k_w)	0.9544	0.4575	47.8%
DS2 (k_w)	1.0437	0.5497	52.7%

Table 7.8-2 represents the numerically calculated wave induced vertical, horizontal, still water bending moment and torsion moment at sea state 3 for the duration of 96 hours. It shows extreme design loads in midship of hull 5415. The 'R_Max' is the most probable extreme design load, and 'R_design' is extreme design load with a probability of exceedance of 0.01 in N encounters. In computations of short term prediction Pierson-Moskowitz spectrum was used at sea state 3. The time period was 96 hours. Table 7.8-3 represents the mean and standard deviation of model uncertainties factor, k_w, used in the equation 7.8-2 and 7.8-3.These calculated values are for a short-term wave load prediction for the hull 5415

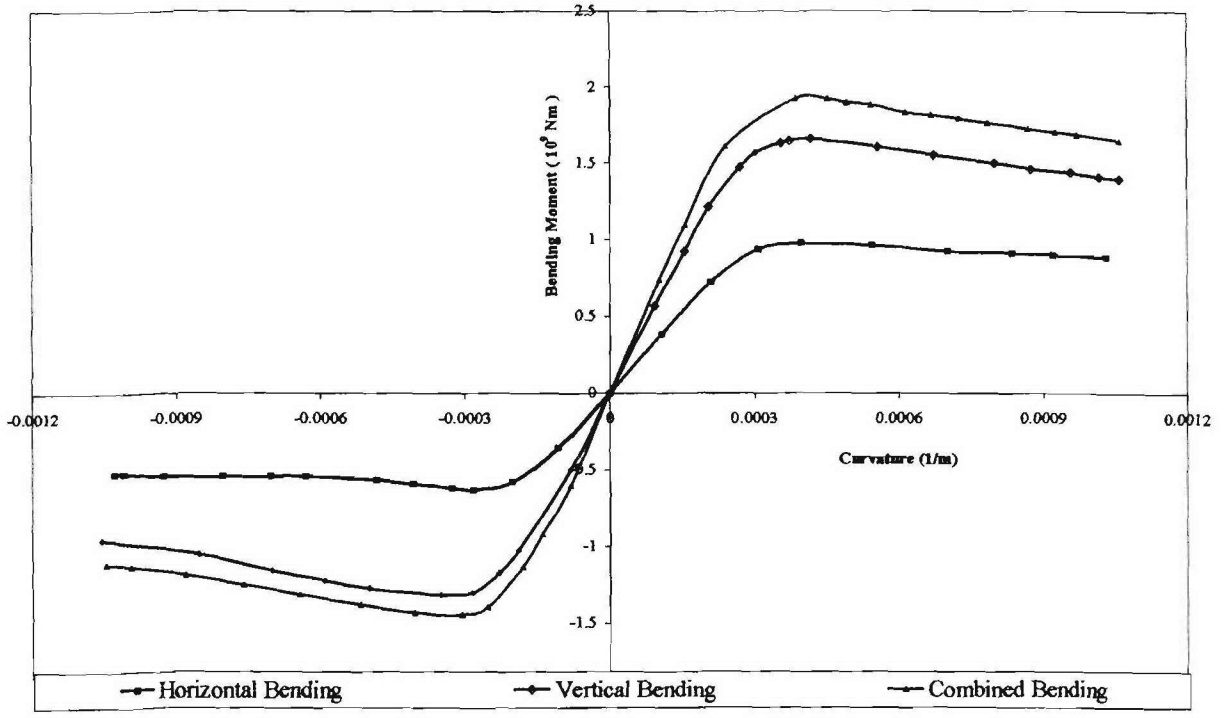

Fig. 7.8-2: Moment-Curvature relationship when the angle between the neutral axis and the base line (θ, see Fig. 4.3-1) is 22 degree for mid-ship section in intact condition.

Figure 7.8-2 represents the combined bending moment when the angle between the neutral axis and the base line is 22 degree for mid-ship section. The horizontal bending moment is less than the vertical bending moment for that particular phase angle, but as the phase angle increases the horizontal bending moment exceeds the vertical bending moment. By continuous increment of phase angle the interaction equation between the horizontal and vertical bending moment can be derived by performing regression analysis. For the present ship, hull 5415 the coefficient has been derived as 2.26 and 1.55 (as mentioned in Fig. 7.8-3) for hogging and sagging conditions in intact scenario respectively.

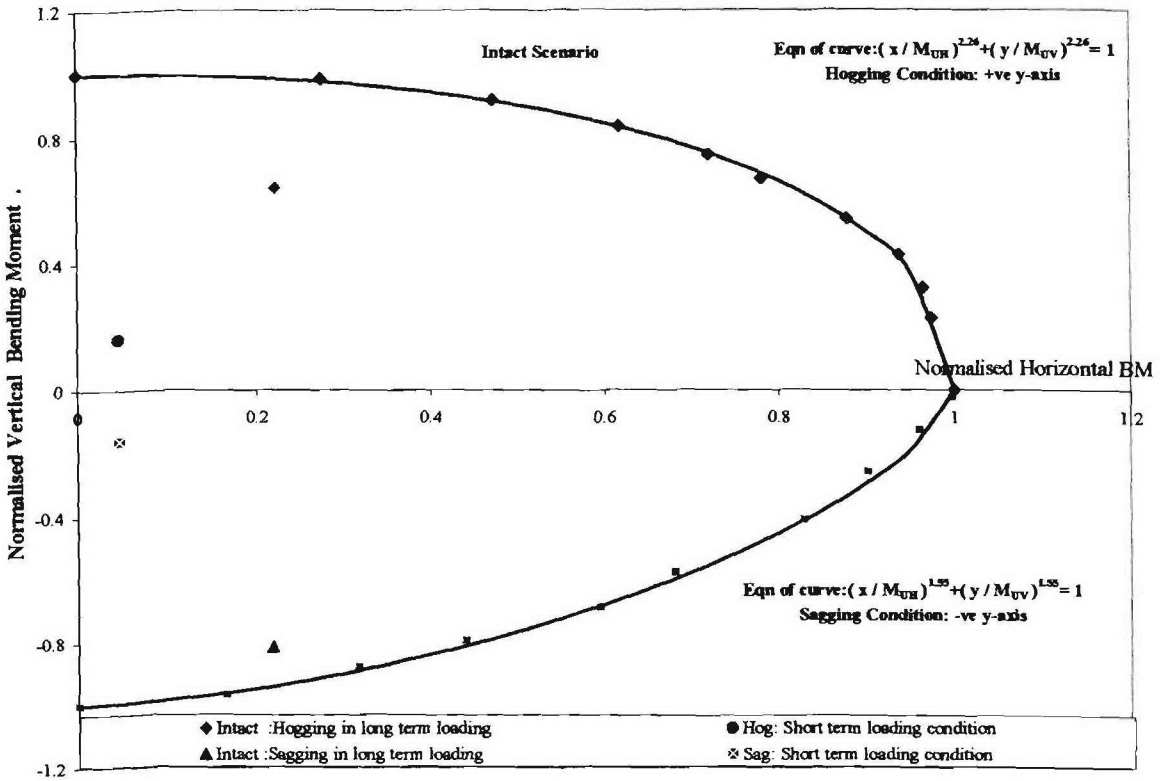

Fig. 7.8-3: The interaction curve between the horizontal and vertical bending moment for hull 5415 in intact condition

Table 7.8-4: Values of coefficients *m,n* in different scenarios

Scenario	Bending Condition	*m*	*n*
Intact scenario	Hogging condition	2.26	2.26
	Sagging condition	1.55	1.55
Damage Scenario 2	Hog: Starboard in tension	1.97	1.97
	Sag: Starboard in tension	1.44	1.44
	Hog: Starboard in compression	1.90	1.90
	Sag: Starboard in compression	1.40	1.40

Similarly for damage scenario 2 the interaction equation changes depending on the direction of the horizontal bending mending moment in hogging or sagging condition. Form Fig. 7.8-4 and Table 7.8-4 it can be noticed that that during hogging condition when the starboard (damaged) side undergoes tension and compression the value of the coefficient (*m* and *n*) are 1.97 and 1.9 respectively. Similarly for sagging condition the value of coefficient are 1.44 and 1.4 for

starboard being under tension and compression respectively. Since when the starboard is under compression the horizontal residual strength is higher than that when it is under tension, and M_{UH} being in denominator in the 2nd term of equation 7.8-1, this difference in the value of the coefficient *m* and *n* is noticed.

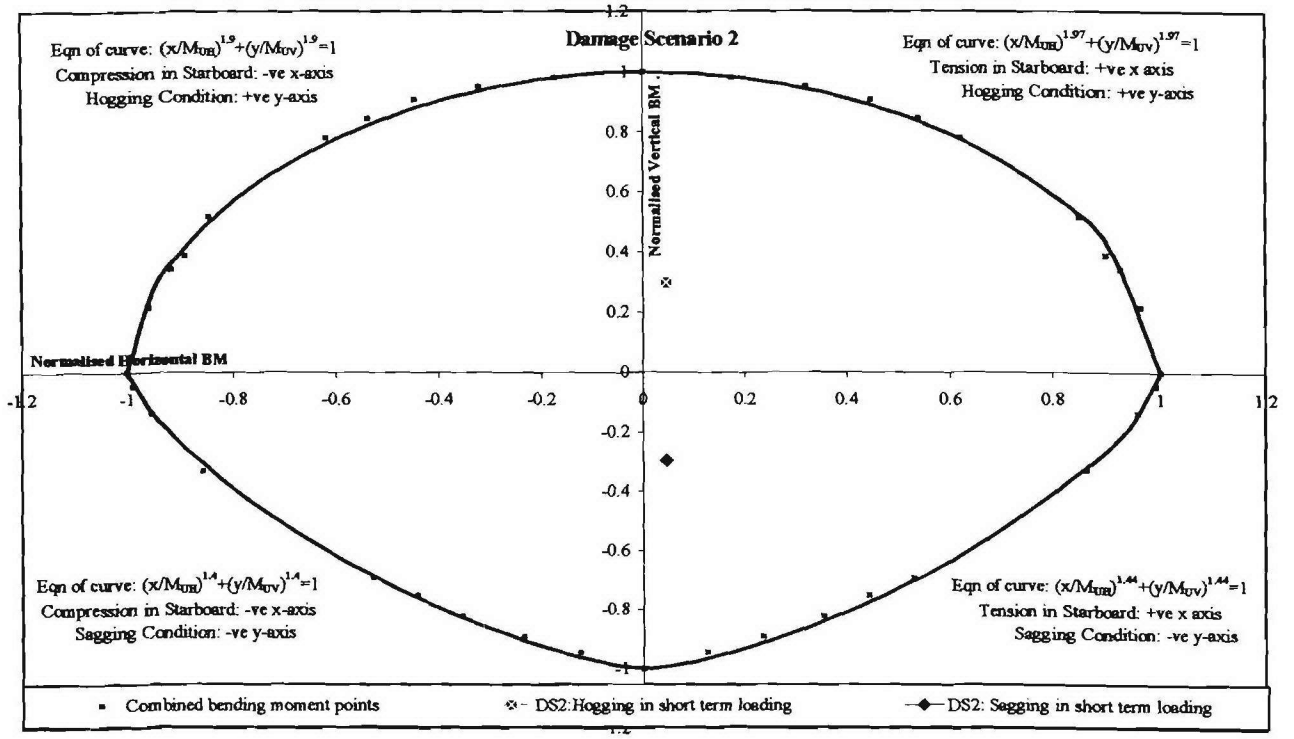

Fig. 7.8-4: The interaction curve between the horizontal and vertical bending moment for hull 5415 in damage scenario 2.

Table 7.8-5: The load to moment ratio in Eq. 7.8-1

Scenario	Bending Condition	$\frac{f.(M_{WH})}{M_{UH}}$ x co-ordinate	$\frac{f.(M_s+M_{WV})}{M_{UV}}$ y co-ordinate
Intact scenario	Intact: Hogging in long term loading	0.2200	0.6422
	Intact: Sagging in long term condition	0.2200	-0.8120
Damage Scenario 2	DS2: Hogging in short term loading	0.0461	0.2976
	DS2: Sagging in short term loading	0.0461	-0.2976

(*f*=1.54 when the IACS formula is used to calculate the value of wave induced BM, else 1.)

Table 7.8-5 represents the values of terms M_{WH}/M_{UH} and $(M_S+M_{WV})/M_{UV}$ of the equation 7.8-1. To calculate the wave induced bending moments and still water bending moment IACS formulae give acceptable values. Since hull 5415 is build for military purposes, for the long-term loading, a factor *f* of 1.54 has been multiplied to the IACS values for the intact conditions. For the short-term loading the wave induced bending moments and still water bending moment have been calculated for both intact and damage scenario 2 as given in table 7.8-2. These co-

ordinates have been plotted in Figures 7.8-3 and 7.8-4. In Figures 7.8-3 and 7.8-4 it can be claimed that when the co-ordinates of Table 7.8-5 are within the interaction curves, the structure is safe. If in any condition a co-ordinate point is outside the interaction curve the ship is not structurally safe in that condition. It can be noticed from Fig. 7.8-3 that during intact scenario the hull 5415 is relatively safer in hogging than in sagging condition for long term loading. Similarly the hull 5415 is very much safe in damage scenario 2, since the load to moment ratio co-ordinates are very close to the axes.

Tosional strength analysis

Design loads may generally be defined as loads that give the response values equivalent to the long-term predicted values (e.g. exceedance probability $Q=10^{-8}$ corresponding to ship's design life) of response. In this context, design loads for torsional strength assessment can be discussed considering that they give the values of warping stress and relative deformation equivalent to the respective long-term predicted values.

If the values of long-term predictions are mostly represented by response values in a certain regular wave (termed as dominant wave), the torsional moments as design loads can be discussed based on the torsional moments under the dominant wave condition.

The largest response which a ship may encounter once or a few times during her lifetime will be attained in extreme waves. In such extreme waves, nonlinear effects appear in various hull responses such as ship motions, hull girder moments and pressures. Thus, the effects of nonlinearity are to be considered when setting the final design loads. It can be shown that the long-term predicted values of wave induced Torsional Moment (T) are well approximated using the classification societies' rules and may be given by

$$T = M_{MT} = 1.3C_1 L d_f C_b (0.65 d_f + e) + 0.2 C_1 L B^2 C_w \qquad (kNm) \qquad (7.8\text{-}10)$$

Where
L: ship length between perpendiculars (m)
B: moulded breadth (m)
d_f: design moulded draught of ship (m)
e : the distance from the shear centre to the base line (m)
C_w : the water plane co-efficient (assumed as 0.9)
C_b : the block coefficient
C_1: the wave height coefficient corresponding to the IACS vertical bending moment and is given by equation 7.8-8:

There are two components in Eq. (7.8-10). The first component of the equation Eq. (7.8-10) is the torsional moment due to shear force multiplied by the distance to shear center from the working point (base line). And the other one is mainly from moment due to the bottom pressure distribution. Similarly from the torsional constant and shear stress the ultimate torsional strength (T_U) can be calculated as

$$T_U = J\frac{\tau}{r} \qquad (7.8\text{-}11)$$

Where
J : St. Venant's Torsional Constant
τ : Shear Stress ($\sigma_{y\text{-}average}/\sqrt{3}$)
r : Distance between the shear centre and the side shell along the base line.
T_U = Torsional Strength

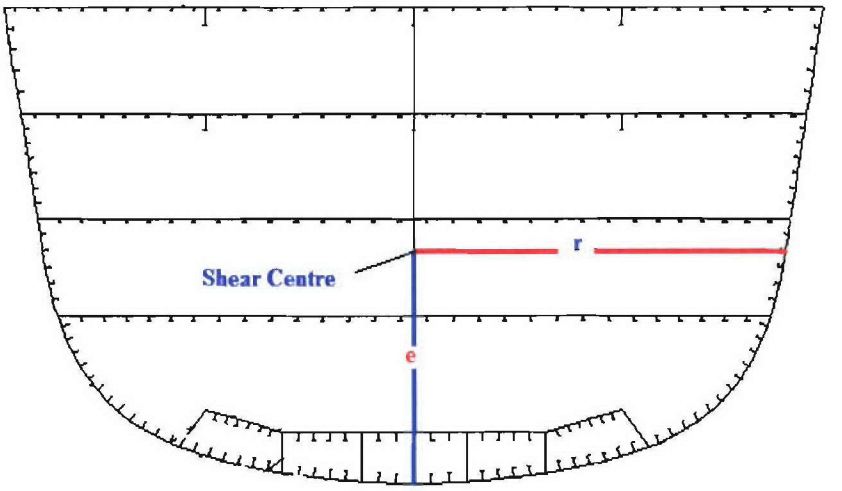

Figure 7.8-5 : Location of shear centre for the intact condition for hull 5415

Table 7.8.3: Torsional and shear properties for the hull 5415 at the mid-ship

Particulars	**Intact**	**Damage Scenario 2**
Cross-section Area of Mid-ship section	**1.593 m^2**	**1.426 m^2**
Elastic Neutral Axis	**6.35 m**	**6.34 m**
Second Moment of Area at centroid about x-axis (I_x)	**32.95 m^3**	**31.48 m^3**
Second Moment of Area at centroid about y-axis (I_y)	**47.7 m^3**	**35.013 m^3**
YY Shear Area	**0.3314m^2**	**0.2434m^2**
XX Shear Area	**0.6851m^2**	**0.5487m^2**
Torsional Constant (J)	**29.87 m^4**	**12.76 m^4**
Shear Centre	**0, 6.786m** (taking bilge pt. as origin)	**-4.18,-8.05m** (taking bilge pt. as origin, starboard side damaged)
Min. distance between shear centre and side shell (r)	**10.543 m**	**6.363 m**
Distance from the base line to the shear centre (e)	**6.786m**	**8.05 m**
Average Shear Stress (τ)	**217.7 MPa**	**215.9 MPa**
Ultimate Torsional Strength (T_U)	**6.168 x 10^8 Nm**	**4.33 x 10^8 Nm**
Wave induced Torsional Moment (T)	**1.445 x 10^8 Nm**	**1.51 x 10^8 Nm**

From Table the 3rd term of Eq. 7.8-4, (T/T_U) for intact and damage scenario 2 is 0.234 and 0.349 respectively for long term loading. Similarly for short-term loading the (T/T_U) ratio for damage scenario 2 is 0.0034. Even though in short-term loading term in the equation 7.6-4 are small individually, but these coefficients combined together may create hull 5415 structurally very much unsafe.

7.9 Reliability analysis of hull 5415

Traditionally, in the design process, practitioners and designers have used fixed deterministic values for loads acting on the girder and for its strength. In reality these values are not unique values but rather have probability distributions that reflect many uncertainties in the load and strength of the girder. Structural reliability theory deals mainly with the assessment of these uncertainties and the methods of quantifying and rationally including them in the design process. The load and strength are thus modelled as random variables

The interaction of only vertical and horizontal bending moment (not including torsion) will be considered in the reliability analysis of the hull 5415. The interaction equations between the vertical and horizontal bending moment in different damage and bending scenarios have been discussed in the section 7.8. Hence the limit state function for reliability analysis of hull 5415 may be expressed as:

$$g(\mathbf{X}) = 1 - \left(\frac{M_V}{M_{UV}}\right)^m - \left(\frac{M_H}{M_{UH}}\right)^n \qquad (7.9\text{-}1)$$

In which

M_{UV} and M_{UH} are maximum capacities in vertical and horizontal bending moment (separately)

M_V and M_H are applied vertical and horizontal bending moments, and expressed as:

$$M_V = k_s M_s + k_w M_{wv} \qquad (7.9\text{-}2)$$

$$M_H = k_w M_{wh} \qquad (7.9\text{-}3)$$

Where

k_s and k_w are model uncertainty factors for still-water bending moment and wave-induced bending moment. M_s is still-water bending moment, M_{wv} and M_{wh} are wave-induced vertical and horizontal bending moment respectively. Equation 7.9-1 can be re written as

$$g(\mathbf{X}) = 1 - \left(\frac{k_s M_s + k_w M_{wv}}{M_{UV}}\right)^m - \left(\frac{k_w M_{wh}}{M_{UH}}\right)^n \qquad (7.9\text{-}4)$$

For reliability analysis of the hull 5415, a factor (f) of 1.54 has been multiplied with the wave induced vertical , horizontal and still water bending moments considering the fact that the present ship has been built according to MOD rules, rather than the classification societies rule. As a practice adopted by the British MOD, the value for the factor (f) has been decided. Hence when the IACS rules have been followed to calculate the wave induced and still water moments, the limit state function for the reliability analysis for the hull 5415 has been taken as:

$$g(\mathbf{X}) = 1 - \left(\frac{f k_s M_s + f k_w M_{wv}}{M_{UV}}\right)^m - \left(\frac{f k_w M_{wh}}{M_{UH}}\right)^n \qquad (7.9\text{-}5)$$

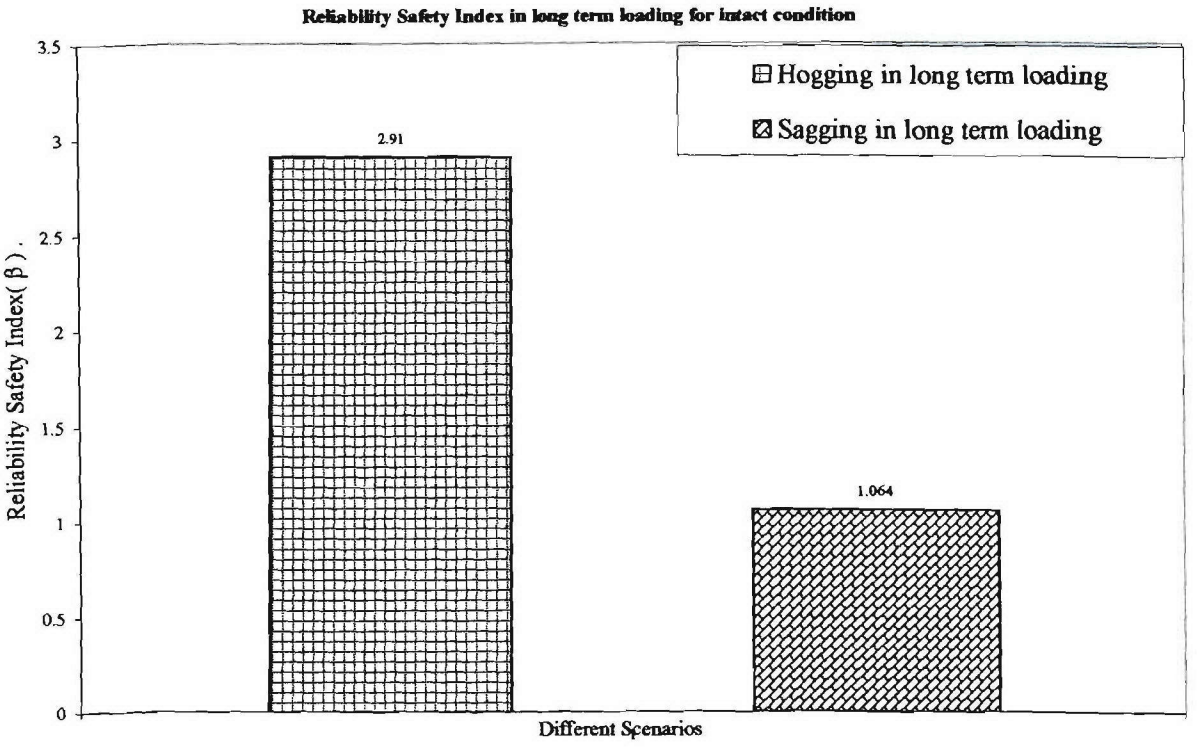

Figure 7.9-1: Reliability safety index (β) at different scenarios for the long term loading in intact condition for the mid-ship section.

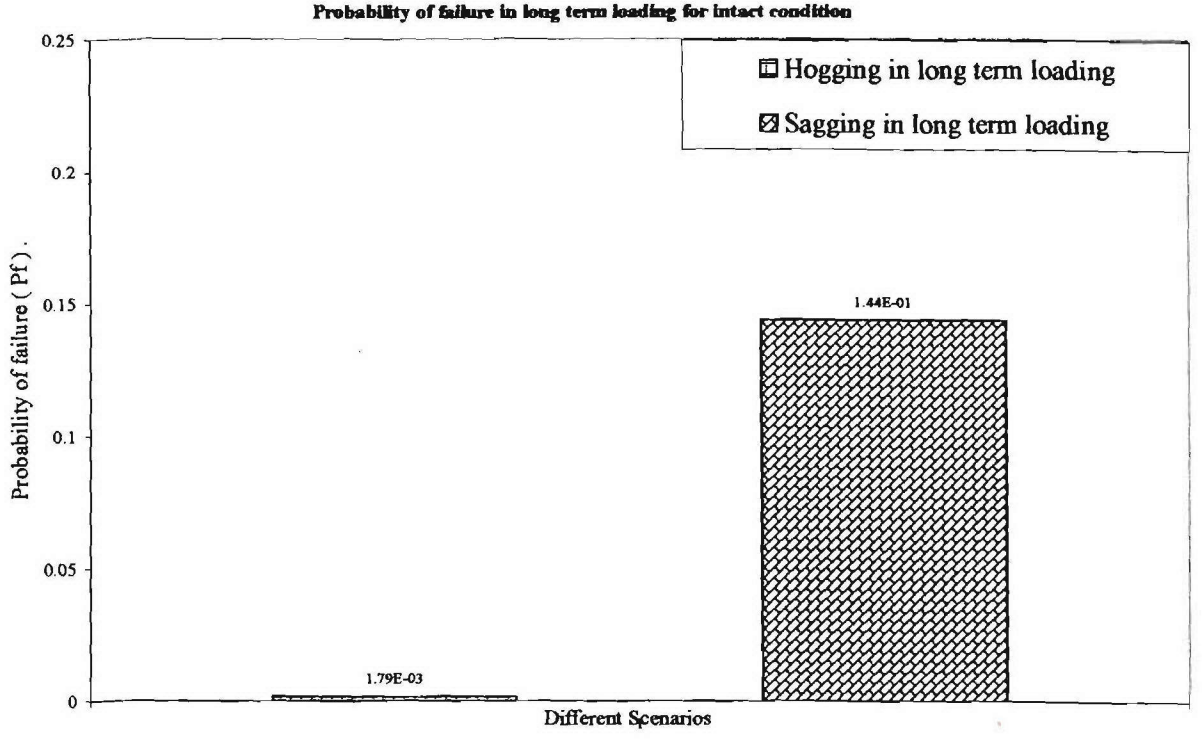

Figure 7.9-2: Probability of failure at different scenarios for the long term loading in intact condition for the mid-ship section.

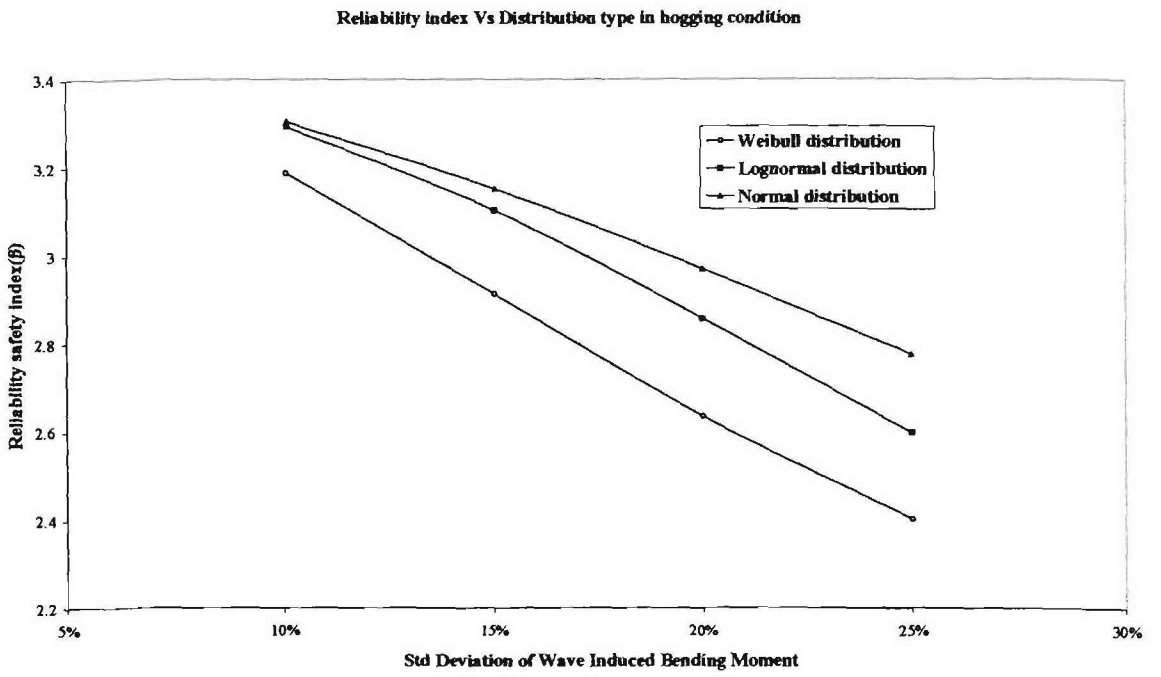

Figure 7.9-3: The variation of the reliability safety index with respect to the change of the standard deviation of the wave induced vertical and horizontal bending moment in hogging.

Table 7.9-5: Extreme design loads in mid-ship of hull 5415 in DS2 at sea state 3 for 96 hours

	M_{wv} (Nm)	M_{wh} (Nm)	TM (Nm)	M_S (Nm)
R_Max	1.4552×10^7	1.0007×10^7	1.4795×10^6	3.748×10^7
R_Design	1.7394×10^7	1.1961×10^7	1.7685×10^6	

(M_{wv}-wave induced vertical BM; M_{wh}-wave induced horizontal BM; M_s- Still water bending moment; TM-tosional moment)

Table 7.9-6: Model uncertainties of wave induced loads

	Mean	St. Dev	COV
Intact (k_w)	0.9544	0.4575	47.9%
DS2 (k_w)	1.0437	0.5497	52.7%
k_s	1	1.04	-

The short term load presented in Table 7.9-5, have been used to find out the probability of failure and reliability index for damage scenario 2. Since the last two terms in the equation 7.9-4 for the short term load are comparatively small (see Fig. 7.8-4), so the deterministic value of g(X) in equation 7.9-4 is not small enough to converge for the short term load condition. So it can be claimed that during short term loading the hull 5415 is relatively safe. On the other hand for the long term load condition the hull 5415 has reliability index of 2.91 and 1.064 for hogging and sagging conditions respectively. The low safety index gives rise to high probability of failure (0.1437) in sagging condition. So the hull is more prone to failure during sagging than hogging.

The distribution type chosen for the mean values during the reliability analysis can alter the prediction over its safety index and probability of failure. As it can be seen from Fig. 7.9-3 that the reliability index decreases with increment of standard deviation and it is also minimum for weibull distribution.

Finally it can be concluded that the hull is safe for the short term load of 96 hours, in sea state 3, but it is unsafe in long-term load scenario and it is more prone to failure during sagging condition.

8. DISCUSSIONS AND CONCLUSIONS

When a ship is damaged, the operators need to decide the immediate repair actions by evaluating the effects of the damage on the safety of the ship using residual strength assessment procedure. In this study, a procedure has been developed to assess structural integrity of damaged ships. The state of the art of the methods for predicting environmental loads and assessing the structural safety has been reviewed. The developed procedure is applied to a sample vessel, HULL5415, to demonstrate the accuracy of these methods.

The hydrodynamic loads in regular waves have been calculated by a 2D linear method. Experimental tests on a ship model with a scale of 1/100 have also been carried out to predict the hydrodynamic loads in regular waves. The results of the theoretical method and experimental tests are compared to validate the theoretical method and to calculate the model uncertainties of the theoretical method for probabilistic strength assessment.

It is found that in head waves a large opening, such as damage scenario 2, can dramatically increase wave-induced vertical bending moment. This is mainly attributed to the large increase of draught. But in damage scenarios 3 and 4 the vertical bending moment is slightly reduced.

In stern quartering waves the vertical bending moment in intact condition is larger than those in damaged conditions. However the horizontal bending moment RAOs in damage scenario 2 are the largest, and followed by damage scenario 1, intact condition and others. The torsional moment in the intact ship is the least amongst all the conditions, while damage scenario 2 has the largest torsional moment. Bearing in mind that damage scenario 2 has the largest opening, its torsional strength could be a concern.

In beam waves the magnitude of wave-induced loads is much smaller than those in other headings, so this would not cause any concern from structural strength point of view.

The comparison of theoretical results with experimental results has revealed that:

a) In intact condition, the agreement in large waves is slightly better than those in small waves. But the differences in the experiment results according to wave amplitudes are small. The computations and measurements of global dynamic wave induced load response amplitudes are in good agreement in head and stern quartering waves while the differences of the results in beam waves are significant. Nevertheless the magnitude of loads in beam waves is usually very small, so the large difference in numerical prediction would not cause much concern in the strength assessment of hull girders. Overall the 2D linear strip method presents acceptable agreements with the measurements.

b) In damage scenario 2 the 2D linear method has acceptable agreements with the measurements for vertical and horizontal bending moments. However the differences between the predictions and measurements of dynamic torsion moments are significant. And these phenomena could be caused by the effects

of sloshing and slamming within the damaged compartments, which could reduce the global dynamic wave load components. The measured and predicted dynamic wave induced loads in beam waves are in good agreements for vertical shear forces and vertical bending moments while there are significant differences in the results of horizontal dynamic wave induced load components. The possible reasons for this difference are the sloshing and slamming effects within the damaged compartment. In addition the drift of model may also be attributed to this difference.

c) In damage scenario 3, the measurements in large waves produce slightly better agreements with numerical results than those in small waves. In head and stern quartering waves, the correlation between the computations and measurements of dynamic load response amplitudes for DS3 ship is satisfactory. The wave induced loads in beam waves are not important because they are small values compared to the other load components.

d) It is observed that the accuracy for vertical bending moment is generally better than that for horizontal bending moment, and the COV of horizontal bending moment is almost as twice as that of vertical bending moment. It may be logical to consider model uncertainties for vertical bending moment and horizontal bending moment separately in reliability analysis. However this could be the further research topic. The accuracies at different floating conditions (intact, DS2 and DS3) are slightly different, but are comparable.

The extreme design wave-induced loads have been calculated by short term and long term prediction. For the loads in intact condition, long term prediction with duration of 20 years is used, while for loads in damaged conditions short term prediction is used. The maximum values of the most probable extreme amplitudes of dynamic wave induced loads in damaged conditions are much less than those in intact condition, because the most probable extreme design load in intact condition is based on long term prediction, while the most probable extreme design load for damaged conditions is based on short term prediction (sea state 3 for 96 hours).

It is noticed that when a ship is damaged, the critical cross sections, whose strength need to be assessed, are not necessarily limited to the damaged cross sections only. Although some cross sections are not structurally damaged, the total loads acting on these cross sections after damage (in other locations) may be increased dramatically compared to the original design load in intact condition. In this case the strength of these cross sections also needs to be assessed.

The ultimate strength of the hull 5415 has been analysed using the progressive analysis and also has been compared with another program. The accuracy of the program has been validated before proceeding to other cases. The M-Φ curves have been continuous and smooth and shown post collapse behaviour with increment of curvature. The high yield strength for the hull 5415 demonstrates that in hogging and sagging conditions the elements of the hull have under gone either flexural buckling or tripping. For the mid-ship section the ultimate strength in vertical bending during hogging condition is about 21 % higher than that in sagging condition. Since more elements during hogging conditions have undergone tensile stress the ultimate strength in hogging has been higher than that in the sagging condition.

Since the breadth of the ship is higher than its depth, the horizontal ultimate strength is higher than vertical ultimate strength (hogging or sagging). Due to symmetry about the central line in the intact case the horizontal ultimate strength is independent of the direction from which side the ship horizontally bents.

The residual strength for the different damage scenarios has been compared. During damage scenarios 1 and 2, since the location of the damages have been around the elastic neutral axis, the residual strength has been about 96.6% and 93 % of the ultimate strength during hogging condition. Similarly the residual strength case 3 and 4 shows significant decrease compared to the ultimate strength at the station 5. The ultimate strength calculated at station 5 may be designated as the local strength of that station, since with that amount of damage at station 5, the ultimate strength at the mid-ship section may be higher. In progressive collapse analysis it is challenging to take into account of the damage at the forward or at the aft of the ship while calculating the ultimate strength of the whole ship at the mid-ship section.

When the ship is damaged in one side, it is of considerable importance to pay attention from which side the ship bents horizontally. When the damaged side of the ship undergoes tension and undamaged side undergoes compression, the horizontal residual strength is less compared to when the damaged side is compression. It can observed that when the damaged side is in tension, total the stress contribution of individual element decreases, because more number of elements being in compression contribute less towards the bending moment, since the tensile stress is higher than the compressive stress. This kind of behaviour is expected when the structure is damaged asymmetrically.

In damaged conditions the wave induced vertical and horizontal bending moments combine together and the combined wave-induced bending moment achieve maximum at different phase angles. So the load combination becomes very essential part of structural safety assessment. For the deterministic analysis a rational interaction equation combining vertical and horizontal bending has been presented. Later the interaction equation will be extended to combine torsional strength with vertical and horizontal bending moment. The coefficient of the interaction curve has been determined using the regression analysis and the value of the coefficients m and n has been taken same for one condition. It is observed that the coefficient m and n for intact case has been different for hogging and sagging condition. Since the vertical ultimate strength (M_{UV}) in hogging is higher than that in sagging, and M_{UV} being in denominator, the value of m and n has been higher for the hogging case. For the unsymmetrical damage scenario for hogging case there has been two set of values for m and n, depending from which side the ship has horizontal bent. Similarly for sagging condition there have been two different values of the coefficients of the interaction equation. So there have been four set of values for m and n for the unsymmetrical damage in the damaged scenario 2. The normalised value vertical and horizontal loads have been plotted in the interaction curve to assess the safety of the hull in different scenarios. It is observed that the hull 5415 is more likely to fail in sagging than hogging condition for long term loading. For short-term loading the hull 5415 is observed to be relatively safe.

The limit state function for combined vertical and horizontal bending moment has been discussed. It is observed that during long term loading the hull 5415 has high probability of failure than that in hogging condition as found out in the deterministic safety assessment. The limit state function to combine the torsional strength with the vertical and horizontal bending moment has also been discussed. It is observed that during the damaged condition the ultimate torsional strength decreases rapidly and the wave induced torsional load increases, making the hull 5415 more likely to fail due to torsion. It can be summarised that the combined effect of torsion with vertical and horizontal load can be very much dangerous for the ship to fail in sagging condition.

In the future more work could be carried out to further improve the understanding of the structural behaviour of a damaged ship. Firstly 2D non-linear method could be used to predict the wave-induced loads and the results will be compared with linear method and experiment. In NSWCCD a commercial software, LAMP, in which nonlinear methods are used, is applied to predict the wave-induced loads. It would be very interesting to compare all these results. Secondly, the effects of forward speed on the wave-induced loads need to be investigated if the damaged ship needs to travel on itself. Thirdly, the current experimental results reveal large discrepancy between small waves and large waves at high wave frequency areas. One of the possible reasons is the small scale (1/100) used in the tests. It would be useful to run the tests with larger scale in the future.

Furthermore, Smith's progressive collapse analysis method has been used to determine the residual strength of the damaged ship. In this method the damaged parts of the ship are assumed to be inert or removed. It can be observed that this simplified method to consider the effects of damage is conservative. To investigate the accuracy of Smith's method it is necessary to perform the non-linear finite element analysis of the ship taking the effects of the damages into account.

The location of the structural damage is an important aspect that should be considered in future studies. When the ship is damaged in the aft or forward, it is advised to study the effect of the damage on the whole ship. During progressive collapse analysis it is challenging to summarise the effect of loss of local strength on the global strength.

Many authors have studied the effect of torsion on the collapse behaviour of ships. But in most of the cases the contribution of torsion has been considered separately, in 2D way. The combination of the torsion, vertical and horizontal bending represents a 3 dimensional surface and combinations of either of the two remain in one plane. Using progressive collapse analysis the interaction equation considering combined effect of horizontal and vertical bending has been done. Since for torsional strength analysis the assumptions taken for progressive collapse analysis (plane sections are assumed to remain plane when curvature is increasing) doesn't remain same, it is challenging to combine torsional moment with vertical and horizontal bending moment in a 3D approach in analytical method. When a ship is damaged the combined effect of torsion, horizontal and vertical bending is very dangerous for its survivability. So it advised to perform non-linear finite element analysis to derive an interaction equation taking into account the effect of torsion, horizontal and vertical bending moment.

ACKNOWLEDGEMENT

The authors would like to thank ONR for sponsoring this research. During the execution of this project Dr Roshdy S. Barsoum has provided a lot of help for us to understand how to meet the requirements of ONR. We are very grateful to this help. Thanks are also due to Ms Diane Gales and Mr Richard Ortisi for their assistance in contract issues. We would also like to thank Dr Jonathan Downes for his contribution to the work of this project.

REFERENCES

ABS.(2003). *"Rules for Building and Classing Steel Vessels, American Bureau of Shipping"*, Houston TX, USA.

Adegeest, L. J. M. (1995). *"Non-linear hull girder loads in ships"*, Thesis, Delft Univ. Technology.

Akita, Y. (1982). "Lessons learned from failure and damage of ships", *Joint Sessions 1, 8th International Ship Structures Congress*, Gdansk, Poland.

Ang H.S., Ma H.F. (1981). "On the reliability of structural systems", *Proc. of the Int. Conf. on Structural Safety and Reliability*, Trondheim.

Aryawan, I. D. (2000). *"Development of Analysis Methods for the Assessment of Hull Girder Loading and Strength of a Turret Moored FPSO"*, PhD thesis, University of Newcastle upon Tyne.

Bai Y., Bendiksen E., Terndrup Pederson P. (1993). *"Collapse Analysis of Ship Hulls, Marine Structures"*, Elsevier Science Ltd, Vol. 6, pp.485-507.

Borges Ferry, J., Castanheta, M. (1971). *"Structural Safety 2nd Edition"*, Laboratorio Nacional de Engenharia Civil, Lisbon, Portugal.

Borresen, R. & Tellsgard, F. (1980). *"Time history simulation of vertical motions and loads on ships in regular head waves of large amplitude"*, Norwegian Maritime Research, 3.

Brebbia, C. A. & Walker, S. (1979). *"Dynamic analysis of offshore structures"*, Butterworth & Co. ISBN: 0-408-00393-6.

Bucher C.G., Bourgound U. (1990). *"A Fast and Efficient Response Surface Approach for Structural Reliability Problems"*, Structural Safety, 7 (57-66).

Bureau Veritas, (2003): *"Rules for the Classification of Steel Ships"*, Bureau Veritas, France.

Caldwell J.B., Ultimate Longitudinal Strength, *Trans. RINA*, 1965.

Carlsen CA, Czujko J. (1978). "SPECIFICATION OF POST-WELDING DISTORTION TOLERANCES FOR STIFFENED PLATES IN COMPRESSION". Vol. 56A, No. 5, pp.133-141.

Chan, H. S. (1992). "Dynamic structural responses of a mono-hull vessel to regular waves", *International Shipbuilding Progress, Vol.* 39, pp.287-315.

Chan, H. S. (1993). "Prediction of motion and wave loads of twin-hulled ships", *J Marine Structures, Vol. 16*, pp.75-102.

Chan, H. S. (1995). "On the calculations of ship motions and wave loads of high-speed catamarans", *International Shipbuilding Progress, Vol. 42*, pp.181-95.

Chan, H. S. (1998). "Prediction of large amplitude motions and wave loads on a RoRo ship in regular oblique waves in intact and damage conditions", *DTR-4.1-UNEW-12.98, DEXTREMEL project BE97-4375.*

Chan, H. S., Voudouris, G.; Servis, D. P. and Samuelides, M. (2000). "Residual Strength of a Damaged RO RO Ship", *DTR-4.3-UNEW-04.00, DEXTREMEL project BE97-4375.*

Chan, H. S.; Atlar, M. and Incecik, A. (2002). "Large-amplitude motion responses of a Ro-Ro ship to regular oblique waves in intact and damaged conditions", *J Marine Science and Technology Vol. 7*, pp.91-99.

Chan, H. S.; Atlar, M. and Incecik, A. (2003). "Global wave loads on intact and damaged RO-RO ships in regular oblique waves", *J Marine Structures Vol. 16*, pp.323-344.

Chan, H.S., Incecik, A. and Atlar, M. (2001). "Structural Integrity of a Damaged Ro-Ro Vessel" Proceedings of the second international conference on collision and grounding of ships, Technical University of Denmark, Lybgby, pp. 253-258.

Chang, M. S. (1977). "Computations of three-dimensional ship motions with forward speed", *Proc the Second International Conf on Numerical Ship Hydrodynamics*, University of California, Berkeley, pp.124-135.

Chen, Y-K, Kutt, LM, Piaszcyk, CM and P. BM. (1983). "Ultimate Strength of Ship Structures". *Transactions of SNAME*, Vol. 91, pp.149-168.

Chiu, F. C. and Fujino, M. (1989). "Nonlinear prediction of vertical motions and wave loads of high-speed crafts in head sea", *International Shipbuilding Progress, Vol. 36*, pp.193-232.

Class NK, (2003). *"Guidelines for Torsional Strength Assessment".*

Collette, M. (2005a). "Draft Deliverable D4.2: p-4-21-RD-2004-16-01-0", *POP&C project FP6-PLT-506193* (Confidential).

Collette, M. (2005b). *"Front End: Documentation and User's Guide Version 0.1"*, University of Newcastle.

COMREL & STRUREL Manual, RCP GmbH, Federal Republic of Germany.

Cornell C.A.(1967). "Bounds on the reliability of structural systems", *Journal of the Structural Division*, ASCE (ST1), 93, pp.171-200.

Dalzell, J.F., Maniar, N.M., Hsu, M.W. (1979). "Examination of service and stress data of three ships for development of hull girder load criteria", *Report No. SSC-287, Ship Structures Committee*, Washington DC, USA.
Das P.K, Fang C., (2005). "Survivability and reliability of damaged ships after collision and grounding". *Ocean Engineering*, Vol. 32, pp 293-307.

Das P.K., Fang C.,(2006). "Residual Strength and Survivability of Ships after Grounding and Collision", Article in Press, *Journal of Ship Research*.

Das P.K., Zheng Y. (2000). "Cumulative formation of Response Surface and its use in Reliability Analysis", *Probabilistic Engineering Mechanics*, Elsevier Science Ltd., 15 (309-315).

De Kat, J. O. (1990). "The numerical modeling of ship motions and capsizing in severe seas", *J Ship Research, Vol. 34*, pp.289-301.

Ditlevsen, H.O.Madsen.(1996). *"Structural Reliability Methods"*, John Wiley & Sons, England.

Ditlevsen.(1979). "Narrow reliability bounds for structural systems", *Journal of Structural Mechanics*, Vol. 7(4), pp 453-472.

DNV (1994). *"Hull structural design of ships with length 100 metres and above"*, Rules for Classification of Ships. Part 3.Chapter 1, Det Norske Veritas, Norway.

DNV. (July 1999). *"Corrosion Prevention of Tanks and Holds"*, Classification Notes No. 33.1, Det Norske Veritas, Hovik, Norway.

DNV (2000). *"DNV Classification Note 30.5: Environmental Conditions and Environmental Loads"*.

Dow RS, Hugill RC, Clark JD, Smith CS. (1981). "Evaluation of Ultimate ship Hull Strength". *Extreme Loads Response Symposium*, Arlington, VA, October 19-20, 1981.pp 133-148.

Dow, R.S. (1980). "N106C: "A computer program for elasto-plastic, large deflection buckling and post-buckling behaviour of plane frames and stiffened panels". *AMTE(S) R80726.*

Downes, J. and Pu, Y. (2005). "Reliability-based Sensitivity Analysis of Ships", *Proc. IMechE 2005.*

Dwight JB, Moxham KE. (1969). "Welded steel plates in compression". Structural Engineer, Vol. 47, No. 2, pp. 54.

Faltinsen, O.M. (1990). *"Sea Loads on Ships and Offshore Structures"*, Cambridge Ocean Technology Series, Cambridge University Press. ISBN: 0-521-45870-6.

Fang C, Das PK. (2005). "Survivability and Reliability of Damaged Ships after Collision and Grounding", *Ocean Engineering*, 32: 3-4, pp 293-307.

Fang, C. C.; Chan, H. S. & Incecik, A. (1997), "Investigation of motions of catamarans in regular waves – II", *J Ocean Engineering, Vol. 24*, pp.949-66.
Fang, M. C. and Her, S. S. (1995). "The non-linear SWATH ship motion in large longitudinal waves", *International Shipbuilding Progress, Vol. 42*, pp.197-220.

Faulkner D, Adamchak JC, Snyder GJ, Vetter MF. (1973). "SYNTHESIS OF WELDED GRILLAGES TO WITHSTAND COMPRESSION AND NORMAL LOADS". *Computers and Structures*, Vol. 3, No. 2, pp.221-246.

Faulkner D. (1975): "A Review of Effective Plating for the Analysis of Stiffened Plating in Bending and Compression". *Journal of Ship Research*, Vol. 19, No.1, pp 1-17.

Faulkner, J.A., Clarke J.D., Smith C.S., and Faulkner D. (1984). "The loss of the HMS Cobra-a reassessment". *RINA Transactions*, Vol. 126, pp.125-151,.

Frank, W. (1967). "Oscillation of Cylinders in or Below the Free Surface of Deep Fluids", *Hydromechanics Laboratory Research and Development Report.*

Frieze, P.A., Dogliani, M., Huss, M., Jensen, J.J., Kunow, R., Mansour, A.E, Murotsu, Y., Valsgard, S.(1991). "Applied Design Report of Committee V.1", *The 11th International Ship & Offshore Structures Congress*, China.

Fujikubo M., Yao T., Varghese B.(1997)."Buckling and ultimate strength of plates subjected to combined loads", *Proc. 7th Offshore and Polar Engineering Conf.*, Vol. IV, pp.380-387,.

Fujino, M. and Yoo, B. S. (1985). "A study on wave loads acting on ship in large amplitude (3rd Report) ", *J Society of Naval Architects of Japan, Vol. 158.*

Geritsma, J. and Beukelman, W. (1967). "Analysis of the modified strip theory for the calculation of ship motions and wave bending moments", *International shipbuilding progress* Vol.14, no.156.

Ghoneim, G. A.; Tadros, G. (1992). "Finite element analysis of damaged ship hull structures". *Proceedings of the International Offshore Mechanics and Arctic Engineering*, Vol. 1, pt B, (1992), pp. 611-620.

Ghose, D.J., Nappi, N.S. and Wiernicki, C.J. (1995). "Residual strength of damaged marine structures". *Report of Ship Structures Committee*, SSC-381.

Gordo J.M., Guedes Soares C. (1993). "Approximate Load Shortening Curves for Stiffened Plates under Uni-axial Compression", *Integrity of Offshore Structures*, EMAS, pp.189-211.

Gordo J.M., Guedes Soares C., Faulkner D. (1996): "Approximate Assessment of the Ultimate Longitudinal Strength of the Hull Girder". *Journal of Ship Research*, 1996, Vol. 40, N° 1, pp. 60-69.

Gordo JM, Guedes Soares C. (1996): "Approximate Method to evaluate the Hull Girder Collapse Strength". *Marine Structures* Vol. 9. Pages 449-470.

Gordo, J.M., Guedes Soares, C. (1997). "Interaction equation for the collapse of tankers and containerships under combined vertical and horizontal bending moments". *Journal of Ship Research*, Vol. 41:3, pp.230-240.

Guedes Soares C, Moan T. "Statistical analysis of Stillwater load effects in ship structures", *SNAME Transaction*, Vol. 96, pp.129-156, 1988.

Guedes Soares C., Soreide T.H.(1983): "Behaviour and Design of Stiffened Plates Under Predominantly Compressive Loads". *International Shipbuilding Progress*, Vol. 30, N° 341, pp. 13-27.

Guedes Soares, C. (1984). "Probabilistic Models for Load Effects in Ship Structures", *Report UR-84-83, Div. Marine Structures*, Norwegian Institute of Technology.

Guedes Soares C.(1988). "Design equation for the compressive strength of unstiffened plate elements with initial imperfections" Journal of Construction Steel Research, Vol. 9, No. 4, pp 287-310.

Hasselmann, K. at al (1973). "Measurements of wind wave growth and swell decay during the Joint North Sea Wave Project (JONSWAP)". *Deutsches Hydrographisches institut*, Hamburg, Report Series A. No. 12.

IACS, (1989). IACS Requirement S7, "Minimum Longitudinal Strength Standards", *Revision 3, International Association of Classification Societies*, London, United Kingdom.

IACS. (2001). "Bulk Carriers: Guidelines for Surveys, Assessment and Repair of Hull Structure", *International Association of Classification Societies*, No. 76, London UK.

Incecik, A.; Pu, Y. Aryawan, I. D. (2001). "Hydro-Structural Aspects of Floating Production Storage and Offloading Systems (FPSOs)", *Proc the 1st PNU International Colloquium*, Pusan National Unv., Korea, pp.7-17.

Inglis, R. B. (1980*). "A three-dimensional analysis of the motion of a rigid ship in waves"*, PhD thesis, Department of Mechanical Engineering, University College London.

ISSC, 1997. "Ultimate Strength". Report of Committee III.1, *International Ships and Offshore Structures Congress*.

ISSC Committee (1979). "ISSC Report of Committee 1.1: Environmental Conditions", *7th International Ship Structures Congress*, Paris.

Ivanov, L., Madjarov, H. (1975). "The statistical estimation of SWBM (still water bending moment) for cargo ships", *Shipping World & Shipbuilder*, Vol. 168, pp.759-762.

Jacobs, W.R. (1958). "The analytical calculation of ship bending moments in regular waves". J Ship Research, June, pp.20-29.

Jacobs, W.R.; Dalzell, J. & Lalangas, P. (1960). "Guide to computational procedure for analytical evaluation of ship bending-moments in regular waves", *US Navy, Davidson Laboratory*, Report No.791.
Jensen J.J. et al. (1994). "Report of Committee III.1, Ductile Collapse", *Proc. 12th International Ship and Offshore Structures Congress*, Vol. 1, pp.229-387.

Jensen, JJ, Amdahl, J, Caridis, P, Chen, TY, Cho, S-R, Damonte, R, Kozliakov, VV, Reissmann, C, Rutherford, SE, Yao, T and Estefen, SF. (1994). "Report of ISSC Technical Committee III.1 - Ductile Collapse". In: Jeffrey NE and Kendrick AM, editors. *12th International Ship and Offshore Structures Congress*; St John's, Canada: Elsevier Science Ltd, pp. 299-387.

JMT (Japan Ministry of Transport) (1997). "Report on the Investigation of Causes of the Casualty of Nakhodka". *The Committee for the Investigation on Causes of the Casualty of Nakhodka*.

John W.G.(1874). "On the strength of the iron ship", *Trans. Inst. Naval Arch.*, Vol. 15, pp.74-93.

Kaplan, M. Benatar, M., Bentson, J., Achtarides, T.A. (1984). "Analysis and assessment of major uncertainties associated with ship hull ultimate failure", Report No. SSC-322, *Ship Structure Committee*, Washington DC, USA.

Khan I.A., Das P.K., Permentier G.(2006). "Ultimate Strength and Reliability Analysis of a VLCC". *Proceedings of the 3rd International ASRANet Colloquium*, Glasgow.

Khan I.A.(2004). "Ultimate Strength of Ship: A Case Study, Bachelor of Technology Thesis". Dept. of Naval Architecture & Ocean Engineering, *Indian Institute of Technology Madras*, India.

Khan IA, Das PK, Zheng Y, (2005). "Structural Response of Intact and Damaged Stiffened Plated Structure for Ship Structures". Proceedings of Maritime Transportation and Exploitation of Ocean and Coastal Resources-Guedes Soares, Garbatov & Fonseca (eds),Lisbon,Portugal, © 2005 Taylor & Francis Group, London. Pages- 455-460.

Khan IA, Guedes Soares C, Teixeira AP, Luis RM,Quesnel T, Nikolov PI, Steen E, Toderan C, Olaru VD, Bollero A, Taczala,(2005): "Effect of the Shape of Localized Imperfections on the Collapse Strength of Plates. Proceedings of Maritime Transportation and Exploitation of Ocean and Coastal Resources-Guedes Soares", Garbatov & Fonseca (eds),Lisbon,Portugal, © 2005 Taylor & Francis Group, London. Pages- 429-437

Kim S.H., Na S.W. (1997). "Response surface method using vector projected sampling points", *Strucutral Saefty*, 19(1) (3-19).

Kim, C. H.; Chou, F. S. & Tien, D. (1980) "Motions and hydrodynamic loads of a ship advancing in oblique waves", *Trans SNAME Vol. .88,* pp.225-56.

Korkut, E.; Atlar, M. & Incecik, A. (2004), "An experimental study of motion behaviour with an intact and damaged Ro-Ro ship model", *J Ocean Engineering* v.31, pp.483-512.
Korkut, E.; Atlar, M. & Incecik, A. (2005), "An experimental study of global loads acting on an intact and damaged Ro–Ro ship model", *J Ocean Engineering* v.32, pp.1370-1403.

Korvin-Kroukovsky, B.V. (1955). "Investigation of ship motions in regular waves", *Transactions SNAME Vol. 63,* pp.386-435.

Korvin-Kroukovsky, B.V.and Jacobs, W.R (1957). "Pitching and heaving motions of a ship in regular waves". SNAME Trans Vol. 65, pp.590-632.

Kutt L.M., Piaszczyk C.M., Chen Y.K. (1985). "Evaluation of longitudinal ultimate strength of various ship hull configurations", *Trans. SNAME*, Vol. 93, pp.33-55.

Larrabee, R.D. and Cornell, C.A. (1981). "Combination of various load processes, Journal of Structural Division", *ASCE*, Vol.107, pp.223-238,.

Larrabee, R.D.(1978). *"Stochastic analysis of multiple load: load combination and bridge loads"*, Ph.D. thesis, Department of Civil engineering, MIT, Cambridge MA, USA,.

Lee, C. M. & Curphey, R. M. (1977). "Prediction of motion, stability and wave load of small-waterplane-area, twin-hull ships", *Trans SNAME v.85,* pp. 94-130.

Lee, Dongkon; Lee, Soon-Sup; Park, Beom-Jin & Kim, Soo-Young. (2005). "A study on the framework for survivability assessment system of damaged ships", *J Ocean Engineering v.32*, pp.1122-1132.

Lewis, E.V. (1957). "A study of midships bending moments in irregular head seas", *Journal of Ship Research*, Vol.1.

Lewis, E.V. et al. (1973), "Load criteria for ship structural design", Report No. SSC-224, *Ship Structrure Committee*, Washington DC, USA.

Lloyd's Register of Shipping, 2002, *"Rule and Regulations for Classification of Naval Ships"* Vol.1.

Lloyd's Register, (2000). *"World Casualty Statistics: annual statistical summary of reported loses and disposals of propelled sea-going merchant ships of not less than 100 GT".*

Lua J. and Hess P.E. (2003). "Hybrid Reliability Predictions of Single and Advanced Double-Hull Ship Structures", *Journal of Ship Research*, 47:2,155-176.

Maestro M., Marino A. (1989). "An Assessment of the structural capacity of damaged ships: The plastic approach in longitudinal symmetrical bending and the influence of buckling", *Int. Shipbuilding Progress*, Vol 36:408, pp.255-265.

Mano, H., Kawabe, H., Iwakawa, K., Mitsumune, N. (1977). „Statistical character of the demand on longitudinal strength (second report)-long term distribution of still water bending moment", *Journal of the Society of Naval Architects of Japan*, Vol. 142, in Japanese.
Mansour A.E., Yang J.M., Thayamballi A. (1990). "An experimental investigation on ship hull ultimate strength", *Trans. SNAME* 98:411-440.

Mansour, A.E., Lin, Y.H., Paik, J.K. (1995). "Ultimate strength of ships under combined vertical and horizontal moments". *Proceedings of the 6th International Symposium PRADS*, Seoul Korea, Vol. 2, pp.844-851.

Mansour, A.E., Thayamballi, A. (1993). "Probability-based ship design procedures", Draft Report SR-1337, *Ship Structure Committee*, Washington DC, USA.

Melchers, R.E. (1998). *"Structural Reliability Analysis and Prediction 2nd Edition"*, John Wiley & Sons, Chichester, England.

Meyerhoff, W.K., Arai, M., Chen, H.H., Day, Y.-S., Isaacson, M., Jankowski, J., Jefferys, E.R., Lee, S.-C., Mathisen, J., Richer, J.-Ph, Riska, K., Romeling, J.U.(1991). "Loads", *report of Committee I.2, 11th International Ship & Offshore Structures Congress*, Wuxi, China.

Moan, T. and Jiao, G. (1988). "Characteristic still-water load effects for production ships", Report MK/R 104/88, *The Norwegian Institute of Technology*.

Moan, T., Wang, X.(1996). "Stochastic and Deterministic Combinations of Still Water and Wave Bending Moments in Ships", *Marine Structures*, Elsevier Science Ltd, Vol.9, pp.787-810.

Newman, J. N. (1978). "The theory of ship motions", *Advances in Applied Mechanics v.18*, pp.221-83.

Nielsen, L. P. (1998). *"Structural Capacity of the Hull Girder."* PhD Thesis. Department of Naval Architecture and Offshore Engineering, Technical University of Denmark, Lyngby, Denmark. pp.211.

Nishihara S., (1983). "Analysis of ultimate strength of stiffened rectangular plate (4th Report)- On the ultimate bending moment of the ship hull girder", *Journal of the Soc. Naval Arch. Of Japan*, Vol 154, pp.367-375, in Japanese.

Nitta, A.(1994). "On C. Guedes Soares discussion of paper by A. Nitta et al. Basis of IACS unified longitudinal strength standard", Vol. 5, (1992) 1-21, *Marine Structures*, Vol. 7, pp.567-572,.

Nordenstrom, N. (1971). "Methods for predicting long term distributions of wave loads and probability of failure of ships", *DNV*, Research and Development Report 71-2-S.

Ochi, M.K. (1973). "On prediction of extreme values". *J Ship Research*, v.17 n.1, Mar, pp.29-37.

Ochi, M.K. (1981). "Principles of extreme value statistics and their application". *Extreme Loads Response Symposium (SNAME)*, Arlington, VA, October 19-20, SNAME, pp.15-30.
Ogilvie, T. F. & Tuck, E. O. (1969). "A rational strip theory for ship motions", *part 1, Report no. 013, Department of Naval Architecture and Marine Engineering, University of Michigan.*

Ozguc O, Das P.K., Barltrop N. (2005). "A comparative study on the structural integrity of single and double side skin bulk carriers under collision damage". *Marine Structures*. Vol. 18. pp 511-547.

Paik J.K. (1992). "Ultimate hull girder strength analysis using Idealized Structural Unit Method: A case study for double hull girder with transverseless system", *PRADS '92*, Elsevier, Vol. 2, pp.745-763, Newcastle upon Tyne.

Paik J.K. (1993). "Hull Collapse of an aging Bulk Carrier under combined Longitudinal Bending and Shearing Force", *Trans. RINA.*

Paik J.K. (1999). "SPINE, A computer program for analysis of elastic –plastic large deflection behaviour of stiffened panels. User's Manual", *Pusan National Univ.*, Korea.

Paik J.K., Kim D.H., Bong H.S., Kim M.S., Han S.K. (1992). "Deterministic and probabilistic safety evaluation for a new double-hull tanker with transverseless system". *Trans. SNAME*, Vol. 100, pp.173-198,.

Paik J.K., Kim S.K., Yang S. H., Thayamballi A.K. (1997). "Ultimate Strength Reliability of Corroded Ship Hulls", *Trans. RINA*.

Paik J.K., Lee D.H. (1990). "Ultimate strength-based safety and reliability assessment of ship's hull girder", *Journal Soc. Naval Arch. Of Japan*, Vol. 168, pp.397-409, in Japanese.

Paik J.K., Lee J.M.(1995). "An empirical formulation for predicting ultimate compressive strength of plates and stiffened plates", *Journal of Ship Research*.

Paik J.K., Mansour A.E. (1995). "A simple formulation for predicting the ultimate strength of ships", *Journal of Marine Science and Technology*.

Paik JK, Thayamballi A and Che JS. (1996). "Ultimate Strength of Ship Hulls Under Combined Vertical Bending, Horizontal Bending and Shearing Forces". *Transactions of SNAME* 1996, Vol. 104, pp.31-59.

Paik, J. K.; Thayamballi, A. K.; Yang, S. H. (1998). "Residual strength assessment of ships after collision and grounding". *Marine Technology*, v 35, n 1, pp. 38-54.

Paik, J.K., Pedersen, T. (1996). "A simplified method for predicting ultimate compressive strength of ship panels". *Int. Shipbuilding Progress*, Vol. 43, No. 434, pp.139-157.

Paik, Jeom K. (1992). "Reserve/residual strength of a double hull girder in intact/damaged condition". *Proceedings of the Second International Offshore and Polar Engineering Conference*, Jun 14-19 1992.
Paik, Jeom K.; Lee, Tak K. (1995). "Damage and residual strength of double-hull tankers in grounding". *International Journal of Offshore and Polar Engineering*, v 5, 4, (Dec 1995), pp. 286-293.

Pu Y., Das P.K. and Faulkner D. (1997): 'Ultimate Compression Strength and Probabilistic Analysis of Stiffened Plates', *Journal of Offshore Mechanics and Arctic Engineering*, Vol. 119, No.4, pp. 270-275.

Qi, Enrong; Cui, Weicheng; Peng, Xingning; Xu, Xiangdong. (1999). "Reliability assessment of ship residual strength after collision and grounding". *Journal of Ship Mechanics*, v 3, n 5, pp. 40-46.

Raff, A. I., (1972). "Program Scores-Ship structural response in waves", Final report on Project SR-174, "Ship Computer Response" to the Ship Structure Committee, SSC-230, Washington D.C.

Rahman M.K., Chowdhury M. (1996). "Estimation of Ultimate Longitudinal Bending Moment of Ships and Box Girders". *Journal of Ship Research*, Vol. 40. No. 3. pp 244-257.

Rajashekhar M.R., Ellingwood B.R.(1993). "A new look at the response Surface approach for Reliability Analysis", *Structural Safety*, Elsevier Science Publishers B.V., 12 (205-220).

Rigo, P., C. Toderan and T. Quesnel (2002). "Sensitivity Analysis on Ultimate Hull Bending Moment and Multi - Criteria Comparative Analysis of exisiting Methods." *In: 1st ASRANet International Colloquium*, 8-10th July 2002, Glasgow, Scotland. P. K. Das. (Ed.) ASRANet. pp.10

Rigo, P., T. Moan, P. A. Frieze and M. Chryssanthopoulos (1995). "Benchmarking of Ultimate Strength Predictions for Longitudinally Stiffened Panels." *In: PRADS '95*: The Sixth International Symposium on Practical Design of Ships and Mobile Units, 17th-22nd Sept 1995, Seoul, Korea. H. Kim and J. W. Lee. (Eds.) SNAK. pp.2.869 - 2.882

Rutherford S.E., Caldwell J.B. (1990). "Ultimate Longitudinal Strength of Ships: A Case Study", *Trans. SNAME.*

Salvesen, N.; Tuck, E.O. & Faltinsen, O. (1970). "Ship motion and sea loads", *SNAME Trans v.78*, pp.1-30.

Santos, T.A.; Winkle, I.E. & Soares, C. Guedes (2002). "Time domain modelling of the transient asymmetric flooding of Ro-Ro ships", *J Ocean Engineering* v.29, pp.667-688.

Smith C.S., DowR.S. (1986): "Ultimate Strength of Ship's Hull under Biaxial Bending", ARE TR86204, *ARE Dunfermline*, Scotland.

Smith, C.S. (1977). "Influence of Local Compressive Failure on Ultimate Longitudinal Strength of a Ship's Hull". In: Zosengakkai N, editor. *Proceedings of the PRADS*: International Symposium on Practical Design in Shipbuilding; 18-20 October 1977; Tokyo, Japan: Society of Naval Architects of Japan, pp. 73-79.
Smith, C.S. and Dow, R., 1981. "Residual Strength of Damaged Steel Ships and Offshore Structures". *Journal of Constructional Steel Research*, Vol. 1, No. 4, September.

Soding, H. (1979). "The prediction of still-water wave-bending moments in containerships", *Schiffstechnik*, Vol. 26, pp.24-41.

Song B.F.(1992). "A numerical method in affine space and amethod with high accuracy for computing structural system reliability", *Computers and Structures*, 42(2).

Special Task Committee VI.2 . (October 2000). "Ultimate Hull Girder Strength", *Proceedings of the 14th International Ship and Offshore Structures Congress*, Nagasaki Japan, Vol. 2, pp.321-391.

Steen, E. (1995), *"Buckling of stiffened plates under combined loads-ABAQUS analysis"* DNV Report No. 95-0445,.

Steen, E., Balling Engelsen, A. (1997). *"ABAQUS analysis- Plate buckling/GL code."*, DNV Report No. 97-05606,.

Tao, Z. & Incecik, A. (1996). "Large amplitude ship motions and bow flare slamming pressures in regular head seas", *Proc ISOPE-Conf* v.1, pp.16-20.

Technical Committee III.1 (October 2000). "Ultimate Strength", *Proceedings of the 14th International Ship and Offshore Structures Congress*, Nagasaki Japan, Vol. 1, pp.253-321.

Technical Committee III.1 (August 2006). "Ultimate Strength", *Proceedings of the 16th International Ship and Offshore Structures Congress*, Southampton, UK, Vol. 1, pp.369-457,.

Ueda Y., Rashed S.M.H., Paik J.K.(1984), "Plate and stiffened plate units of the idealized structural unit method-Under in-plane loading", *Journal Soc. Naval Arch. Of Japan*, Vol. 156, pp.336-375, in Japanese.

Ueda, Y. and Rashed, SMH. (1984). "The idealised structural unit method and its application to deep girder structures". *Computers and Structures*, Vol. 18, No. 2, pp.227-293.

Ursell, F. (1949). "On the heaving motion of a circular cylinder on the surface of a fluid", *J Mechanics and Applied Mathematics* v.2, pp.218-31.

Valsgaard S., Jorgensen L., Boe A.A., Thorkildsen H. (1991). "Ultimate hull girder strength margins and present class requirements", *Proc. SNAME Symp. '91 on Marine Structural Inspection*, Maintenance and Monitoring, Arlington, March, B., pp.1-19,.

Valsgaard, S. and Steen, E.(1991). "Ultimate hull girder strength margins in present class requirements". *Proceedings of the Marine Structural Inspection*, Maintenance and Monitoring Symposium, SSC/SNAME, Arlington Virginia, III.B.1-III.B.19, 1991.

Wang, Ge; Chen, Yongjun; Zhang, Hanqing; Peng, Hua. (2002). "Longitudinal strength of ships with accidental damages". *Marine Structures*, v 15, n 2, 2002, p 119-138.

Wei-Biao Shi.(1992). "In-Service Assessment of Ship Structures: Effects of General Corrosion on Ultimate Strength", *RINA Spring Meetings.*

Yamamoto, Y.; Fujino, M. & Fukasawa, T. (1978). "Motion and longitudinal strength of a ship in head sea and effects of nonlinearities", (1st & 2nd Reports). *J Society of Naval Architects of Japan*, pp.143-144.

Yao T. (1993). *"Analysis of ultimate longitudinal strength of a ship's hull"*. Text Book of Mini-Symposium on Buckling/Plastic Collapse and Fatigue Strength; State of the Art and Future Problems, The West-Japan Soc. Naval Arch., pp.154-177, in Japanese.

Yao T., Fujikubo M., Kondo K., Nagahama S. (1994). "Progressive collapse behaviour of double hull tanker under longitudinal bending", *Proc. 4th Int. Offshore and Polar Engineering Conf.*, Vol. VI pp.570-577, Osaka,.

Yao T., Fujikubo M., Varghese B., Yamamura K., Niho O.(1997). "Buckling/plastic collapse strength of rectangular plate under combined pressure and thrust", *Journal Soc. Naval Arch. Of Japan*, Vol. 182, pp.561-570.

Yao T., Niho O., Fujikubo M., Varghese B., Mizutani K. (1997). "Buckling/ultimate strength of ship bottom plating", *Proc. Int. Conf. on Advances in Marine Structures III*, Paper 28, Dunfermline UK.

Yao T., Nikolov P. I. (1991). "Progressive Collapse Analysis of a Ship's Hull under Longitudinal Bending", *Journal of the Society of Naval Architects of Japan*, Vol. 170, pp.449-461.

Yao T., Nikolov P. I.(Nov 1992). "Progressive Collapse Analysis of a Ship's Hull under Longitudinal Bending (2nd Report)", *Journal of the Society of Naval Architects of Japan*, Vol. 172, pp.437-446.

Yao, T. (1999). "Ultimate longitudinal strength of ship hull girder; historical review and state of the art". *International Journal of Offshore and Polar Engineering*. Vol. 9, No. 1, pp. 1-9.

Yu L., Das P.K., Zheng Y., (2001). "Stepwise Response Surface Method and its Application in Reliability Analysis of Ship Hull Structure", *Proceedings of OMAE 2001, 20th International Conference on Offshore Mechanics and Arctic Engineering*, A.S.M.E., Rio de Janeiro, Brazil.

Zhang, Sheng-Kun; Yu, Qing; Mu, Yang. (1996). "Semi-analytical method of assessing the residual longitudinal strength of damaged ship hull". *Proceedings of the International Offshore and Polar Engineering Conference*, v 4, (1996), p 510-516.

Zheng Y., Das P.K.(2000). "Improved Response Surface Method and its application to Stiffened Plate Reliability Analysis", *Engineering Structures*, Elsevier Science Ltd., 22 (544-551).

APPENDIX A:
COMPUTATION PROCEDURE OF 2D LINEAR METHOD

A.1 Numerical Computation Procedure

There are several programmes for linear strip theory which use slightly different assumptions to compute different parts of response. One of the popular programs is the Ship Motion Programme (SMP), originally developed by the U.S. Navy and now widely distributed. HSSE has developed a version of SMP that can be linked with the salvage response software, HECSALV. This program can produce the vessel's damage equilibrium position and generate SMP input files for the vessel's hull and weight distribution in the damage condition. A wide range of damage cases can be investigated quickly. However the SMP can not consider asymmetric vessel cross section. This means that the vessel has to be always modelled in the upright condition without heel, although the longitudinal trim and changed weight distribution resulting from the damage can be included (Collette, 2005a). UNEW has developed a series of internal sea-keeping and loading prediction programmes, UNEW Hydro Programme set, using linear strip theory. UNEW Hydro Programme does not assume symmetric sections, therefore can consider the effects of heel. UNEW Hydro Programme also includes GUI programme, Hydro Front End (HEF), for quickly generating the hull form with new weight distribution, draught, trim and heel values of a damaged ship (Collette, 2005b). The computation procedure of this study using UNEW Hydro Programme is provided in Figure A.1. Here computation procedure on 2D linear suite are presented.

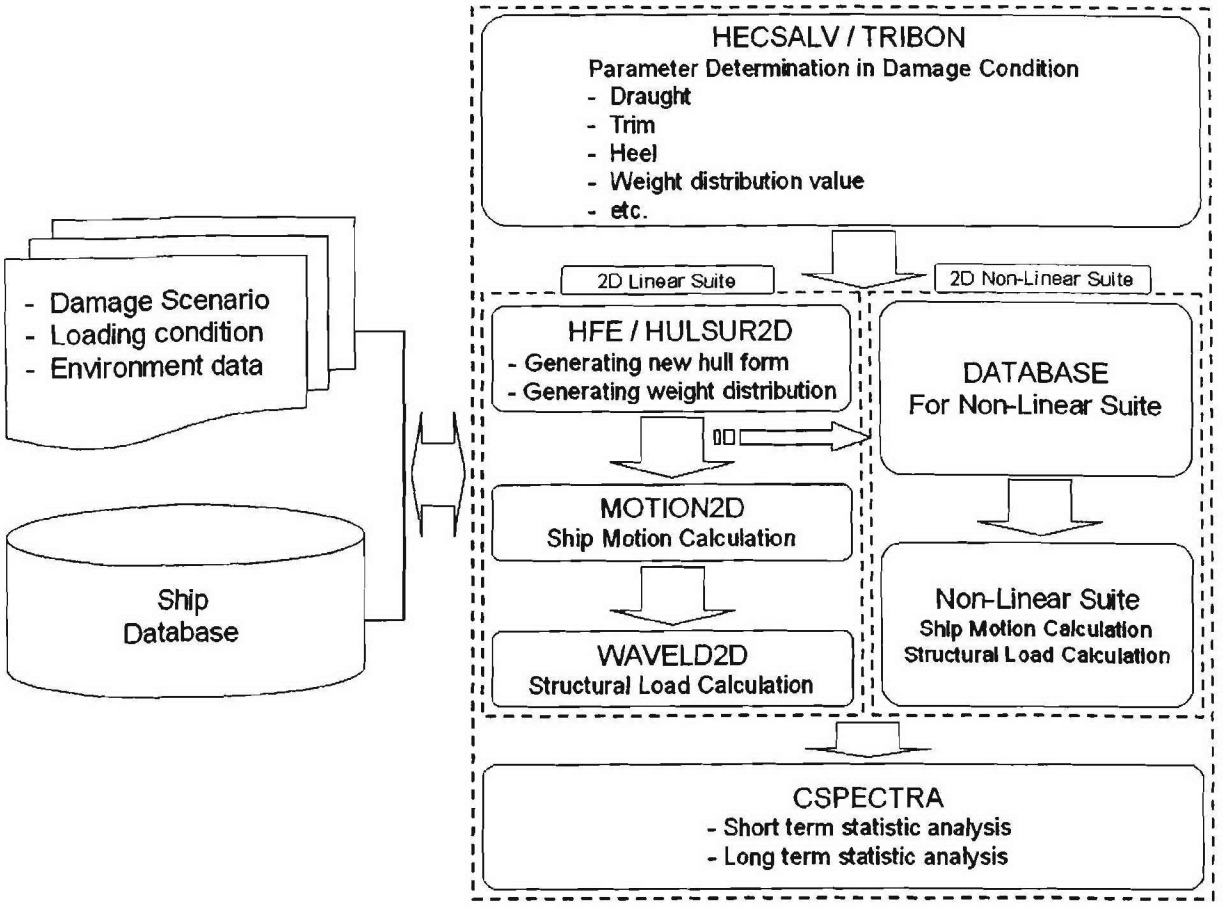

Figure A.1: Computation procedure of UNEW Hydro Programme

A.2 UNEW Hydro Programme

UNEW Hydro Front End Programme

Hydro Front End (HFE) is a LabVIEW 7.1 program designed to serve as a graphical front end to the series of linear 2-D strip theory programs developed by Dr. Chan at Newcastle. The whole package of the strip theory programs with HFE will be referred to as the "UNEW Hydro Programme" in the remainder of this document. The program automates the production of the hull geometry (*.HCS) and to a lesser extent the weights (*.FRA) FORTRAN input files for the strip theory programs.

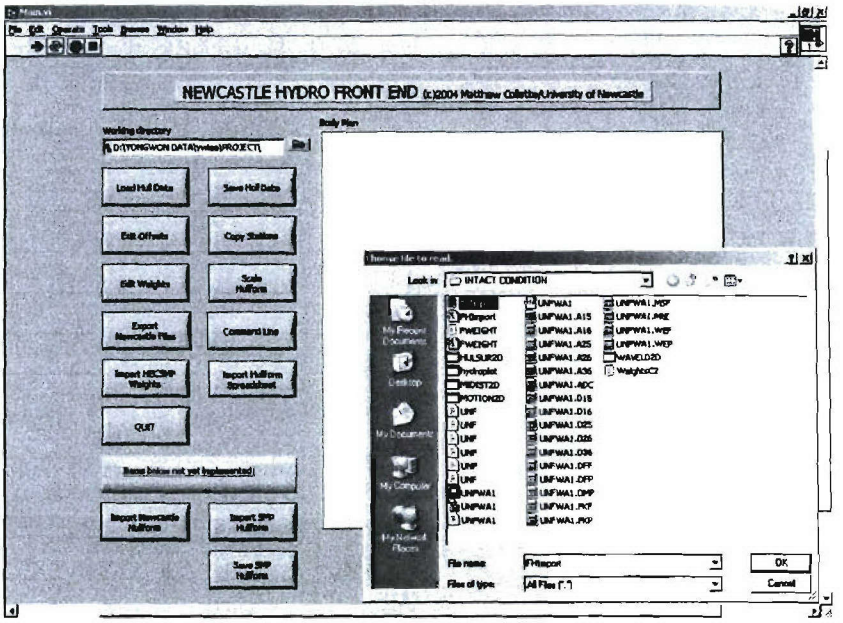

Figure A.2: Main desk of UNEW Hydro Front End Programme

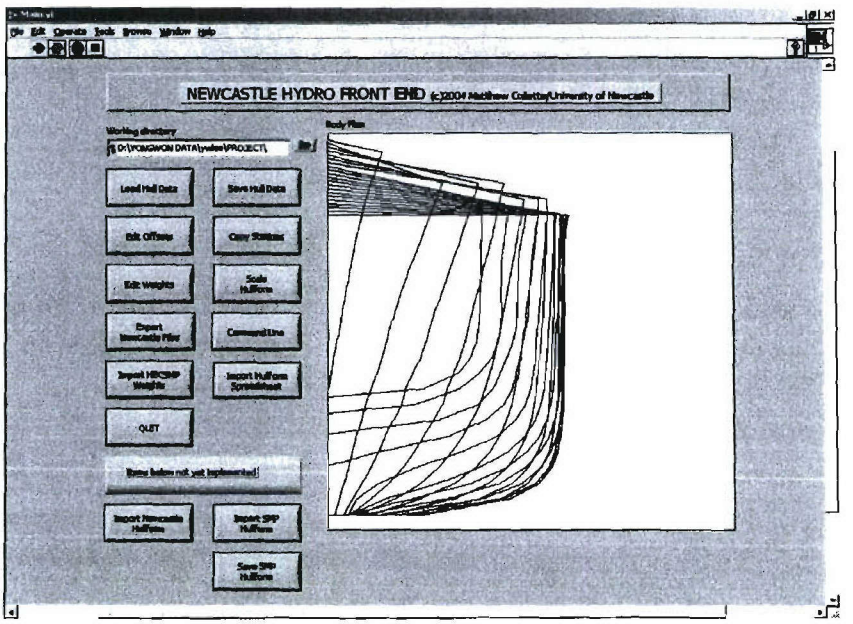

Figure A.3: Main desk after a hull form data import

The hull geometry *.HCS file requires the hull form up to the still waterline, which means a new versions of the *.HCS file is required for every draft, trim, and heel combination to be investigated. Normally, this is a time consuming operation, however HFE will allow the hull form to be entered once to the main deck, and then an unlimited number of *.HCS files can be generated for desired draft, trim, and heel conditions in damage conditions. HFE also allows for visual editing of the weight distribution for writing to a *.FRA file, and automated conversion of weight distributions from the HECSALV/HECSMP suite of damage stability and motion prediction software. This is useful for generating a large number of damage hydrodynamic analyses. The limited ability to scale hull forms (but not weight distributions) is also provided (Collette, 2005b). Figure A.2 shows the main window of UNEW Hydro Front End Programme, here the vessel geometry is imported into UNEW Hydro Programme from a tab-delimitated text file which can be easily generated from Excel or other spreadsheet files. The main desk after a hull form data import is also shown in Figure A.3.

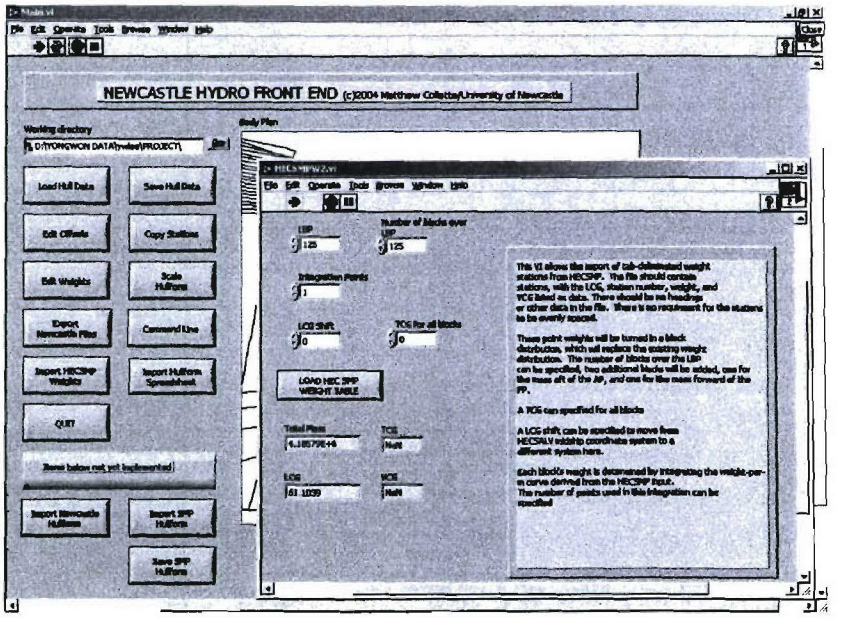

Figure A.4: Weight distribution import window

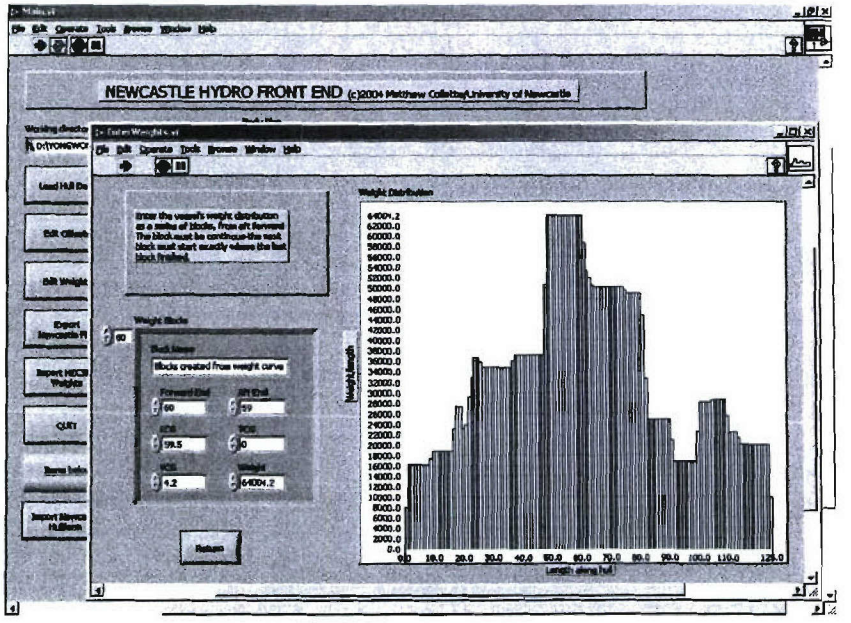

Figure A.5: Weight distribution window after a weight data import

Entering the weight distribution

The vessel's weight distribution is represented by a series of weight blocks over the vessel's length. At the moment only uniformly distribution weight blocks are allowed. Each block is defined by a forward end, an aft end, a LCG (which MUST be the average of the forward and aft ends at the moment), a VCG, a TCG, and total weight. The weight block can be entered manually by clicking on the "Edit Weights" button on the main screen. A graphical depiction of the weights is also shown. Editing the weights in this way is very similar to editing the offsets manually. For cases where an entire weight distribution needs to be defined, or a distribution is available as non-evenly spaced point masses, a spreadsheet import tool is available. This was designed to work directly with the mass distribution from the Herbert Software HECSMP sea-keeping program, but a similar mass distribution can be created easily in Excel or other spreadsheet files.

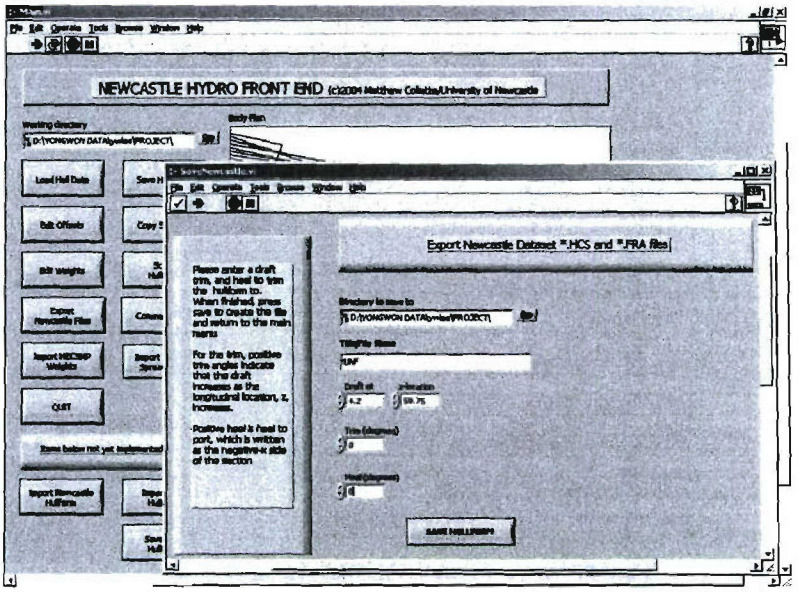

Figure A.6: Generating the information to motion and load calculations

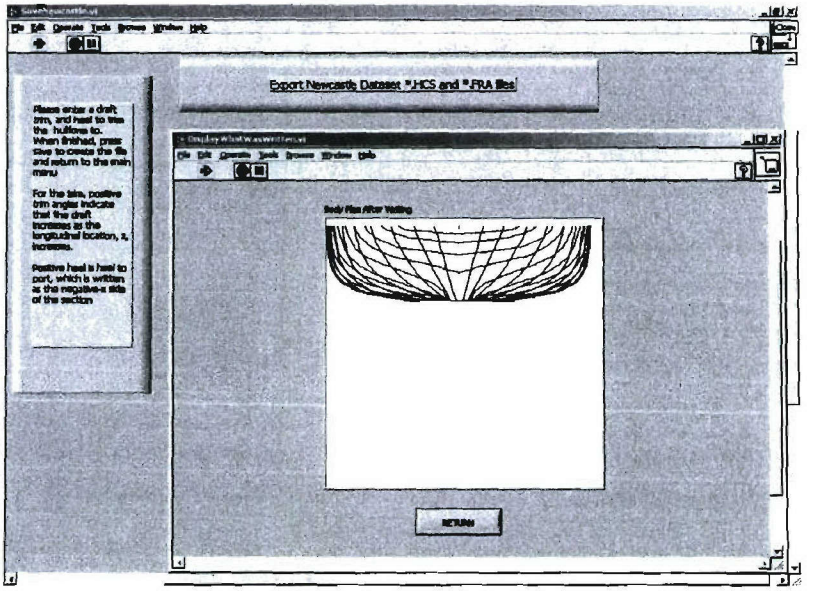

Figure A.7: Hull form display in intact condition

The file format is again a tab-delimitated text file, as the hull form input described above. To import this file into HFE, click the "Import HECSMP Weights" button on the main screen. This will bring up a screen where several defaults can be set before the weights are imported. Figure A.4 and Figure A.5 show a weight import window and weight distribution window after a weight data import respectively (Collette, 2005b).

Generating the information to motion and load calculations

With the hull form and weight distribution set, the final step is to export the required file to UNEW Hydro Programme. This can be achieved by clicking on the "Export Newcastle Files" button.

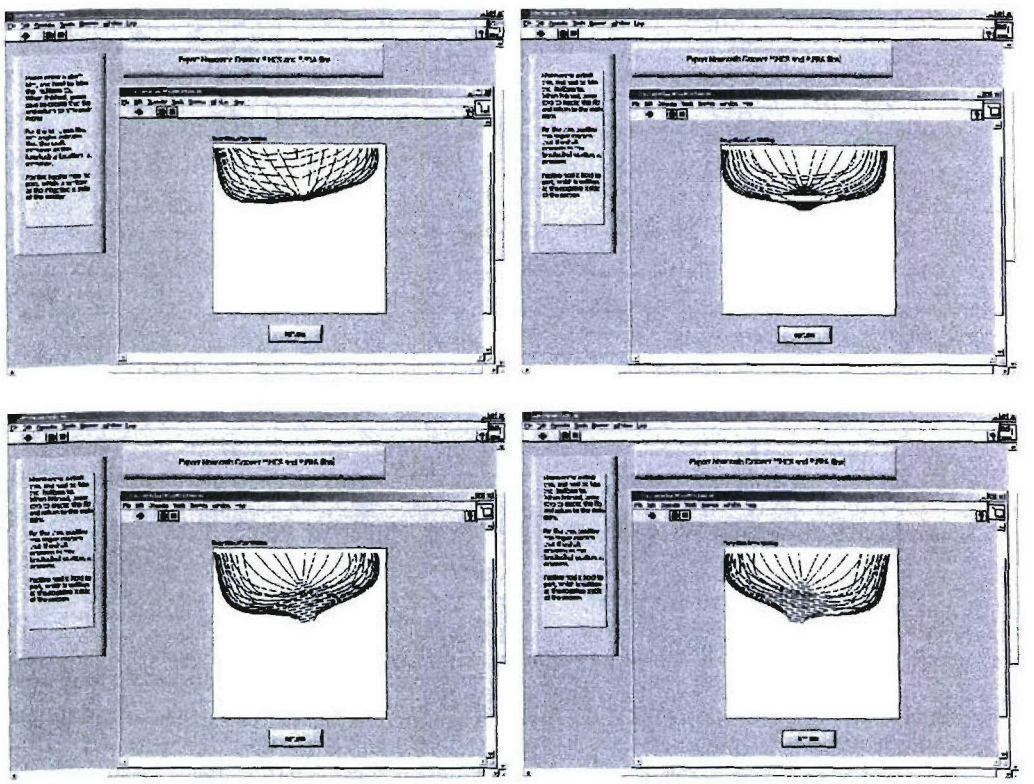

Figure A.8: Hull form display in various damaged conditions

On the resulting screen, the directory to save to and the file name can be specified, along with the draft, trim, and heel of the hull form in the required damaged condition. The entered hull form will be automatically mirrored and trimmed to the requested water plane, and written as an asymmetric *.HCS file. The weight distribution will also be written as an *.FRA file. The written hull form will then be plotted on a pop-up window so you can check that the geometry is at least mostly sensible before running the Motion2D suite. It is recommend that after running Hulsur2D and Midist2D in the Motion2D suite, the results are checked with Hydroplot, to ensure that the files are written correctly (see Figure A.9). A command prompt can be accessed from the main screen of HFE. Figures A.6 and A.7 show the geometry generator window to motion and load calculations and hull form in intact condition. The hull form display in various damaged conditions is also provided in Figure A.8.

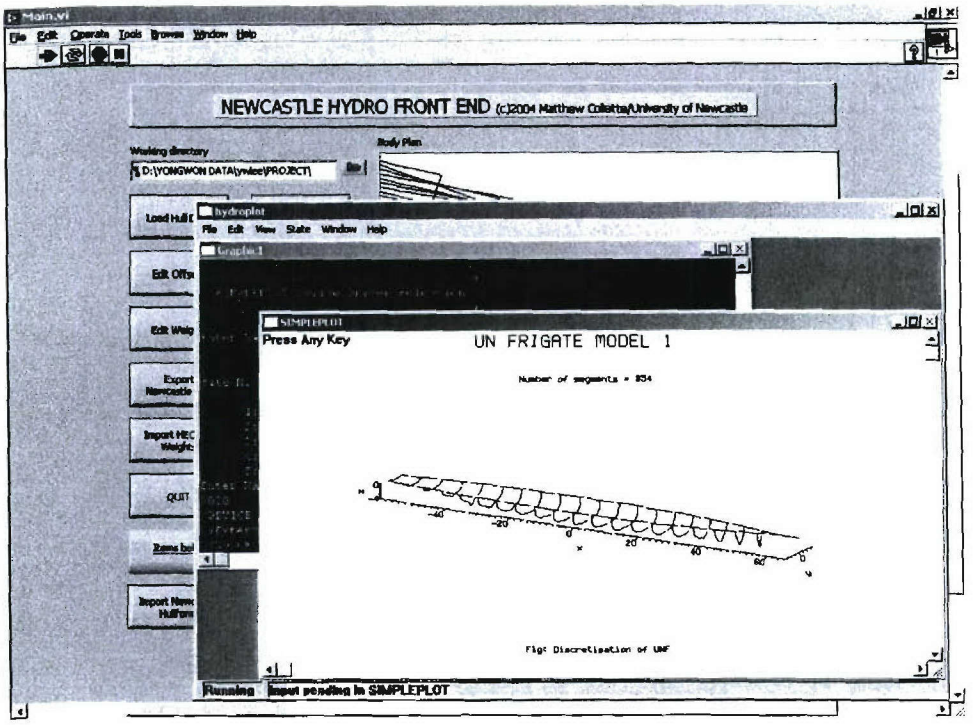

Figure A.9: Surface discretisation of a sample vessel

Static load programme

Results on global static analyses can be calculated and displayed by Hydroplot program, which is a part of UNEW Hydro Programme set. Figure A.10 displays the mass distribution, hull buoyancy and still water load of a sample vessel. In addition Figure A.11 shows the shear force and bending moment diagram of a sample vessel (also see Figure A.12).

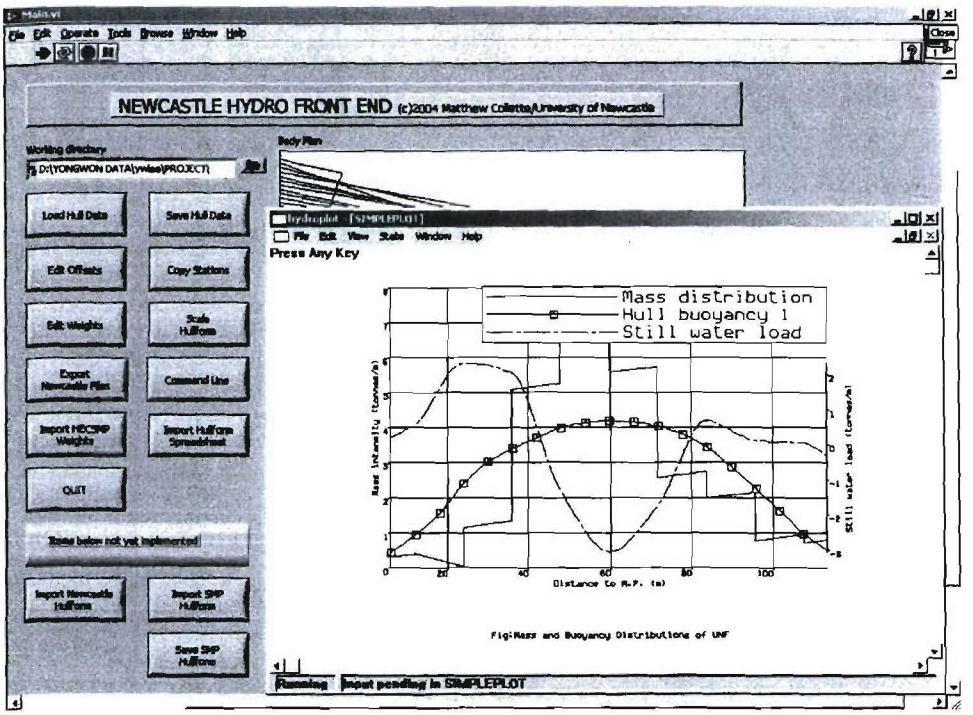

Figure A.10: Mass distribution, hull buoyancy and still water load

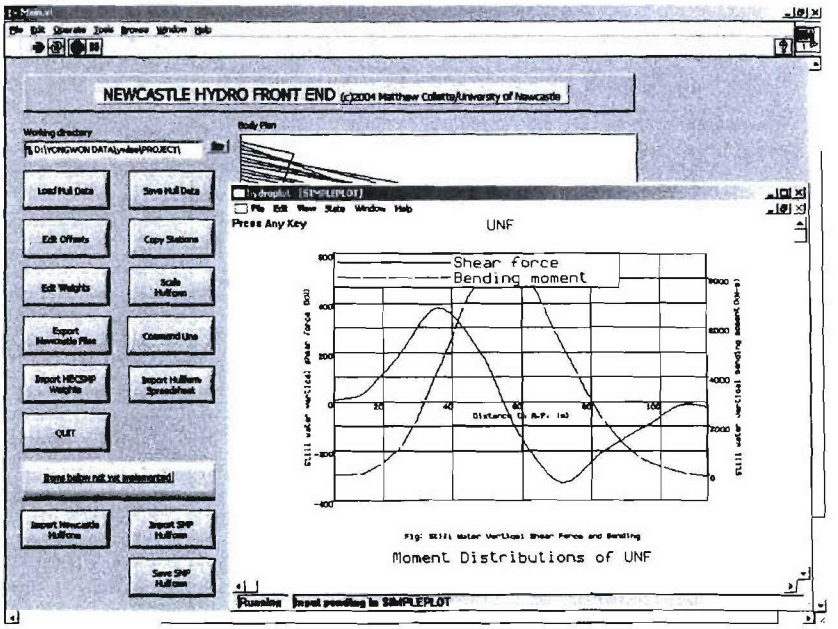

Figure A.11: Shear force and bending moment

Motion and load simulation programme

UNEW Hydro Programme calculates ship motions and dynamic wave induced loads in intact and various damaged conditions. Following representative results are obtained from the above computation.

- Ship Motion calculation.
- Static loading.
- Dynamic longitudinal force.
- Dynamic vertical and horizontal shear force.
- Dynamic vertical and horizontal bending moment.
- Dynamic torsion moment.

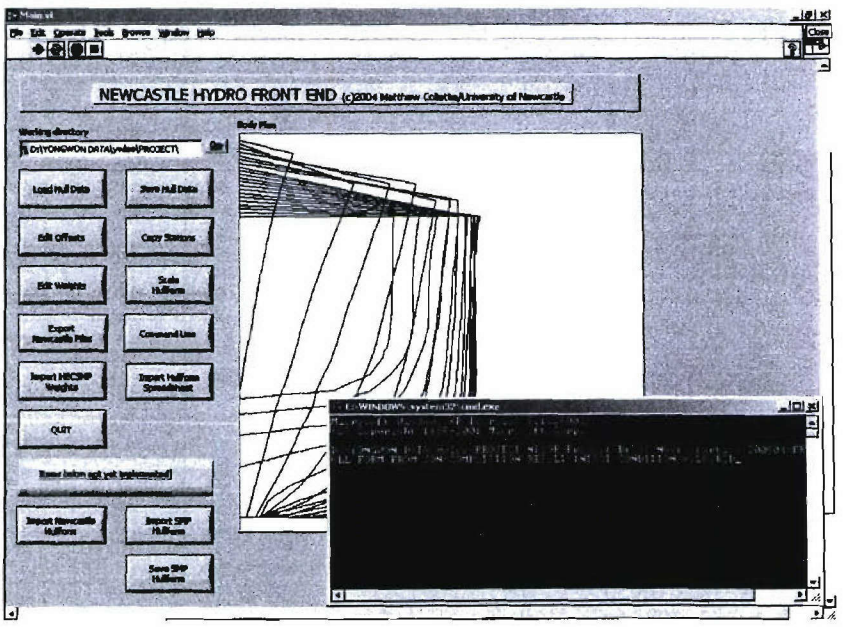

Figure A.12: Motion and load calculation command window

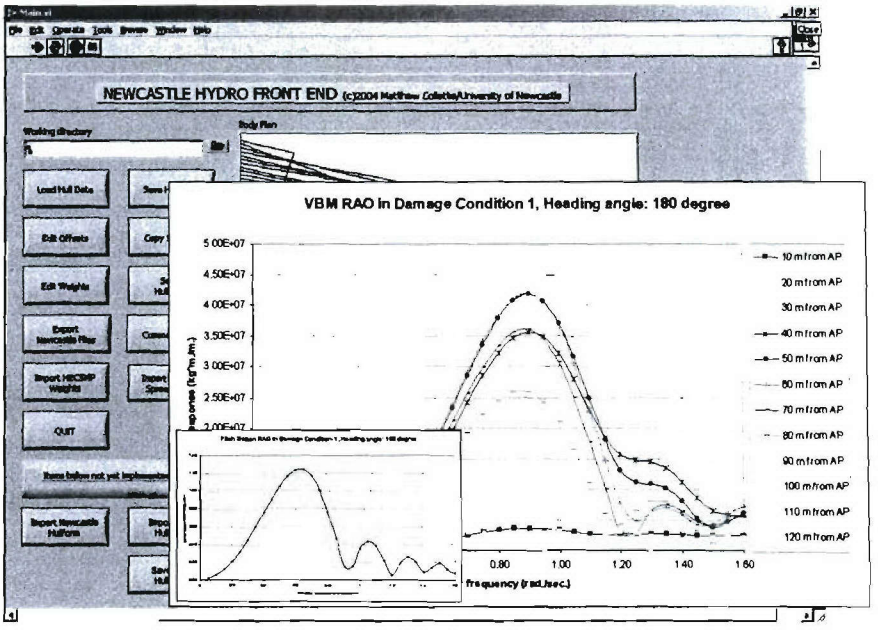

Figure A.13: An example of wave induced motion and load calculations

The motion and load calculation command window and one example of wave induced motions and load calculations are respectively shown in Figures A.12 and A.13.

APPENDIX B:

A SAMPLE VESSEL – HULL 5415

(Notional US Navy Destroyer)

By Paul E. Hess III, NSWCCD

There is a need for a simple ship design that reflects traditional US Navy combatant design for use in collaborative research projects with non-US institutions. To meet this need a notional destroyer has been designed based upon the 5415 hull form used in previous international collaborations in the public forum. The development of Hull 5415 preceded the design of the DDG-51. The hull lines of form, seaway design loads, compartmentation and structural scantlings at select stations have been developed and included in this report.

The basic dimensions of Hull Form 5415 are as follows:

Overall Length: 496 ft
Length Between Perpendiculars: 466 ft
Maximum Beam: 69.4 ft
Beam at Waterline: 65.7 ft
Depth of Hull: 41.8 ft
Design Draft: 20.7 ft

The lines of form are shown in Figure B.1, with the detailed coordinates in Table B.4 at the end of this paper. The seaway loads are shown in Tables B.1, B.2 and B.3 and Figures B.2, B.3 and B.4. Structural scantlings are shown in Figures, B.5 through B.10 for Stations 5, 10 and 15.

Mr. Ed Devine, Mr. John Noland and Ms. Samar Malek assisted in the development of this design.

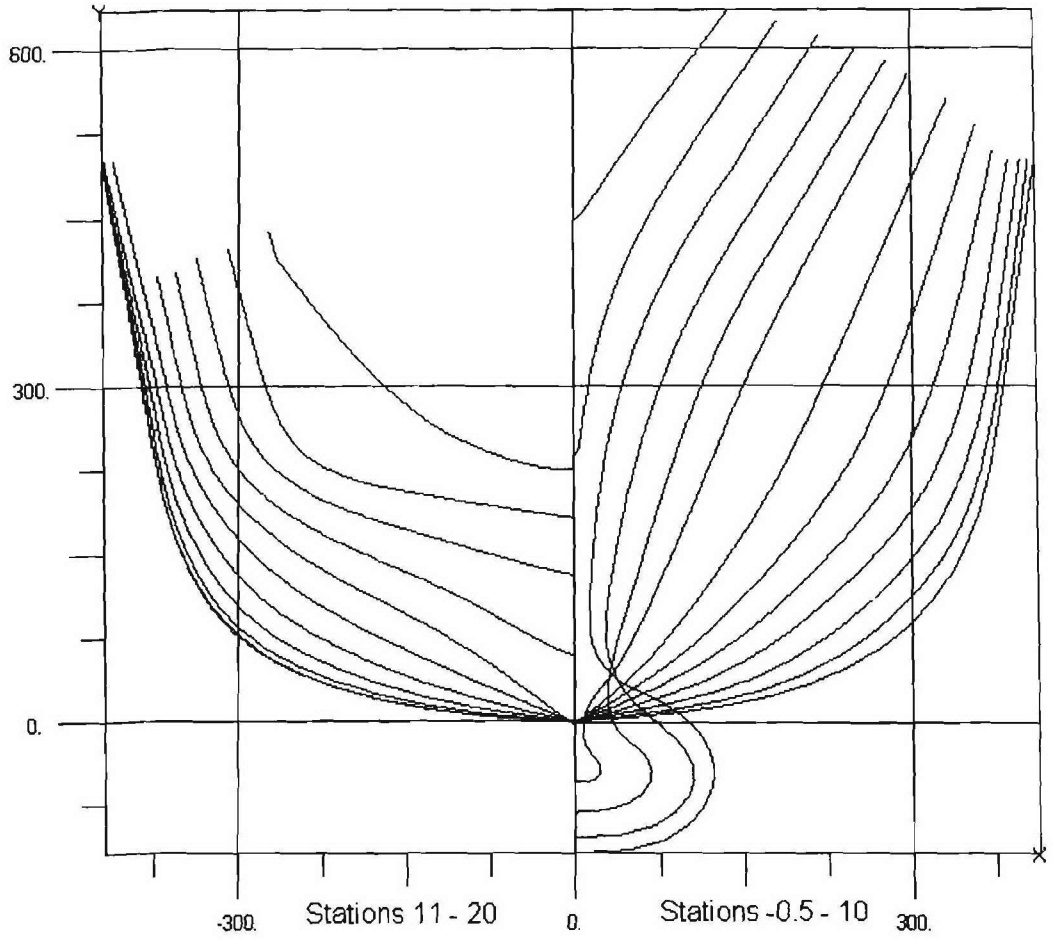

Figure B.1: Hull 5415

Table B.1: Weight and Buoyancy

Location from FP	Weight (Ltons)	Stillwater (Ltons)	Hogging (Ltons)	Sagging (Ltons)
-19	-50	0	0	7.36
11.65	-224	135.06	79.98	271.19
34.95	-256	169.86	61.7	400.02
58.25	-274	207.74	28.52	480.99
81.55	-365	304.62	83.4	545.32
104.85	-392	388.7	183.65	541.55
128.15	-442	469.57	345.59	499.97
151.45	-519	574.19	579.38	481.45
174.75	-575	622.69	781.18	418.02
198.05	-607	687	973.04	398.23
221.35	-618	716.56	1081.31	374.17
244.65	-607	710.62	1086.85	355.95
267.95	-603	702.39	1025.23	369.21
291.25	-579	674.59	887.41	398.12
314.55	-551	627.81	707.65	436.96
337.85	-520	562.56	503.55	481.85
361.15	-502	483.38	312.14	524.77
384.45	-390	381.27	141.23	547.2
407.75	-267	261.38	28.19	527.34
431.05	-265	151.64	0	482.34
454.35	-249	58.37	0	347.96
471.5	-35	0	0	0

Table B.2: Shear

Station	ft from FP	Stillwater (LT-ft)	Hogging (LT-ft)	Sagging (LT-ft)
-1.5	-38	0	0	0
-0.5	-11.6	34.73	34.7	29.6
0	0.0	50	50	42.64
0.5	11.6	94.9	122.01	19
1	23.3	138.94	194.02	-4.55
1.5	34.9	181.825	291.08	-76.5
2	46.6	225.08	388.31	-148.57
3	69.9	291.34	633.8	-355.57
4	93.2	351.72	915.4	-535.89
5	116.5	355.02	1123.76	-685.44
6	139.8	327.45	1220.17	-743.41
7	163.1	272.26	1159.78	-705.86
8	186.3	224.57	953.61	-548.89
9	209.6	144.58	587.57	-340.12
10	232.9	46.01	124.26	-96.29
11	256.2	-57.61	-355.59	154.76
12	279.5	-156.99	-777.82	388.55
13	302.8	-252.59	-1086.23	569.43
14	326.1	-329.39	-1242.88	683.47
15	349.4	-371.96	-1226.44	721.61
16	372.7	-353.34	-1036.57	698.84
17	396.0	-344.61	-787.81	541.64
18	419.3	-338.99	-549	281.3
19	442.6	-225.63	-284	63.96
20	465.9	-35	-35	-35
21	477.0	0	0	0

Table B.3: Vertical Bending Moments

Station	ft from FP	Stillwater (LT-ft)	Hogging (LT-ft)	Sagging (LT-ft)
-0.5	-11.6	443.52	442.68	432.6
0	0.0	638.4	638.4	623.9
0.5	11.6	2053.65	2230.7	1254.4
1	23.3	3481.1	3823	1890.3
1.5	34.9	5590.9	7133.6	1077.6
2	46.6	7718.9	10449.9	257.8
3	69.9	13927.1	22429.7	-5413.1
4	93.2	21611.5	40641.1	-15732.5
5	116.5	30030.3	64674.9	-29990.2
6	139.8	38166.6	92381.4	-46695.4
7	163.1	45144.7	120386.5	-63821.5
8	186.3	51094.1	145452.6	-78471.3
9	209.6	55497.6	163721.9	-88858.7
10	232.9	57693.2	172075.2	-94015.9
11	256.2	57601.8	169383.3	-93284.3
12	279.5	55108.4	156019	-86871.4
13	302.8	50303	134024.7	-75604.5
14	326.1	43451.8	106547.5	-60887
15	349.4	35173.9	77421.2	-44395.8
16	372.7	26593.3	50742.1	-27733.3
17	396.0	18259.7	29218.4	-13258.3
18	419.3	10077.4	13520.4	-3726.8
19	442.6	3330.9	3834	181.3
20	465.9	135.2	134.5	134.8
aft	477.0	0.8	0.1	0.4

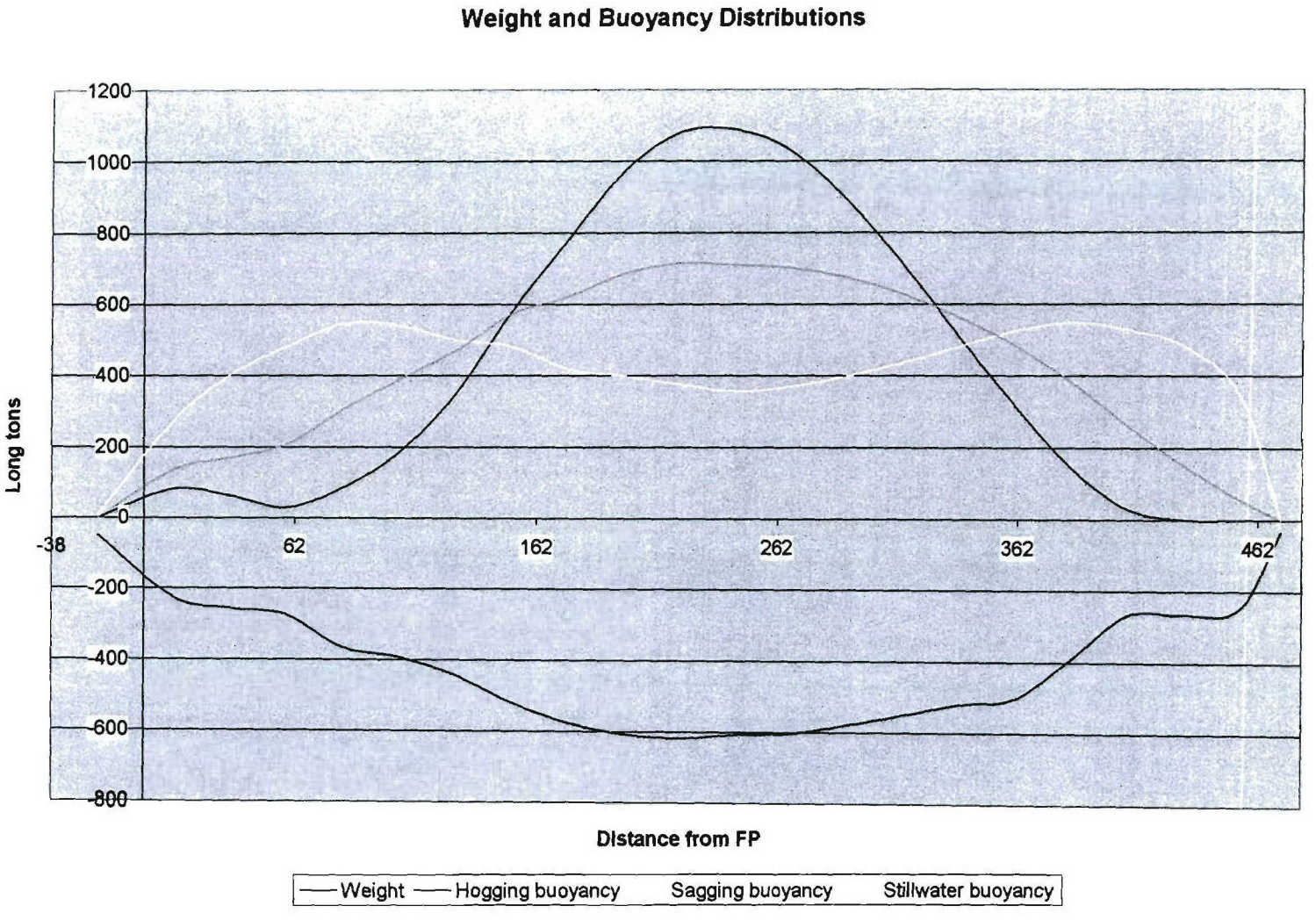

Figure B.2: Weight and Buoancy Distributions

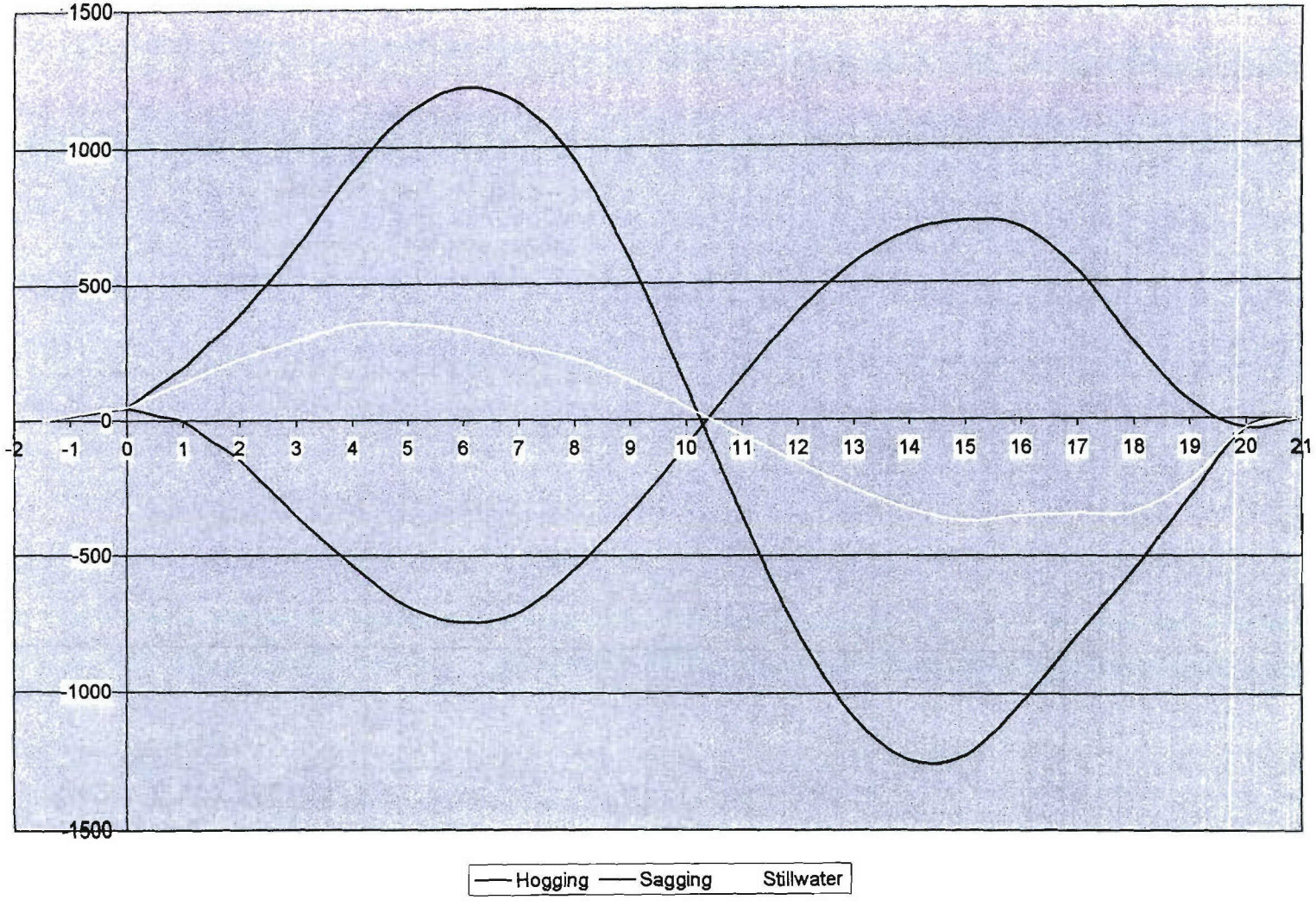

Figure B.3: Shear Distributions

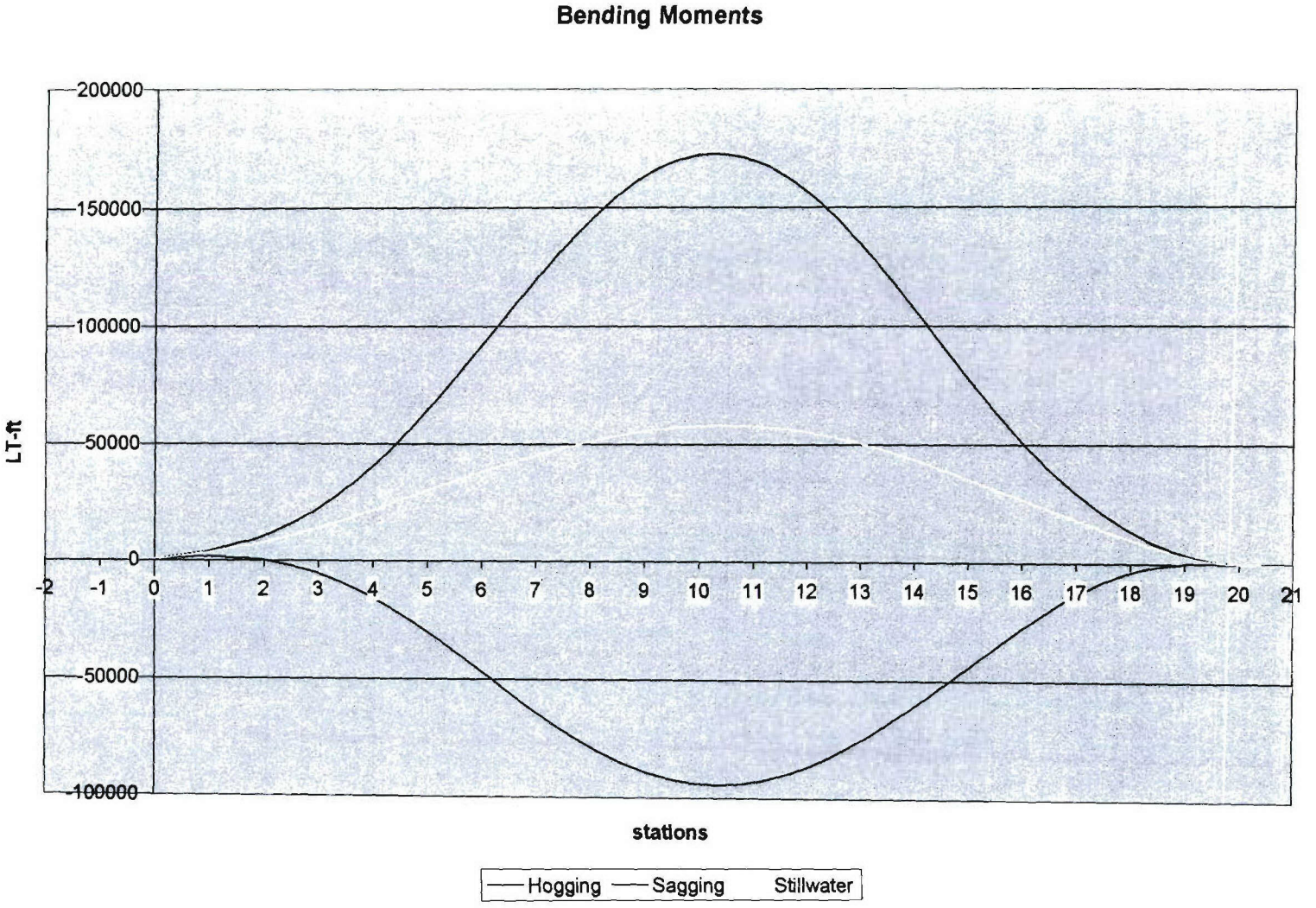

Figure B.4: Bending Moment Distributions

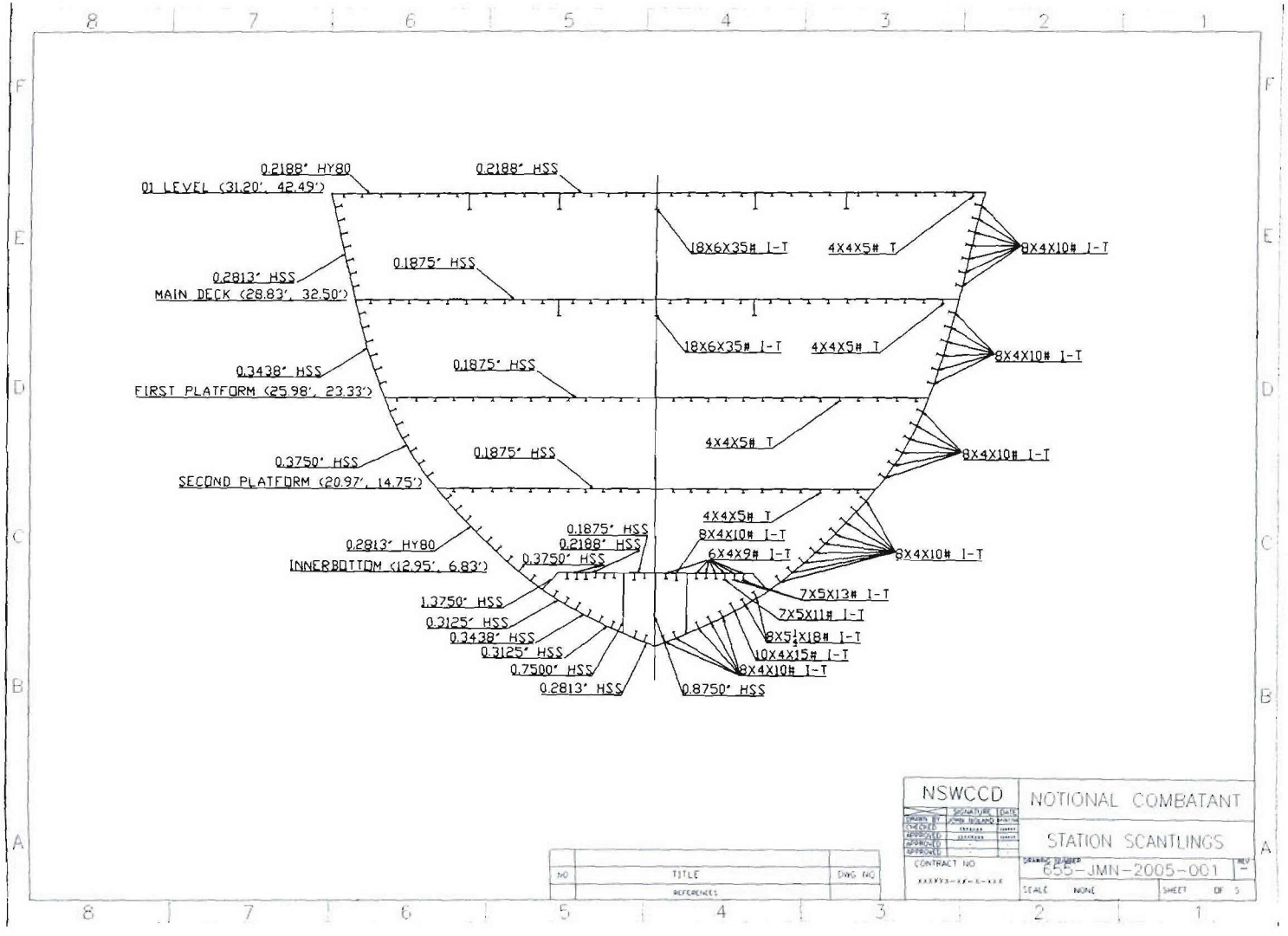

Figure B.5: Station 5 Longitudinal Structural Scantlings

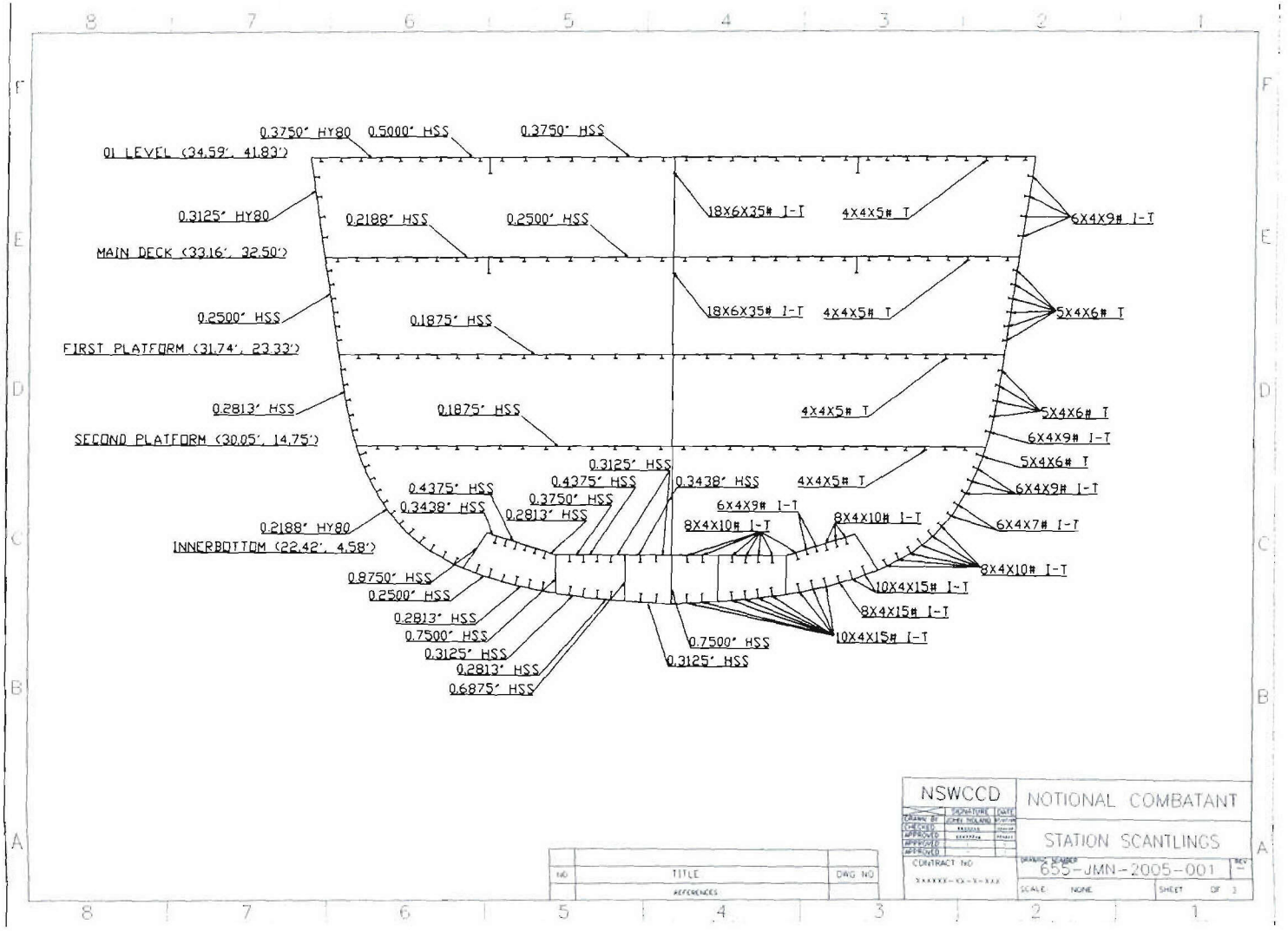

Figure B.6: Station 10 Longitudinal Structural Scantlings

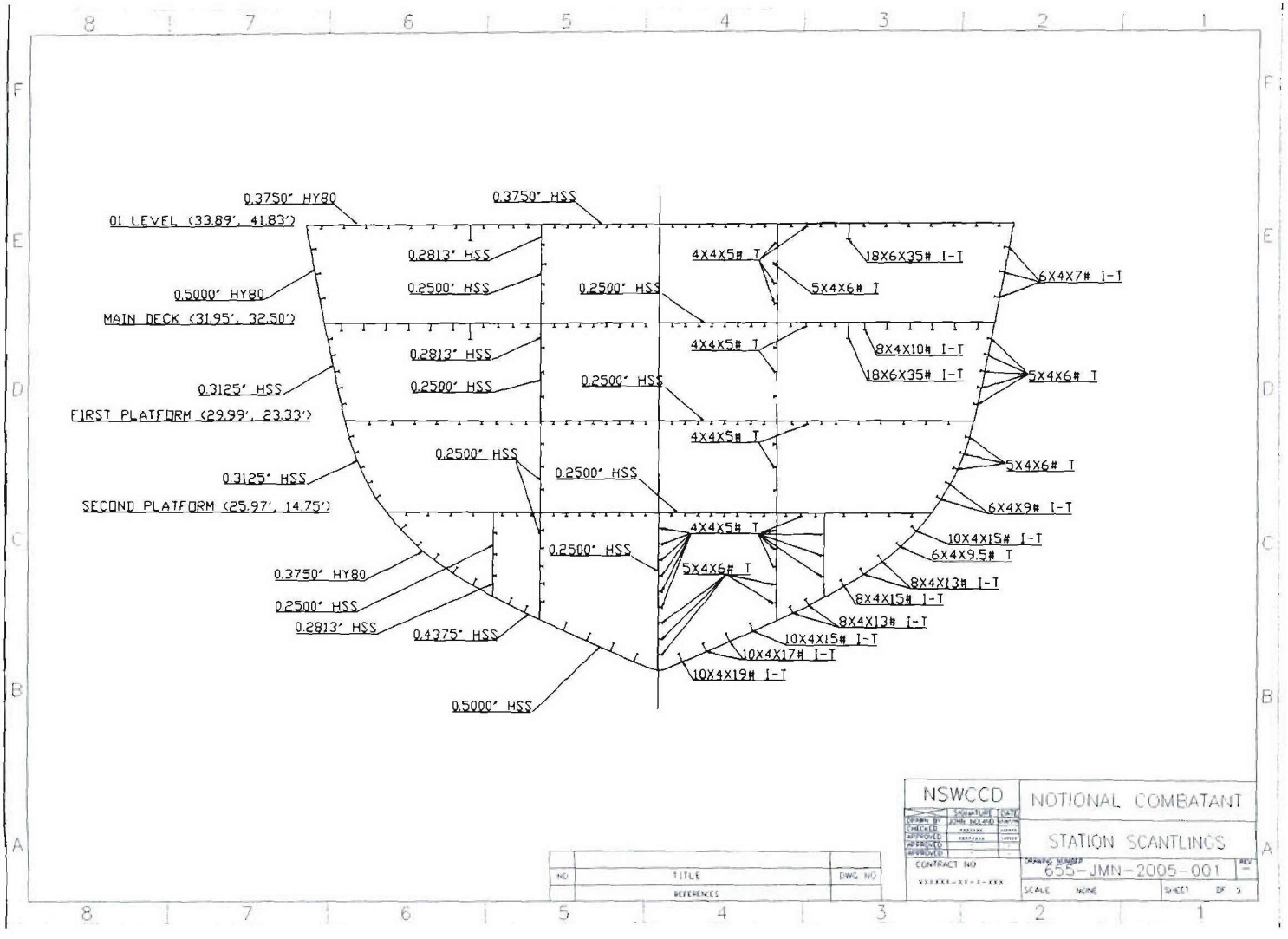

Figure B.7: Station 15 Longitudinal Structural Scantlings

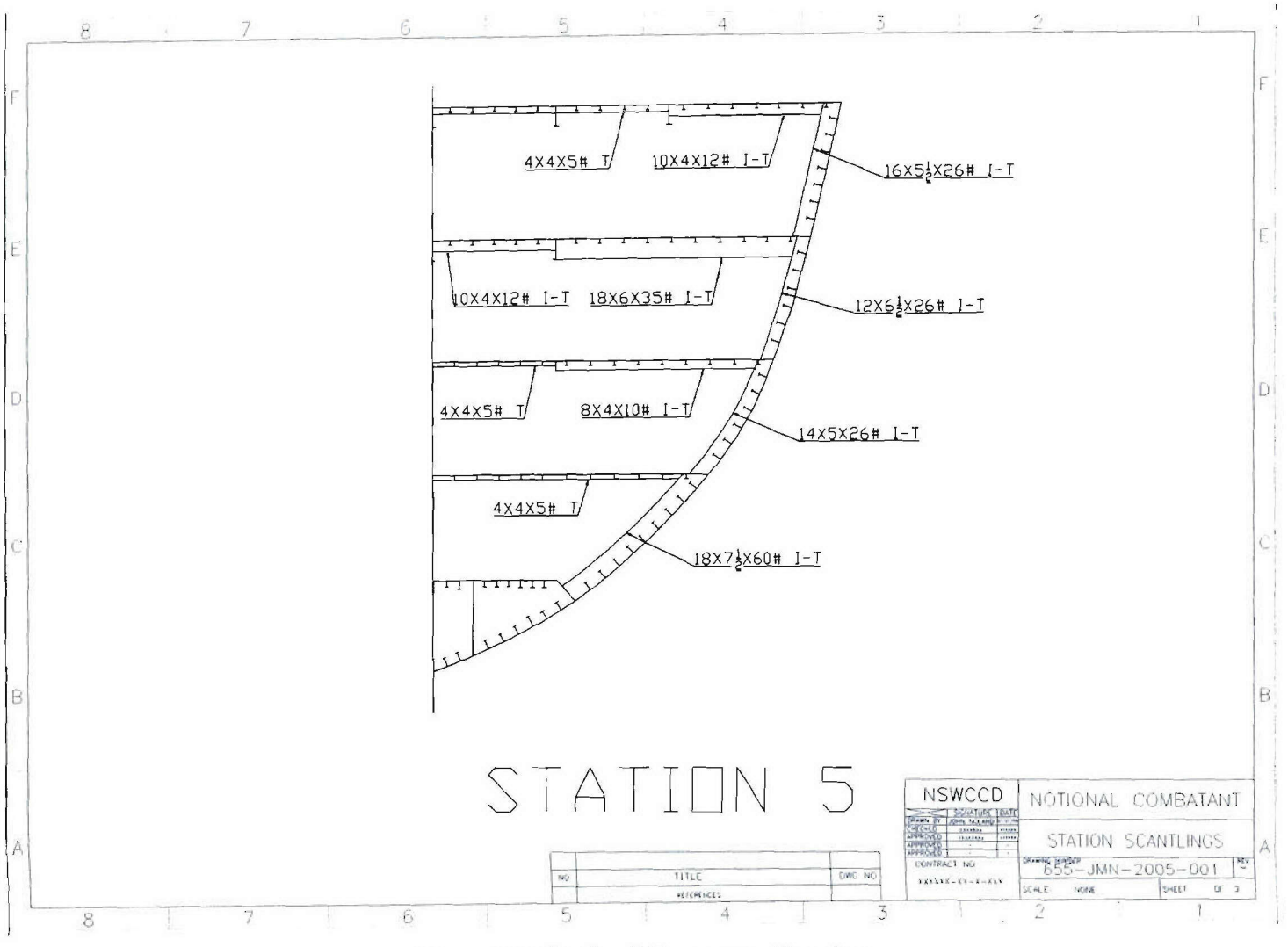

Figure B.8: Station 5 Transverse Framing

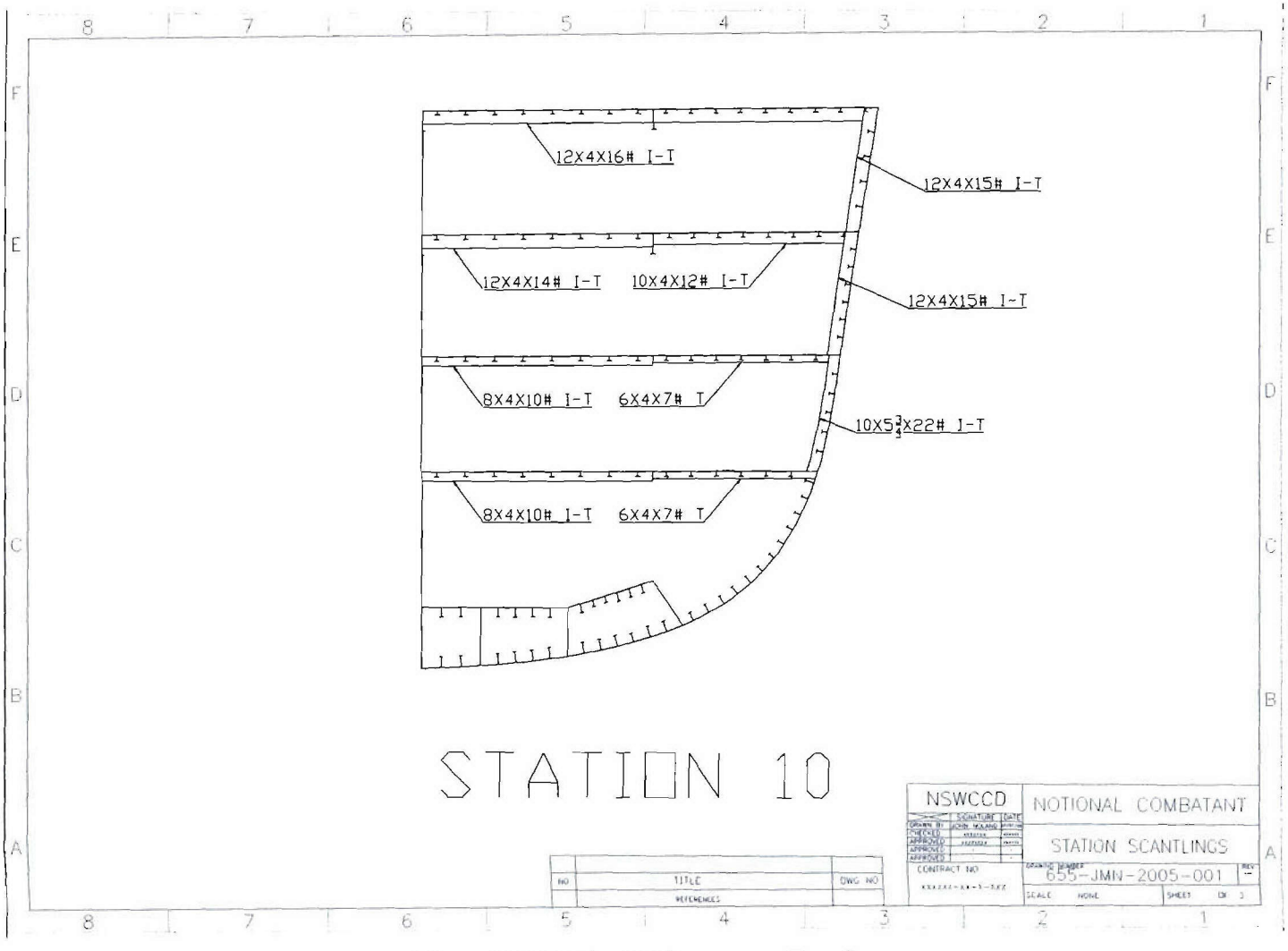

Figure B.9: Station 10 Transverse Framing

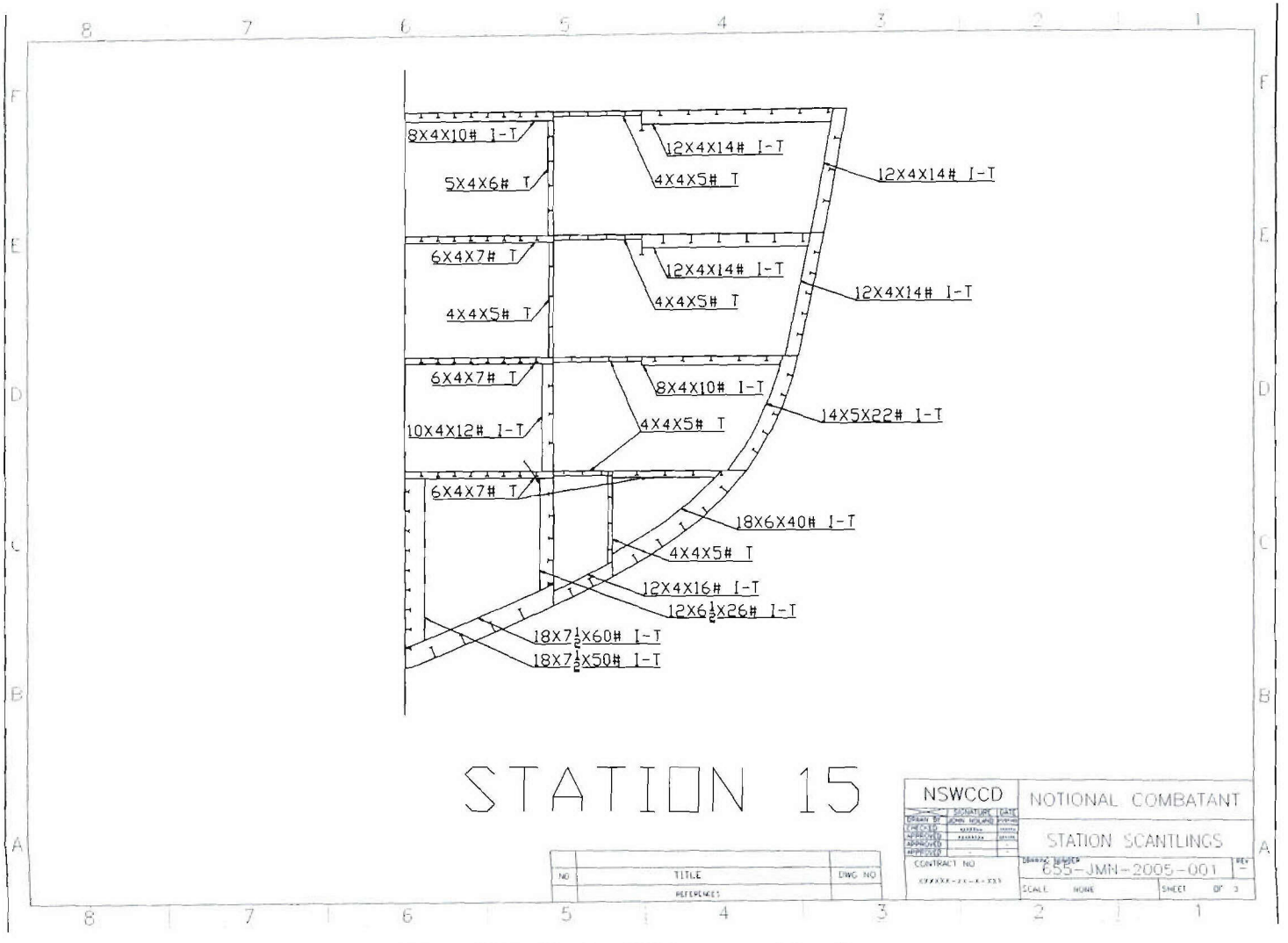

Figure B.10: Station 15 Transverse Framing

Table B.4: Offsets for Hull 5415

Station	Dist from FP	Half-breadth	Ht abv BL
-0.5	-11.6465	0	37.24
-0.5	-11.6465	0.48	37.63
-0.5	-11.6465	1.25	38.7
-0.5	-11.6465	2.37	40.36
-0.5	-11.6465	2.61	40.71
-0.5	-11.6465	3.86	42.53
-0.5	-11.6465	5.93	45.43
-0.5	-11.6465	6.22	45.82
-0.5	-11.6465	8.88	49.35
-0.5	-11.6465	11.25	52.4
0	0	0	19.72
0	0	0.28	20.26
0	0	0.52	21.68
0	0	0.61	22.26
0	0	0.83	23.73
0	0	1.09	25.24
0	0	1.29	26.29
0	0	1.8	28.45
0	0	2.08	29.45
0	0	2.9	31.88
0	0	3.49	33.36
0	0	4.53	35.61
0	0	5.92	38.21
0	0	6.86	39.8
0	0	9.5	43.83
0	0	10.27	44.93
0	0	13.75	49.86
0	0	15.11	51.79
0.5	11.6465	0	-9.88
0.5	11.6465	4	-9.6
0.5	11.6465	6.61	-8.85
0.5	11.6465	8.29	-7.76
0.5	11.6465	9.43	-6.45
0.5	11.6465	10.07	-5.03
0.5	11.6465	10.24	-3.62
0.5	11.6465	9.94	-2.31
0.5	11.6465	9.3	-1.14
0.5	11.6465	8.46	**-0.15**
0.5	**11.6465**	**7**.52	0.65
0.5	11.6465	6.55	1.27
0.5	11.6465	5.6	1.76
0.5	11.6465	4.69	2.18
0.5	11.6465	3.83	2.62
0.5	11.6465	3.03	3.15
0.5	11.6465	2.29	3.87
0.5	11.6465	1.68	4.76
0.5	11.6465	1.26	5.82
0.5	11.6465	1.08	7.04
0.5	11.6465	1.07	8.47
0.5	11.6465	1.18	10.17
0.5	11.6465	1.32	12.17
0.5	11.6465	1.53	14.43

0.5	11.6465	1.82	16.88
0.5	**11.6465**	**2.**23	19.47
0.5	11.6465	2.61	21.4
0.5	**11.6465**	**2.7**9	22.19
0.5	11.6465	3.54	25.05
0.5	**11.6465**	**4.5**4	28.05
0.5	**11.6465**	**5.**48	30.35
0.5	11.6465	5.9	31.27
0.5	**11.6465**	**7.**71	34.77
0.5	**11.6465**	**9.4**2	37.6
0.5	11.6465	10.15	**38.74**
0.5	**11.6465**	**13.**54	43.8
0.5	11.6465	13.9	44.32
0.5	11.6465	18.39	51.01
1	23.293	0	-8.73
1	23.293	3.49	-8.47
1	23.293	5.84	-7.78
1	23.293	7.36	-6.8
1	23.293	8.3	-5.65
1	23.293	8.72	-4.43
1	23.293	8.64	-3.25
1	23.293	8.1	-2.18
1	23.293	7.27	-1.24
1	23.293	6.36	-0.42
1	23.293	5.54	0.28
1	23.293	4.84	0.89
1	23.293	4.28	1.43
1	23.293	3.83	1.93
1	23.293	3.47	2.46
1	23.293	3.13	3.08
1	23.293	2.78	3.85
1	23.293	2.47	4.76
1	23.293	2.27	5.83
1	23.293	2.25	7.06
1	23.293	2.38	8.49
1	**23.293**	2.63	10.19
1	23.293	2.97	12.19
1	**23.293**	3.39	14.44
1	**23.293**	3.92	16.87
1	23.293	3.97	17.06
1	**23.293**	4.57	19.42
1	23.293	5.35	22.07
1	**23.293**	6.29	24.81
1	**23.2**93	7.41	27.61
1	23.293	8	28.91
1	**23.293**	8.82	30.57
1	**23.293**	10.6	33.76
1	23.293	12.46	36.75
1	**23.293**	**12.**89	37.42
1	23.293	16.17	42.41
1	23.293	17.81	44.94
1	23.293	21.1	50.06
1.5	34.9395	0	-6.81
1.5	34.9395	2.3	-6.62
1.5	34.9395	3.91	-6.11

1.5	34.9395	4.93	-5.39
1.5	34.9395	5.49	-4.56
1.5	34.9395	5.62	-3.71
1.5	34.9395	5.36	-2.9
1.5	34.9395	4.77	-2.2
1.5	34.9395	4.02	-1.57
1.5	34.9395	3.33	-0.95
1.5	34.9395	2.87	-0.31
1.5	34.9395	2.61	0.35
1.5	34.9395	2.48	1.01
1.5	34.9395	2.46	1.15
1.5	34.9395	2.42	1.65
1.5	34.9395	2.42	2.3
1.5	34.9395	2.48	3.01
1.5	34.9395	2.6	3.83
1.5	34.9395	2.81	4.76
1.5	34.9395	3.09	5.83
1.5	34.9395	3.46	7.06
1.5	34.9395	3.91	8.5
1.5	34.9395	4.43	10.19
1.5	**34.9395**	**5.0**4	12.19
1.5	**34.9395**	**5.7**2	14.43
1.5	**34.9395**	**6.4**7	16.82
1.5	**34.9395**	**6.**76	17.72
1.5	34.9395	7.29	19.3
1.5	**34.9395**	**8.1**9	21.84
1.5	34.9395	9.18	24.41
1.**5**	**34.9395**	10.29	27
1.5	**34.9395**	**11**.6	29.7
1.5	34.9395	12.5	31.38
1.5	**34.9395**	**13**.2	32.6
1.5	34.9395	15.26	35.98
1.5	**34.9395**	**18**.38	40.96
1.5	34.9395	19.63	43
1.5	34.9395	23.22	48.94
2	46.586	0	-4.6
2	46.586	0.82	-4.54
2	46.586	1.38	-4.35
2	46.586	1.71	-4.06
2	46.586	1.84	-3.71
2	46.586	1.8	-3.34
2	46.586	1.63	-2.99
2	46.586	1.36	-2.66
2	46.586	1.06	-2.3
2	46.586	0.79	-1.8
2	46.586	0.61	-1.1
2	46.586	0.58	-0.35
2	46.586	0.58	-0.25
2	46.586	0.75	0.63
2	46.586	1.15	1.44
2	46.586	1.3	1.66
2	46.586	1.71	2.21
2	46.586	2.33	2.98
2	46.586	2.86	3.69
2	46.586	2.94	3.82

2	46.586		
2	46.586	4.15	5.84
2	46.586		
2	46.586	4.41	6.32
2	46.586		
2	46.586	5.46	8.5
2	46.586		
2	46.586		
2	46.586	7.1	12.19
2	46.586		
2	46.586	9.06	16.76
2	46.586		
2	46.586	11.07	21.58
2	46.586		
2	46.586		
2	46.586		
2	46.586		
2	46.586	15.82	31.56
2	46.586		
2	46.586		
2	46.586		
2	46.586	24.81	47.78
3	69.879	0	0
3	69.879	0.21	0.08
3	69.879	0.57	0.29
3	69.879	1.04	0.62
3	69.879	2.02	1.39
3	69.879	3.12	2.33
3	69.879	4.22	3.35
3	69.879	5.77	4.96
3	69.879	7.16	6.58
3	69.879	8.49	8.29
3	69.879	9.88	10.15
3	69.879	11.31	12.15
3	69.879	12.72	14.24
3	69.879	14.07	16.4
3	69.879	15.34	18.61
3	69.879	16.53	20.85
3	69.879	17.64	23.15
3	69.879	18.75	25.59
3	69.879	19.94	28.3
3	69.879	21.4	31.61
3	69.879	23.66	36.81
3	69.879	27.38	45.39
4	93.172	0	0
4	93.172	0.23	0.07
4	93.172	0.64	0.25
4	93.172	1.2	0.54
4	93.172	2.37	1.21
4	93.172	3.72	2.04
4	93.172	5.09	2.93
4	93.172	7.1	4.36
4	93.172	8.9	5.83
4	93.172	10.64	7.4
4	93.172	12.39	9.13

4	93.172	14.13	11
4	93.172	15.84	12.95
4	93.172	17.45	14.95
4	93.172	18.94	16.99
4	93.172	20.29	19.07
4	93.172	21.47	21.22
4	93.172	22.56	23.52
4	93.172	23.63	26.07
4	93.172	24.84	29.23
4	93.172	26.63	34.41
4	93.172	29.5	43.27
5	116.465	0	0
5	116.465	0.24	0.05
5	116.465	0.7	0.21
5	116.465	1.34	0.45
5	116.465	2.7	1
5	116.465	4.27	1.68
5	116.465	5.89	2.43
5	116.465	8.27	3.66
5	116.465	10.42	4.97
5	116.465	12.44	6.41
5	116.465	14.42	8.04
5	116.465	16.35	9.81
5	116.465	18.21	11.68
5	116.465	19.99	13.58
5	116.465	21.62	15.53
5	116.465	23.07	17.54
5	116.465	24.31	19.63
5	116.465	25.39	21.88
5	116.465	26.39	24.35
5	116.465	27.44	27.43
5	116.465	28.85	32.58
5	116.465	30.99	41.59
6	139.758	0	0
6	139.758	0.26	0.04
6	139.758	0.77	0.16
6	139.758	1.49	0.34
6	139.758	3.02	0.75
6	139.758	4.8	1.28
6	139.758	6.65	1.87
6	139.758	9.37	2.9
6	139.758	11.82	4.05
6	139.758	14.09	5.37
6	139.758	16.24	6.89
6	139.758	18.3	8.59
6	139.758	20.26	10.39
6	139.758	22.12	12.25
6	139.758	23.82	14.18
6	139.758	25.29	16.19
6	139.758	26.51	18.29
6	139.758	27.53	20.54
6	139.758	28.44	22.99
6	139.758	29.35	26.01
6	139.758	30.47	31.13
6	139.758	32.06	40.17

7	163.051	0	0
7	163.051	0.28	0.03
7	163.051	0.82	0.11
7	163.051	1.6	0.23
7	163.051	3.27	0.53
7	163.051	5.24	0.9
7	163.051	7.28	1.35
7	163.051	10.32	2.16
7	163.051	13.06	3.12
7	163.051	15.57	4.3
7	163.051	17.9	5.71
7	163.051	20.08	7.32
7	163.051	22.1	9.09
7	163.051	23.97	10.97
7	163.051	25.65	12.95
7	163.051	27.07	15.02
7	163.051	28.18	17.19
7	163.051	29.08	19.49
7	163.051	29.85	21.97
7	163.051	30.61	24.97
7	163.051	31.53	30.03
7	163.051	32.81	38.97
8	186.344	0	0
8	186.344	0.28	0.02
8	186.344	0.86	0.07
8	186.344	1.68	0.15
8	186.344	3.46	0.34
8	186.344	5.55	0.6
8	186.344	7.74	0.92
8	186.344	11.03	1.55
8	186.344	14.03	2.35
8	186.344	16.76	3.38
8	186.344	19.26	4.67
8	186.344	21.54	6.19
8	186.344	23.61	7.93
8	186.344	25.46	9.85
8	186.344	27.07	11.92
8	186.344	28.37	14.1
8	186.344	29.36	16.36
8	186.344	30.11	18.73
8	186.344	30.73	21.25
8	186.344	31.35	24.26
8	186.344	32.14	29.23
8	186.344	33.31	37.91
9	209.637	0	0
9	209.637	0.29	0.01
9	209.637	0.88	0.05
9	209.637	1.73	0.1
9	209.637	3.56	0.23
9	209.637	5.73	0.42
9	209.637	8.01	0.66
9	209.637	11.46	1.18
9	209.637	14.62	1.88
9	209.637	17.52	2.8
9	209.637	20.16	3.96

9	209.637	22.55	5.37
9	209.637	24.66	7.06
9	209.637	26.47	9.02
9	209.637	27.97	11.19
9	209.637	29.16	13.48
9	209.637	30.03	15.82
9	209.637	30.68	18.24
9	209.637	31.19	20.8
9	209.637	31.71	23.82
9	209.637	32.44	28.65
9	209.637	33.6	36.9
10	232.93	0	0
10	232.93	0.29	0.01
10	232.93	0.89	0.03
10	232.93	1.75	0.08
10	232.93	3.61	0.18
10	232.93	5.82	0.33
10	232.93	8.14	0.55
10	232.93	11.66	1.03
10	232.93	14.91	1.7
10	232.93	17.89	2.55
10	232.93	20.64	3.62
10	232.93	23.09	4.94
10	232.93	25.23	6.59
10	232.93	27	8.58
10	232.93	28.42	10.82
10	232.93	29.52	13.18
10	232.93	30.32	15.56
10	232.93	30.9	18.01
10	232.93	31.36	20.58
10	232.93	31.81	23.59
10	232.93	32.5	28.23
10	232.93	33.69	35.97
11	256.223	0	0
11	256.223	0.3	0.01
11	256.223	0.9	0.03
11	256.223	1.76	0.08
11	256.223	3.63	0.18
11	256.223	5.85	0.34
11	256.223	8.18	0.56
11	256.223	11.72	1.06
11	256.223	14.99	1.74
11	256.223	17.99	2.6
11	256.223	20.76	3.65
11	256.223	23.23	4.94
11	256.223	25.36	6.57
11	256.223	27.11	8.57
11	256.223	28.49	10.84
11	256.223	29.55	13.21
11	256.223	30.33	15.58
11	256.223	30.9	18
11	256.223	31.34	20.55
11	256.223	31.76	23.5
11	256.223	32.42	27.94
11	256.223	33.59	35.12

12	279.516	0	0
12	279.516	0.31	0.01
12	279.516	0.92	0.05
12	279.516	1.77	0.11
12	279.516	3.62	0.25
12	279.516	5.83	0.46
12	279.516	8.15	0.73
12	279.516	11.67	1.32
12	279.516	14.9	2.09
12	279.516	17.87	3.02
12	279.516	20.59	4.11
12	279.516	23.02	5.43
12	279.516	25.12	7.05
12	279.516	26.84	9.03
12	279.516	28.21	11.25
12	279.516	29.28	13.56
12	279.516	30.09	15.86
12	279.516	30.69	18.19
12	279.516	31.16	20.66
12	279.516	31.59	23.53
12	279.516	32.23	27.73
12	279.516	33.38	34.39
13	302.809	0	0
13	302.809	0.35	0.02
13	302.809	0.95	0.09
13	302.809	1.78	0.19
13	302.809	3.59	0.43
13	302.809	5.76	0.74
13	302.809	8.05	1.14
13	302.809	11.5	1.9
13	302.809	14.65	2.82
13	302.809	17.54	3.88
13	302.809	20.16	5.07
13	302.809	22.51	6.44
13	302.809	24.54	8.06
13	302.809	26.23	9.96
13	302.809	27.62	12.06
13	302.809	28.73	14.22
13	302.809	29.59	16.36
13	302.809	30.27	18.55
13	302.809	30.8	20.89
13	302.809	31.27	23.63
13	302.809	31.96	27.61
13	302.809	33.14	33.81
14	326.102	0	0
14	326.102	0.39	0.04
14	326.102	0.98	0.16
14	326.102	1.78	0.34
14	326.102	3.53	0.74
14	326.102	5.65	1.26
14	326.102	7.87	1.85
14	326.102	11.22	2.89
14	326.102	14.26	4.02
14	326.102	17.02	5.23
14	326.102	19.51	6.52

14	326.102	21.74	7.92
14	326.102	23.69	9.5
14	326.102	25.37	11.26
14	326.102	26.78	13.16
14	326.102	27.94	15.1
14	326.102	28.89	17.03
14	326.102	29.65	19.04
14	326.102	30.27	21.21
14	326.102	30.83	23.8
14	326.102	31.57	27.56
14	326.102	32.78	33.36
15	349.395	0	0
15	349.395	0.43	0.07
15	349.395	1.01	0.27
15	349.395	1.76	0.57
15	349.395	3.44	1.28
15	349.395	5.46	2.14
15	349.395	7.6	3.06
15	349.395	10.81	4.49
15	349.395	13.7	5.84
15	349.395	16.3	7.16
15	349.395	18.65	8.47
15	349.395	20.75	9.82
15	349.395	22.63	11.25
15	349.395	24.29	12.8
15	349.395	25.74	14.44
15	349.395	26.98	16.12
15	349.395	28	17.83
15	349.395	28.85	19.63
15	349.395	29.55	21.64
15	349.395	30.18	24.07
15	349.395	30.94	27.62
15	349.395	32.08	33.12
16	372.688	0	0
16	372.688	0.53	0.11
16	372.688	1.09	0.44
16	372.688	1.78	0.95
16	372.688	3.33	2.12
16	372.688	5.24	3.52
16	372.688	7.26	4.92
16	372.688	10.28	6.78
16	372.688	13	8.25
16	372.688	15.44	9.49
16	372.688	17.63	10.65
16	372.688	19.61	11.82
16	372.688	21.42	13.03
16	372.688	23.07	14.33
16	372.688	24.56	15.72
16	372.688	25.85	17.17
16	372.688	26.91	18.69
16	372.688	27.78	20.33
16	372.688	28.51	22.2
16	372.688	29.16	24.48
16	372.688	29.93	27.88
16	372.688	31.03	33.2

17	395.981	0	4.93
17	395.981	0.26	4.98
17	395.981	0.78	5.14
17	395.981	1.52	5.44
17	395.981	3.1	6.26
17	395.981	4.95	7.3
17	395.981	6.86	8.39
17	395.981	9.71	9.85
17	395.981	12.26	11
17	395.981	14.53	11.97
17	395.981	16.57	12.88
17	395.981	18.42	13.78
17	395.981	20.15	14.74
17	395.981	21.78	15.8
17	395.981	23.27	16.96
17	395.981	24.56	18.23
17	395.981	25.61	19.61
17	395.981	26.46	21.14
17	395.981	27.16	22.88
17	395.981	27.79	25.03
17	395.981	28.57	28.3
17	395.981	29.73	33.55
18	419.274	0	10.91
18	419.274	0.26	10.94
18	419.274	0.75	11.03
18	419.274	1.45	11.18
18	419.274	2.94	11.55
18	419.274	4.68	12.02
18	419.274	6.48	12.53
18	419.274	9.13	13.29
18	419.274	11.49	13.99
18	419.274	13.59	14.63
18	419.274	15.48	15.23
18	419.274	17.19	15.85
18	419.274	18.8	16.55
18	419.274	20.34	17.36
18	419.274	21.75	18.32
18	419.274	22.96	19.42
18	419.274	23.94	20.68
18	419.274	24.72	22.11
18	419.274	25.36	23.74
18	419.274	25.98	25.74
18	419.274	26.8	28.9
18	419.274	28.1	34.17
19	442.567	0	15.21
19	442.567	0.25	15.23
19	442.567	0.73	15.29
19	442.567	1.4	15.38
19	442.567	2.82	15.58
19	442.567	4.47	15.82
19	442.567	6.17	16.08
19	442.567	8.65	16.48
19	442.567	10.82	16.84
19	442.567	12.73	17.19
19	442.567	14.44	17.52

19	442.567	15.98	17.89
19	442.567	17.41	18.37
19	442.567	18.74	19
19	442.567	19.94	19.8
19	442.567	20.96	20.78
19	442.567	21.77	21.95
19	442.567	22.42	23.29
19	442.567	22.98	24.81
19	442.567	23.55	26.66
19	442.567	24.4	29.75
19	442.567	25.85	35.14
20	465.86	0	18.75
20	465.86	0.25	18.75
20	465.86	0.48	18.76
20	465.86	0.7	18.76
20	465.86	0.94	18.77
20	465.86	1.21	18.78
20	465.86	1.58	18.82
20	465.86	2.16	18.9
20	465.86	3.04	19.06
20	465.86	3.42	19.14
20	465.86	4.19	19.34
20	465.86	5.18	19.65
20	465.86	6.17	20.01
20	465.86	7.23	20.43
20	465.86	7.24	20.44
20	465.86	8.39	20.94
20	465.86	9.41	21.45
20	465.86	9.63	21.57
20	465.86	10.94	22.39
20	465.86	11.21	22.57
20	465.86	12.32	23.42
20	465.86	13	23.99
20	465.86	13.75	24.66
20	465.86	15.16	26
20	465.86	15.22	26.06
20	465.86	16.87	27.8
20	465.86	18.21	29.37
20	465.86	19.4	30.84
20	465.86	22.29	34.53
20	465.86	22.29	34.53
20	465.86	22.75	36.33

APPENDIX C:
MODEL UNCERTAINTIES OF NUMERICAL METHOD

Table C.1: Model uncertainties of numerical method

load	β	Hw	exp.	pred.	Xm	mean, L1	COV, L1	mean, L2	COV, L2	mean, L3	COV, L3	mean, L4	COV, L4	mean, L5	COV, L5
VBM	180	small	0.003917	0.002850	1.3743	0.8861	0.3166	0.8637	0.2787	0.9503	0.3283				
			0.005089	0.004800	1.0603										
			0.006873	0.005900	1.1649										
			0.008674	0.008600	1.0086										
			0.012370	0.018170	0.6808										
			0.012457	0.020750	0.6003										
			0.005529	0.008400	0.6582										
			0.001515	0.001800	0.8417										
			0.002518	0.004300	0.5857										
		large	0.002281	0.002750	0.8295										
			0.004719	0.003850	1.2256										
			0.006477	0.005900	1.0977										
			0.007800	0.008500	0.9176										
			0.013636	0.018550	0.7351										
			0.011989	0.020650	0.5806										
			0.006624	0.008700	0.7613										
			0.001296	0.002000	0.6478										
			0.002405	0.003100	0.7760										
	45	small	0.002182	0.001300	1.6783	1.0393	0.3203								
			0.002176	0.002150	1.0120										
			0.003285	0.002900	1.1329										
			0.003952	0.004250	0.9299										
			0.008639	0.011500	0.7512										
			0.008869	0.013450	0.6594										
			0.011553	0.017100	0.6756										
			0.016781	0.013700	1.2249										
			0.017281	0.013400	1.2896										
		large	0.002442	0.001250	1.9538										
			0.002205	0.002000	1.1027										
			0.003664	0.003400	1.0776										
			0.004458	0.004350	1.0249										
			0.008302	0.011500	0.7219										
			0.009274	0.014950	0.6203										
			0.011774	0.017050	0.6906										
			0.012825	0.013500	0.9500										
			0.006849	0.005850	1.1707	1.0347	0.3843	1.0370	0.3431						
	180	small	small values ≈ 0												

			large	small values ≈ 0								
Intact	HBM											
			small	0.000852	0.000400	2.1302						
				0.000269	0.000600	0.4491						
				0.000211	0.000775	0.2720						
				0.000452	0.001150	0.3933						
				0.002179	0.003850	0.5661						
				0.002964	0.004725	0.6273						
				0.008494	0.006575	1.2919						
				0.008157	0.004800	1.6995						
		45		0.008409	0.004750	1.7704	1.0222	0.6891				
			large	0.000848	0.000355	2.3878						
				0.000160	0.000550	0.2913						
				0.000259	0.000900	0.2880						
				0.000427	0.001175	0.3633						
				0.002402	0.003850	0.6239						
				0.003870	0.005425	0.7134						
				0.006594	0.006550	1.0067						
				0.006790	0.004800	1.4146						
				0.003554	0.003425	1.0375	0.9030	0.7483	0.9626	0.6986	0.9626	0.6986
	TM		small	small values ≈ 0								
		180										
			large	small values ≈ 0								
			small	0.000243	0.000185	1.3160						
				0.000043	0.000290	0.1491						
				0.000071	0.000380	0.1872						
				0.000112	0.000550	0.2041						
				0.000990	0.001430	0.6923						
				0.001537	0.001650	0.9315						
				0.000913	0.001570	0.5818						
				0.000723	0.001070	0.6759						
		45		0.000713	0.001060	0.6725	0.6012	0.6369				
			large	0.000160	0.000175	0.9146						
				0.000048	0.000270	0.1780						
				0.000091	0.000440	0.2073						
				0.000131	0.000575	0.2277						
				0.001143	0.001430	0.7990						

				0.002131	0.001810	1.1776								
				0.000874	0.001570	0.5570								
				0.000494	0.001060	0.4664								
				0.000398	0.000530	0.7516	0.5866	0.5979	0.5939	0.5999	0.5939	0.5999	0.8643	0.5320
				0.003519	0.003200	1.0996								
				0.004525	0.004900	0.9235								
				0.007218	0.006200	1.1642								
				0.009442	0.009000	1.0491								
			small	0.015019	0.019000	0.7905								
				0.013752	0.020900	0.6580								
				0.004328	0.006600	0.6558								
				0.002133	0.004500	0.4740								
		180		0.002523	0.002900	0.8701	0.8538	0.2702						
				0.002859	0.003300	0.8663								
				0.005020	0.004950	1.0141								
				0.007051	0.006100	1.1560								
				0.009966	0.009100	1.0952								
			large	0.015704	0.019200	0.8179								
				0.012674	0.020950	0.6050								
				0.004962	0.006900	0.7191								
				0.001632	0.004600	0.3548								
				0.002482	0.002500	0.9929	0.8468	0.3024	0.8503	0.2781				
				0.001434	0.001750	0.8197								
				0.002048	0.002700	0.7586								
				0.004998	0.003950	1.2654								
				0.006084	0.004950	1.2292								
			small	0.011392	0.011700	0.9737								
				0.011078	0.013250	0.8361								
				0.010732	0.015100	0.7107								
				0.011813	0.012800	0.9229								
	VBM	45		0.007286	0.006250	1.1658	0.9647	0.2159						
				0.001538	0.001750	0.8788								
				0.002142	0.002600	0.8240								
				0.004176	0.003650	1.1442								
				0.005396	0.004950	1.0901								
			large	0.010546	0.011650	0.9052								
				0.010360	0.013250	0.7819								
				0.012230	0.015100	0.8100								
				0.010533	0.012600	0.8359								
				0.006816	0.006200	1.0994	0.9299	0.1520	0.9473	0.1833				
				0.002312	0.001700	1.3602								
				0.002462	0.002500	0.9849								
				0.005620	0.003900	1.4410								
				0.006638	0.005000	1.3276								
			small	0.010139	0.011700	0.8666								
				0.010632	0.014700	0.7233								
				0.024071	0.015300	1.5733								
				0.012189	0.012800	0.9523								
		315		0.006789	0.006100	1.1129	1.1491	0.2518						
				0.001875	0.001800	1.0414								
				0.002856	0.002700	1.0577								
				0.004982	0.003800	1.3111								
				0.005680	0.005100	1.1138								
			large	0.010065	0.011800	0.8530								
				0.010659	0.014400	0.7402								

				0.017999	0.015300	1.1764						
				0.015267	0.012700	1.2021						
				0.008328	0.006200	1.3432	1.0932	0.1816	1.1212	0.2162	0.9729	0.2502
		180	small	small values ≈ 0								
			large	small values ≈ 0								
		45	small	0.000891	0.000325	2.7406						
				0.000413	0.000500	0.8259						
				0.000163	0.000775	0.2102						
				0.000225	0.001025	0.2194						
				0.002637	0.003625	0.7276						
				0.003267	0.004450	0.7341						
				0.005144	0.007050	0.7296						
				0.004658	0.005750	0.8102						
DS2	HBM			0.007443	0.003150	2.3628	1.0400	0.8593				
			large	0.000546	0.000325	1.6797						
				0.000261	0.000475	0.5485						
				0.000132	0.000700	0.1889						
				0.000208	0.001025	0.2027						
				0.002585	0.003625	0.7132						
				0.003083	0.004450	0.6929						
				0.005417	0.007050	0.7684						
				0.003455	0.005600	0.6170						
				0.006287	0.003075	2.0445	0.8284	0.7589	0.9342	0.8108		
		315	small	0.001357	0.000300	4.5250						
				0.000488	0.000450	1.0839						
				0.001025	0.000775	1.3225						
				0.001136	0.001050	1.0821						
				0.003253	0.003625	0.8973						
				0.005056	0.005300	0.9540						
				0.010414	0.007300	1.4266						
				0.006573	0.005800	1.1332						
				0.002945	0.002950	0.9984	1.4914	0.7711				
			large	0.000568	0.000325	1.7470						
				0.000412	0.000500	0.8244						
				0.000833	0.000725	1.1487						
				0.000991	0.001000	0.9908						
				0.003398	0.003500	0.9709						
				0.005374	0.005100	1.0538						
				0.011157	0.007400	1.5078						

			0.008617	0.006200	1.3898						
			0.004198	0.002750	1.5265	1.2400	0.2524	1.3657	0.6062	1.1500	0.7061
			0.000088	0.000725	0.1220						
			0.000101	0.001225	0.0825						
			0.000178	0.001650	0.1080						
			0.000243	0.002500	0.0970						
		small	0.000748	0.005775	0.1295						
			0.001255	0.006450	0.1945						
			0.000248	0.003450	0.0720						
			0.000100	0.006925	0.0145						
	180		0.000037	0.001400	0.0267	0.0941	0.5800				
			0.000063	0.000750	0.0843						
			0.000084	0.001250	0.0671						
			0.000131	0.001650	0.0792						
			0.000193	0.002500	0.0771						
		large	0.000939	0.005800	0.1620						
			0.001323	0.006450	0.2050						
			0.000210	0.003450	0.0608						
			0.000116	0.007000	0.0166						
			0.000031	0.001500	0.0208	0.0859	0.7146	0.0900	0.6278		
			0.000062	0.000230	0.2701						
			0.000046	0.000375	0.1233						
			0.000038	0.000550	0.0684						
			0.000017	0.000700	0.0237						
		small	0.000325	0.001710	0.1903						
			0.000471	0.001900	0.2480						
			0.000491	0.001380	0.3559						
			0.000718	0.000800	0.8975						
TM	45		0.000241	0.000840	0.2871	0.2738	0.9409				
			0.000040	0.000230	0.1756						
			0.000036	0.000355	0.1003						
			0.000038	0.000510	0.0749						
			0.000039	0.000700	0.0563						
		large	0.000373	0.001690	0.2208						
			0.000481	0.009200	0.0522						
			0.000581	0.001380	0.4213						
			0.000717	0.000760	0.9436						
			0.000262	0.000840	0.3115	0.2618	1.0878	0.2678	0.9840		
			0.000078	0.000230	0.3390						
			0.000071	0.000350	0.2018						
			0.000187	0.000550	0.3409						
			0.000208	0.000720	0.2883						
		small	0.000681	0.001740	0.3916						
			0.001320	0.002120	0.6228						
			0.000316	0.001440	0.2197						
			0.000345	0.007900	0.0437						
	315		0.000290	0.000880	0.3295	0.3086	0.5097				
			0.000041	0.000250	0.1638						
			0.000075	0.000370	0.2035						
			0.000155	0.000560	0.2761						
			0.000206	0.000730	0.2818						
		large	0.000851	0.001750	0.4862						
			0.001688	0.002090	0.8077						
			0.000490	0.001420	0.3453						
			0.000470	0.000770	0.6101						

				0.000269	0.000800	0.3356	0.3900	0.5346	0.3493	0.5267	0.2357	0.9110	0.7407	0.8092
				0.003981	0.002600	1.5311								
				0.004898	0.004000	1.2246								
				0.006449	0.005350	1.2055								
				0.008071	0.007800	1.0347								
			small	0.012380	0.017400	0.7115								
				0.012805	0.019650	0.6516								
				0.005558	0.009600	0.5790								
				0.001165	0.003250	0.3585								
		180		0.002204	0.003200	0.6889	0.8873	0.4276						
				0.003789	0.002500	1.5155								
				0.004759	0.004200	1.1331								
				0.006572	0.005800	1.1331								
				0.007879	0.007900	0.9974								
			large	0.012310	0.017500	0.7034								
				0.012560	0.018100	0.6939								
				0.005665	0.009000	0.6294								
				0.001009	0.002900	0.3479								
	VBM			0.002087	0.003000	0.6955	0.8721	0.4035	0.8797	0.4037				
				0.001516	0.001100	1.3782								
				0.001969	0.001900	1.0361								
				0.002794	0.002500	1.1177								
				0.003582	0.003800	0.9427								
			small	0.008834	0.010500	0.8414								
				0.008337	0.011100	0.7511								
				0.012165	0.016000	0.7603								
				0.010882	0.012700	0.8569								
		45		0.006547	0.006150	1.0646	0.9721	0.2069						
				0.001500	0.001050	1.4288								
				0.002040	0.001750	1.1655								
				0.003061	0.002350	1.3023								
				0.003897	0.003800	1.0256								
			large	0.008489	0.010400	0.8163								
				0.008052	0.011100	0.7254								
				0.013147	0.015900	0.8268								
				0.009586	0.012500	0.7669								
				0.007614	0.006150	1.2381	1.0329	0.2524	1.0025	0.2275	0.9411	0.3195		
			small	small values ≈ 0										
		180												
			large	small values ≈ 0										
DS3	HBM													

			0.000846	0.000250	3.3856										
			0.000226	0.000800	0.2822										
			0.000355	0.000950	0.3736										
			0.000245	0.001375	0.1785										
		small	0.001532	0.003900	0.3927										
			0.001490	0.004150	0.3591										
			0.007341	0.006025	1.2184										
			0.006015	0.004325	1.3907										
	45		0.002795	0.003025	0.9241	0.9450	1.0735								
			0.000406	0.000500	0.8122										
			0.000120	0.000725	0.1649										
			0.000106	0.000925	0.1142										
			0.000229	0.001375	0.1665										
		large	0.001644	0.003850	0.4270										
			0.001628	0.004150	0.3923										
			0.006126	0.005950	1.0296										
			0.004460	0.004400	1.0136										
			0.003459	0.002975	1.1628	0.5870	0.7132	0.7660	1.0118	0.7660	1.0118				
TM	180	small	small values ≈ 0												
		large	small values ≈ 0												
			0.000051	0.000170	0.2989										
			0.000025	0.000290	0.0852										
			0.000039	0.000365	0.1080										
			0.000055	0.000540	0.1017										
		small	0.000311	0.001420	0.2188										
			0.000294	0.001490	0.1973										
			0.000256	0.001560	0.1640										
			0.000416	0.001040	0.4001										
	45		0.000115	0.000695	0.1648	0.1932	0.5291								
			0.000033	0.000170	0.1916										
			0.000027	0.000260	0.1029										
			0.000042	0.000340	0.1224										
			0.000069	0.000540	0.1279										
		large	0.000393	0.001400	0.2808										
			0.000385	0.001490	0.2585										
			0.000266	0.001520	0.1750										
			0.000301	0.001000	0.3008										
			0.000115	0.000700	0.1647	0.1916	0.3784	0.1924	0.4468	0.1924	0.4468	0.7101	0.7530	0.7640	0.7236